TECHNISCHE UNIVERSITÄT MÜNCHEN

Institut für Siliciumchemie

WACKER-Lehrstuhl für Makromolekulare Chemie

Synthesis and Reactivity of Acyclic Silylenes: On the Way to Metal-free Catalysis

Daniel Andreas Wolfgang Wendel

Vollständiger Abdruck der von der Fakultät für Chemie der Technischen Universität München zur Erlangung des akademischen Grades eines

Doktors der Naturwissenschaften

genehmigten Dissertation.

Vorsitzender:	Prof. Dr. Tobias A. M. Gulder
Prüfer der Dissertation:	1. Prof. Dr. Dr. h.c. Bernhard Rieger
	2. Prof. Dr. Shigeyoshi Inoue
	3. Prof. Dr. Dr. h.c. mult. Herbert W. Roesky / apl. Prof. Dr. Wolfgang Eisenreich

Die Dissertation wurde am 05.03.2018 bei der Technischen Universität München eingereicht und durch die Fakultät für Chemie am 11.04.2018 angenommen.

“Nothing can be more certain than this: that we are just beginning to learn something of the wonders of the world on which we live and move and have our being.”

William Ramsay (1852-1916)

Diese Arbeit wurde in der Zeit von Februar 2015 bis Februar 2018 am WACKER-Lehrstuhl für Makromolekulare Chemie der Technischen Universität München unter der Betreuung von Herrn Prof. Dr. Dr. h.c. Bernhard Rieger durchgeführt.

Acknowledgments

Mein besonderer Dank gilt Herrn Professor Dr. Dr. h.c. Bernhard Rieger für die herzliche Aufnahme in seinen Arbeitskreis und das entgegengebrachte Vertrauen ein spannendes Projekt des WACKER-Instituts für Siliciumchemie bearbeiten zu dürfen. Bedanken möchte ich mich ebenfalls für sein persönliches Interesse an meiner Arbeit sowie die zahlreichen Anregungen und Diskussionen.

Daneben bin ich meinem Mentor „Shige“ (Herr Prof. Dr. Shigeyoshi Inoue) zu großem Dank verpflichtet. Bei seiner Ankunft an unserer Fakultät hat er es als selbstverständlich angesehen, mich als „quasi“-Mitglied in seiner Gruppe willkommen zu heißen und es geschafft mein Projekt durch sein Know-how und seine Expertise auf dem Gebiet des niedervalenten Siliciums stetig voranzutreiben.

Danken möchte ich darüber hinaus Herrn Dr. Thomas Renner, Herrn Dr. Richard Weidner, Frau Dr. Elke Fritz-Langhals und Herrn Dr. Jan Tillmann von der WACKER Chemie AG für die gemeinsame Projektarbeit, die vielen fachlichen Diskussionen sowie die produktive und angenehme Atmosphäre bei den regelmäßigen Treffen.

Im Zuge des Silicium-Instituts bin ich auch meinem direkten Projektpartner und gutem Freund Fabian „Febbien“ Herz sehr dankbar. Wir waren ein exzellentes Team und haben gemeinsam viel Gutes auf die Beine gestellt. Ebenso gebührt mein Dank dem „Silanon-/Bierkönig“ Dominik Reiter. Zusammen sind wir der Erfüllung von Kipping’s Traum ein großes Stück näher gekommen. Im gleichen Sinne möchte ich mich bei Amelie Porzelt und Tibor Szilvási für die unzähligen Stunden bedanken, die sie in Rechnungen zur Aufklärung der elektronischen Struktur meiner doch teilweise zu groß geratenen Moleküle gesteckt haben. Dem XRD-Team – bestehend aus Dr. Alexander Pöthig, Christian Jandl und Philipp Altmann – danke ich für die zahlreichen Messungen, sowie die Geduld und das Engagement jeden noch so winzigen „Kristall“ in einen Strukturvorschlag zu verwandeln. Ein herzliches Dankeschön gebührt Ulrike Ammari, Rodica Dumitrescu und Maria Weindl, deren analytische Dienste außerordentlich wichtig für die Anfertigung meiner Arbeit waren.

Für die technische Unterstützung und Anlaufstelle bei Problemen jeglicher Art möchte ich Dr. Carsten Troll und Dr. Sergei Vagin recht herzlich danken. Darüber hinaus gilt mein Dank Annette Bauer für die Unterstützung bei sämtlichen organisatorischen Aufgaben.

Des Weiteren danke ich meinem ehemaligen Masterarbeitsbetreuer Sven Heidsieck und allen früheren Kollegen des ehemaligen Silicium-Instituts (insbesondere Matthias Grübel und Sebastian Kraus), die mir die Tür zur Siliciumorganischen Chemie geöffnet haben. Im gleichen Maße möchte ich mich bei der jüngeren Generation des Silicium-Instituts (vor allem Philipp Frisch, Richard Holzner und Debotra Sarkar) sowie den Mitgliedern des AK Inoue und des WACKER-Lehrstuhls für Makromolekulare Chemie für das angenehme und produktive Arbeitsklima und die Hilfsbereitschaft bei Fragen und Problemen jeglicher Art bedanken.

Herausheben möchte ich hier, meine ständigen Begleiter im Studium, langjährigen Laborpartner und sehr guten Freunde Philipp Pahl und Martin Machat. Ich werde die Zeiten in denen wir als die drei unzertrennlichen „Chipmunks“ das Labor, die Münchner Nachtclubs und all die schönen Plätze dieser Welt unsicher gemacht haben, sehr vermissen. Ich hoffe aber wir können in Zukunft, wann immer es die Zeit zulässt, daran anschließen. Selbstverständlich bin ich auch meinen Studenten, insbesondere meiner brillanten Masterandin Katharina Kaiser, dankbar, die über die letzten Jahre wichtige Arbeit für mich geleistet haben.

Ich danke auch Marko „Sranje“ Cigler, Dr. Françoise „Fritzo“ Schaefers und den restlichen Doktoranden der Arbeitskreise Gulder und Lang, die es als direkte Labornachbarn immer verstanden haben für eine lockere und lustige Arbeitsatmosphäre und sehr viel Spaß, auch außerhalb des Labors, zu sorgen. Außerdem gebührt sämtlichen Korrekturlesern dieser Arbeit mein besonderer Dank.

Abschließend möchte ich mich bei meiner Familie für das entgegengebrachte Vertrauen und die fortwährende Unterstützung während der gesamten Studienzeit bedanken. Ich weiß, dass ich in sämtlichen Lebenslagen auf euch zählen kann! Zuallerletzt: Danke Nadine, dass du immer für mich da bist, mich Saukerl auch in schwierigeren Zeiten aushältst, mich stets wieder aufbaust und mir, wenn nötig, das Licht am Ende des Tunnels zeigst. Ohne dich, stände ich jetzt nicht hier!

List of Abbreviations

$\Delta E_{S,T}$	singlet-triplet energy
λ	wavelength [nm]
θ	bent angle [°]
τ	twist angle [°]
A	anion
Å	Ångström
*a*AAC	acyclic alkyl(amino)carbene
AG	german (*Aktiengesellschaft*): “stock company”
approx.	approximately
BCF	tris(pentafluorophenyl)borane
Bn.	billion
*c*AAC	cyclic alkyl(amino)carbene
*c*AASi	cyclic alkyl(amino)silylene
cat.	catalyst
CGMT	“Carter-Goddard-Malrieu-Trinquier”
Cp*	pentamethylcyclopentadienyl
Cy	cyclohexyl
DFT	density functional theory
Dipp	2,6-di*iso*-propylphenyl; C_6H_3-2,6-*i*-Pr_2
DME	dimethyl ether
E	element
e.g.	latin (*exempli gratia*): “for example”
E_{Hybrid}	energy of hybridization
Et	ethyl
et al.	latin (*et alii*): “and others”
eV	electronvolt
FLP	“Frustrated Lewis Pair”
h	hour
HBcat	catecholborane
HBpin	pinacolborane
HT	high temperature
HOMO	highest occupied molecular orbital
I*i*-Pr_2Me_2	1,3-bis(*iso*-propyl)-4,5-dimethylimidazol-2-yildene
in situ	latin: “on site”
IPr	1,3-bis(2,6-di*iso*-propylphenyl)-imidazol-2-ylidene
i-Pr	*iso*-propyl

IR	infrared spectroscopy
I*t*-Bu	1,3-bis(*tert*-butyl)imidazol-2-ylidene
kcal	kilocalorie
kJ	kilojoule
L-	literature reported compound
LT	low temperature
LUMO	lowest unoccupied molecular orbital
M	metal
Me	methyl
Mes	2,4,6-trimethylphenyl; C_6H_2-2,4,6-Me_3
min	minute
m.p.	melting point
m-Tol	*meta*-toluoyl
MWh	megawatt hour
NHC	*N*-heterocyclic carbene
NHI	*N*-heterocyclic imine
NHSi	*N*-heterocyclic silylene
NMR	nuclear magnetic resonance spectroscopy
Ph	phenyl
ppm	parts per million
R	functional group
r.t.	room temperature
SC XRD	single-crystal X-ray diffraction
t	ton
TBon	$[B(NDippCH)_2NTMS]$
t-Bu	*tert*-butyl
thf	tetrahydrofuran
Tipp	2,4,6-tri*iso*-propylphenyl; C_6H_2-2,4,6-*i*-Pr_3
TMS	trimethylsilyl
TOF	turnover frequency
UV-vis	ultraviolet–visible spectroscopy
vice versa	latin: “the other way around”
WBI	“Wiberg Bond Index”
X	halogen atom or related substituent

Publication List

- Wendel, D.; Eisenreich, W.; Jandl, C.; Pöthig, A.; Rieger, B., *Organometallics* **2016**, *35*, 1-4. “Reactivity of an Acyclic Silylsilylene toward Ethylene: Migratory Insertion into the Si–Si Bond”.

- Wendel, D.; Szilvási, T.; Jandl, C.; Inoue, S.; Rieger, B., *J. Am. Chem. Soc.* **2017**, *139*, 9156-9159. “Twist of a Silicon–Silicon Double Bond: Selective *Anti*-Addition of Hydrogen to an Iminodisilene”.

- Wendel, D.; Porzelt, A.; Herz, F. A. D.; Sarkar, D.; Jandl, C.; Inoue, S.; Rieger, B., *J. Am. Chem. Soc.* **2017**, *139*, 8134-8137. “From Si(II) to Si(IV) and Back: Reversible Intramolecular Carbon–Carbon Bond Activation by an Acyclic Iminosilylene”.

- Wendel, D.; Reiter, D.; Porzelt, A.; Altmann, P. J.; Inoue, S.; Rieger, B., *J. Am. Chem. Soc.* **2017**, *139*, 17193-17198. “Silicon and Oxygen’s Bond of Affection: An Acyclic Three-Coordinate Silanone and Its Transformation to an Iminosiloxysilylene”.

- Wendel, D.; Szilvási, T.; Henschel, D.; Altmann P. J.; Jandl, C.; Inoue, S.; Rieger, B., *ready-to-publish*. “Precise Ammonia Activation and Oxygenation by an Iminodisilene”.

Publications beyond the scope of this thesis:

- Sarkar, D.; Wendel, D.; Ahmad, S. U.; Szilvasi, T.; Pothig, A.; Inoue, S., *Dalton Trans.* **2017**, *46*, 16014-16018. “Chalcogen-atom transfer and exchange reactions of NHC-stabilized heavier silaacylium ions”.

Table of Contents

1. Introduction

"Catalysis" – a term once implemented by Berzelius in the early 19th century, has undoubtedly shaped the history of modern chemistry like no other. In industry, it was the development of catalysis that enabled the soaring rise of today's multi-million ton scale chemical processes, that confronted the ever increasing demand of the constantly growing world population and ensured the continued existence of mankind.[1] In the same way, but on a smaller scale, in terms of academic research, laboratory experiments commonly rely heavily on the use of suitable, highly effective catalysts. To quote the German chemist Alwin Mittasch, co-inventor of the world-famous Haber-Bosch process:

"Chemistry without catalysis, would be a sword without a handle, a light without brilliance, a bell without sound."[2]

Alwin Mittasch (1869-1953)

According to estimations, today nearly 85-90% of industrially relevant chemicals require catalysts in at least one stage of their manufacture.[3] Hence, the current catalyst market size was valued at $28 Bn., approximately reaching $40 Bn. by 2022, and generating chemical products with a value that is a hundredfold higher.[4] The supremacy still clearly belongs to heterogeneous systems, where catalyst and reactants are in different phases, but due to the superior chemo- and stereoselectivity, combined with frequently milder reaction conditions, there has been a steadily growing number of homogenously catalyzed processes. Presumably, the first industrially applied catalyst working in solution and containing organometallic intermediates is mercury(II) sulfate, which was used by the WACKER Chemie AG in the 1920s for the production of acetaldehyde from acetylene. Nowadays, its use is receding. The more environmentally friendly "second WACKER process" uses a homogenous palladium(II) dichloride/water mixture and ethylene as feedstock instead. But in general, molecular catalysts are found in several industrially relevant processes such as the cobalt- or rhodium-based "Oxo synthesis" of aldehydes from olefins and carbon monoxide, the rhodium-catalyzed carbonylation of methanol which gives acetic acid ("Monsanto process") or the widely applied catalytic hydrogenation or isomerization reactions of olefins (e.g. "Wilkinson hydrogenation" or "Shell's higher olefins process").[5] All of the mentioned processes involve transition metal complexes as catalytically active species. In most cases, the metals used, such

as platinum, palladium or iridium, are rare and thus inherently expensive. Even the full recovery of the precious catalyst, like in the platinum-based addition curing of silicone elastomers (estimated loss of 5.6 t Pt/year)[6], cannot always be guaranteed. Furthermore, the incomplete removal of toxic, heavy transition metal residues may pose a significant health threat, in particular in applications in the pharmaceutical sector.[7]

As a consequence, recent years have brought forth a new concept that, in addition to the departure from limited fossil fuels and towards "greener" renewable resources, involves the pursuit of alternative catalyst solutions that provide comparable results but are less costly or toxic than transition metals. In this context, in the last decade main group compounds from nearly all groups of the periodic table have emerged as non-toxic, fairly abundant and efficient replacements of conventional *d*-block metals.[7] One nearly forgotten element that humanity will most certainly not run out of in the near future, and whose compounds – if put into the right environment – exhibit a distinct metallic character, is silicon.

2. The Element Silicon and Organosilicon Compounds

The ability to form strong single and multiple bonds with itself and many nonmetal elements of the periodic table – in particular hydrogen, oxygen and nitrogen – makes carbon the undisputed "carrier of life". Carbon-based compounds are found everywhere, from simple hydrocarbons in fossil fuels and chemical products to complex polymeric structures in enzymes or nucleic acids – vital components of all living organisms. However, the importance of carbon to life and the richness of organic chemistry are in strong contrast to carbon's actual abundance in the Earth's crust with just about 0.18%. Its direct heavier congener of group 14, silicon, is far more abundant, accounting for approximately one quarter (27%) of the lithosphere, directly after the most relevant element oxygen (46%).[8] Similarly to carbon, silicon is capable to form bonds with up to four partners, which raises the legitimate question why evolution has not preferred a silicon-based life form.[9] Indeed, organosilicon compounds structurally resemble their lighter analogues, however, their chemical and physical properties differ massively. Silanes, for example, are much more reactive than their alkane counterparts, mainly due to the inverse polarization of the $Si^{\delta+}$–$H^{\delta-}$ bond and the lower Si–Si bond strength.[10] Thus, the simplest compound, silane SiH_4, combusts in air and reacts violently with halogens, totally opposed to the reactivity of methane. In addition, the larger atomic radius of silicon minimizes the effective mixing of s- and p-orbitals and reduces the preference of silicon to form multiple bonds,[11] which has been a key requirement in terms of carbon to access the variety of known organic geometries. It is, therefore, fair to say that the lack of alleged structural diversity and the lower stability of organosilicon compounds clearly impede the use of silicon as hypothetical life source.[12]

Nevertheless, the element silicon has found other ways into our daily lives. Due to its semiconducting properties, silicon is an inherent part of microchip, processor and transistor manufactures. Likewise, the solar cell industry depends heavily on purified silicon for the production of photovoltaic cells. As a result of its high affinity to oxygen, silicon does not occur elementarily, but only covalently bound as quartz or in siliceous minerals. Thus, the industrial preparation of silicon necessarily proceeds by reduction of these silicon-oxygen precursors with coke in an electric arc furnace at 1900 °C. Although this process is highly energy consuming (about 12.5-14 MWh/t)[13], it nowadays accounts for roughly 7 million tons (2016)[14] of crude silicon worldwide. Silicon's oxophilic nature was also reflected in its long

overdue discovery in elemental form, in comparison to other much rarer elements. Initial efforts to prepare elemental silicon were made by Antoine Lavoisier in 1787, who mistakenly considered the semi-metal to be a compound. In 1811, Joseph-Louis Gay-Lussac and Louis Jaques Thénard succeeded in producing elemental, amorphous silicon by reacting silicon tetrafluoride with potassium. The big breakthrough was achieved in 1824 by Jöns Jakob Berzelius in Sweden, who used a similar method to react hexafluorosilicate with elemental potassium and recognized the elemental nature of silicon during purification. It is through his work that silicon owes its name, which is derived from the Latin word *silex* meaning "pebble". Today's metallurgical grade silicon with a purity of 98-99% is directly used as alloying component and deoxidant in the steel industry or as starting material for the production of chlorosilanes. Applications in solar and semiconductor technologies, however, require significantly higher purities of silicon, reaching up to 99.99% or higher. To achieve this, the so called "Siemens process" is most commonly used. Here, the crude silicon is treated with hydrochloric acid to form trichlorosilane, which is purified by distillation and finally reduced with hydrogen to polycrystalline silicon. For monocrystalline semiconductor silicon (>99.99% purity) a second entrenched method is applied, the "Czochralski process", in which a seed crystal is separated from impurities by pulling it under rotation from a polycrystalline silicon melt.[12]

Akin to carbon, silicon compounds have shown a rich variety of industrial applications that are almost indispensable in this day and age. For instance, organofunctional silanes containing two reactive side groups are sold as coupling agents for composite and hybrid materials, while fumed silica, an amorphous SiO_2 powder, is used as thixotropic thickener or reinforcing filler. By far the widest range of applications, however, are covered by the class of polysiloxanes.[15] Due to their excellent thermal and mechanical properties that are attributed to the flexible and highly stable Si–O chains, they are commonly used as flagship-fluids, -elastomers and -resins in applications in the construction, electronic and automotive industry. Furthermore, their outstanding biocompatibility and remarkable hydrophobic character make polysiloxanes convenient solutions for products in the medicine, cosmetic and textile sector.[16] Fairly, this impact and diversity of applications has developed steadily over the years. Polysiloxanes, colloquially referred to as silicones, have originally already been discovered in the early part of the 20th century by the pioneering work of Frederic S. Kipping.[17] In 1901, he targeted the isolation of silicon analogues of ketones containing a Si=O double bond, but due to the strong $Si^{\delta+}-O^{\delta-}$ polarization and a high tendency for head-to-tail polymerization,[18] he ended up with

the unintentional discovery of polysiloxanes, which he accordingly, but misleadingly named "sili-cones". As the following quote illustrates, the enormous potential of this compound class and, in general, the entire organosilicon chemistry remained initially unrecognized.[19]

"We have considered all the known types of organic derivatives of silicon and we see how few are their number in comparison with the purely organic compounds. Since the few which are known are very limited in their reactions, the prospect of any immediate and important advance in this section of chemistry does not seem very hopeful."[19]

Organosilicon pioneer Frederic S. Kipping, 1934, Bakerian Lecture Royal Society

And indeed, Kipping's discovery had not been industrially meaningful until the 1940s, when the chemists R. Müller and E. Rochow independently found a way to prepare the silicone precursor Me_2SiCl_2 in a commercial process.[20] The today well-established "Direct Synthesis" or "Müller-Rochow Process" converts silicon and alkyl halides such as methyl chloride to the corresponding organochlorosilanes. Subsequent hydrolysis results in linear and cyclic oligosiloxanes, which are further elongated by polycondensation or ring opening polymerization to form high-molecular polysiloxanes.[12] Since its discovery, this process has met the ever-increasing demand for silicones, with today's annual worldwide production estimated at several million tones[21] and a market value of roughly $14 Bn. (2017)[22] – numbers that will surely rise together with the not yet fully exploited potential of silicones.

The silicon structures described so far are all four-coordinate, with the silicon atom occurring in the most stable oxidation state +IV. Another, still developing class are organosilicon compounds in lower oxidation states and with reduced coordination numbers. For a long time these were considered to be extremely unstable and synthetically challenging to isolate. Intensive research has changed this situation in recent years and established the chemistry of low-valent silicon compounds as emerging field of research that is still searching for industrial relevance.[23]

3. Low-Valent Silicon Chemistry: An Overview

In knowing the multitude of potential oxidation states of *d*-block metals and their pivotal impact on reactivity and catalytic activity, chemists have been excited for decades to transfer this concept to main group chemistry and stabilize *s*- and *p*-block elements in non-classical oxidations states. Due to the fundamentally smaller number of valence electrons in contrast to transition metals, only a limited number of oxidation states are accessible for main group elements. Furthermore, compounds comprising these elements in such unpreferred electronic environments are basically highly reactive and tend to oligomerize or disproportionate to the respective element and compounds with the element in its most stable oxidation state. To access low-valent structures, sterically encumbered and often heteroatom-based ligands have proven themselves as effective protectors that hamper potential decomposition pathways.

Regarding the element silicon, low-valent by definition implies all oxidation states that deviate from the most favorable and stable +IV, thus ranging from zero to +III. Historically, in particular the similarities and differences to compounds of the lighter homologue carbon have aroused the interest of main group chemists. The journey of stable low-valent silicon compounds began in 1981 with the groundbreaking isolation of the first disilene, a silicon analogue of ubiquitous alkenes, with both silicon atoms in the unusual oxidation state +II ($Mes_2Si{=}SiMes_2$; Mes = C_6H_2-2,4,6-Me_3).[24] This pioneering work by West *et al.* not only helped to revolutionize the mindset of heavier group 14 multiple bonding, but has been the beginning of a success story that has lasted for over 35 years and brought forth a wide spectrum of different silicon compounds in low oxidation states. Nowadays with a vast number of isolable representatives, the disilene compound class has already accomplished the transition from once transient species to functional molecules utilizing the Si=Si motif as linking unit in organic synthesis[25] or as prototype for silicon surfaces in material science[26]. Especially in the last two decades, a plethora of further low-valent silicon compounds with unique electronic properties have been made accessible that, prior to their isolation, had been widely considered as elusive and unstable.[27] For instance, in 2004 Sekiguchi and coworkers reported the successful isolation of a compound containing a Si≡Si triple bond in analogy to the well-established class of alkynes.[28] Later, with the help of external donors (*N*-heterocyclic carbenes (NHCs) or cyclic alkyl(amino)carbenes (*c*AACs)), the zero oxidation state of silicon was also attained in the form of "naked" Si=Si dimer by Robinson *et al.*[29] or separately as

monomeric Si(0) complex in a silylone by Roesky *et al.*[30]. In addition, the class of silyliumylidenes RSi^+ as ionic Si(II) species[31] have as well joined the list of milestones that can be extended almost endlessly. The following chapter, however, shall limit its focus on the description of monomeric, divalent Si(II) species and their dimers.

3.1 Silylenes and Disilenes: Characteristics and Properties

Silylenes are mononuclear, divalent Si(II) compounds with the general molecular formula $R_2Si(II)$, where R^- is a monodentate, σ- or π-coordinating ligand (homo- or heteroleptic) or R_2^{2-} a bidendate chelating ligand. They owe their name to the much more investigated carbon analogues, carbenes, that until today have been applied as useful ligands in all parts of organometallic chemistry due to their excellent σ-donating properties.[23a] Despite the name-giving, silylenes, and in fact all heavier tetrylenes, differ distinctively in their electronic properties from their carbon congeners (Figure 1).

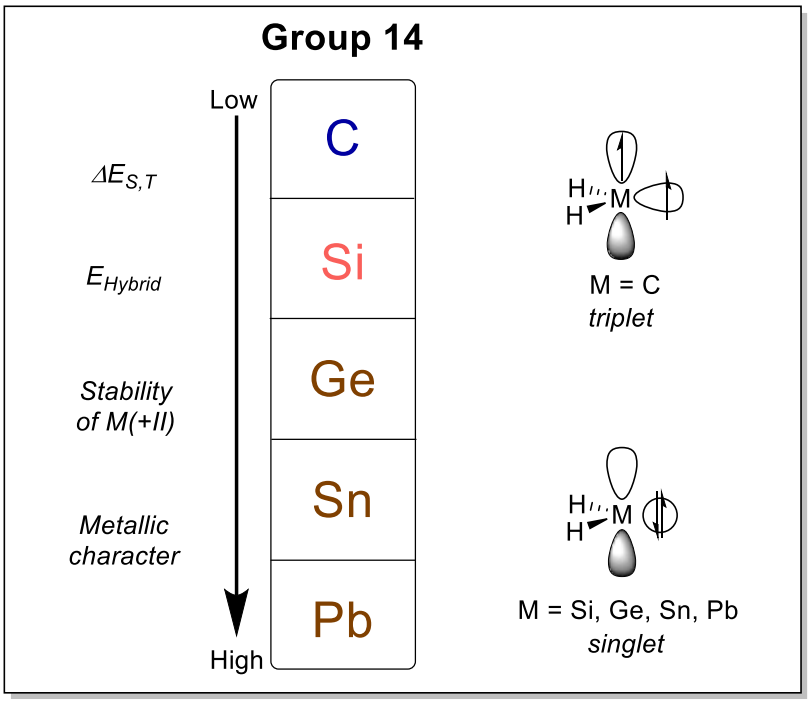

Figure 1. General trends of electronic properties of group 14 elements and schematic representation of the frontier orbitals of tetrylenes.

In general, group 14 elements possess four valence electrons and an electronic configuration of $(ns)^2(np)^2$. However, for divalent carbon species, as in methylene $H_2C(II)$, carbenes mainly favor a triplet ground state due to a negative singlet-triplet splitting ($\Delta E_{S,T}$ = –14 kcal/mol).[32] The resulting diradical has two unpaired electrons with parallel spin in two sets of orbitals. On

the contrary, as the singlet-triplet energy increases down group 14, silylenes and heavier tetrylenes generally possess a singlet ground state (e.g. $H_2Si(II)$; $\Delta E_{S,T}$ = 16.7 kcal/mol).[32] Here the two electrons are located in the lower lying sp^2-character orbital, while the energetically much higher p-orbital remains vacant. A strongly related value is the energy of hybridization (E_{Hybrid}) that rises as well as the group is descended. One reason explaining the low tendency of hybridization of heavier group 14 elements is the higher effective nuclear charge and the reduced overlap between s- and p-orbitals as a result of the increasing energy separation and diverging spatial extension of both orbitals. The filled sp^2-type orbital in silylenes and heavier analogues therefore has a high s-character, while the ligand bonding orbitals instead have a high p-character. The latter is best demonstrated by the continuous decrease of the interligand angle of parent $H_2M(II)$ by going down group 14 (H_2Si 92.7°, $H_2Ge(II)$ 91.5°, $H_2Sn(II)$ 91.1°, $H_2Pb(II)$ 90.5°). Again, the deviating, large bonding angle of methylene ($H_2C(II)$ 134°) reflects its triplet state and the convergence to an ideally linear sp-type (180°) geometry.[32] Another apparent trend in group 14, following the former two, is the increase of stability of oxidation state +II upon descending the *p*-block, with the heaviest element lead even preferring the low oxidation state in its compounds (e.g. $PbCl_2$). This phenomenon goes hand in hand with the already mentioned increase of E_{Hybrid} and the relativistic effect of the "inert pair", which suggests that electrons in valence s-orbitals of heavier group 14 elements are more tightly bound to the nucleus due to the weak shielding of the intervening d-orbitals and therefore need more energy to be ionized than electrons in p-orbitals.[33] This means that, especially for plumbylenes and stannylenes, the s-type lone pair and the +II oxidation state often remains unaffected. This preference toward oxidation state +II and the energetically facile alternation between the higher and the lower oxidation state may also be associated with an emerging metallic character of the tetrylene species, similar to the generally accepted trend of tetrel elements themselves. If, in principle for the lighter tetrylenes, the energy barrier between both states is reduced, then a fine interplay between oxidative addition and reductive elimination of substrates similar to transition metals could be achieved.[34] The propensity of hybridization of carbon gave access to the omnipresent variety of multiple bonded hydrocarbon structures that have shaped main parts of organic chemistry. Regarding the valence bond theory of olefins, it is assumed that a complementary interaction of two triplet carbenes are responsible to form the common sp^2-hybridized, planar C=C bond (Figure 2).[35] For singlet heavier tetrylenes, the interatomic Pauli repulsion of the inner-shell electrons in combination with the repulsion of the filled lone pairs between both fragments prohibits such classical double bond formation.[36] Therefore, until the mid-1970s there was the

tenacious belief, commonly referred to as “double bond rule”, that heavier group 14 elements with a principal quantum number greater than 2 cannot form multiple bonds.[37] The isolation of several group 14 alkene analogues including the already mentioned seminal disilene[1] by West *et al.* eventually disproved this hypothesis.[38] In this context, an adapted bonding model by Carter-Goddard-Malrieu-Trinquier (CGMT) was developed, which rationalized the formation of ditetrelenes by electron donation from one sp^2-type lone pair orbital into a vacant p-orbital of another molecule (and *vice versa*).[39] This distortion then forms a double donor–acceptor type bond with *trans*-pyramidalization at both tetrel centers. Accordingly, the extent of the interaction and the degree of *trans*-bending is largely dictated by the singlet-triplet energy of both tetrylene fragments.[11] Thus, by following this approach a smaller $\Delta E_{S,T}$ gives a more planar, while a larger $\Delta E_{S,T}$ a more bent double bond.[40] One way to influence this element-specific electronic parameter is the choice of ligands that shall be explained exemplarily with silylenes.

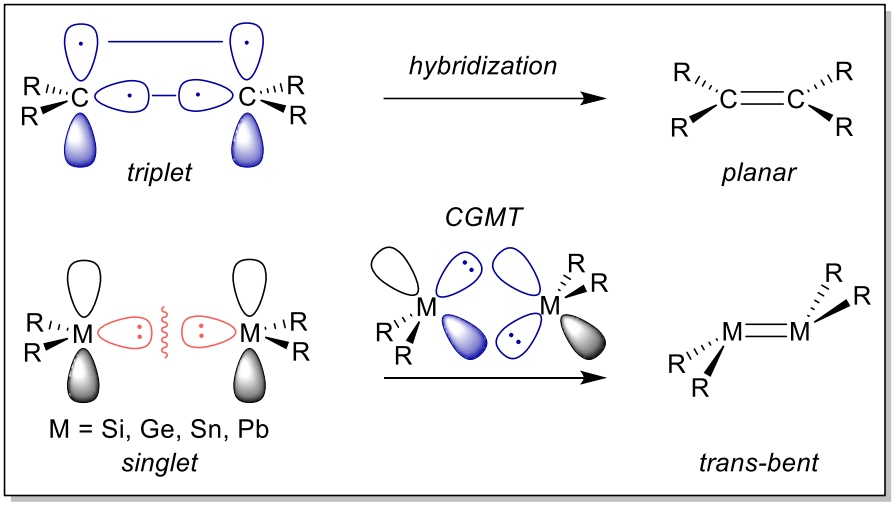

Figure 2. Bonding models for the dimerization of singlet and triplet tetrylene fragments.

Silylenes and all heavier tetrylenes are ambiphilic molecules – they possess both a vacant 3p-orbital generating a highly Lewis acidic silicon center and at the same time a filled Lewis basic lone pair. In total, the six valence electron count deviates from the generally accepted “octet rule” and makes silylenes electron deficient species that rapidly undergo dimerization to form disilenes, or react with a variety of substrates typically in form of insertions into E-E (e.g. O–H, N–H, C–X, X = halogen) single bonds or cycloadditions with unsaturated molecules (e.g. C=C, C≡C, C=O).[32] Due to a weak π-orbital overlap and a small HOMO-LUMO gap (≈ 3 eV),[41] disilenes themselves exhibit a reactive Si=Si bond that is susceptible to oligomerization or polymerization reactions. Therefore, to isolate both

otherwise elusive species, the protection and stabilization of the low-valent silicon center is absolutely essential. One reliable method has been the utilization of heteroatom-based ligands that thermodynamically influence the electronic properties of the silylene center (Figure 3).[32] It is assumed that the introduction of electron-withdrawing substituents such as nitrogen, sulfur or phosphorus inductively stabilize the non-bonding orbital (HOMO) at the silicon center by increasing its s-character and lowering its energy, thereby favoring the singlet state. Furthermore, in terms of mesomeric stabilization, the lone pair of the π-donor ligand can donate electrons into the empty 3p-orbital (LUMO), leading to a reduction of the electrophilicity and a larger HOMO-LUMO gap (and a simultaneously higher $\Delta E_{S,T}$).[36]

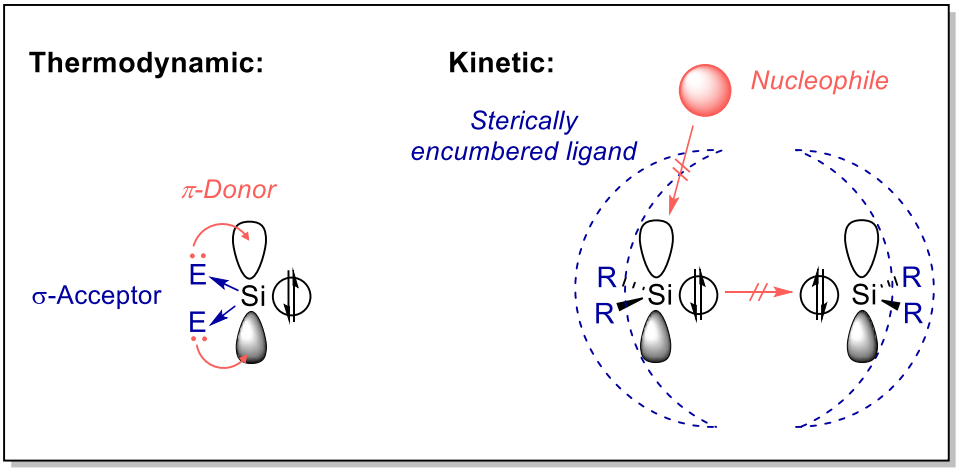

Figure 3. Thermodynamic stabilization of silylenes by π-donor and σ-acceptor ligands (e.g. E = NR_2, SR, PR_2) and illustration of kinetic shielding of the Si(II) center by sterically demanding substituents.

In strong contrast, electropositive ligands such as silyl and boryl groups or alkali metals without any π-donor effect inductively decrease the orbital separation and promote the reactive triplet state.[42] These species tend to instantly dimerize, but in literature first occurrences of silylenes ((t-$Bu_3Si)_2$Si(II) and (t-Bu_3Si)MSi(II); M = Li, Na, K) in the triplet state were observed *via* EPR experiments in frozen hydrocarbon matrices.[43] The second key stabilization method is the use of sterically bulky ligands that kinetically prevent dimerization or oligomerization and protect the electropositive Si(II) center from attacks by nucleophiles. For this purpose a huge number of different ligands (e.g. silyl, alkyl, aryl) with adjustable steric bulk have been developed over the years. However, it is noteworthy, that in principle, counteracting to the stabilization effect, an exaggerated steric encumbrance increases the repulsion of the ligands, which leads to a widening of the bonding angle and thereupon a favored triplet state.[42, 44]

3.2 Historic Milestones in Silylene Chemistry

The last couple of decades have seen a burst of reported isolable silylenes with plenty of exotic structures in some cases even containing more than one silylene function ("bis(silylenes)" for example)[45]. However, the majority of these reports involve only three- or four-coordinate silylenes in which the imbalanced electrophilicity of the Si(II) center was additionally tamed by external donor molecules.[46] This chapter will instead give a historic overview of important milestones and developments regarding the still limited number of original two-coordinate silylenes.

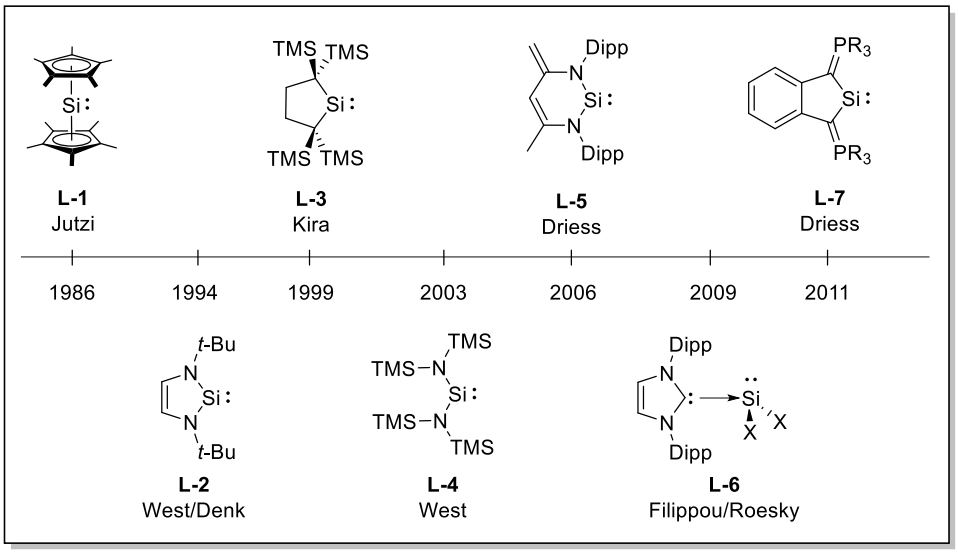

Figure 4. Early stages and essential historic landmarks of silylene chemistry; only monomeric two-coordinate Si(II) compounds (except structures **L-1** and **L-6**) are considered (X = Cl, Br, I, R = Ph, *m*-Tol).

Apart from the discovery of the first disilene by West *et al.*, 1981 was a year of success for the chemistry of main group and in particular low-valent silicon compounds. The origin of today's flourishing silylene chemistry dates back to the 1960s and the pioneering studies by Goldstein and coworkers.[47] In their experiments, the reduction of dimethyldichlorosilane at 260 °C with sodium-potassium vapor in the presence of trimethylsilane gave pentamethyldisilane, whose formation was attributed to the insertion of a short-lived dimethylsilylene, $Me_2Si(II)$, species into the Si–H bond of the trapping reagent. In the following years, numerous photochemical and thermal experiments were performed in order to identify elusive silylene species. Until the 1980s, however, silylenes could only be isolated in hydrocarbon matrices or argon atmosphere, at temperatures of 77 K or lower. The first major breakthrough was achieved by Jutzi *et al.* in 1986 with the synthesis of the first monomeric Si(II) compound, decamethylsilicocene **L-1**, stable under ambient conditions

(Figure 4).[48] The chemistry of this extraordinary compound has been extensively studied in recent years, but due to its hyper coordination (η^{10}) and its resulting highly nucleophilic silicon site, **L-1** cannot be, according to the definition, considered as a true silylene.[49] Therefore, with the discovery of the first stable *N*-heterocyclic carbene (NHC) by Arduengo *et al.* in 1991, silicon still remained as the only element of group 14 with no monomeric, room temperature stable divalent compound. In 1994, the group around West and Denk finally isolated silylene **L-2**, the first member of a nowadays large class of *N*-heterocyclic silylenes (NHSi).[50] **L-2** was prepared by reduction of the corresponding dichlorosilane with elemental potassium at elevated temperatures to yield a colorless, crystalline substance with surprising thermal stability up to 220 °C. As described in the previous chapter, the stabilization of the Si(II) species was achieved on an electronic level by two π-donating adjacent amino groups, which push electron density to the empty 3p-orbital of silicon, and by steric shielding with the help of two voluminous *tert*-butyl groups. Shortly after, the same group isolated the structural analogue of **L-2** with a saturated backbone. In the following years, based on this common mode of stabilization, a handful of NHSis with congeneric five-membered ring systems and different wing-tips have been reported.[45a, 51] Excitingly, in 1999 Kira *et al.* set a milestone with the isolation of carbocyclic bis(alkyl)silylene **L-3**. Hereby, they illustrated that silylenes did not necessarily need a π-donor ligand and can be stabilized solely by steric shielding of the central Si(II) with four large $SiMe_3$ groups, although some electronic contribution of the conjugation of the C–Si σ-bonds and the Si_{3p}-orbital was proposed.[52] However, the silylene turned out to only be persistent up to 0 °C and decomposed above this temperature *via* an intramolecular 1,2-silyl migration to the corresponding cyclic silene (Si=C). Nevertheless, silylene **L-3** possesses a highly electrophilic silicon site, which is directly reflected by a strongly downfield shifted ^{29}Si NMR resonance at 567.4 ppm compared to those of classical, rather nucleophilic NHSis (δ = 78-199 ppm)[32] and even approaches the calculated values of transient silylenes H_2Si (771.8 ppm) and Me_2Si (739.6 ppm). A few years later, in 2003, the group of West followed a new, quite challenging idea to stabilize a Si(II) moiety in a more flexible acyclic framework. Their reported acyclic bis(amino)silylene **L-4** was formed by reduction of the respective dibromosilane $(TMS_2N)_2SiBr_2$ with potassium graphite (KC_8), but unfortunately it could not be characterized by X-ray analysis, presumably due to the lack of kinetic stabilization (persistent for approx. 12 h at –20 °C).[53] In 2006, Driess and coworkers revitalized the class of NHSis, by isolation of an akin *N*-heterocyclic silylene **L-5** imbedded in a conjugated six-membered heterofulvene ring.[54] Interestingly, beside the standard Si(II) reaction site, compound **5** features an additional ambivalent reactivity with the exocyclic

methylene backbone prone to electrophilic attacks.[55] A brand-new strategy was developed in 2009, when Roesky *et al.* succeeded in synthesizing the NHC-stabilized dichlorosilylene **L-6**, which is accessible by reductive dehydrochlorination of $HSiCl_3$ with two equivalents of NHC.[56] Regarding the list of two-coordinate silylenes, this three-coordinate structure obviously falls out of line. This achievement, however, is still worth mentioning, as the general synthetic route dispensing the use of strong reducing agents, has become a viable method to access several more base-stabilized structures as implied at the beginning of this chapter. Moreover, silylene **L-6** is the first direct Si(II) precursor for salt metathesis reactions and a model compound of transient dichlorosilylene, an extremely reactive intermediate in the industrial preparation of elemental silicon. In this context, it should be noted that, with a similar approach, the stable NHC-coordinated dibromo- and diiodosilylenes were isolated by the group of Filippou.[57]

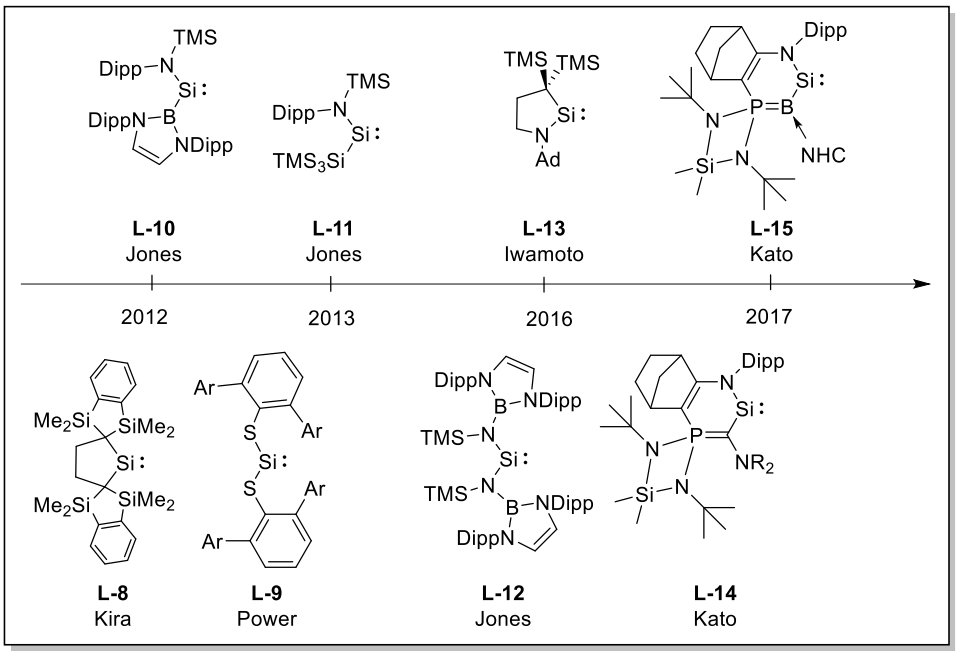

Figure 5. Recent milestones in the timeline of monomeric, two-coordinate silylenes (Ar = aryl, R = *i*-Pr, cHex, NHC = I*i*-Pr_2Me_2).

In 2009, the group of Driess successfully developed and implemented a remarkable carbon-based donor ligand in their aromatic ylide-stabilized silylene **L-7**.[58] In contrast to related semi-stable carbocyclic silyene **L-3**, the increased electron density at the carbon center, due to the zwitterionic phosphonium ylidic $R_3P^+–C^-$ character, provided the fragment with additional π-donor properties. In comparison to nitrogen containing ligands, the poorer σ-acceptor strength due to the smaller electronegativity of carbon and the experimentally determined moderate ^{29}Si NMR shift of **L-7** at 213.3 ppm, however, allow the conclusion,

that the electronic stabilization and, therefore, the reactivity of **L-7** shall be classified in between the one of NHSis and carbocyclic silylene **L-3**. Shortly after, Kira *et al.* reported a third carbocyclic silylene **L-8** by modifying the primal ligand system of **L-3** with spirocyclic 1,3-disilaindane functions (Figure 5).[59] This sterical adjustment turned out to be essential to avoid the prior observed 1,3-silyl migration and stabilize the silylene at ambient conditions. Furthermore, it was impressively demonstrated that the flexible steric bulkiness of **L-8** allows this compound to equilibrate in solution with its isolable dimer, the corresponding disilene, which is the first observation of such a dynamic equilibrium.

So far, the Si(II) center of all reported compounds, with the exception of semi-stable bis(amino)silylene **L-4**, were stabilized by the inclusion in cyclic systems or by an increased coordination number. However, to truly understand the intrinsic nature of silylenes, the goal to stabilize an acyclic silylene has been desperately targeted for decades, until finally in 2012 two different approaches solved this task (see structures **L-9** to **L-12**). Based on the relevance of this milestone to this thesis, these results are separately addressed and discussed in detail in the following chapter. For the sake of completeness, recently, Iwamoto *et al.* reported a two-coordinate cyclic alkyl(amino)silylene **L-13**, in analogy to the well-known carbon derivatives (*c*AACs).[60] By combining the electronic properties of both ligand systems, cAASi **L-13** exhibits an improved thermal stability (two days at 150 °C) compared to bis(alkyl)silylenes **L-3** and **L-8**, while still maintaining high levels of reactivity which is in accordance with, the generally, rather low-field shifted ^{29}Si NMR signal (274.7 ppm). This silylene, for instance, readily undergoes cycloadditions with alkynes, Si–H insertions and even intermolecular benzylic C–H bond activations at elevated temperatures. Very recently, two more two-coordinate cyclic silylenes **L-14** and **L-15** were isolated by the groups of Baceiredo and Kato.[61] Here, the established amino group was combined with another π-donating phosphonium or bora-ylide ligand, respectively. In spite of this second donor, the ^{29}Si NMR shifts of **L-14** (R = *i*-Pr, 202.2 ppm) and **L-15** (295.5 ppm) point to a similar electronic behavior as cAASi **L-13** with just one π-donor. In terms of reactivity, and parallel to the results of this work, both structures have emerged as ideal precursors to fulfill "Kipping's" long-term dream of isolation of room temperature stable, three-coordinate silanones containing Si=O double bonds.[62] Despite all mentioned achievements, the structural diversity of two-coordinate silylenes is still very limited compared to the large family of carbenes and, without a doubt, this field needs further research to isolate silylene structures in novel, precisely designed chemical environments.

3.3 Acyclic Silylenes as Transition Metal Mimics

In 2012, the groups of Jones and Aldridge[63] and, separately but almost simultaneously, the group of Power[64] set a landmark discovery with the isolation of two-coordinate acyclic silylenes stable at ambient temperatures (Figure 6). Thereby, they finally put an end to the long time belief that acyclic silylenes only exist as elusive, short-lived species observable in photolytic trapping experiments. To put it into historic context, these findings shall, of course, be seen as continuation of the initial work of West *et al.* and their reported semi-stable acyclic bis(bis(trimethylsilyl)amino)silylene **L-4**.[53] One key advantage of acyclic silylene structures, in comparison to Si(II) centers integrated in a rigid cyclic framework, is their much larger flexibility that facilitates coordination and oxidative addition of substrates – an essential criterion for selective bond activation.[65] Moreover, due to the more obtuse bonding angle at the silicon center in combination with energetically narrow frontier orbital separations (small HOMO-LUMO gap and $\Delta E_{S,T}$), it is generally believed that acyclic silylenes are promising candidates not only to give access to a silylene with a triplet ground state[43] (ideal linear geometry), but to open the door to a potentially increased "transition metal-like" reactivity, creating new opportunities for small molecule activation and even main group catalysis. In this context, one goal that still remains a "holy grail" in low-valent silicon chemistry is the successful splitting of the C–H bond of methane.[46a]

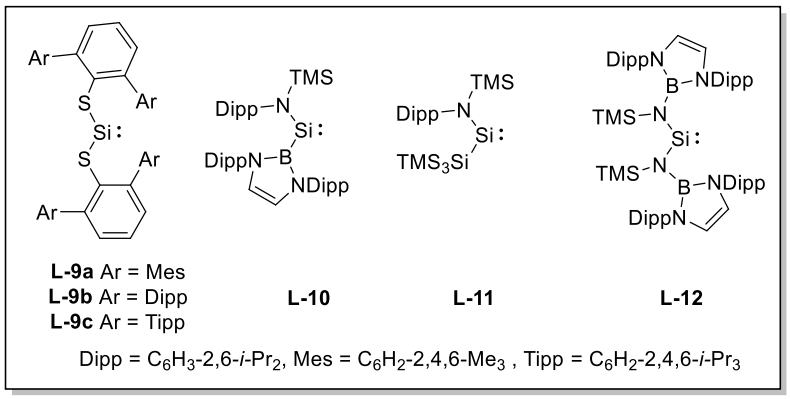

	L-9a	L-10	L-11	L-12
HOMO-LUMO [eV]	4.26	2.04	1.99	2.55
$\Delta E_{S,T}$ [kJ/mol]	-	103.9	103.7	158.3
R–Si–R [°]	90.5	109.7	116.9	110.9
^{29}Si NMR [ppm]	285.5	439.7	438.2/467.4	204.6

Figure 6. Structures of reported room temperature stable, two-coordinate acyclic silylenes **L-9-12** and summary of HOMO-LUMO gaps, singlet-triplet energies ($\Delta E_{S,T}$), bonding angles and ^{29}Si NMR data of the central silicon atom of all reported compounds.

In Powers' synthetic approach[64], he and his group reported the successful reduction of the precursor $Br_2Si(S(m\text{-terphenyl}))_2$ with Jones' reducing complex (Mg(I) dimer) to give acyclic bis(arylthiolato)silylene **L-9a** as colorless crystals in moderate yields 51%. The ^{29}Si NMR shift of the central silicon atom at 285.5 ppm is low-field shifted in comparison to those of classical NHSis (δ = 78-199 ppm)[32] or semi-stable acyclic bis(amino)silylene **L-4** (δ = 223.9 ppm)[53], indicating less π-donation of the sulfur based ligands into the vacant Si_{3p}-orbital. However, their structure proved to be surprisingly stable up to 146 °C, thereby reflecting not only sufficient kinetic stabilization, but also thermodynamic shielding by both flanking arylthiolato ligands. As mentioned before, the bonding angle at the Si(II) center is one decisive parameter to evaluate the electronics and reactivity of silylenes. The S–Si–S angle of **L-9a** is extremely acute (90.5°) and in fact comparable with cyclic NHSi **L-2** (N–Si–N 88.6°)[66]. Power and coworkers later isolated two analogous structures with more sterically demanding ligands **L-9b** (Ar = Dipp) and **L-9c** (Ar = Tipp).[67] Contrary to the normal steric expectations that would presume a widening of the bond angle, both structures have even narrower interligand angles (**L-9b** 85.1°, **L-9c** 84.8°). In-depth DFT calculations and further experimental data of other group 14 tetrylenes indicated, that this phenomenon is best explained by increasing London dispersion effects between the C–H moieties of the bulky terphenyl substituents.[67-68] The second parameter that is assumed to be strongly connected to the size of the bonding angle, but as well to the nature of ligand, is the HOMO-LUMO gap and consequently the singlet-triplet gap ($\Delta E_{S,T}$).[69] For silylene **L-9a**, the determined acute angle in combination with the good σ-acceptor and moderate π-donor qualities of the sulfur ligand afforded a calculated HOMO-LUMO gap of 4.26 eV. Regarding selective small molecule activation, the splitting of highly apolar and inert dihydrogen is often considered as prime example for a pronounced reactivity of main group compounds mimicking typical reactions of transition metal complexes.[70] Bis(thiolato)silylene **L-9a**, however, cannot activate H_2 at ambient conditions, most likely as a result of the wider frontier orbital separation. Still, silylene **L-9a** has shown to cleave the more polar bond of MeI and excitingly both compounds **L-9a** and **L-9b** are capable to activate ethylene by forming a unique dissociation equilibrium with the respective silacyclopropane ring (silirane) **L-16a** and **L-16b** (Scheme 2).[71] In terms of potential main group catalysis, this reversibility, where oxidative addition and reductive elimination alternate with each other, can be considered as foundation for a catalytic cycle. Power *et al.* could later demonstrate that, similarly, alkynes such as phenylacetylene and diphenylacetylene can quantitatively be bound in silacyclopropene (silirene) rings.[72]

In contrast to silylene **L-9** by Power *et al.*, the groups of Jones and Aldridge relied on the established π-donor strength of one amino group (DippNTMS) in their silylene design, but intentionally implemented an electropositive σ-donating boryl **L-10** and later also a silyl ligand **L-11** that effectively reduces the HOMO-LUMO gap and $\Delta E_{S,T}$ as described in Chapter 3.1.[63, 73] Such ligand combination ensures that, on the one hand, the Si(II) center is effectually stabilized, but on the other hand the original, untamed Lewis acidity of transient silylenes is largely preserved. This effect is best seen through the ^{29}Si NMR shifts of **L-10** (439.7 ppm)[63] and **L-11** (two conformers, 438.2/467.4 ppm)[73], which are extremely low-field shifted in comparison to those of Powers's silylene **L-9a** (285.5 ppm)[64] and even approach the one of cyclic bis(alkyl)silylene **L-3** (567.4 ppm)[52] without any π-donor stabilization. From a synthetic perspective, both compounds were prepared from a single-step, one-pot reaction of the aminotribromosilane DippNTMSSiBr$_3$ with two equivalents of lithium boryl reagent or potassium hypersilanide, respectively (Scheme 1A).

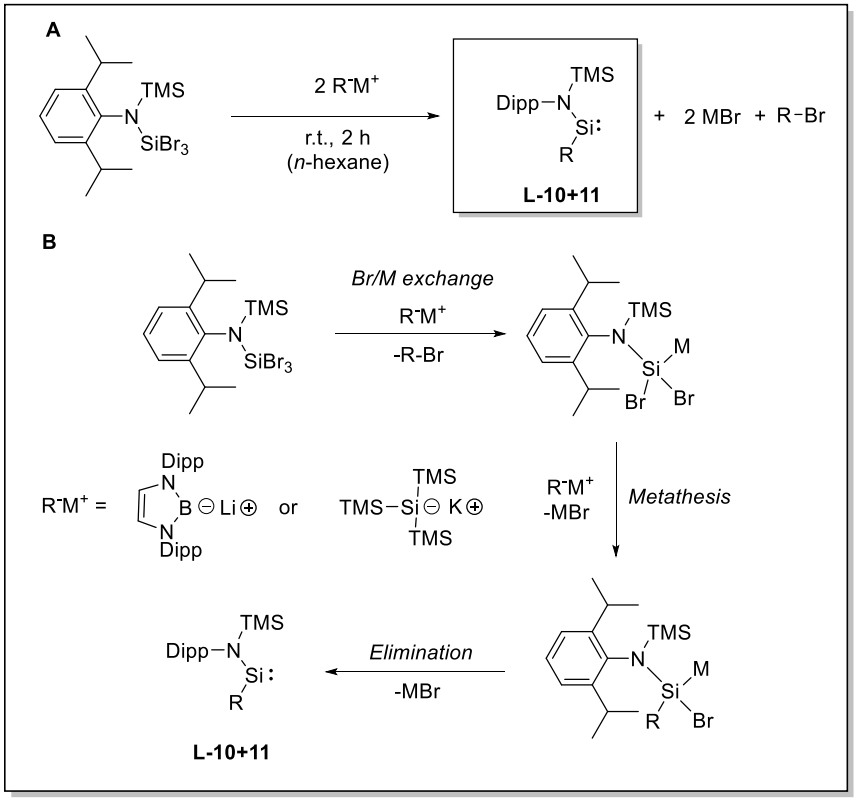

Scheme 1: A) Synthesis route of acyclic amino(boryl) **L-10** and amino(silyl)silylene **L-11**. B) Proposed mechanism for the one-pot formation of both silylenes (R^-M^+ = $(thf)_2LiB(NDippCH)_2$ or $(thf)_2KSiTMS_3$).

In this elegant route the alkali salts R^-M^+ act not only as reductants, but simultaneously as nucleophiles so that the anion is incorporated into the ligand framework. Jones and Aldridge *et al.* proposed a mechanism where initially a metal-halogen exchange on DippNTMSSiBr$_3$

affords an intermediary bromosilylenoid and liberates the respective boryl- or silylbromide as side product (Scheme 1B). In the next step, the second equivalent of main group anion instantly attacks the silicon center in a salt metathesis to give another silylenoid species that finally eliminates the respective alkali bromide salt to yield acyclic silylenes **L-10** and **L-11**. Both compounds were separated from inorganic residues by extraction and filtration with *n*-hexane, but due to the similar solubility as the boryl- or silylbromide co-product, pure isolation and up-scaling turned out to be quite challenging (yield: **L-10** 39% (only NMR scale ≈ 20-30 mg, still 12% $BrB(NDippCH)_2$ impurity); **L-11** 51% (≈ 60-70 mg scale, only traces of $BrSiTMS_3$)).[73] In contrast to bisthiolato silylenes **L-9**, the crystal data of both silylenes feature a more obtuse interligand angle (**L-10** N–Si–B 109.7°, **L-11** N–Si–Si 116.9°), illustrating a much higher triplet silylene character that is directly manifested in a narrower HOMO-LUMO gap (around 2 eV) and $\Delta E_{S,T}$ (approx. 100 kJ/mol). Still, both silylenes are thermally robust and stable as solids up to 130-140 °C for a short period of time. Excitingly, in solution (C_6D_6) and already at 50-80 °C, they slowly (several days) undergo a highly selective, intramolecular C–H bond activation with the ancillary ligand to form silacycles **L-17** and **L-18** – a reactivity pattern that is reminiscent of the well-investigated C–H bond activation by transition metal complexes.[74] Furthermore, due to their precisely adjusted electronic properties,[75] both compounds, as first silylenes, have been able to successfully activate dihydrogen under mild conditions (r.t. or even 0 °C, 1 bar, between 30 min to 2.5 hours) to give the monosilanes **L-19** and **L-20**.[63, 73]

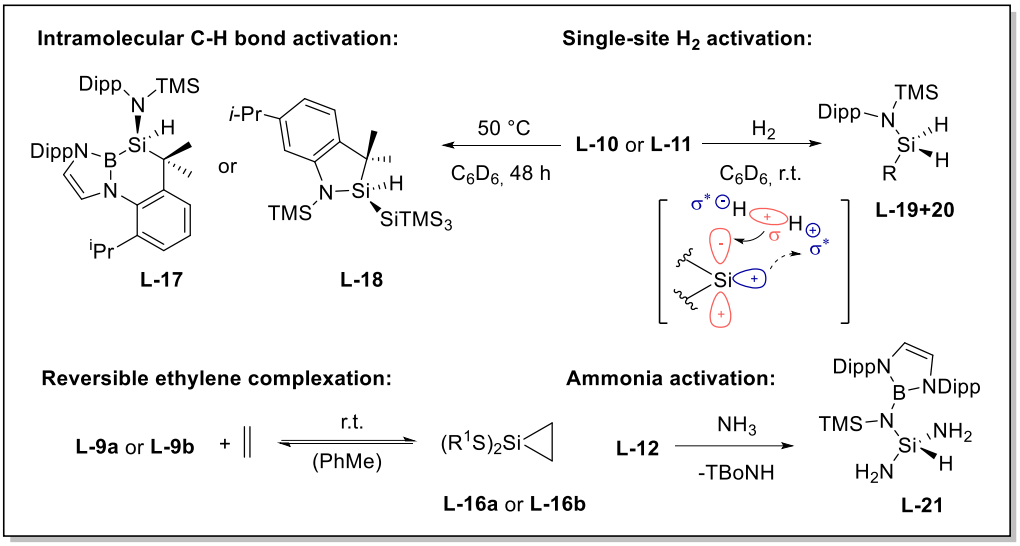

Scheme 2: First promising results of reactivity studies with room temperature stable acyclic silylenes **L-9-12** (R = $B(NDippCH)_2$ or $SiTMS_3$, R^1 = *m*-terphenyl (Ar = Mes, Dipp), TBon = $[B(NDippCH)_2]NTMS$).

Theoretical calculations were carried out in order to explain the mild addition of H_2 to amino(boryl)silylene **L-10**. It has been shown that this activation is distinguished by a moderate energy barrier of 97.2 kJ/mol, that is much lower compared to those of computed bis(amino)silylenes (e.g. acyclic $Si(NH_2)_2$ 190.0 kJ/mol or cyclic $Si(NHCH)_2$) 277.8 kJ/mol)[73, 75], thus illustrating the necessity of a σ-donor ligand to selectively cleave strong, low polarity E–E bonds. From a mechanistic perspective, a transition state was located that represents a side-on approach of the H_2 molecule perpendicular to the N–Si–B plane, with an electron donation from the σ-bond of H_2 (HOMO) into the Si_{3p} orbital (LUMO) of the highly electrophilic Si(II) center. Thereby, the conclusion was drawn that the H_2 splitting by silylenes is distinguishable from the proposed nucleophilic approach of related acyclic and cyclic alkyl(amino)carbenes (*a*AAC and *c*AAC), proposed by Betrand *et al.*[76]. This rather resembles the classical behavior of transition metal complexes with a similar donation of electron density from the filled H_2 frontier orbital into a vacant metal d-orbital.[70a] In total, both the C–H and H–H bond activation are, indeed, the first proofs of the promising "transition metal-like" reactivity of acyclic silylenes that, paired with their potential to even achieve catalytic transformations, have been the stimulation for global on-going investigations[77] and, in particular, the development of this thesis.

Parallel to this work, a fourth room temperature stable acyclic bis(amino)silylene **L-12** was reported by Jones *et al.* (Figure 6).[78] By isolating the silicon analogue of acyclic bis(amino)tetrylenes, their findings eventually completed the long search for such compounds that originated more than 40 years ago with the pioneering work of Lappert *et al.*[79] (Ge, Sn, Pb in 1974) and later Alder *et al.*[80] (C in 1996). In their silylene, Jones *et al.* implemented the boryl fragment, previously employed as independent substituent in **L-10**, into a novel amine ligand system (TBoN = $[B(NDippCH)_2]NTMS$).[78] As stated, the primal idea suggested that a potential N–B π-backbonding could reduce the degree of N–Si(II) electron donation and thereby enhance the electrophilicity of the silylene center. The crystal data, however, mostly excluded this hypothesis due to the presence of almost orthogonal, planar boryl fragments relative to the Si_2NB least square planes. For the preparation of **L-12** an elegant non-reductive pathway was chosen, in which the lithiated ligand Li[TBoN] was converted with Roesky's NHC-stabilized Si(II) dichloride **L-6** in a salt metathesis reaction. To separate the silylene species from liberated NHC (IPr), the reaction mixture was treated either with $SiBr_4$ or CO_2 (surprisingly neither of which react with **L-12**), which led to the instant precipitation of poorly soluble $[IPrSiBr_3]Br$ or $IPr{\cdot}CO_2$ adduct respectively, and gave bis(amino)silylene **L-12**

in 51% yield.[78] The silylene is thermally stable (m.p. 152-160 °C) and shows no sign of decomposition in hydrocarbon solutions even at 60 °C. The ^{29}Si NMR shift of **L-12** at 204.6 ppm is similar to the one of related bis(amino)silylene **L-4** (223.9 ppm)[53] and reflects the strong π-donation of both amino groups compared to bis(thiolato) silylene **L-9a** (285.5 ppm)[64]. The interligand N–Si–N angle (110.9°) turned out to be quite obtuse, similar to those of **L-12** and **L-11**, but nevertheless much larger than the one of **L-9a**. Likewise, the respective calculated HOMO-LUMO gap (2.55 eV) and $\Delta E_{S,T}$ (158.3 kJ/mol) of **L-12** joins the trend, that a reactivity is expected in between the highly reactive class of silylene **L-10** and **L-11** and the moderate one of **L-9**. This hypothesis was experimentally proven by the lack of reactivity of **L-12** towards molecular hydrogen, similarly to **L-9a**. However, with ammonia a rarely known N–H bond activation by a silylene was discovered.[81] Here, triaminosilane **L-21** was isolated, which was presumed to be formed *via* a σ-bond metathesis of **L-12** and NH_3 to split off protonated TBoNH and give a new, transient bis(amino)silylene TBoN(NH_2)Si(II), that subsequently oxidatively adds another NH_3 molecule.[78] The proposed σ-bond metathesis, that traditionally poses one elemental step in many lanthanide catalyzed transformations, re-emphasizes the huge potential of acyclic silylenes to mimic typical reactions of transition metals. A complete catalytic cycle will, hopefully, be enlightened in the near future.

3.4 *N*-Heterocyclic Iminato Ligand for Low-Valent Main Group Compounds

The previous chapters illustrated the importance of bulky heteroatom (e.g. N, S, C=P) π-donor ligands to effectively compensate the electron-deficiency of sub-valent silicon compounds. As seen in the reported silylene structures (e.g. NHSi **L-2** or bis(amino)silylene **L-12**), nitrogen-containing ligands such as amines R_2N-Si(II) have successfully enforced their way into this field. However, the class of imidazolin-2-imines **A**, also denoted as *N*-heterocyclic imines (NHIs) (Scheme 3A), possess a potent electron pair on the exocyclic nitrogen atom as well, that can readily be shared with an electron-poor main group element. Beside this metalla-2-aza-allene character **A'**, the positive charge can further be delocalized in the imidazoline ring system, as seen in the metalimide form **A''**. This additional electronic contribution may be regarded as key advantage of NHIs over amine ligands and is often associated with a short M–N bond length, an elongation of the $C–N_{imino}$ distance and a widening of the C–N–M angle toward the ideal 180° of an allene-type structure. In addition to their excellent 2π- and even 4π-donor qualities, derivatization of the imidazoline wingtips enables the facile adjustment of the steric demand of NHIs; a key requirement to individually control the magnitude of kinetic stabilization.[82]

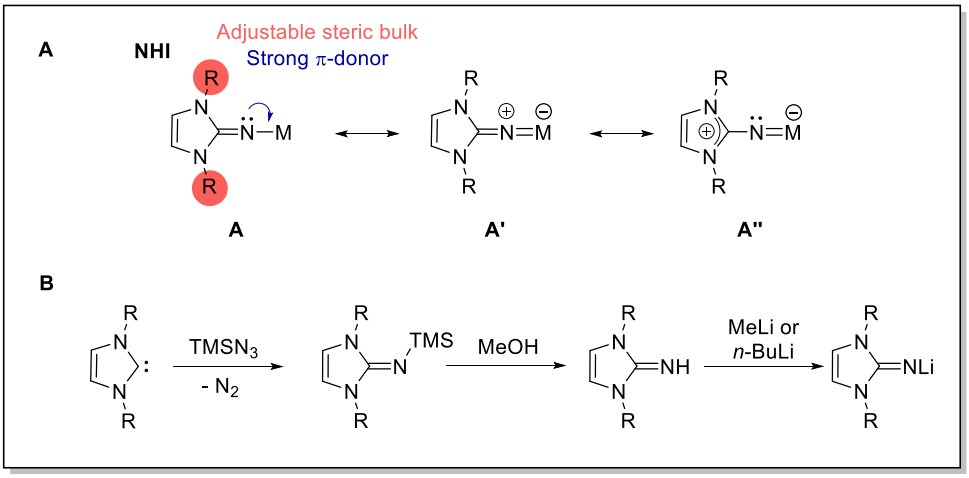

Scheme 3. A) Selected resonance structures of a model NHI-metal (M = metal, R = alkyl, aryl) complex. B) General synthesis of imidazolin-2-imines including desilylation and deprotonation to the lithiated NHI ligand.

Despite these promising characteristics, the utilization of *N*-heterocyclic imines as ligands in low-valent main group chemistry is still in its infancy. Nevertheless, enormous progress has been made in recent years to give rise to hope for a widespread application in this field.[82a] The NHI ligand system was first introduced by Kuhn and coworkers more than 20 years ago[83], but

it took until the year 2004 and great efforts by Tamm *et al.* to establish a simple and high-yielding method for the convenient bulk-scale synthesis of imidazolin-2-imines (Scheme 3B).[84] In general, the trimethylsilyl substituted ligand NHISiMe$_3$, which can directly be used as transmetalation reagent, is prepared by a Staudinger-type reaction with Me_3SiN_3 under elimination of dinitrogen starting from the respective readily available and easy modifiable NHC.[85] Furthermore, desilylation with methanol leads to the free, protonated ligand NHIH, which can simply be converted into its lithium salt NHILi using organolithium reagents (MeLi or *n*-BuLi).[86] The exocyclic nitrogen atom in its anionic imido form is highly nucleophilic and eligible to undergo salt metathesis reactions with metal halides. Following this straight-forward pathway, a plethora of transition metal complexes using NHIs as ancillary ligands have been reported to date, that found diverse application in homogenous catalysis such as in olefin polymerization or alkyne metathesis.[82b, 82c]

The breakthrough in main group chemistry, however, has been achieved just within the last decade, when Bertrand *et al.* utilized the potential of NHIs to stabilize highly reactive species such as a phosphorous-centered radical[87], a radical cation[88] or a phosphinonitrene[89]. Since then, the number of reported NHI-containing pnictogen compounds steadily increased[90], but also for group 13 elements and the chemistry of boron and aluminum compounds[91], NHIs helped to stabilize otherwise elusive species such as B=S[92] or Al=Te[93] double bonds. Regarding group 14, the area of NHI-stabilized low-valent heavier tetrel compounds has mainly been shaped in recent years by Inoue and coworkers.[82a, 94] In this context, his group reported the synthesis of divalent, mixed amino-imino tetrylenes of germanium **L-22a**[95] and tin **L-22b**[96] (Figure 7) by selective deamination of the respective low-valent metal precursor $(Me_3Si)_2N)_2E$(II) (E = Ge, Sn) with one equivalent of IPrNH (IPrN = 1,3-bis(2,6-di*iso*-propylphenyl)imidazolin-2-iminato). Interestingly, treatment of both compounds with tris(pentafluorophenyl)borane (BCF) led to the respective cyclic germanium(II) **L-23a** and tin(II) monocations **L-23b** *via* Lewis acid mediated methyl group abstraction and ring-closing. The crystallographic and theoretical data suggested a distinct metallyliumylidene character with an intramolecular coordination of the N_{imino} atom to the cationic tetrel center. However, a delocalization of the positive charge across the adjacent imidazoline ring was discussed as well. Both isolated compounds thereby represent prime examples for the suitability of NHIs to effectively stabilize highly electrophilic cationic main group species. Inoue *et al.* showed further, that treatment of amino(imino)germylene **L-22a** with $BF_3{\cdot}OEt_2$ afforded bis(imino)germylene-germyliumylidene **L-24**, possessing both a two-coordinate

germylene and a three-coordinate germyliumylidene moiety combined in a single molecule.[97] Here, DFT calculations indicated that the formation of **L-24** proceeds *via* an intermediary four-membered fluorogermylene dimer, which rapidly loses a fluoride ligand to boron trifluoride to afford the monocation. Although the isolation of this intermediate was not reported, a similar bridged $N_2Sn(II)$ dimer **L-25a** was isolated in the reaction of the respective stannylene **L-22b** with azido trimethylsilane.[96] Interestingly, the product was proven to be in equilibrium in solution with its monomeric stannylene form. In this connection, further substituted iminostannylene dimers with halide (R = Cl **L-25b**, Br **L-25c**) and cyclopentadienyl ligands **L-25d** have been made accessible.[98]

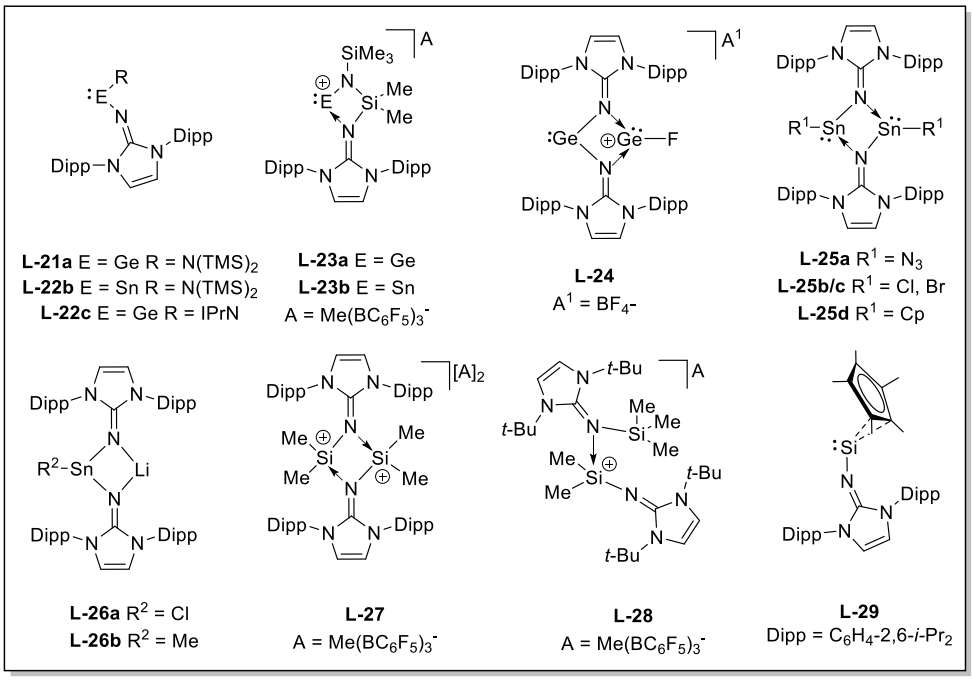

Figure 7. Selected examples of reported NHI-stabilized group 14 compounds (Si, Ge and Sn).

Moreover, Inoue *et al.* could prove that the structural motif of a four-membered bisimino ring system occurred, when IPrNLi was treated with 0.5 equivalents of $Sn(II)Cl_2$·(1,4-dioxane). This pathway did not lead to the expected bis(imino)stannylene $IPrN_2Sn(II)$ *via* salt metathesis, but formed a rarely found tin analogue of a carbenoid **L-26a**.[99] The chlorostannylenoid has unique ambiphilic properties; it possesses both a nucleophilic character to oxidatively activate I_2 or MeI, but also shows distinct electrophilicity to form for instance product **L-26b** with MeLi. Regarding the entity of reported structures, the general trend becomes clear, that especially compounds comprising two NHI ligands tend to form bridged dimers, yet also intermolecularly coordinated dimers of monoimino stabilized silyl cations **L-27** and **L-28** have been reported.[100] These compounds are prepared similarly to

L-23a and **L-23b** by addition of BCF to IPrNSiMe$_3$ or I*t*-BuNSiMe$_3$ (I*t*-BuN = 1,3-bis(di*tert*-butyl)imidazolin-2-iminato), respectively. For this reason, it is quite peculiar that Rivard and coworkers have been able to isolate a monomeric bis(imino)germylene **L-22c** by an alternative reductive route from IPr$_2$NGeCl$_2$ with sodium naphthalenide.[101] This compound has a rather small singlet-triplet energy (191.6 kcal/mol) and therefore activates dihydrogen under ambient conditions, even if the resulting germane IPrN$_2$GeH$_2$ is labile and cleaves of protonated IPrNH ligand. His group also attempted the isolation of the respective bis(imino)silylene IPrN$_2$Si(II) *via* an analogous reductive pathway from the dibromosilane IPrN$_2$SiBr$_2$ **L-30**. However, several reducing agents (elemental Na or K, Jones' Mg(I) dimer) did not show any reactivity toward this promising precursor. Astonishingly, the authors could verify that, if KC$_8$ was used instead, a rare NHI ligand activation by cleavage of the N–aryl bond and a transfer of the Dipp groups to the silicon center occurred (Scheme 4). This particular, obviously NHI-silicon specific, rearrangement was investigated by computational methods, which suggested that the undesired side-reaction is mainly triggered by over-reduction to Si(I) and Si(0) species.[101]

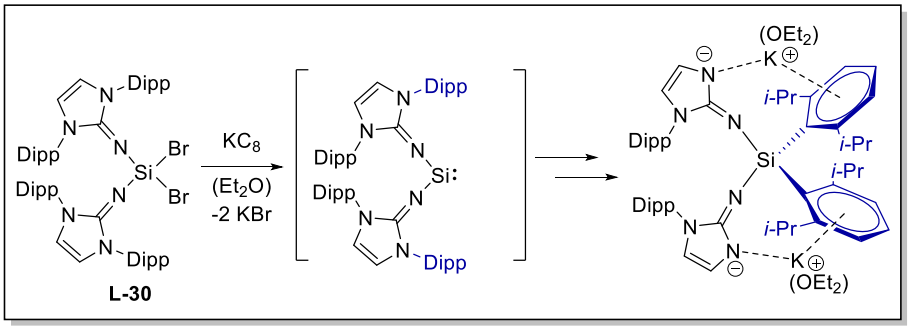

Scheme 4. Reported NHI ligand activation of Si(IV) precursor **L-30** under harsh reducing conditions with KC$_8$.

A similar problem under harsh reducing conditions with an NHI-containing Si(IV) halide precursor was identified in the synthesis of the only reported low-valent silicon compound IPrNCp*Si(II) **L-29** exhibiting an NHI ligand, which was already isolated in 2012 by Inoue and coworkers.[102] Here the synthetic pathway *via* reductive dehalogenation of the dibromosilane IPrNCp*SiBr$_2$ with sodium naphthalenide or KC$_8$ gave **L-29** solely in low yields (less than 10%). If instead the more favorable salt metathesis route *via* the silyliumylidene cation [Cp*Si]$^+$[B(C$_6$F$_5$)$_4$]$^-$ and IPrNLi was chosen, the yield increased significantly to 57%. Therefore it seems that new strategies are necessary to further access low-valent silicon compounds containing NHI ligands – a synthetic goal that has been tackled extensively as part of this thesis.

4. Main Group Catalysis: A Sustainable Alternative to Transition Metals

The last decade has witnessed tremendous advances in the field of main group catalysis with nearly countless reports of catalytic applications that are clearly on the verge of industrial implementation. Though, most certainly, some isolated examples of main group compounds involved significantly in catalytic transformations have already been reported in the 20th century, the primal idea to use "greener" main group compounds only consisting of *s*- and *p*-block elements as cheap, less toxic and fairly abundant transition metal alternatives in catalysis, is still very young. This field has its origin in the hydrogenation experiments of Power *et al.*, who was the first to recognize the strong similarities between the electronics of transition and main group metals. In 2005, he and his group demonstrated for the first time that a simple main group compound in form of digermyne **L-31** willingly reacts with molecular hydrogen without the use of any catalyst, under mild conditions (25 °C, 1 bar), to form a mixture of mono-, di- and tri-hydrogenation products (Scheme 5).[103]

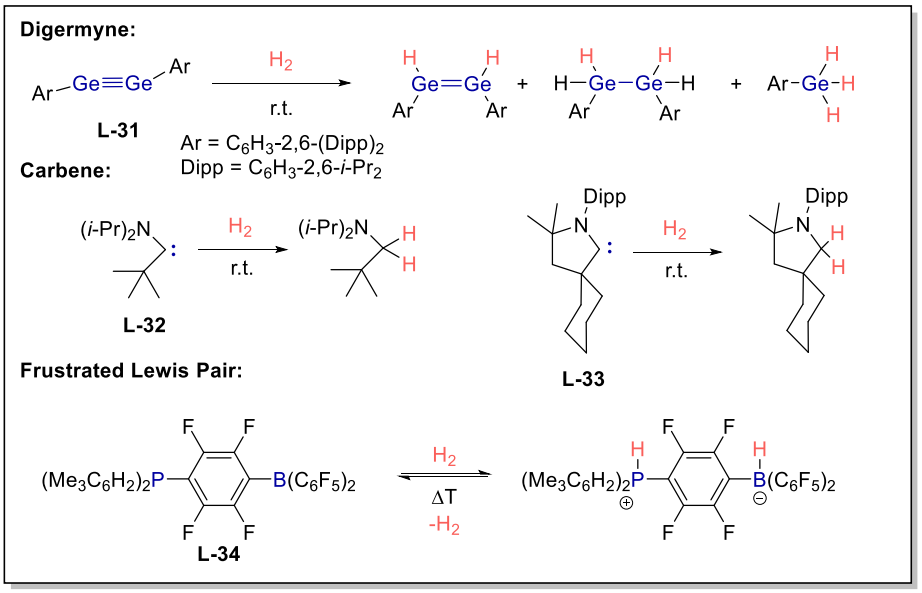

Scheme 5. First examples of metal-free activations of hydrogen by a digermyne, acyclic and cyclic carbenes (*a*AACs and *c*AACs) and a bulky phosphino borane as Frustrated Lewis Pair (FLP).

Since then, several more hydrogen activations mediated by main group compounds have followed.[104] One outstanding example is the single-site activation of hydrogen by acyclic and cyclic carbenes (*a*AAC **L-32** and *c*AAC **L-33**) reported in 2007 by Bertrand and coworkers[76] – a groundbreaking result which paved the way for further hydrogenations by heavier

tetrylenes (Si, Ge and Sn), following piece by piece in the years after.[63, 73, 77, 105] The real breakthrough towards catalysis was already achieved one year earlier, in 2006, by the group of Stephan, who presented a temperature-dependent reversible splitting of hydrogen by the sterically encumbered phosphino-borane **L-34**.[106] This simple concept using the unquenched reactivity of sterically restricted Lewis Pairs laid the foundation for the rapidly expanding field of Frustrated Lewis Pairs (FLPs). FLPs today encompass plenty of diverse structural motifs, as well as known applications, arising from the almost endless combination of bulky Lewis acids (e.g. boranes, borocations or alanes) and Lewis bases (e.g. phosphines, amines or carbenes).[107] Beside the stoichiometric activation of small molecules (e.g. CO_2, SO_2, N_2O or ethylene), also in terms of catalysis, FLPs have emerged as effective metal-free hydrogenation catalysts for imines[108], ketones[109], alkynes[110] and many other double bond containing substrates[107], in some examples even in asymmetric fashion[111]. But beyond hydrogenation, a vast multitude of catalytic reactions, as for instance the highly challenging FLP-catalyzed transformations of CO_2 to CH_4[112] or the conjugate-addition polymerizations mediated by FLPs[113] as initiating example of polymer catalysis, have been reported until today.[107] As these applications represent only a glimpse of the actual potential of FLPs, this field will surely grow in the future to one of the most important areas of modern chemistry, and fairly, it is already the indisputable signboard of main group catalysis. Right next to FLPs, and currently receiving more and more attention, are main group complexes consisting of group 2 metal ions, such as magnesium(II), calcium(II) or strontium(II), that due to their large ionic radii and their intrinsic electropositive nature, have appeared as effective Lewis acid catalysts in the selective formation of C–C, C–H and C–N bonds.[7, 114]

In terms of the here relevant group 14 elements, the most prominent classic-oxidation state example is presumably the Sn(IV) catalyst, dibutyltin dilaurate, used for the room temperature vulcanization of silicones, but as well silylium cations R_3Si^+ as highly Lewis acidic species[115] and recently even neutral tetra- and penta-coordinate organosilanes as hydrosilylation/-boration or cyanosilylation catalysts[116] have forced their way into this field. With the same goal in mind, in the last decade the development started to build single-site catalysts of *p*-block elements in non-classical oxidation states that benefit from additional coordination sites and higher redox flexibility. The results of catalysis initiated by sub-valent group 14 compounds shall be briefly discussed here.

4.1 Low-Valent Heavier Group 14 Compounds as Molecular Catalysts

Though heavier tetrylenes, by possessing a filled lone pair and an empty p-orbital as potential coordination sites, resemble the ideal electronic constitution of transition metal complexes, the field of sub-valent heavier group 14 compounds as homogeneous catalysts is still in its infancy. Within the last decade, a few catalytic examples have been reported, but all of these studies were strongly restricted to the easier redox prospects germanium(II) and tin(II). The transfer of knowledge to the environmentally more benign, but highly challenging, element silicon and the implementation of a Si(II) complex in an effective catalytic cycle is still under ongoing investigation.[70b]

As so often in catalysis, the discovery of catalytic activity of compounds results from initial stoichiometric studies towards small molecules. Admittedly, the reactivity of heavier tetrylenes has been intensively investigated over the years. The first hint, that a tetrylene mediated catalytic transformation may be feasible, was given by Roesky *et al.* in 2010 (Scheme 6).[117]

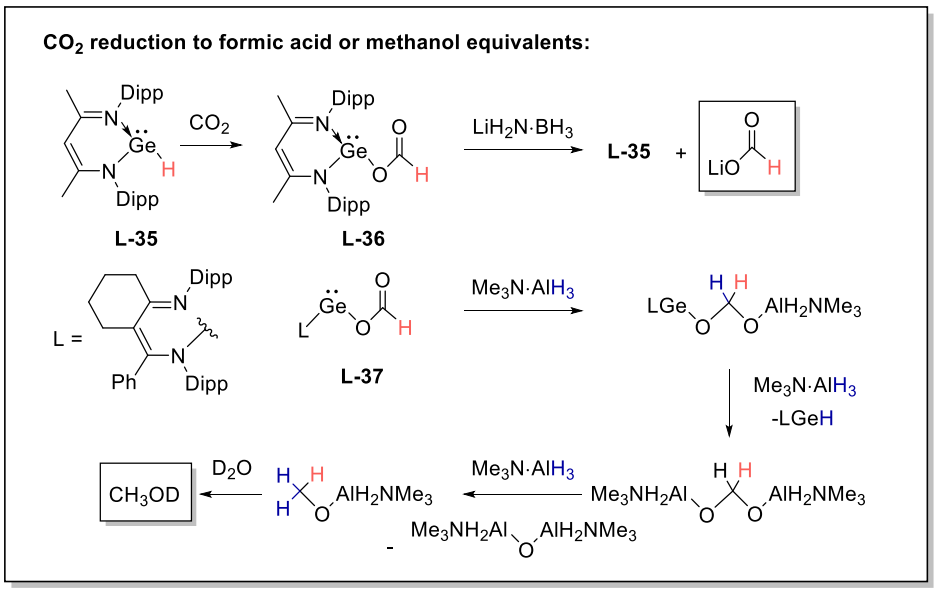

Scheme 6. First pioneering experiments of CO_2 reduction to formic acid and methanol equivalents mediated by germanium(II) hydride complexes.

In their experiments towards main group metal-mediated CO_2 reduction, they used a three-coordinate germanium(II) hydride complex **L-35** that formed the respective Ge(II) formate **L-36** under CO_2 atmosphere. In a second, separately conducted step this compound

then reacted with $LiH_2N{\cdot}BH_3$ to give lithium formate along with the regeneration of **L-35**. Although within this study the catalytic cycle could not be enlightened, it was further demonstrated that if instead ammonia borane ($H_3N{\cdot}BH_3$) was used as hydrogen source, methanol, a valuable C1 building block, was accessible upon aqueous work-up.[117] Later, Driess and coworkers investigated the mechanistic details of the methanol formation using a related germanium(II) formate system **L-37** and alane $Me_3N{\cdot}AlH_3$ as hydride source. They were able to elucidate a three-step hydrogenation process to form an alane-substituted methanol derivative that, upon hydrolysis with deuterated water, yielded CH_3OD.[118] Inspired by these results, Nagendran *et al.* reported in 2014 a full catalytic example with a similar germylene system (Scheme 7, left).[119] In their study, they could demonstrate that the conversion of aminotroponiminato-stabilized Ge(II) cyanide complex **L-38** with different aldehydes led to the clean formation of the isolable germylene alkoxides, that upon addition of TMSCN instantly underwent σ-bond metathesis to formally cyanosilylate the carbonyl compounds and regenerate germylene **L-38**. Hence, a quantitative cyanosilylation of the tested substrates was obtained with catalyst loadings of 1 mol% of germanium(II) catalyst.

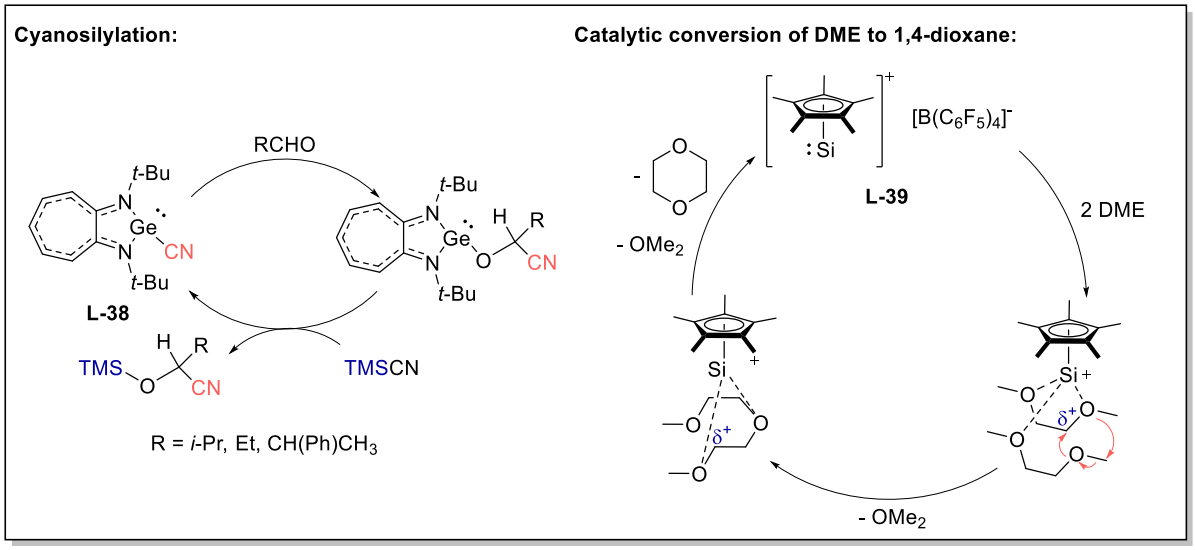

Scheme 7. Ge(II)-mediated cyanosilylation of carbonyl compounds and conversion of DME to 1,4-dioxane catalyzed by ionic Si(II) compound **L-39**.

Until now, the only example of a low-valent silicon compound as homogenous catalyst has been found by Jutzi *et al.* in 2011 (Scheme 7, right).[120] During reactivity studies of half-sandwich pentamethylcyclopentadienyl silicon(II) cation **L-39**,[31] he and his team astonishingly found out, that this compound catalytically converts 1,2-dimethoxyethane (DME) to 1,4-dioxane and dimethyl ether. The underlying mechanism, studied by *ab inito* calculations, proposed an electrostatic interaction of two molecules of DME with the highly

positively charged silicon center of the silylium ylidene cation. These dative Si–O contacts then induce a rearrangement of the σ-bond and the lone-pair electrons in the ether framework to eventually free one molecule of dimethyl ether and 1,4-dioxane, respectively, and regenerate the catalyst. It has been reported that, for this specific reaction, high conversions were obtained even with low catalyst loadings of 0.5 mol%, and, in general, this controlled ether degradation process turned out to be transferable to a series of oligo(ethyleneglycol)diethers.[121]

Within low-valent group 14 catalysis, the yet most impressive example has been achieved by Jones *et al.* in 2014.[122] They illustrated that the catalytic hydroboration of ketones, a standard transition metal catalyzed procedure to prepare protected alcohols, can also be initiated by well-defined, low-valent germanium or tin hydrides. Their developed two-coordinate acyclic hydrido germylene or stannylene complexes **L-40** have shown to be effective single-site catalysts for the hydroboration of several unactivated aldehydes and ketones, even if applied at low catalyst loadings (0.05 mol %), reaching turnover frequencies (TOF) of up to 13300 h^{-1} – a value that clearly rivals those of classic transition metal catalysts for such reactions (Scheme 8).

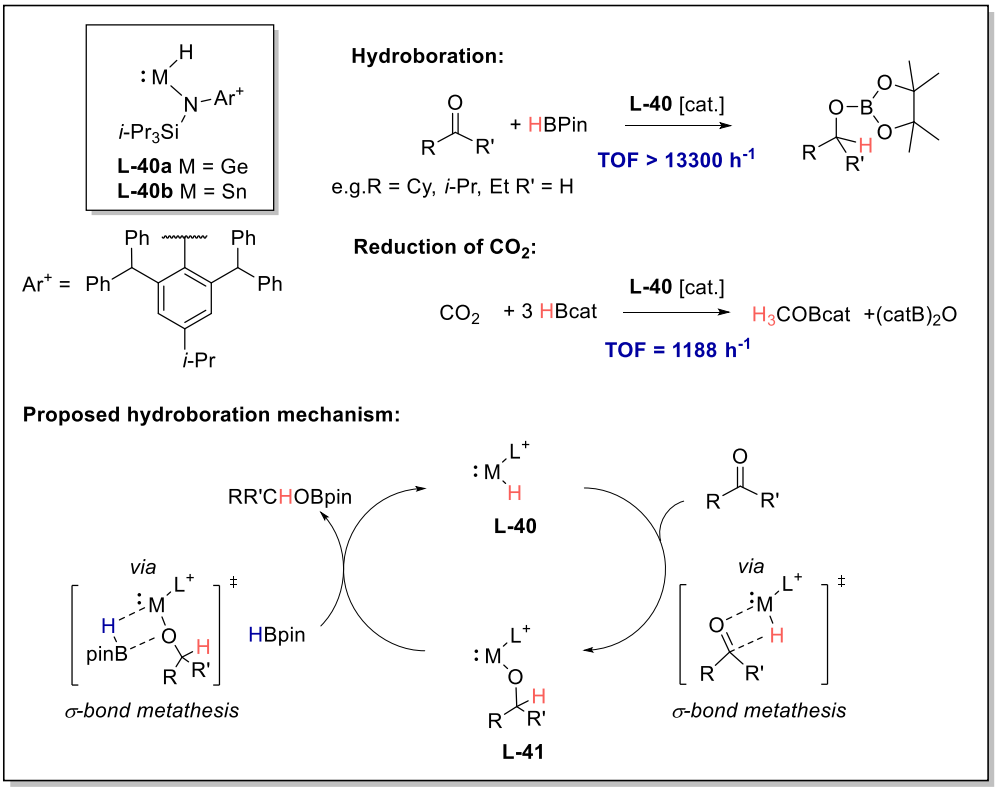

Scheme 8. Hydroboration of carbonyl compounds (including mechanistic details) and reduction of CO_2 to methanol equivalents catalyzed by two-coordinate Ge(II) and Sn(II) hydride complexes **L-40**.

In terms of the underlying mechanism, it was proposed that the catalytic cycle is initiated by a σ-bond metathesis step of the respective carbonyl compound with the M(II)–H bond of the tetrylene, leading to an alkoxy substituted germylene or stannylene intermediate **L-41**, respectively. The mild borane reagent HBpin (pin = pinacolo), as a result of the oxophilicity of boron, could then split the M–O bond, again in a four-membered transition state, to release the borate ester as product and reproduce the hydridotetrylene **L-40**. As continuation of the mentioned pioneering work of Roesky *et al.*, most recently, both Ge(II) and Sn(II) catalysts **L-40** were also found to be applicable in the hydroboration of CO_2 to methanol equivalents, using either HBpin or HBcat (cat = catecholato) as hydrogen source. In this regard, the Sn(II) hydride derivative of **L-40** has been the most active non-transition metal catalyst for such reactions reported to date with TOF values of 1188 h^{-1}, nearly approaching the activity of a competing palladium thiolate system (TOF 1780 h^{-1}) as most effective transition metal complex.[123]

In summary, the latest two achievements by Jones *et al.* point out that monomeric, low-valent compounds of group 14 (Ge, Sn) are not only applicable as single-site catalysts in organic transformations, but they even achieve comparable efficiencies to transition metal-based systems. In order to approach the next step and test similar conversions with more economical silicon(II) congeners, first the accessibility and diversity of these structures has to be expanded greatly.

5. Scope of This Work

Recent years have established main group catalysis as a flourishing field with a multitude of remarkable catalytic applications, but the involvement of silicon-containing compounds clearly lags behind. As pointed out in the introduction, two-coordinate acyclic silylenes, due to their close frontier orbitals separation and their vacant coordination sites, are considered as the most promising Si(II) structures to mimic transition metals in small molecule activation or even catalytic processes. Yet, prior to the outset of this thesis, the number of accessible two-coordinate acyclic silylenes, with only three reported representatives (**L-9-11**), has been very limited, never mind their chemistry that despite the early results mentioned in Chapter 3.3 has hardly been explored. This work therefore aimed to close the gap and expand the chemistry of this novel compound class. The primary focus was the activation of small molecules, especially of industrially relevant targets, such as carbon dioxide, olefines or ammonia. Particular attention was paid to the investigation of the activated products for potential reversibility – a fundamental part of catalysis (Figure 8).

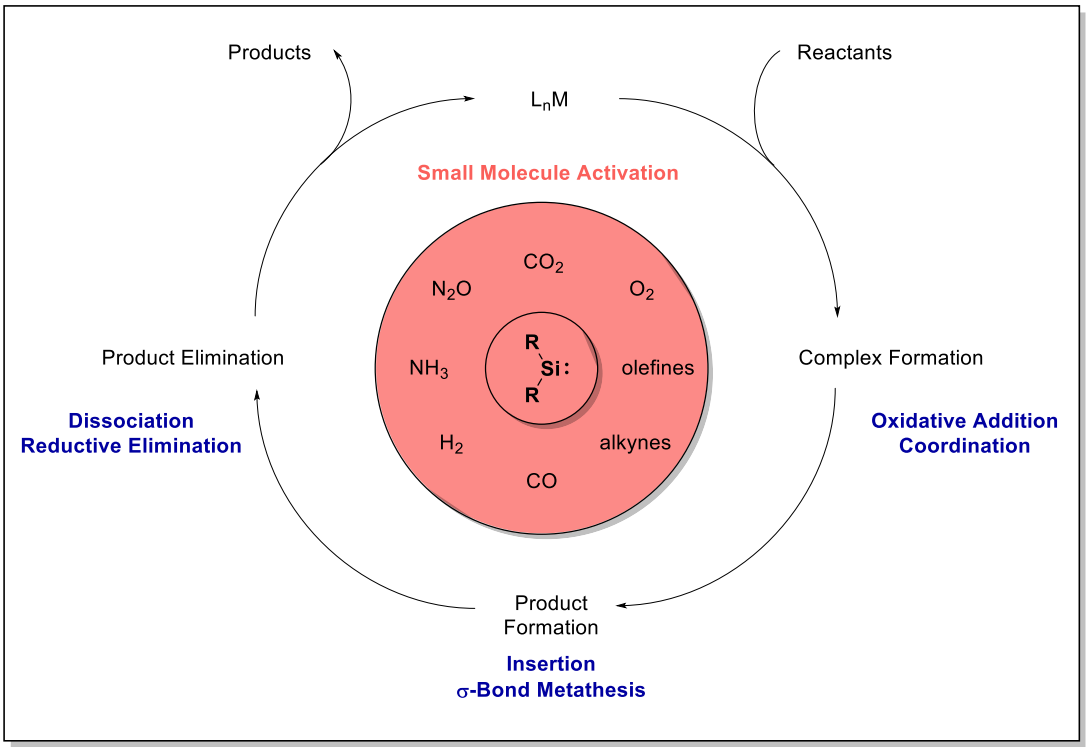

Figure 8. Small molecule activation of potential substrates by a two-coordinate acyclic silylene; Representation of a conventional catalytic cycle and its most common elemental steps.

More precisely, the question arose, if the activation proceeds in all cases *via* oxidative addition of substrates to the Si(II) center, or if instead further fundamental steps of a catalytic cycle, like simple coordination-dissociation of substrates or more preferably insertion reactions could be detected. In particular, the quest for a σ-bond metathesis or a reductive elimination at a silicon center to formally regenerate the silylene species was pursued. If successful, this would give the first proof for a viable catalytic system based on the Si(II)/Si(IV) redox couple.

To achieve this ambitious task, the initial build-up of knowledge and expertise on this, for our group completely foreign, field was absolutely essential. Therefore as an entry point, we set the goal to reproduce the synthesis of one two-coordinate acyclic silylene, namely Jones' amino(silyl)silylene **L-11** (for synthetic details see Chapter 3.3), and intensively investigate its reactivity with different substrates. Most notably, the behavior towards olefines was of great interest since, at that time, the remarkable ethylene dissociation equilibrium with related bis(thiolato)silylene **L-9** had already been reported, and for us a similar reactivity seemed plausible.

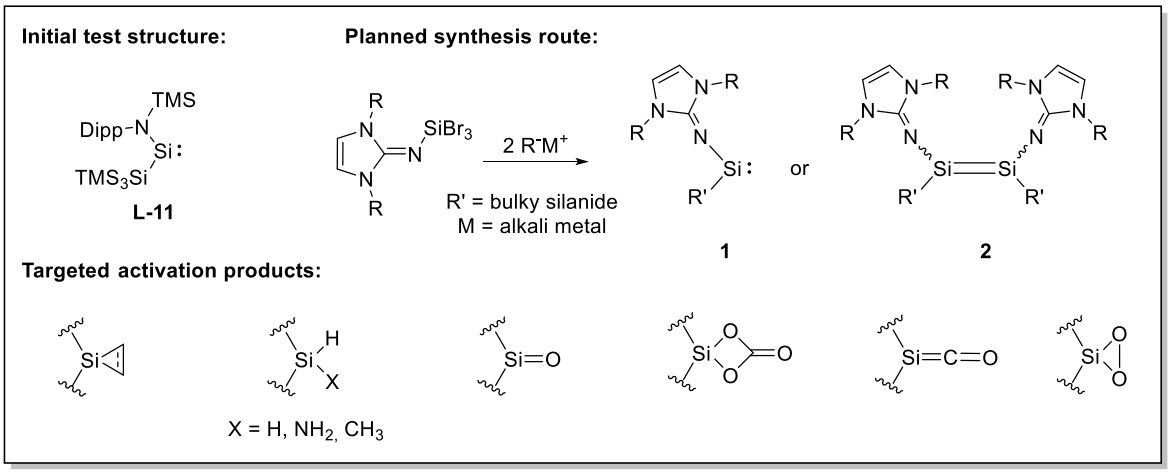

Scheme 9. Initial test structure **L-11** and planned synthesis route to new, acyclic imino(silyl)-silylene **1** or -disilene **2** including potential activation products.

With the gained knowledge in hand, we would, afterwards, shift the focus of our work to the synthesis of an independent system. In our silylene concept, we envisioned the NHI ligand as excellent π-donor to thermodynamically stabilize the Si(II) moiety in combination with a counteracting σ-donating silyl group (e.g. hypersilyl ($SiTMS_3$)), that maintains the small frontier orbitals separation necessary for the activation of more challenging molecules. Inspired by Jones's one-pot synthesis, we targeted the respective iminotribromosilane with different substituents at the imino and the silyl group (Scheme 9). Following the procedure

described in Chapter 3.3, the monomeric acyclic imino(silyl)silylene **1** could be obtained by the reduction with two equivalents of a respective bulky silanide. Depending on the sterical encumbrance of the NHI and the silyl ligand the formation of an imino(silyl)disilene **2** was also considered, an option that seemed particularly beneficial since nitrogen-substituted disilenes are generally quite rare.[124] This prompted us to investigate, if the combination of such contrasting ligands, one favoring a planar (silyl), the other a *trans*-bent (NHI) type Si=Si geometry, may lead to unusual electronic properties and new insights into multiple bonding of silicon or even give access to yet unknown modes of reactivity.

In respect to small molecule activation with potential acyclic imino(silyl)silylene **1**, several peculiar products were targeted (Scheme 9 bottom). Among them have, of course, been silirane or silirene rings from the reaction of silylenes with olefines or alkynes, respectively, with the intended goal in mind to depart stoichiometric conversions and approach reversible dissociation equilibria. The activation of hydrogen, ammonia or even the yet unsolved C–H activation of methane would be tested in the same fashion with the newly developed system. Furthermore, we were convinced that acyclic silylenes are predestinated precursors for the isolation of a three-coordinate silanone containing a Si=O double bond, an eagerly awaited species that after more than 100 years of silicone chemistry still lacks of experimental proof. In this connection, a monomeric four-coordinate silicon carbonate complex, a formal [2+2] cycloaddition product of the silanone with CO_2, may be obtainable as well. Interestingly, so far all reported attempts to isolate such a compound led to the formation of dimers or larger rings structures.[125] In addition, acyclic silylenes could be the key for the isolation of a silicon analogue of a ketene (Si=C=O) resulting from yet unprecedented reaction of a silylene with carbon monoxide. In the same way, the activation of molecular oxygen has been of great interest, because it may lead to the formation of a strained three-membered dioxasilirane ring, an ideal molecule to transfer oxygen to other organic molecules under regeneration of the former Si(II) species. To conclude, as discoveries of catalytic activity of main group compounds often grow from initial stoichiometric reactivity studies, the results of these activation experiments shall eventually facilitate the evaluation of the catalytic potential of this special compound class and ideally trigger further investigations towards silylene-based metal-free catalysis.

6. Reactivity of an Acyclic Silylsilylene toward Ethylene: Migratory Insertion into the Si–Si Bond

Title: "Reactivity of an Acyclic Silylsilylene toward Ethylene: Migratory Insertion into the Si–Si Bond"

Status: Communication, published online October 13, 2015

Journal: Organometallics, 2016, 35 (1), 1–4.

Publisher: American Chemical Society

DOI: 10.1021/acs.organomet.5b00797

Authors: Daniel Wendel, Wolfgang Eisenreich, Christian Jandl, Alexander Pöthig, Bernhard Rieger[a]

Content: This publication has been the entry for our group into the field of low-valent silicon chemistry. The reaction of Jones' acyclic amino(silyl)silylene toward ethylene was investigated with the ulterior motive to achieve an olefin polymerization to poly(ethylene). In contrast to the mentioned reports of Power's bis(thiolato)silylene, no direct dissociation equilibrium between the free silylene and the respective silirane ring was detectable. Instead, in ethylene atmosphere under ambient conditions a full stoichiometric conversion to the silirane was observed. However, at elevated temperatures (60 °C, 1 bar) the system performed a remarkable migratory insertion of the coordinated ethylene of the silirane ring into the Si–Si bond of the hypersilyl ligand. The subsequently formed Si(II) center of the intermediary alkyl(amino)silylene was then instantly trapped by a second ethylene molecule of the reaction solution. This proposed mechanism was verified by separate reactivity studies with deuterated ethylene (C_2D_4). By taking a closer look into the mechanistic details, it became noticeable that our reaction largely resembles the well-known mechanism of the Ziegler-Natta polymerization of olefins. Our study revealed, however, that in strong contrast to classic group IV polymerization catalysis, the modified silirane ring cannot undergo a second or even more ethylene insertions to extend the alkyl chain, most likely due to the formation of a stable Si–C bond. Nevertheless, this work visualized the general possibility of insertion reactions into labile ligand bonds of acyclic silylenes, an important step towards catalytic transformations.

[a]D. Wendel planned and executed all experiments and wrote the manuscript. W. Eisenreich helped with the evaluation of NMR data. C. Jandl conducted all SC XRD-measurements and managed the processing of the respective data. All work was performed under the supervision of B. Rieger.

Coverpage of Organometallics, Vol. 35, Issue 1, 2016

"This photorealistic cover picture displays the key step in the reaction sequence of the only known room-temperature-stable, acyclic silylsilylene with ethylene – a migratory insertion of the coordinated ethylene into the Si–Si bond of the ligand framework with subsequent addition of a second ethylene molecule."

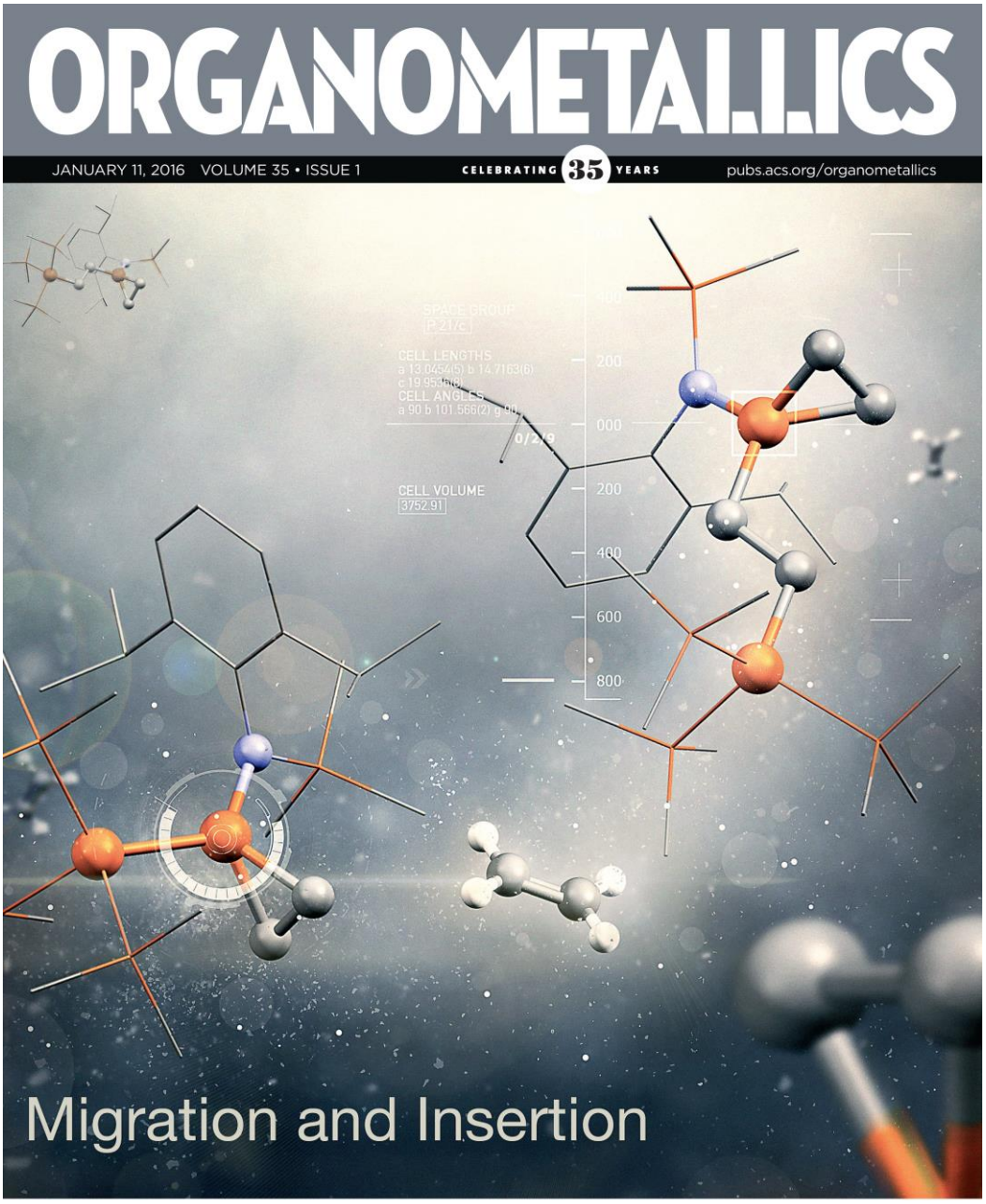

Coverart designed and created by Johannes Richers (jo@jorichers.com).

ORGANOMETALLICS

Communication

pubs.acs.org/Organometallics

Reactivity of an Acyclic Silylsilylene toward Ethylene: Migratory Insertion into the Si–Si Bond

Daniel Wendel,[†] Wolfgang Eisenreich,[‡] Christian Jandl,[§] Alexander Pöthig,[§] and Bernhard Rieger*[,†]

[†]WACKER-Lehrstuhl für Makromolekulare Chemie and [‡]Lehrstuhl für Biochemie, Technische Universität München, Lichtenbergstraße 4, 85747 Garching bei München, Germany

[§]Zentralinstitut für Katalyseforschung, Technische Universität München, Ernst-Otto-Fischer Straße 1, 85747 Garching bei München, Germany

Supporting Information

ABSTRACT: The reaction of the only known room-temperature-stable, acyclic silylsilylene, Si{NDipp(SiMe$_3$)}{Si(SiMe$_3$)$_3$}, toward ethylene was investigated. A full conversion to the silirane product Si{CH$_2$–CH$_2$}{NDipp(SiMe$_3$)}{Si(SiMe$_3$)$_3$} (**1**) was observed at ambient temperature. However, heating of the benzene solution under an ethylene atmosphere led to an exceptional Si–Si bond insertion to give the modified silirane Si{CH$_2$–CH$_2$}{NDipp-(SiMe$_3$)}{CH$_2$–CH$_2$–Si(SiMe$_3$)$_3$} (**2a**). With respect to the mechanism, an NMR experiment using C_2D_4 revealed this reaction to proceed via a migratory insertion of the coordinated ethylene of **1** into the Si–Si bond of the ligand framework and subsequent addition of a second ethylene molecule. Moreover, [4+1] cycloaddition with 2,3-dimethyl-1,3-butadiene to give the corresponding silacyclopent-3-ene ring Si{CH$_2$–CH$_3$C═CCH$_3$–CH$_2$}{NDipp(SiMe$_3$)}{Si(SiMe$_3$)$_3$} (**3**) is reported. All structures were fully characterized by single-crystal X-ray analysis and ^{1}H, ^{13}C, and ^{29}Si NMR spectroscopy.

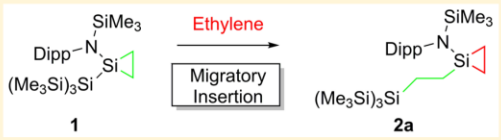

About 50 years ago Goldstein et al. proposed a transient, low-valent SiMe$_2$ species in the reduction of dimethylchlorosilane with sodium–potassium vapor at elevated temperatures.[1] From the time of this pioneering work up to now, exceptional efforts have been made in exploring and elucidating the nature of these elusive silicon compounds.[2] The foundation of this development was laid in 1986, when Jutzi and co-workers isolated decamethylsilicocene as the first room-temperature-stable, monomeric Si(II) compound, in which the central silicon atom is protected between two bulky Cp* ligands.[3] In 1994 the group of West followed with the groundbreaking discovery of the first room-temperature-stable N-heterocyclic silylene (NHSi),[4] whose structural motif has been transferred to a wide variety of stable structures which represent the most investigated silylene class.[2] To date, several interesting reactions with small molecules have been reported with NHSis, but more ambitious targets which demand a reactivity more similar to that of transition metals, such as the activation of H_2, NH_3, CO, and strong C–H bonds, still remain a challenge.[2c] A step toward this goal was achieved only recently, due to the remarkable work by the groups of Power[5] and Aldridge,[6] who simultaneously illustrated the highly difficult task of stabilizing silylenes in an acylic framework (Chart 1).[7] In contrast to conventional NHSis, acyclic silylenes are ideal candidates for selective small-molecule activation and lead structures for potential metal-free catalysts. This is attributed to their coordinative and oxidative flexibility in connection with the implementation of less π-donating but extremely bulky ligands.[2b,8]

Chart 1. Room-Temperature-Stable, Monomeric, Acyclic Silylenes I–III

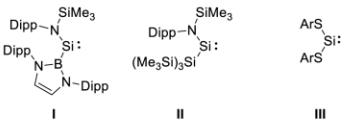

Dipp = C$_6$H$_3$-2,6-^{i}Pr$_2$, Mes = C$_6$H$_2$-2,4,6-Me$_3$, **IIIa** Ar = C$_6$H$_3$-2,6-Mes$_2$, **IIIb** Ar = C$_6$H$_3$-2,6-Dipp$_2$

A key factor for the evaluation of silylene reactivity is the HOMO–LUMO gap, which in the case of silylenes **I** and **II** (2.04 and 1.99 eV, respectively) is assumed to be lowered due to the strong σ-donation from the coordinating boryl/silyl groups.[8,9] Both structures have been reported to cleave dihydrogen at ambient temperatures, the prime example demonstrating their enhanced reactivity.[6] The HOMO–LUMO gap of bis(arylthio)-substituted silylene **III** is clearly larger (4.26 eV for **IIIa**), which presumably prohibits the single-site activation of hydrogen.[5] This compound, however, shows remarkable behavior toward ethylene by reversibly binding the olefin in a dissociation equilibrium with its corresponding silirane ring (silacyclopropane) under ambient conditions.[10] This unprecedented behavior by an acyclic, two-coordinate silylene raises the question if such a system is capable of

Received: September 17, 2015
Published: October 13, 2015

DOI: 10.1021/acs.organomet.5b00797
Organometallics 2016, 35, 1–4

eventually playing a role in catalytic transformations. Still, the chemistry of acyclic silylenes is largely unexplored.

The proposed extended reactivity with the chance to use acyclic silylenes as molecular catalysts in macromolecular chemistry inspired our group to investigate the reactivity of the most reactive acyclic silylene, **II**, toward the simplest olefin monomer, ethylene (Scheme 1).

Scheme 1. Reaction Pathway of Silylsilylene II with Ethylene To Afford Siliranes 1 and 2a,b

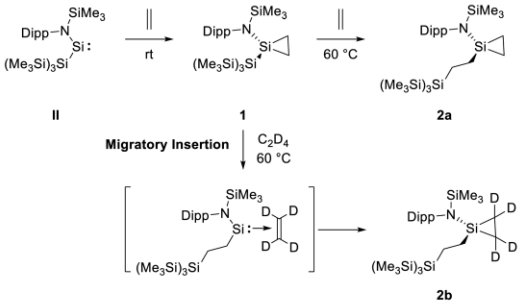

Herein we report the irreversible reaction of **II** to the silirane **1** with no dissociation equilibrium at room temperature. Increasing the temperature commonly favors the regeneration of the silylene with olefin elimination.[10,11] In this case the unexpected formation of the modified silirane **2a** was observed at elevated temperatures. An NMR experiment with C_2D_4 indicates the mechanism of this process to follow a migratory insertion pathway of the coordinated ethylene into the Si–Si bond with subsequent silirane formation with a deuterated ethylene molecule (Scheme 1; **2b**). Moreover, the behavior of **II** toward the butadiene derivative 2,3-dimethyl-1,3-butadiene was analyzed. Monitoring the reaction via NMR spectroscopy proved the exclusive formation of the [4+1] cycloaddition product **3** with no observable vinylsilirane byproduct (Scheme 2).

Scheme 2. Reaction of Silylsilylene II with 2,3-Dimethyl-1,3-butadiene To Afford Silacylopentene 3

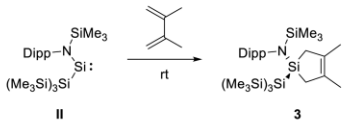

Exposure of a solution of **II** in C_6D_6 to ethylene at room temperature led to the full decolorization of the characteristic purple color within seconds. Subsequent NMR analysis confirmed the sole formation of the silirane **1** with no remaining silylsilylene **II**. The ^{29}Si NMR spectrum of **1** displays an upfield signal at −80.76 ppm for the central silicon atom, which represents a shift of more than 500 ppm in comparison to the original silylsilylene **II** signal (two conformers due to the restricted rotation around the Si–N bond at 438.20 and 468.46 ppm).[6] Hereby the change in oxidation state and the presence of a single conformer with free rotation around the Si–N bond are demonstrated. Interestingly the ^1H NMR spectrum reveals two signal groups for the four ring-bound protons (0.91 and 0.37 ppm) with higher-order multiplets, indicating the different chemical surroundings in a heteroleptic ligand framework (see the Supporting Information). This statement is in line with analoguous silirane products using Power's homoleptic silylene **III** in which only one singlet (**IIIa** 0.64 ppm and **IIIb** 0.4 ppm in toluene-d_8) for the four chemical equivalent protons is observed.[10]

The structural details of **1** were determined by single-crystal X-ray analysis and are depicted in Figure 1.

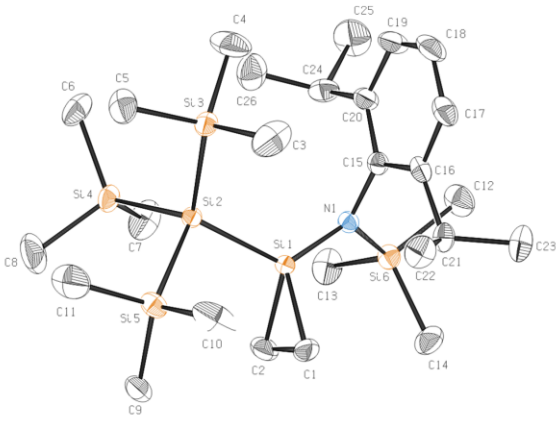

Figure 1. Molecular structure of **1**. Hydrogen atoms are omitted for clarity, and displacement ellipsoids are set at the 50% probability level. Selected bond lengths (Å) and angles (deg): C1–C2 1.554(3), C1–Si1 1.850(2), C2–Si1 1.847(2), Si2–Si1 2.3439(6), N1–Si1 1.747(1); C2–Si1–C1 49.71(8), C2–C1–Si1 65.0(1), C1–C2–Si1 65.2(1), N1–Si1–Si2 126.88(5).

The central silicon atom is tetracoordinated, with a widened N1–Si1–Si2 angle (126.88(45)°) in comparison to the previous silylene **II** (116.49°)[6b] and a much smaller C2–Si1–C1 angle (49.71(8)°), which is in accordance with those of similar siliranes.[10,12] Regarding the bond lengths, the newly formed carbon–silicon bonds (C1–Si1 1.850(2) Å and C2–Si1 1.847(2) Å) are very close to standard Si–C single-bond lengths (1.87 Å).[13] Similarly, the measured C1–C2 bond (1.554(3) Å) clearly show its single-bond character (standard C–C 1.54 Å).[13]

A solution of **1** in C_6D_6 was heated to 60 °C under an ethylene atmosphere and monitored via NMR spectroscopy. The primary idea behind this experiment was the insertion of a second ethylene molecule into the Si–C bond to enlarge the ring system to a silacyclopentane. Ideally, further insertions would then increase the ring chain to build up polyethylene in a fashion similar to that in the polymerization of ethylene with Phillips catalyst.[14] Instead, the NMR data after 3 days revealed that a complete conversion to silirane **2a** was afforded in which apparently a second ethylene molecule inserted into the Si–Si bond of the ligand. A mechanistic study using C_2D_4 in an identical experimental setup elucidated that actually the coordinated ethylene unit in **1** migrates into the Si–Si bond and a deuterated ethylene molecule forms the novel silirane ring to give **2b** (see the Supporting Information for NMR details). To the best of our knowledge, this transformation is the first reported migratory insertion of an olefin into a Si–Si bond. Related work by Baceiredo et al. illustrated the possibility of a reversible insertion of ethylene into a Si–Sn bond of a stable silylene–phosphine complex.[15] Furthermore, a compa-

DOI: 10.1021/acs.organomet.5b00797
Organometallics 2016, 35, 1–4

rable reaction has been discovered by Marschner et al., who proposed a migratory insertion of phenylacetylene into a Si–Ge bond of a donor-stabilized silylgermylene to build vinylgermylenes.[16] In a recent investigation the group of Aldridge conducted the same experiment with silylsilylene **II** and phenylacetylene but only identified the appropriate silirene (silacyclopropene) as the sole product.[17]

The newly formed Si–C bonds of **2a** give rise to a high-field-shifted signal for the silirane silicon atom at −51.88 ppm in the ^{29}Si NMR spectrum, whereas the signal of the quaternary silicon of the hypersilyl group shifts from −118.94 ppm in **1** to −76.47 ppm. The proposed structure of **2a** was verified by single-crystal X-ray analysis and is illustrated in Figure 2. The

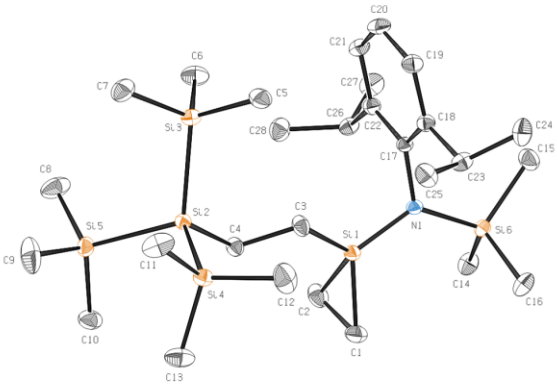

Figure 2. Molecular structure of **2**. Hydrogen atoms are omitted for clarity, and displacement ellipsoids are set at the 50% probability. level. Selected bond lengths (Å) and angles (deg): C1–C2 1.584(2), C1–Si1 1.828(1), C2–Si1 1.836(1), C3–Si1 1.863(1), C4–Si2 1.908(1), C3–C4 1.539(2); C2–Si1–C1 51.24(6), C2–C1–Si1 64.64(7), C1–C2–Si1 64.12(7), N1–Si1–C3 112.69(5).

introduced ethyl spacer of **2a** causes a considerable contraction of the N1–Si1–C3 angle from 126.88(5)° to 112.69(5)°, thereby releasing tension of the strained silacycle, whose C2–Si1–C1 angle (51.24(6)°) slightly increases in comparison to that of **1** (49.71(8)°). The cleavage of a labile Si–Si bond in combination with the formation of two more stable Si–C single bonds presumably promotes this rearrangement.

A diverse reactivity of silylenes with 1,3-dienes has been reported in the literature.[12] Here, the bulkiness of the substituents of the silylene turned out to be crucial for product formation to either give silacyclopent-3-enes via [4+1] cycloaddition or vinylsiliranes via [2+1] cycloaddition.[18] Therefore, the reactivity of **II** toward 2,3-dimethyl-1,3-butadiene was investigated. A solution of silylsilylene **II** in C_6D_6 was added to a Young NMR tube filled with 2,3-dimethyl-1,3-butadiene, and the reaction progress was monitored via NMR spectroscopy. The ^{1}H NMR data after 3 days reveal a concerted process to the silacyclopent-3-ene **3** without any sign for a vinylsilirane intermediate (see the Supporting Information). The ^{29}Si NMR spectrum of **3** displays a signal for the central silicon atom at 7.71 ppm, which is shifted to high field in comparison to the signal of the appropriate silacylopent-3-ene with Power's silylene **IIIb** at 31.49 ppm.[19] The molecular structure obtained by single-crystal X-ray analysis is depicted in Figure 3. The N1–Si1–Si2 angle (121.71(5)°) of **3** is considerably widened in comparison to the angle of the

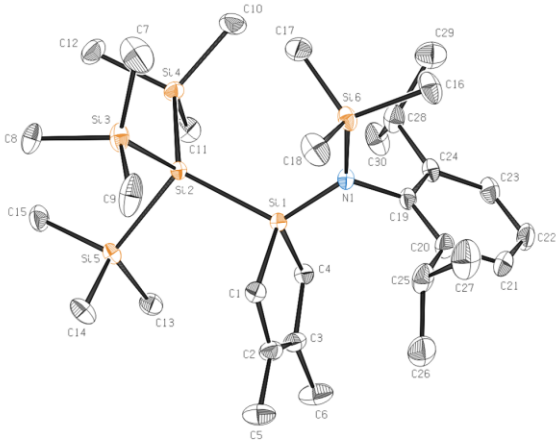

Figure 3. Molecular structure of **3**. Hydrogen atoms are omitted for clarity, and displacement ellipsoids are set at the 50% probability level. Selected bond lengths (Å) and angles (deg): C2–C3 1.336(2), C1–C2 1.518(2), C3–C4 1.515(2), C1–Si1 1.896(2), C4–Si1 1.893(2); C4–Si1–C1 94.50(8), N1–Si1–Si2 121.71(5).

original silylene **II** (116.49°). The C4–Si1–C1 angle (94.50(8)°) and the measured bond lengths are similar to those obtained in the formation of the silacyclopent-3-ene using **IIIb**[19] and are comparable with related published structures.[12,20]

In summary, our reactivity study of the promising acyclic silylsilylene **II** toward ethylene illustrated that under ambient conditions the compound behaves like a classical, transient silylene with full conversion to silirane **1**. The original intended ring enlargement to trigger a polymerization reaction of ethylene was not accomplished. However, at elevated temperatures the system performed a unique migratory insertion of the coordinated ethylene of **1** into the Si–Si bond of the ligand framework and subsequently added a second ethylene molecule to give the modified silirane **2a**. The proposed mechanism of this process was verified by NMR experiments with C_2D_4. The separate reactivity study of **II** toward 2,3-dimethyl-1,3-butadiene yielded exclusively the [4+1] cycloaddition product **3**. Our work demonstrates the first migratory insertion of an olefin into a Si–Si bond with a low-valent silicon compound. Thereby it re-emphasizes the untapped potential of acyclic silylenes to mimic typical reactions of transition-metal complexes and brings researchers in this field closer to the ultimate goal of metal-free catalysis.

■ ASSOCIATED CONTENT

Supporting Information

The Supporting Information is available free of charge on the ACS Publications website at DOI: 10.1021/acs.organomet.5b00797.

Crystallographic data for **1** (CCDC 1424204), **2a** (CCDC 1424205), and **3** (CCDC 1424206) (CIF)

Detailed synthetic procedures, full spectroscopic analysis, and information for single-crystal X-ray structure determinations (PDF)

DOI: 10.1021/acs.organomet.5b00797
Organometallics 2016, 35, 1–4

AUTHOR INFORMATION

Corresponding Author

*E-mail for B.R.: rieger@tum.de.

Notes

The authors declare no competing financial interest.

ACKNOWLEDGMENTS

We are exceptionally grateful to the WACKER Chemie AG for continued financial support. We thank Philipp Pahl, Martin Machat, Benedikt S. Soller, and Matthias Grübel for valuable discussions.

REFERENCES

(1) Skell, P. S.; Goldstein, E. J. *J. Am. Chem. Soc.* **1964**, *86*, 1442−1443.

(2) For reviews on silylenes see (a) Rivard, E. *Chem. Soc. Rev.* **2015**, DOI: 10.1039/C5CS00365B. (b) Blom, B.; Driess, M. *Struct. Bonding (Berlin, Ger.)* **2013**, *156*, 85−123. (c) Yao, S.-L.; Xiong, Y.; Driess, M. *Organometallics* **2011**, *30*, 1748−1767. (d) Asay, M.; Jones, C.; Driess, M. *Chem. Rev. (Washington, DC, U. S.)* **2011**, *111*, 354−396. (e) Mizuhata, Y.; Sasamori, T.; Tokitoh, N. *Chem. Rev. (Washington, DC, U. S.)* **2009**, *109*, 3479−3511. (f) Kira, M.; Iwamoto, T.; Ishida, S. *Bull. Chem. Soc. Jpn.* **2007**, *80*, 258−275. (g) Kira, M. *J. Organomet. Chem.* **2004**, *689*, 4475−4488. (h) Hill, N. J.; West, R. *J. Organomet. Chem.* **2004**, *689*, 4165−4183. (i) Gehrhus, B.; Lappert, M. F. *J. Organomet. Chem.* **2001**, *617*−*618*, 209−223. (j) Tokitoh, N.; Okazaki, R. *Coord. Chem. Rev.* **2000**, *210*, 251−277. (k) Haaf, M.; Schmedake, T. A.; West, R. *Acc. Chem. Res.* **2000**, *33*, 704−714.

(3) Jutzi, P.; Kanne, D.; Kruger, C. *Angew. Chem., Int. Ed. Engl.* **1986**, *25*, 164−165.

(4) Denk, M.; Lennon, R.; Hayashi, R.; West, R.; Belyakov, A. V.; Verne, H. P.; Haaland, A.; Wagner, M.; Metzler, N. *J. Am. Chem. Soc.* **1994**, *116*, 2691−2.

(5) Rekken, B. D.; Brown, T. M.; Fettinger, J. C.; Tuononen, H. M.; Power, P. P. *J. Am. Chem. Soc.* **2012**, *134*, 6504−6507.

(6) (a) Protchenko, A. V.; Birjkumar, K. H.; Dange, D.; Schwarz, A. D.; Vidovic, D.; Jones, C.; Kaltsoyannis, N.; Mountford, P.; Aldridge, S. *J. Am. Chem. Soc.* **2012**, *134*, 6500−6503. (b) Protchenko, A. V.; Schwarz, A. D.; Blake, M. P.; Jones, C.; Kaltsoyannis, N.; Mountford, P.; Aldridge, S. *Angew. Chem., Int. Ed.* **2013**, *52*, 568−71.

(7) A few other stable, acyclic silylenes have been reported that are worth mentioning here (a) Inoue, S.; Leszczynska, K. *Angew. Chem., Int. Ed.* **2012**, *51*, 8589−8593. (b) Jutzi, P.; Leszczynska, K.; Mix, A.; Neumann, B.; Rummel, B.; Schoeller, W.; Stammler, H.-G. *Organometallics* **2010**, *29*, 4759−4761. (c) Jutzi, P.; Leszczynska, K.; Neumann, B.; Schoeller, W. W.; Stammler, H.-G. *Angew. Chem., Int. Ed.* **2009**, *48*, 2596−9. (d) Jutzi, P.; Mix, A.; Rummel, B.; Schoeller, W. W.; Neumann, B.; Stammler, H.-G. *Science (Washington, DC, U. S.)* **2004**, *305*, 849−851.

(8) Driess, M. *Nat. Chem.* **2012**, *4*, 525−526.

(9) Kuriakose, N.; Vanka, K. *Dalton Trans.* **2014**, *43*, 2194−2201.

(10) Lips, F.; Fettinger, J. C.; Mansikkamaki, A.; Tuononen, H. M.; Power, P. P. *J. Am. Chem. Soc.* **2014**, *136*, 634−7.

(11) (a) Seyferth, D.; Annarelli, D. C. *J. Am. Chem. Soc.* **1975**, *97*, 7162−3. (b) Atwell, W. H.; Weyenberg, D. R. *J. Am. Chem. Soc.* **1968**, *90*, 3438−43.

(12) Ishida, S.; Iwamoto, T.; Kira, M. *Heteroat. Chem.* **2011**, *22*, 432−437.

(13) (a) Stark, B. *Electron Diffraction Catalogue and Supplement*; Van Nostrand Reinhold: London, 1979. (b) Sutton, L. E. *Tables of Interatomic Distances and Configuration in Molecules and Ions*; Chemical Society: London, 1958.

(14) McDaniel, M. P. *Adv. Catal.* **2010**, *53*, 123−606.

(15) (a) Rodriguez, R.; Contie, Y.; Gau, D.; Saffon-Merceron, N.; Miqueu, K.; Sotiropoulos, J.-M.; Baceiredo, A.; Kato, T. *Angew. Chem., Int. Ed.* **2013**, *52*, 8437−8440. (b) Rodriguez, R.; Gau, D.; Kato, T.; Saffon-Merceron, N.; De Cozar, A.; Cossio, F. P.; Baceiredo, A. *Angew. Chem., Int. Ed.* **2011**, *50*, 10414−10416.

(16) Walewska, M.; Baumgartner, J.; Marschner, C. *Chem. Commun. (Cambridge, U. K.)* **2015**, *51*, 276−278.

(17) Protchenko, A. V.; Blake, M. P.; Schwarz, A. D.; Jones, C.; Mountford, P.; Aldridge, S. *Organometallics* **2015**, *34*, 2126−2129.

(18) (a) Zhang, S.; Conlin, R. T. *J. Am. Chem. Soc.* **1991**, *113*, 4272−8. (b) Nag, M.; Gaspar, P. P. *Organometallics* **2009**, *28*, 5612−5622.

(19) Lips, F.; Mansikkamaki, A.; Fettinger, J. C.; Tuononen, H. M.; Power, P. P. *Organometallics* **2014**, *33*, 6253−6258.

(20) Xiong, Y.; Yao, S.; Driess, M. *Organometallics* **2010**, *29*, 987−990.

DOI: 10.1021/acs.organomet.5b00797
Organometallics 2016, 35, 1−4

7. Twist of a Silicon–Silicon Double Bond: Selective *Anti*-Addition of Hydrogen to an Iminodisilene

Title: "Twist of a Silicon–Silicon Double Bond: Selective *Anti*-Addition of Hydrogen to an Iminodisilene"

Status: Communication, published online June 22, 2017

Journal: Journal of the American Chemical Society, 2017, 139 (27), 9156–9159.

Publisher: American Chemical Society

DOI: 10.1021/jacs.7b05335

Authors: Daniel Wendel, Tibor Szilvási, Christian Jandl, Shigeyoshi Inoue, Bernhard Rieger[a]

Content: The electronic structure and the chemistry of disilenes, the dimers of silylenes, is well-understood and it is not without reason that they belong to the most investigated low-valent silicon compounds with a plethora of reported compounds. Yet, in comparison to their lighter homologues, alkenes, where this transformation is omnipresent, one of the most fundamental reactions – a hydrogenation of a Si=Si bond remained unknown. This contribution finally contributes to this matter and describes the isolation of a (Z)-imino(silyl)disilene possessing unique electronic and structural properties. In greater detail, the disilene features a highly *trans*-bent and twisted geometry and the longest Si=Si double bond reported to date which, according to DFT calculations, is best described as very weak double donor–acceptor bond. The remarkable properties of this product were used to achieve the first demonstration of hydrogen activation by a multiply bonded silicon compound under ambient conditions (1 bar, r.t.). Excitingly, in-depth studies revealed further that in strong contrast to the hydrogenation of alkenes, which without exception proceed *via syn*-addition to the respective *cis*-product, for the silicon analogue exclusively the *trans*-isomer was formed. The observed odd stereospecificity was rationalized mechanistically by a facilitated concerted *anti*-addition of H_2 due to the twisted geometry of the disilene – a mechanistic pathway that is hardly imaginable for C=C bonds and once again illustrates the immense differences in reactivity between carbon and silicon counterparts.

[a] D. Wendel planned and executed all experiments and wrote the manuscript. T. Szilvási designed and performed the theoretical analyses and contributed with fruitful mental input. C. Jandl conducted all SC XRD-measurements and managed the processing of the respective data. All work was performed under the supervision of B. Rieger and S. Inoue.

JACS
JOURNAL OF THE AMERICAN CHEMICAL SOCIETY
Communication
pubs.acs.org/JACS

Twist of a Silicon–Silicon Double Bond: Selective *Anti*-Addition of Hydrogen to an Iminodisilene

Daniel Wendel,[†] Tibor Szilvási,[§] Christian Jandl,[‡] Shigeyoshi Inoue,*[,∥] and Bernhard Rieger*[,†]

[†]WACKER-Chair of Macromolecular Chemistry, [∥]WACKER-Institute of Silicon Chemistry, [‡]Catalysis Research Center, Technische Universität München, Lichtenbergstraße 4, 85748 Garching bei München, Germany

[§]Department of Chemical and Biological Engineering, University of Wisconsin–Madison, 1415 Engineering Drive, Madison, Wisconsin 53706-1607, United States

Supporting Information

ABSTRACT: Hydrogenation of alkenes with C=C bonds is a ubiquitous reaction in organic chemistry. However, this transformation remains unknown for heavier counterparts, disilenes with Si=Si bonds. Here we report the isolation of (*Z*)-diiminodisilyldisilene **2** featuring a highly *trans*-bent and twisted structure and the longest silicon–silicon double bond reported to date. *In silico* studies suggested that the Si=Si bond in **2** is described as very weak double donor–acceptor bond. We utilized the remarkable electronic and structural features of this product to achieve the first demonstration of hydrogen activation by a multiply bonded silicon compound under ambient conditions. Interestingly, NMR and X-ray analysis gave exclusively racemic (*RR*/*SS*)-1,2-disilane **3a**, indicating a stereospecific *trans*-hydrogenation of the Si=Si bond. In-depth calculations revealed that in strong contrast to the reactivity of C=C bonds, a concerted *anti*-addition pathway was favored due to the twisted structure of **2**.

Hydrogenation of olefins, one of the most fundamental reactions in organic synthesis, is frequently used by chemists from both academia and industry. Large-scale processes such as petrochemical saturation of olefins and aromatics, manufacturing of pharmaceuticals and vitamins and processing of vegetable oils for the food industry, rely heavily on molecular hydrogen as a reducing agent. To activate this strongly bound, nonpolar dihydrogen molecule, the general use of transition metal catalysts (e.g., Pd and Rh) is unavoidable.[1] Disilenes, the heavier congeners of alkenes, feature increased reactivity because of their small HOMO–LUMO gap (~3 eV) and the biradical character of their π-bond.[2] Ever since the landmark discovery of the first stable disilene ($Mes_2Si{=}SiMes_2$; Mes = 2,4,6-Me_3-C_6H_2) in 1981 by West et al.,[3] considerable attention has been paid to elucidating the molecular structure, bonding nature and reactivity of unsaturated silicon compounds.[2] To date, a plethora of disilene derivatives containing silicon–silicon double bonds and even triple bonds have been isolated, characterized and intensively studied.[2a,4] In 2005, Power et al. opened a new chapter in modern main group chemistry by exemplifying the analogy between classical transition metal complexes and low-valent main group compounds in small molecule activation.[5] His group reported that unlike conventional alkynes, a digermyne (ArGe≡GeAr; Ar = C_6H_3-2,6-$(Dipp)_2$, Dipp = 2,6-*i*-$Pr_2C_6H_3$) readily reacts with molecular hydrogen without any catalyst under mild conditions (25 °C, 1 bar) to give a mixture of mono-, di- and trihydrogenation products.[6] In the past decade this concept has not only been applied to distannynes[7] but several hydrogen activations initiated by main group compounds have been discovered. For instance carbenes[8] and heavier tetrylenes[9] are capable to easily split dihydrogen under ambient conditions, and even the flourishing field of frustrated Lewis pairs (FLP) that generated significant applications in main group catalysis originated in a reversible hydrogen reaction.[10] Despite these achievements, hydrogenation of multiply bonded silicon-bearing compounds has proven to be a difficult endeavor.

In recent work, we have utilized *N*-heterocyclic imines (NHI) for the stabilization of unique structural motifs of group 13 and 14 main group elements including silicon.[11] Here we extended this strategy to synthesize and characterize a novel heteroatom-substituted disilene, **2** (Scheme 1).

By combining bulky NHI and hypersilyl groups, we achieved an unusually twisted and bent Si=Si bonding geometry, which is discussed in detail and analyzed by quantum chemical

Scheme 1. (A) Preparation of Iminosilyldisilene 2 and Depiction of Related Compounds. (B) *Trans*-Hydrogenation of the Si=Si Bond of 2

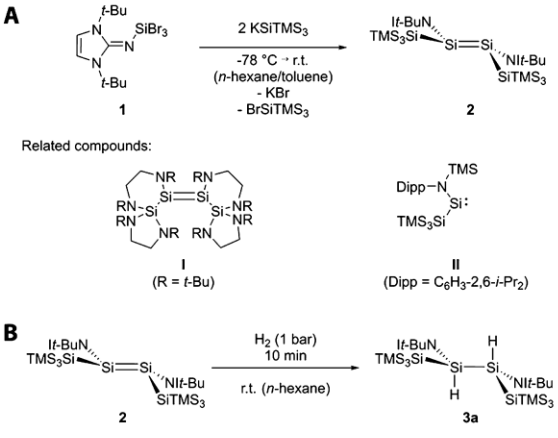

Received: May 24, 2017
Published: June 22, 2017

DOI: 10.1021/jacs.7b05335
J. Am. Chem. Soc. 2017, 139, 9156–9159

calculations. The outstanding properties of **2** were evidenced by its unique reactivity toward dihydrogen under mild conditions. Inspired by the elegant one-pot method that Jones and Aldridge et al. used to prepare two acyclic boryl-[9d] and silylaminosilylenes,[9b] we treated one equivalent of bis(*tert*-butyl)imidazolin-2-iminotribromosilane I*t*-BuNSiBr$_3$ **1** in toluene with two equivalents of KSiTMS$_3$ in *n*-hexane at −78 °C to produce an instant dark-purple solution and precipitate KBr (Scheme 1A). Instead of the acyclic iminosilylsilylene, the dimeric product **2** was formed quantitatively and isolated in 64% yield as dark-purple crystals.

The ^{29}Si NMR spectrum of **2** (Figure S4) displayed a signal at 72.0 ppm for both central silicon atoms; this value is in the range reported for typical disilenes (155−50 ppm).[2f] However, because of the strong donor qualities of the imino group, the signal is high field shifted in comparison with that of the related cyclic (*Z*)-diaminodisilyldisilene **I** by West et al. (119.5 ppm).[12] Structural analysis of **2** (Figure 1A) confirmed the (*Z*)-

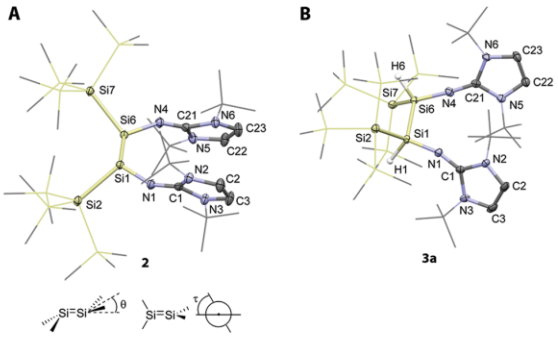

Figure 1. Molecular structures of **2** and **3a**. Hydrogen atoms are omitted for clarity and TMS- and *t*-Bu-groups are simplified as wireframes. Displacement ellipsoids are set at 50% probability level. Selected bond lengths (Å) and angles (deg): (A) **2** Si1−Si6 2.3124(7), Si1−Si2 2.3991(7), Si6−Si7 2.3886(7), Si1−N1 1.672(2), Si6−N4 1.681(2), N1−C1 1.281(2), N4−C21 1.280(2), N1−Si1−Si2 105.16(6), N4−Si6−Si7 106.78(6), Si2−Si1−Si6−Si7 78.12(4), N1−Si1−Si6−N4−22.35(9). Definition of bent (θ) and twist (τ) angles (B) **3a** Si1−Si6 2.4142(7), Si1−Si2 2.3931(9), Si6−Si7 2.4144(7), Si1−N1 1.674(2), Si6−N4 1.661(2), N1−C1 1.275(3), N4−C21 1.267(3), Si1−H1 1.45(2), Si6−H6 1.43(2), N1−Si1−Si2 110.19(6), N4−Si6−Si7 110.98(6).

diiminodisilyldisilene, which is in line with theoretical calculations that predict that the (*E*)-isomer is 3.4 kcal/mol less stable. The Si═Si bond observed (2.3124(7) Å) was extremely elongated, well exceeding the length of typical double bonds of disilenes (2.14−2.29 Å).[2f] In fact, the Si═Si bond found even approached the first dative Si—Si bond (2.324(2) Å) of the base-stabilized disilene adduct $Me_2EtN \rightarrow SiCl_2 \rightarrow Si(SiCl_3)_2$ as reported by Holthausen et al.[13]

Disilene **2** exhibits a strongly *trans*-bent structure with significant pyramidalization at both central silicon atoms (bent angles θ(Si1) = 37.86° and θ(Si6) = 39.03°) and a highly twisted geometry around the central Si═Si bond (twist angle τ = 23.1°) (see Figure 1 for definition of bent and twist angle). Interestingly, both NHI ligands are nearly eclipsed, forming a torsion angle of merely −22.35(9)° (ω(N1−Si1−Si6−N4)), and hypersilyl groups are intensively staggered (ω(Si2−Si1−Si6−Si7) = 78.12(4)°). All of the structural characteristics are comparable with those of **I** (θ = 32.3° and 33.8°, τ = 25.1°) including the longest Si═Si bond (2.2890(14) Å) reported to date.[12] Disilene **I** was formed by tetramerization of the corresponding diaminosilylene *via* insertion of one silylene into the Si—N bond of another, followed by subsequent dimerization. In fact, time-dependent NMR and UV−vis data revealed a dynamic equilibrium between diaminodisilyldisilene and diaminosilylene. Therefore, a solution of **2** in C_7D_8 was monitored over 2 weeks at room temperature via ^{29}Si NMR spectroscopy. The spectra obtained showed full degradation of **2** to a variety of uncharacterized products, and no signal of an acyclic iminosilylsilylene I*t*-BuNSi(II)SiTMS$_3$ with an expected ^{29}Si NMR shift in the range of aminosilylsilylene **II** (438.2/467.5 ppm) was found.[9b] This result is in line with variable temperature (VT) UV−vis studies of **2** (Figure S7) indicating a dissociation and decomposition process only at elevated temperatures and no distinguishable dynamic equilibrium. To obtain further insights into the bonding properties of **2**, we performed density functional theory (DFT) calculations. The HOMO and LUMO of **2** (Chart 1A) are mainly located on the Si═Si moiety and exhibit significant lone-pair character.

Chart 1. (A) DFT-Calculated HOMO *E* = −3.83 eV and LUMO *E* = −1.16 eV of 2[a]; (B) Resonance Structure 2′ Revealing a Double Donor−Acceptor Bond According to Natural Resonance Theory (NRT) Analysis

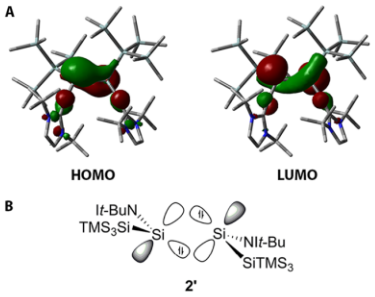

[a]Hydrogens are Omitted for Clarity.

The two frontier orbitals are separated by only 2.67 eV, which indicates the high reactivity of the double bond. The corresponding singlet−triplet energy gap (22.8 kcal/mol) is relatively small; this energy gap may be accessible at room temperature but is still higher in comparison to the energy necessary (7.3 kcal/mol) to excite highly twisted tetrakis(di*tert*-butylmethylsilyl)disilene to the triplet state by rotation around the Si═Si bond.[14] Natural bond orbital analysis suggest bonding orbitals for the Si═Si bond, although only a weak double bond can be considered due to the low orbital occupancy (1.81e) of the π bond. This finding is in full agreement with the calculated Wiberg Bond index of the Si═Si bond (1.41) in **2** and its experimentally observed elongated bond length. NRT analysis (Chart 1B) revealed the bonding nature of Si═Si to be best described as a double donor−acceptor bond, as shown in **2′**, which corresponds well to the results of previous quantum chemical investigations conducted on related tetraaminodisilenes.[15] Specifically, the bonding situation of **2** is similar to the calculated structure of highly *trans*-bent (θ = 42.6°) and twisted (τ = 55.5°) (*i*-Pr$_2$N)$_2$Si═Si(N*i*-Pr$_2$)$_2$, which as well exhibits a surprisingly long Si═Si bond (2.472 Å), and therefore is better described as a very weak donor−acceptor adduct of two silylenes rather than a typical disilene.[15c]

DOI: 10.1021/jacs.7b05335
J. Am. Chem. Soc. 2017, 139, 9156−9159

Motivated by the unique bonding feature of **2**, we were interested in whether the Si═Si bond shows any reactivity toward molecular hydrogen. Indeed, the exposure of a solution of disilene **2** in *n*-hexane to hydrogen (1 bar) at room temperature led to full decolorization of its characteristic purple color within 10 min. Subsequent NMR analysis confirmed the complete conversion of **2** to 1,2-disilane (**3a**), which was isolated as a colorless solid in 95% yield (Scheme 1B). The ^{1}H NMR spectrum of **3a** (Figure S8) displayed a low field shifted signal at 6.17 ppm for both silicon-bound protons with a ^1J (Si−H) = 146 Hz; this value is distinctly smaller than the coupling constant of the monomeric hydrogen activation product of **II** (^1J (Si−H) = 195 Hz).[9b] Proton-coupled ^{29}Si NMR spectroscopy (Figure S10) showed a doublet at −62.4 ppm for both central silicon atoms with the identical coupling constant, thus pointing to a dimeric structure. To confirm that hydrogen is the reactive agent of **2**, the reaction was repeated with deuterium gas to produce the deuterated analog **3b** (see SI). X-ray analysis of **3a** (Figure 1B) clearly showed elongation of the central Si−Si bond by *ca.* 0.1 to 2.4142(7) Å, which is in the range of a typical Si−Si single bond.[16] The centrosymmetric structure elucidated exclusive *trans*-addition to the (*Z*)-isomer of **2** to give a racemic mixture (*RR*/*SS*) of **3a**. NMR spectroscopy did not indicate the presence of *meso*-**3a** (*RS*/*SR*) as well, thereby suggesting a stereospecific reaction. To exclude explicitly a potential mechanism involving dissociation of **2** to I*t*-BuNSi(II)SiTMS$_3$ followed by H_2 activation and Si−H insertion to give **3a**, we monitored the hydrogenation reaction at −20 °C (toluene-d_8, 1 bar) via ^{1}H NMR spectroscopy. At this low temperature, the reaction time to reach full conversion to *racemic*-**3a** was prolonged to approximately 4 h. At all times, no intermediary species (I*t*-BuNSi(II)SiTMS$_3$ or monomeric silane I*t*-BuNSiH$_2$SiTMS$_3$) were detectable. In analogy to the room temperature experiment, no *meso*-**3a** was observed. In a second NMR experiment, the reaction of **2** (1 equiv, C_6D_6) with *t*-Bu$_2$SiH$_2$ (2 equiv) was carried out to re-enact an insertion of a potential dissociated I*t*-BuNSi(II)SiTMS$_3$ into a Si—H bond of a comparable R$_2$SiH$_2$ compound. Monitoring this reaction via ^{1}H NMR spectroscopy did not show any conversion to the respective disilane I*t*-BuNSiTMS$_3$HSiSiH*t*-Bu$_2$ even after 1 day at room temperature. Both experimental results clearly point to a concerted hydrogenation of **2**, which was further supported by a relatively high 19.2 kcal/mol theoretical energy barrier of H_2 insertion to I*t*-BuNSiH$_2$SiTMS$_3$.[17]

Direct hydrogenation of olefinic C═C bonds with molecular hydrogen exclusively proceed via *syn*-addition to the corresponding *cis*-product (Scheme 2A) without exception. We studied the reaction mechanism of **2** and the parent disilene (Si$_2$H$_4$) with molecular hydrogen using DFT and ab initio methods (see SI). *Syn*-addition for C═C double bonds is well-established in the literature from both the theoretical and experimental point of view.[1] Theoretical work on analogous Si═Si bonds suggest a similar mechanism.[18] *Syn*-addition to planar alkenes (Scheme 2A) requires slight reorganization of the ligands to reach the activation barrier. However, disilenes are not planar due to the small $\pi-\pi^*$ energy gap of the planar disilene, which induces a second-order Jahn−Teller distortion resulting in a *trans*-bent structure (Scheme 2B).[2c] Therefore, one silicon center must first be planarized to achieve a *syn*-addition transition state (TS) and then inverted to the final *cis*-product. Although planarization is not an energetically demanding process for the parent disilene molecule (Si$_2$H$_4$) and requires only 0.5 kcal/mol, planarization of a silicon center in **2** demands a substantial energy investment (17.7 kcal/mol).

Scheme 2. Mechanisms of 1,2-Hydrogen Addition to C═C and Si═Si Double Bonds[a]

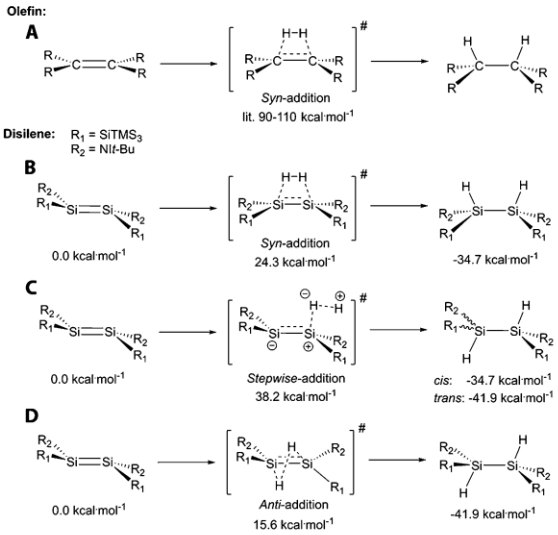

[a](A) General *Syn*-Addition of H_2 to C═C Double Bonds.[18] R Groups Refer to Arbitrary Ligands. (B) Calculated *Syn*-Addition of H_2 to **2**. (C) Calculated *Stepwise*-Addition of H_2 to **2**. (D) Calculated *Anti*-Addition of H_2 to **2**.

This is because of the steric congestion induced by the very bulky ligands of the molecule. This large initial energy penalty immediately disfavors classic *syn*-addition for **2**. The *syn*-addition barrier presents an associated energy of 24.3 kcal/mol (Scheme 2B). Power et al. previously reported that multiply bonded Ge and Sn compounds can activate H_2 in a manner similar to that promoted by transition metals.[5b,6] Thus, we sought to determine a stepwise reaction mechanism that is logically similar to these authors' suggestion (Scheme 2C). Because the interaction of the σ-orbital of H_2 with the LUMO of **2** is dominant in the transition state (TS), the process is more ionic than Powers' mechanism. In the TS, one Si−H bond is formed, and another proton migrates to a second Si atom to afford a *cis*- (i.e., *meso*-**3a**) or *trans*-product (i.e., *racemic*-**3a**). We note that *racemic*-**3a** is more stable than *meso*-**3a** by 7.2 kcal/mol as consequence of steric effects. This large energy difference appears to be adequate to yield *racemic*-**3a** exclusively in our experiments. However, because of the large activation barrier (38.2 kcal/mol), this mechanism may not be viable. The twisted structure of **2** suggests that rotation of the ligands occurs relatively freely and may result in unexpected direct *anti*-addition (Scheme 2D). Calculations revealed that this mechanism presents a low energy barrier (15.6 kcal/mol), thus corroborating the experimentally observed mild H_2 activation. In the TS, the σ-orbital of H_2 interacts with the LUMO of **2**. Calculations involving the parent disilene (Si$_2$H$_4$) showed that the interaction of the LUMO of **2** (Chart 1A) with hydrogen occurs because of its twisted structure (see SI). The σ^*-orbital of H_2 and the HOMO of **2** also interact because of the staggered structure of the latter, thereby resulting in a homolytic H_2 cleavage. Additional calculations showed further that the staggered ligand structure can be responsible for the low barrier

DOI: 10.1021/jacs.7b05335
J. Am. Chem. Soc. 2017, 139, 9156−9159

as it reduces the stability of the Si=Si structure and preorganizes the Si=Si bond for concerted *anti*-addition (see SI).

In summary, we synthesized and fully characterized the first example of an iminodisilene **2** with a highly *trans*-bent and twisted geometry including the longest reported Si=Si bond. However, theoretical calculations of **2** suggested that this bond is better described as double donor–acceptor bond between two silylene fragments. This unique bonding feature was used to demonstrate the first hydrogen activation by a multiply bonded silicon compound under mild conditions. As confirmed by NMR and X-ray analysis, solely racemic (*RR*/*SS*)-1,2-disilane **3a** was formed in this reaction, indicating a stereospecific *trans*-hydrogenation of the Si=Si bond. To elucidate the underlying mechanism, a detailed theoretical study was carried out, which revealed that the steric congestion of the bulky ligands of **2** induced a twisted Si=Si bond and prearranged the compound for facile homolytic *anti*-addition of H_2.

■ ASSOCIATED CONTENT

Supporting Information

The Supporting Information is available free of charge on the ACS Publications website at DOI: 10.1021/jacs.7b05335.

Experimental procedures (PDF)
Crystallographic data for **1**, **2** and **3a** (CIF)

■ AUTHOR INFORMATION

Corresponding Authors

*rieger@tum.de
*s.inoue@tum.de

ORCID

Tibor Szilvási: 0000-0002-4218-1570
Shigeyoshi Inoue: 0000-0001-6685-6352
Bernhard Rieger: 0000-0002-0023-884X

Notes

The authors declare no competing financial interest.

■ ACKNOWLEDGMENTS

We are grateful to WACKER Chemie AG for continued financial support. We thank Dominik Reiter, Martin Machat and Philipp Pahl for revising the paper. We thank Dr. Alexander Pöthig for his advice pertaining to crystallography and Fabian Linsenmann and Manuel Kaspar for IR and (VT) UV–vis measurements.

■ REFERENCES

(1) Vries, J. G.; Elsevier, C. J. *The Handbook of Homogeneous Hydrogenation*; Wiley-VCH: Weinheim, 2008.

(2) Recent reviews on disilene chemistry: (a) Präsang, C.; Scheschkewitz, D. *Chem. Soc. Rev.* **2016**, *45*, 900–921. (b) Iwamoto, T.; Ishida, S. In *Functional Molecular Silicon Compounds II: Low Oxidation States*, Scheschkewitz, D., Ed.; Springer International Publishing: Cham, 2014; pp 125–202. (c) Kira, M. *Proc. Jpn. Acad., Ser. B* **2012**, *88*, 167–191. (d) Kira, M.; Iwamoto, T. *Adv. Organomet. Chem.* **2006**, *54*, 73–148. (e) Weidenbruch, M. *J. Organomet. Chem.* **2002**, *646*, 39–52. (f) Weidenbruch, M. In *The Chemistry of Organic Silicon Compounds*, Rappoport, Z., Apeloig, Y., Eds.; John Wiley & Sons: Chichester, U. K., 2001; Vol. 3, pp 391–428. (g) Power, P. P. *Chem. Rev.* **1999**, *99*, 3463–3504. (h) Okazaki, R.; West, R. *Adv. Organomet. Chem.* **1996**, *39*, 231–273.

(3) (a) West, R.; Fink, M. J.; Michl, J. *Science* **1981**, *214*, 1343–1344. (b) Pioneering work on *trans*-bent distannene by Lappert et al.: Goldberg, D. E.; Harris, D. H.; Lappert, M. F.; Thomas, K. M. *J. Chem. Soc., Chem. Commun.* **1976**, 261–262.

(4) Selected examples of reported Si–Si triple bonds: (a) Ishida, S.; Sugawara, R.; Misawa, Y.; Iwamoto, T. *Angew. Chem., Int. Ed.* **2013**, *52*, 12869–12873. (b) Murata, Y.; Ichinohe, M.; Sekiguchi, A. *J. Am. Chem. Soc.* **2010**, *132*, 16768–16770. (c) Sasamori, T.; Hironaka, K.; Sugiyama, Y.; Takagi, N.; Nagase, S.; Hosoi, Y.; Furukawa, Y.; Tokitoh, N. *J. Am. Chem. Soc.* **2008**, *130*, 13856–13857. (d) Jung, Y.; Brynda, M.; Power, P. P.; Head-Gordon, M. *J. Am. Chem. Soc.* **2006**, *128*, 7185–7192. (e) Sekiguchi, A.; Kinjo, R.; Ichinohe, M. *Science* **2004**, *305*, 1755–1757. (f) Wiberg, N.; Vasisht, S. K.; Fischer, G.; Mayer, P. *Z. Anorg. Allg. Chem.* **2004**, *630*, 1823–1828.

(5) (a) Yadav, S.; Saha, S.; Sen, S. S. *ChemCatChem* **2016**, *8*, 486–501. (b) Power, P. P. *Nature* **2010**, *463*, 171–177.

(6) Spikes, G. H.; Fettinger, J. C.; Power, P. P. *J. Am. Chem. Soc.* **2005**, *127*, 12232–12233.

(7) (a) Hadlington, T. J.; Hermann, M.; Li, J.; Frenking, G.; Jones, C. *Angew. Chem., Int. Ed.* **2013**, *52*, 10199–10203. (b) Li, J.; Schenk, C.; Goedecke, C.; Frenking, G.; Jones, C. *J. Am. Chem. Soc.* **2011**, *133*, 18622–18625. (c) Peng, Y.; Brynda, M.; Ellis, B. D.; Fettinger, J. C.; Rivard, E.; Power, P. P. *Chem. Commun.* **2008**, 6042–6044.

(8) Frey, G. D.; Lavallo, V.; Donnadieu, B.; Schoeller, W. W.; Bertrand, G. *Science* **2007**, *316*, 439–441.

(9) (a) Protchenko, A. V.; Bates, J. I.; Saleh, L. M. A.; Blake, M. P.; Schwarz, A. D.; Kolychev, E. L.; Thompson, A. L.; Jones, C.; Mountford, P.; Aldridge, S. *J. Am. Chem. Soc.* **2016**, *138*, 4555–4564. (b) Protchenko, A. V.; Schwarz, A. D.; Blake, M. P.; Jones, C.; Kaltsoyannis, N.; Mountford, P.; Aldridge, S. *Angew. Chem., Int. Ed.* **2013**, *52*, 568–571. (c) Filippou, A. C.; Baars, B.; Chernov, O.; Lebedev, Y. N.; Schnakenburg, G. *Angew. Chem., Int. Ed.* **2014**, *53*, 565–570. (d) Protchenko, A. V.; Birjkumar, K. H.; Dange, D.; Schwarz, A. D.; Vidovic, D.; Jones, C.; Kaltsoyannis, N.; Mountford, P.; Aldridge, S. *J. Am. Chem. Soc.* **2012**, *134*, 6500–6503. (e) Peng, Y.; Guo, J.-D.; Ellis, B. D.; Zhu, Z.; Fettinger, J. C.; Nagase, S.; Power, P. P. *J. Am. Chem. Soc.* **2009**, *131*, 16272–16282. (f) Peng, Y.; Ellis, B. D.; Wang, X.; Power, P. P. *J. Am. Chem. Soc.* **2008**, *130*, 12268–12269.

(10) (a) Stephan, D. W. *Acc. Chem. Res.* **2015**, *48*, 306–316. (b) Stephan, D. W.; Erker, G. *Angew. Chem., Int. Ed.* **2015**, *54*, 6400–6441. (c) Stephan, D. W. *J. Am. Chem. Soc.* **2015**, *137*, 10018–10032. (d) Welch, G. C.; San Juan, R. R.; Masuda, J. D.; Stephan, D. W. *Science* **2006**, *314*, 1124–1126.

(11) (a) Wendel, D.; Porzelt, A.; Herz, F. A. D.; Sarkar, D.; Jandl, C.; Inoue, S.; Rieger, B. *J. Am. Chem. Soc.* **2017**, *139*, 8134–8137. (b) Ochiai, T.; Inoue, S. *RSC Adv.* **2017**, *7*, 801–804. (c) Bag, P.; Ahmad, S. U.; Inoue, S. *Bull. Chem. Soc. Jpn.* **2017**, *90*, 255–271. (d) Ochiai, T.; Franz, D.; Inoue, S. *Chem. Soc. Rev.* **2016**, *45*, 6327–6344. (e) Ochiai, T.; Szilvási, T.; Inoue, S. *Molecules* **2016**, *21*, 1155–1167. (f) Inoue, S.; Leszczynska, K. *Angew. Chem., Int. Ed.* **2012**, *51*, 8589–8593.

(12) Schmedake, T. A.; Haaf, M.; Apeloig, Y.; Müller, T.; Bukalov, S.; West, R. *J. Am. Chem. Soc.* **1999**, *121*, 9479–9480.

(13) Schweizer, J. I.; Scheibel, M. G.; Diefenbach, M.; Neumeyer, F.; Würtele, C.; Kulminskaya, N.; Linser, R.; Auner, N.; Schneider, S.; Holthausen, M. C. *Angew. Chem., Int. Ed.* **2016**, *55*, 1782–1786.

(14) (a) Kostenko, A.; Tumanskii, B.; Karni, M.; Inoue, S.; Ichinohe, M.; Sekiguchi, A.; Apeloig, Y. *Angew. Chem., Int. Ed.* **2015**, *54*, 12144–12148. (b) Sekiguchi, A.; Inoue, S.; Ichinohe, M.; Arai, Y. *J. Am. Chem. Soc.* **2004**, *126*, 9626–9629.

(15) (a) Müller, T.; Apeloig, Y. *J. Am. Chem. Soc.* **2002**, *124*, 3457–3460. (b) Takahashi, M.; Kira, M.; Sakamoto, K.; Müller, T.; Apeloig, Y. *J. Comput. Chem.* **2001**, *22*, 1536–1541. (c) Takahashi, M.; Tsutsui, S.; Sakamoto, K.; Kira, M.; Müller, T.; Apeloig, Y. *J. Am. Chem. Soc.* **2001**, *123*, 347–348. (d) Tsutsui, S.; Sakamoto, K.; Kira, M. *J. Am. Chem. Soc.* **1998**, *120*, 9955–9956.

(16) Krempner, C.; Chtchian, S.; Reinke, H. *Inorg. Chim. Acta* **2004**, *357*, 3733–3738.

(17) Energetics of silylene insertion reactions: Nyiri, K.; Szilvasi, T.; Veszpremi, T. *Dalton Trans.* **2010**, *39*, 9347–9352.

(18) Sakai, S. *J. Phys. Chem. A* **1997**, *101*, 1140–1146.

DOI: 10.1021/jacs.7b05335
J. Am. Chem. Soc. 2017, 139, 9156–9159

8. From Si(II) to Si(IV) and Back: Reversible Intramolecular Carbon–Carbon Bond Activation by an Acyclic Iminosilylene

Title: "From Si(II) to Si(IV) and Back: Reversible Intramolecular Carbon–Carbon Bond Activation by an Acyclic Iminosilylene"

Status: Communication, published online June 6, 2017

Journal: Journal of the American Chemical Society, 2017, 139 (24), 8134–8137.

Publisher: American Chemical Society

DOI: 10.1021/jacs.7b05136

Authors: Daniel Wendel, Amelie Porzelt, Fabian A. D. Herz, Debotra Sarkar, Christian Jandl, Shigeyoshi Inoue, Bernhard Rieger[a]

Content: The reports of room temperature stable two-coordinate acyclic silylenes are still limited to very few examples. Likewise, the *N*-heterocyclic imino ligand (NHI), despite its excellent π-donor properties, has not yet fully accomplished the transition from implementations in low-valent germanium and tin compounds to respective silicon congeners. By picking up both points, this contribution, which represents the main task of this thesis, aimed to establish a new, independent acyclic silylene utilizing the NHI ligand and testing its reactivity towards small molecules. In the planned synthesis route, indeed, an extremely reactive acyclic imino(silyl)silylene was identified at –78 °C using (LT) UV-vis and NMR techniques. However, above this temperature, the silylene rapidly underwent an intramolecular insertion into a C=C bond of its aromatic ligand framework to form a silacycloheptatriene ring (silepin). As confirmed by X-ray analysis, the newly formed Si–C bonds of the silepin were quite labile and facilitated the reductive elimination back to Si(II) in combination with the driving force of rearomatization. This idea was verified by (HT) UV−vis experiments, additional DFT calculations and isolation of a silylene−borane adduct upon addition of BCF. The concept of reversibility was further tested by directly using silepin as a "masked" silylene in the activation of small molecules. Here, the targeted first monomeric, four-coordinate silicon carbonate complex was isolated and fully characterized in the reaction with carbon dioxide. In addition, the activation of ethylene and molecular hydrogen was demonstrated under mild conditions. In total, our work gives the first proof that beside the established oxidative addition of a silylene species, the essential concept of a facile reductive elimination from Si(IV) back to Si(II) is in fact viable – a result that may soon open the door to the ultimate goal of silylene-based metal-free catalysis.

[a]D. Wendel planned and executed all experiments and wrote the manuscript. A. Porzelt designed and performed the theoretical analyses, F. A. D. Herz and D. Sarkar contributed with fruitful mental input. C. Jandl conducted all SC XRD-measurements and managed the processing of the respective data. All work was performed under the supervision of B. Rieger and S. Inoue.

JACS
JOURNAL OF THE AMERICAN CHEMICAL SOCIETY
Communication
pubs.acs.org/JACS

From Si(II) to Si(IV) and Back: Reversible Intramolecular Carbon–Carbon Bond Activation by an Acyclic Iminosilylene

Daniel Wendel,[†] Amelie Porzelt,[‖] Fabian A. D. Herz,[†] Debotra Sarkar,[‖] Christian Jandl,[‡] Shigeyoshi Inoue,*[,‖] and Bernhard Rieger*[,†]

[†]WACKER-Chair of Macromolecular Chemistry, [‖]WACKER-Institute of Silicon Chemistry, [‡]Catalysis Research Center, Technische Universität München, Lichtenbergstraße 4, 85748 Garching bei München, Germany

Supporting Information

ABSTRACT: Reversibility is fundamental for transition metal catalysis, but equally for main group chemistry and especially low-valent silicon compounds, the interplay between oxidative addition and reductive elimination is key for a potential catalytic cycle. Herein, we report a highly reactive acyclic iminosilylsilylene **1**, which readily performs an intramolecular insertion into a C═C bond of its aromatic ligand framework to give silacycloheptatriene (silepin) **2**. UV–vis studies of this Si(IV) compound indicated a facile transformation back to Si(II) at elevated temperatures, further supported by density functional theory calculations and experimentally demonstrated by isolation of a silylene–borane adduct **3** following addition of $B(C_6F_5)_3$. This tendency to undergo reductive elimination was exploited in the investigation of silepin **2** as a synthetic equivalent of silylene in the activation of small molecules. In fact, the first monomeric, four-coordinate silicon carbonate complex **4** was isolated and fully characterized in the reaction with carbon dioxide under mild conditions. Additionally, the exposure of **2** to ethylene or molecular hydrogen gave silirane **5** and Si(IV) dihydride **6**, respectively.

Ever since discovery of decamethylsilicocene $Cp^*_2Si(II)$ in 1986,[1] considerable attention has been paid to explore and elucidate the nature of monomeric low-valent silicon compounds.[2] To date, a plethora of stable silylenes have been isolated and studied. Progress in experimental techniques has even granted synthetic access to acyclic silylenes (Chart 1).[3] These compounds are ideal for selective small molecule activation, due to their coordinative flexibility and reduced HOMO–LUMO gap (~2–4 eV).[2b,4] Both attributes are key to facilitate oxidative addition of targets like NH_3, H_2 or ethylene. Although traditionally these types of activation are associated with *d-block*-metal complexes, acyclic silylenes have proven their potential as transition metal mimics. For instance, oxidative cleavage of the strong σ-bond of dihydrogen was accomplished with silylenes **I**[3c] and **II**.[3d] Further studies show easy splitting of ammonia under mild conditions by **I**[5] and **IV**.[3a] In terms of a potential silylene-based catalytic cycle, this oxidative step is only considered as one substep; far more complex is the regeneration of the Si(II) species via reductive elimination. First approaches toward this goal were accomplished for heavier germanium[6] and tin[5] analogs, but for subvalent silicon compounds this reverse reaction remains challenging. Silylene **III**[7] shows behavior toward ethylene by reversibly binding the olefin in a dissociation equilibrium with the corresponding silirane ring under ambient conditions. The same reversible [2+1]-cycloaddition with ethylene was reported by Baceiredo et al. for a cyclic phosphine-stabilized silylene.[8] In addition, this structure stands out by unprecedented reversible insertions into Si–X (X = H, Cl) and P–H bonds.[9]

Chart 1. Selected Examples of Room Temperature Stable Acyclic Silylenes with Small HOMO–LUMO Gaps (~2–4 eV)

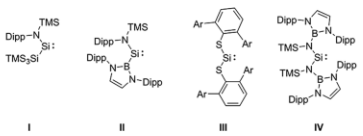

Dipp = C_6H_3-2,6-*i*-Pr_2, Mes = C_6H_2-2,4,6-Me_3, Tripp = C_6H_2-2,4,6-*i*-Pr_3, Ar = Mes, Dipp, Tripp

Recently, we utilized *N*-heterocyclic imino (NHI) ligands for stabilization of low-valent compounds based on group 13 and 14 elements.[10] Herein, we report synthesis of acyclic iminosilylsilylene **1**, which undergoes an intermolecular C═C insertion into its aromatic ligand framework to form room temperature stable silacycloheptatriene (silepin) **2**. Reactivity studies of **2** show this formal Si(IV) compound is easily converted back to Si(II) as a silylene–borane adduct and even acts as "masked" silylene in small molecule activation of carbon dioxide, ethylene and hydrogen.

In analogy to the one-pot method by Jones and Aldridge et al. for the preparation of **I**[3c] and **II**,[3d] we determined Rivard's bis(2,6-diisopropylphenyl)imidazolin-2-iminotribromosilane (IPrN-$SiBr_3$)[11] ideal for our synthetic route. Treatment of 1 equiv of IPrN$SiBr_3$ in toluene with 2 equiv of $KSiTMS_3$ at −78 °C gave a light green solution with precipitation of KBr (Scheme 1). An instant color change to yellow was observed upon warming the solution to room temperature. The ^{1}H NMR spectrum of the crude reaction mixture showed a complicated series of Dipp resonances (Figure S8), similar to those observed for the ligand activation by Rivard et al.,[11] but here the quantitative formation of TMS_3SiBr as side product and distinct signals in the ^{29}Si NMR spectrum (central Si at 16.1 ppm) pointed to a defined product. Yellow crystals of this compound were obtained by crystallization

Received: May 18, 2017
Published: June 6, 2017

DOI: 10.1021/jacs.7b05136
J. Am. Chem. Soc. 2017, 139, 8134–8137

Scheme 1. Reaction Sequence of the Preparation of Silepin 2 via *in Situ* Generated Iminosilylsilylene 1

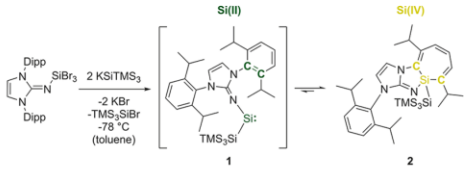

in *n*-hexane (−35 °C, 3 months), but due to its similar solubility to TMS_3SiBr only in low yields (6%).

Subsequently, X-ray analysis revealed the structure of silepin **2**, formed by intramolecular insertion of the *in situ* generated iminosilylsilylene **1** into a C═C bond of one of the Dipp groups (Figure 1). To verify this mechanism, we performed ^{29}Si NMR

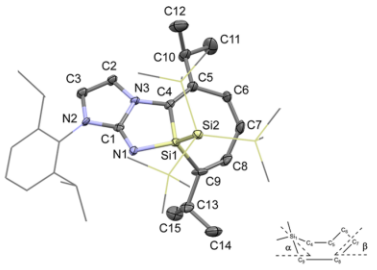

Figure 1. Molecular structure of **2** in the solid state with ellipsoids set at the 50% probability level (one out of two molecules in the asymmetric unit). For clarity, hydrogen atoms and cocrystallized solvent molecules are omitted and TMS as well as Dipp groups are simplified as wireframes. Selected bond lengths (Å) and angles (deg): Si1−C4 1.891(6), Si1−C9 1.876(6), C8−C9 1.333(9), C7−C8 1.433(9), C6−C7 1.354(9), C5−C6 1.452(8), C4−C5 1.352(7), Si1−N1 1.748(5), Si1−Si2 2.342(4), N1−C1 1.279(6), N1−Si1−Si2 109.37(17), C4−Si1−C9 105.3(3), α (C4−Si1−C9 and C4−C5−C8−C9) 41.06, β (C5−C6−C7−C8 and C4−C5−C8−C9) 31.70.

experiments in toluene-d_8 at −78 °C. The initial light green solution gave a characteristic signal at 300.0 ppm for the central silicon atom of **1**, which rapidly vanished upon warming the solution (Figure S2). Even at −78 °C, a further reaction to **2** was detectable. As expected, the shift of **1** lies between the chemical shift of **IV** (204.6 ppm)[3a] or West's $[(SiMe_3)_2N]_2Si(II)$ (223.9 ppm)[12] and **II** (439.7 ppm).[3d] The high-field shift of **1** compared to structural analog **I** (438.2/467.5 ppm)[3c] illustrates the stronger donor qualities of the NHI ligand. For further characterization, we performed variable temperature (VT) UV−vis measurements from −70 to +20 °C with a concentrated reaction solution. A characteristic low intensity band at 612 nm was observed at −70 °C, which, analogously to the NMR study, disappeared upon warming up the solution (Figure S3). Similarly, monitoring a reaction mixture of **2**/TMS_3SiBr from room temperature to 100 °C displayed reversible formation of the same characteristic signal of **1** (617 nm) at elevated temperatures (100 °C), pointing to an equilibrium between silepin and silylene at higher temperatures (Figure S4). To support this and elucidate the mechanism of silepin formation, we performed density functional theory (DFT) calculations (B3LYP/6-311+G(d,p)) with a reduced iminosilylsilylene **1′** (replacement of Dipp substituents with phenyl groups). We determined in fact silylene **1′** is 17.7 kJ/mol lower in energy than silepin **2′** (Figure S26), further suggesting a thermally accessible interconversion. The calculated singlet−triplet energy of **1′** (103.9 kJ/mol) is small, in the range of **I** (103.7 kJ/mol),[3c] and may explain its reactivity. There are two reported examples of insertion of silylenes into aromatic C═C bonds.[13] Here, either a transient silylene is generated at elevated temperatures (>70 °C)[13e] or the Si(II) center is photochemically elevated to an excited state.[13c] Both silylenes react intermolecularly with aromatic compounds, extending the reaction or irradiation times to several hours.[13a−e] As expected due to the close proximity, the first intramolecular ring closure to **2** is much faster and proceeds even at low temperatures. The seven-membered ring system of **2** (Figure 1) is in a typical folded boat conformation with a C4−Si1−C9 angle of 105.3(3)° and angles between the planes of 41.06° (α) and 31.70° (β), which are in the range of reported silepins.[14] However, the silicon−carbon lengths (Si1−C4 = 1.891(6) Å and Si−C9 = 1.876(6) Å) are slightly elongated (cf. 1.82−1.88 Å in literature),[14] presumably a result of the sterically encumbered ligands. This structural feature and the obtained theoretical data aroused our interest in whether a facilitated bond breakage under regeneration of a Si(II) species might be feasible. Recently, Müller et al. introduced a new synthetic approach to NHC-stabilized silylenes by using NHCs to cleave selectively elongated Si−C bonds of 7-silanorbornadienes.[15] We pursued the idea a strong Lewis acid such as $B(C_6F_5)$ (BCF) may break the Si−C bonds of the silepin ring and form the corresponding silylene−borane adduct.[16]

Addition of 1 equiv of BCF to a mixture of **2**/TMS_3SiBr led to rearomatization and full conversion into the respective iminosilylene−BCF adduct **3** within 20 min (Scheme 2). The

Scheme 2. Reaction of 2 with $B(C_6F_5)_3$ To Form Iminosilylene−BCF Adduct 3

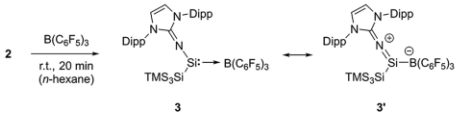

solubility in hexane decreased, presumably a result of the polarized bond between both partners, and adduct **3** could be separated from TMS_3SiBr as yellow crystals in moderate yield (45%). Although compound **3** is only stable in solution at room temperature for a maximum of 1 day, it was fully characterized by NMR, MS and X-ray analysis. The ^{29}Si NMR spectrum of **3** showed a quartet at 160.7 ppm ($^1J_{SiB}$ = 53.9 Hz) arising from the coordination of the central silicon atom to boron.

Compared to related room temperature stable IPrNCp*Si(II)−BCF adduct (114.5 ppm, $^1J_{SiB}$ = 70 Hz),[16d] the downfield shift of around 45 ppm emphasizes decreased electron density at the silicon atom. The crystallographic data of **3** (Figure 2) confirm a trigonal planar Si(II) center (bonding angles at Si1 add up to 360° within their standard deviations) with a Si1−B1 bond of 2.117(2) Å, longer than that of IPrNCp*Si(II)−BCF (2.080(5) Å)[16d] and similar to that of donor−acceptor adduct NHC → $SiCl_2$ → BCF (2.106(6) Å).[16b] Moreover, although the Si1−N1 bond (1.6354(16) Å) is shortened, the N1−C1 bond (1.306(2) Å) is elongated compared to precursor **2** (corresponding distances of 1.748(5) and 1.279(6) Å, respectively). This points to an increase of π-donation to the silicon atom, suggesting a linear 1-sila-2-azaallene resonance form **3′**. However, in comparison to IPrNCp*Si(II)-BCF (Si1−N1 = 1.605(3) Å and N1−C1 = 1.302(4) Å), this structure should be less pronounced (C1−N1−Si1 of **3** 151.10(14)° vs 158.7(3)°).[16d]

DOI: 10.1021/jacs.7b05136
J. Am. Chem. Soc. 2017, 139, 8134−8137

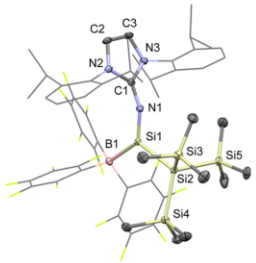

Figure 2. Molecular structure of **3** in the solid state with ellipsoids set at the 50% probability level. For clarity, hydrogen atoms and cocrystallized solvent molecules are omitted and Dipp- as well as C_6F_5-groups are simplified as wireframes. Selected bond lengths (Å) and angles (deg): Si1–B1 2.117(2), Si1–N1 1.6354(16), Si1–Si2 2.3827(6), N1–C1 1.306(2), C1–N2 1.387(2), C1–N3 1.381(2), N1–Si1–Si2 112.26(6), Si2–Si1–B1 118.28(6), B1–Si1–N1 129.45(8), C1–N1–Si1 151.10(14).

After this convincing proof of extrusion of a Si(II) species from silepin **2**, we targeted its direct use as "masked" silylene in small molecule activation (Scheme 3B).

Scheme 3. (A) Selected Examples of Known Silicon Carbonate Complexes (B); Small Molecule Activation of 2 with CO_2, Ethylene and H_2

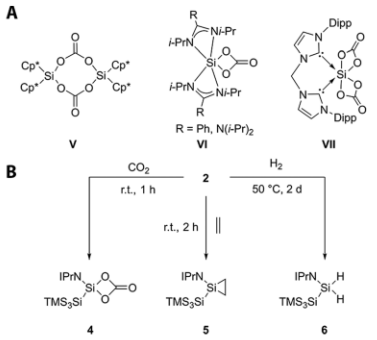

Over the last 3 decades, the metal-free binding of carbon dioxide by low-valent silicon compounds has drawn attention.[17] Jutzi et al. demonstrated the first reduction of carbon dioxide to carbon monoxide via stoichiometric formation of Si(IV) biscarbonato complex **V** (Scheme 3A).[18] Since then, a few other low-valent silicon compounds have been shown to activate successfully CO_2.[17] To the best of our knowledge, all but two of these reaction products are dimeric. Tacke et al. reported formation of six-coordinate, monomeric bis(amidinato/guadinato) silicon carbonate **VI** from the reaction of CO_2 with the respective silylene,[17b,d] and a silicon dicarbonate complex **VII** was isolated by Driess et al. from the activation of CO_2 by a silylone.[17a] The reaction of **2** with CO_2 proceeded rapidly (within 1 h) under mild conditions (1 bar, r.t.). Silepin **2** behaves as dormant form of iminosilylene **1**, which then follows the mechanism described in literature to give the corresponding silicon carbonate **4** (Scheme 3B).[17e,18] As mentioned, these products are usually prone to dimerization, but in our case the first four-coordinate, monomeric carbonato chelated silicon(IV) compound **4** was isolated in 60% yield. The ^{29}Si NMR shift of the central silicon atom of **4** (−35.0 ppm) is in the range of typical four-coordinate silicon compounds and is comparable to that of the biscarbonato dimer **V** (−28.3 ppm).[18] The characteristic C=O stretch of the carbonato unit of **4** was found at 1789 cm^{-1} (cf. **V**[18] $\nu_{C=O}$ = 1760 cm^{-1}, **VII**[17a] $\nu_{C=O}$ = 1746 cm^{-1}). The single crystal X-ray diffraction analysis of **4** (Figure 3) revealed its monomeric structure and exposed the position of the carbonato group in a pocket between the two bulky ligands.

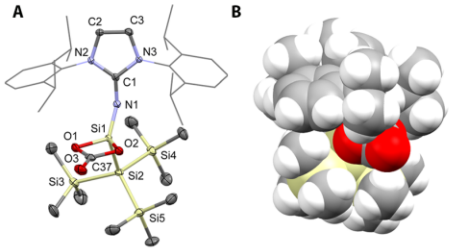

Figure 3. (A) Molecular structure of **4** in the solid state with ellipsoids set at the 50% probability level. For clarity, hydrogen atoms are omitted and Dipp groups are simplified as wireframes. Selected bond lengths (Å) and angles (deg): Si1–O1 1.7413(17), Si1–O2 1.7395(17), Si1–N1 1.6275(19), Si1–Si2 2.3161(10), N1–C1 1.297(3), O1–C37 1.360(3), O2–C37 1.348(3), O3–C37 1.194(3), N1–Si1–Si2 117.94(8), O1–Si1–O2 76.18(8), O1–C37–O2 104.93(18). (B) Space filling representation of **4**.

Because of this protection, no dimerization was observed in solution (C_6D_6) even after several weeks. The bond lengths related to the carbonato group are similar to those of published structures.[17b,d,18] The widening of the N1–Si1–Si2 angle (117.94(8)°) is noticeable in comparison to **3** (112.26(6)°) as a consequence of the lower space requirement of the carbonato moiety compared to the borane group. Acyclic silylenes have shown some reactivity toward ethylene[7,19] and molecular hydrogen.[3c,d] Therefore, we were interested whether silepin **2** was capable of activating such challenging targets. According to NMR studies, exposure of a freshly prepared solution of **2** to ethylene at room temperature gave the corresponding silirane ring **5** within 2 h (Scheme 3B). Despite several isolation attempts, this product could not be purified by crystallization due to its similar solubility properties to TMS_3SiBr, but is characterized sufficiently via ^{1}H, ^{13}C, ^{29}Si and 2D NMR spectroscopy. The ^{29}Si NMR spectrum gave a signal for the central silicon atom at −100.9 ppm, which is slightly high-field shifted compared to the analogous product from using **I** (−80.8 ppm),[19] illustrating once again the donor strength of the imino ligand. In addition, coupling of this central silicon to the ring-bound protons in the ^{1}H-^{29}Si HMBC spectrum confirmed the silirane structure. According to literature, exclusively acyclic silylenes with small HOMO–LUMO gaps (~2 eV) have been able to split the strong and nonpolar bond of dihydrogen.[3c,d] For silepin **2**, NMR studies revealed a slow reaction with hydrogen at room temperature; however, heating to 50 °C led to full conversion within 2 days (Scheme 3B). Here too, isolation of the product was problematic, but the obtained ^{29}Si NMR showed clear evidence for the assumed compound **6** with a triplet for the central silicon atom at −60.7 ppm ($^1J_{SiH}$ = 189 Hz), in accordance with the data of H_2 activation product of **I** (−35.2 ppm, $^1J_{SiH}$ = 195 Hz).[3c]

In summary, we provided proof of the first example of an acyclic iminosilylsilylene **1** via low temperature NMR and UV–vis experiments, which undergoes an intramolecular insertion into an aromatic C=C bond to form silepin **2**. As confirmed by X-ray

DOI: 10.1021/jacs.7b05136
J. Am. Chem. Soc. 2017, 139, 8134–8137

analysis, the newly formed Si—C bonds of **2** are elongated and facilitate the reductive elimination to Si(II) in combination with the driving force of rearomatization. This idea was verified by (HT) UV–vis experiments, DFT calculations and isolation of the silylene–borane adduct **3** upon addition of BCF. Compound **3** belongs to the small list of isolable silylene–BCF adducts and shows a minor contribution of the resonance structure 1-sila-2-azaallene **3′**. The concept of reversibility was further probed by directly using silepin **2** as a "masked" silylene in the activation of small molecules. For CO_2, the first example of a monomeric, four-coordinate silicon carbonate complex **4** was isolated. In addition, the activation of ethylene and molecular hydrogen with **2** was achieved under mild conditions. Beside the established oxidative addition of a silylene species, our work demonstrates the key concept of a reductive elimination from Si(IV) to Si(II), opening the door to the ultimate goal of silylene-based metal-free catalysis.

■ ASSOCIATED CONTENT

Supporting Information

The Supporting Information is available free of charge on the ACS Publications website at DOI: 10.1021/jacs.7b05136.

Experimental details (PDF)
Crystallographic data (CIF)

■ AUTHOR INFORMATION

Corresponding Authors

*rieger@tum.de
*s.inoue@tum.de

ORCID

Shigeyoshi Inoue: 0000-0001-6685-6352
Bernhard Rieger: 0000-0002-0023-884X

Notes

The authors declare no competing financial interest.

■ ACKNOWLEDGMENTS

We are grateful to the WACKER Chemie AG for continued financial support. We thank Dominik Reiter, Martin Machat and Philipp Pahl for revising the paper. We thank Dr. Alexander Pöthig for crystallographic advice, Fabian Linsenmann and Manuel Kaspar for IR and (VT) UV–vis measurements. We also express appreciation to the Leibniz Supercomputing Center of the Bavarian Academy of Science and Humanities for the provision of computing time.

■ REFERENCES

(1) Jutzi, P.; Kanne, D.; Kruger, C. *Angew. Chem., Int. Ed. Engl.* **1986**, *25*, 164–165.

(2) For recent reviews on silylenes, see: (a) Rivard, E. *Chem. Soc. Rev.* **2016**, *45*, 989–1003. (b) Blom, B.; Driess, M. *Struct. Bonding (Berlin, Ger.)* **2013**, *156*, 85–123. (c) Yao, S.-L.; Xiong, Y.; Driess, M. *Organometallics* **2011**, *30*, 1748–1767. (d) Asay, M.; Jones, C.; Driess, M. *Chem. Rev. (Washington, DC, U. S.)* **2011**, *111*, 354–396. (e) Mizuhata, Y.; Sasamori, T.; Tokitoh, N. *Chem. Rev. (Washington, DC, U. S.)* **2009**, *109*, 3479–3511.

(3) (a) Hadlington, T. J.; Abdalla, J. A. B.; Tirfoin, R.; Aldridge, S.; Jones, C. *Chem. Commun.* **2016**, *52*, 1717–1720. (b) Rekken, B. D.; Brown, T. M.; Fettinger, J. C.; Lips, F.; Tuononen, H. M.; Herber, R. H.; Power, P. P. *J. Am. Chem. Soc.* **2013**, *135*, 10134–10148. (c) Protchenko, A. V.; Schwarz, A. D.; Blake, M. P.; Jones, C.; Kaltsoyannis, N.; Mountford, P.; Aldridge, S. *Angew. Chem., Int. Ed.* **2013**, *52*, 568–571. (d) Protchenko, A. V.; Birjkumar, K. H.; Dange, D.; Schwarz, A. D.; Vidovic, D.; Jones, C.; Kaltsoyannis, N.; Mountford, P.; Aldridge, S. *J. Am. Chem. Soc.* **2012**, *134*, 6500–6503. (e) Rekken, B. D.; Brown, T. M.; Fettinger, J. C.; Tuononen, H. M.; Power, P. P. *J. Am. Chem. Soc.* **2012**, *134*, 6504–6507.

(4) Driess, M. *Nat. Chem.* **2012**, *4*, 525–526.

(5) Protchenko, A. V.; Bates, J. I.; Saleh, L. M. A.; Blake, M. P.; Schwarz, A. D.; Kolychev, E. L.; Thompson, A. L.; Jones, C.; Mountford, P.; Aldridge, S. *J. Am. Chem. Soc.* **2016**, *138*, 4555–4564.

(6) Inomata, K.; Watanabe, T.; Miyazaki, Y.; Tobita, H. *J. Am. Chem. Soc.* **2015**, *137*, 11935–11937.

(7) Lips, F.; Fettinger, J. C.; Mansikkamaki, A.; Tuononen, H. M.; Power, P. P. *J. Am. Chem. Soc.* **2014**, *136*, 634–7.

(8) (a) Rodriguez, R.; Gau, D.; Kato, T.; Saffon-Merceron, N.; De Cozar, A.; Cossio, F. P.; Baceiredo, A. *Angew. Chem., Int. Ed.* **2011**, *50*, 10414–10416. (b) Rodriguez, R.; Gau, D.; Contie, Y.; Kato, T.; Saffon-Merceron, N.; Baceiredo, A. *Angew. Chem., Int. Ed.* **2011**, *50*, 11492–5.

(9) (a) Rodriguez, R.; Contie, Y.; Nougué, R.; Baceiredo, A.; Saffon-Merceron, N.; Sotiropoulos, J.-M.; Kato, T. *Angew. Chem.* **2016**, *128*, 14567–14570. (b) Rodriguez, R.; Contie, Y.; Mao, Y.; Saffon-Merceron, N.; Baceiredo, A.; Branchadell, V.; Kato, T. *Angew. Chem., Int. Ed.* **2015**, *54*, 15276–15279.

(10) (a) Ochiai, T.; Inoue, S. *RSC Adv.* **2017**, *7*, 801–804. (b) Bag, P.; Ahmad, S. U.; Inoue, S. *Bull. Chem. Soc. Jpn.* **2017**, *90*, 255–271. (c) Ochiai, T.; Szilvási, T.; Inoue, S. *Molecules* **2016**, *21*, 1155–1167. (d) Ochiai, T.; Szilvási, T.; Franz, D.; Irran, E.; Inoue, S. *Angew. Chem., Int. Ed.* **2016**, *55*, 11619–11624. (e) Ochiai, T.; Franz, D.; Inoue, S. *Chem. Soc. Rev.* **2016**, *45*, 6327–6344.

(11) Lui, M. W.; Merten, C.; Ferguson, M. J.; McDonald, R.; Xu, Y.; Rivard, E. *Inorg. Chem.* **2015**, *54*, 2040–2049.

(12) Lee, G.-H.; West, R.; Müller, T. *J. Am. Chem. Soc.* **2003**, *125*, 8114–8115.

(13) (a) Kosai, T.; Ishida, S.; Iwamoto, T. *Chem. Commun.* **2015**, *51*, 10707–10709. (b) Kira, M.; Ishida, S.; Iwamoto, T.; de Meijere, A.; Fujitsuka, M.; Ito, O. *Angew. Chem., Int. Ed.* **2004**, *43*, 4510–4512. (c) Kira, M.; Ishida, S.; Iwamoto, T.; Kabuto, C. *J. Am. Chem. Soc.* **2002**, *124*, 3830–3831. (d) Suzuki, H.; Tokitoh, N.; Okazaki, R. *Bull. Chem. Soc. Jpn.* **1995**, *68*, 2471–81. (e) Suzuki, H.; Tokitoh, N.; Okazaki, R. *J. Am. Chem. Soc.* **1994**, *116*, 11572–3. Example of a silicon-mediated aryl group activation: (f) Mondal, K. C.; Samuel, P. P.; Roesky, H. W.; Aysin, R. R.; Leites, L. A.; Neudeck, S.; Lübben, J.; Dittrich, B.; Holzmann, N.; Hermann, M.; Frenking, G. *J. Am. Chem. Soc.* **2014**, *136*, 8919–8922.

(14) (a) Sohn, H.; Merritt, J.; Powell, D. R.; West, R. *Organometallics* **1997**, *16*, 5133–5134. (b) Nishinaga, T.; Izukawa, Y.; Komatsu, K. *Tetrahedron* **2001**, *57*, 3645–3656. (c) Nishinaga, T.; Izukawa, Y.; Komatsu, K. *Chem. Lett.* **1998**, *27*, 269–270. (d) Nishinaga, T.; Komatsu, K.; Sugita, N. *J. Org. Chem.* **1995**, *60*, 1309–1314.

(15) Lutters, D.; Severin, C.; Schmidtmann, M.; Müller, T. *J. Am. Chem. Soc.* **2016**, *138*, 6061–6067.

(16) Reported silylene–BCF adducts: (a) Jana, A.; Azhakar, R.; Sarish, S. P.; Samuel, P. P.; Roesky, H. W.; Schulzke, C.; Koley, D. *Eur. J. Inorg. Chem.* **2011**, *2011*, 5006–5013. (b) Ghadwal, R. S.; Roesky, H. W.; Merkel, S.; Stalke, D. *Chem. - Eur. J.* **2010**, *16*, 85–88. (c) Metzler, N.; Denk, M. *Chem. Commun.* **1996**, 2657–2658. (d) Inoue, S.; Leszczynska, K. *Angew. Chem., Int. Ed.* **2012**, *51*, 8589–8593.

(17) Recent examples of activation of CO_2 by low-valent silicon compounds: (a) Burchert, A.; Yao, S.; Müller, R.; Schattenberg, C.; Xiong, Y.; Kaupp, M.; Driess, M. *Angew. Chem., Int. Ed.* **2017**, *56*, 1894–1897. (b) Mück, F. M.; Baus, J. A.; Nutz, M.; Burschka, C.; Poater, J.; Bickelhaupt, F. M.; Tacke, R. *Chem. - Eur. J.* **2015**, *21*, 16665–16672. (c) Wang, Y.; Chen, M.; Xie, Y.; Wei, P.; Schaefer, H. F.; Robinson, G. H. *J. Am. Chem. Soc.* **2015**, *137*, 8396–8399. (d) Junold, K.; Nutz, M.; Baus, J. A.; Burschka, C.; Fonseca Guerra, C.; Bickelhaupt, F. M.; Tacke, R. *Chem. - Eur. J.* **2014**, *20*, 9319–9329. (e) Liu, X.; Xiao, X.-Q.; Xu, Z.; Yang, X.; Li, Z.; Dong, Z.; Yan, C.; Lai, G.; Kira, M. *Organometallics* **2014**, *33*, 5434–5439. (f) Gau, D.; Rodriguez, R.; Kato, T.; Saffon-Merceron, N.; de Cózar, A.; Cossío, F. P.; Baceiredo, A. *Angew. Chem., Int. Ed.* **2011**, *50*, 1092–1096.

(18) Jutzi, P.; Eikenberg, D.; Moehrke, A.; Neumann, B.; Stammler, H.-G. *Organometallics* **1996**, *15*, 753–9.

(19) Wendel, D.; Eisenreich, W.; Jandl, C.; Pöthig, A.; Rieger, B. *Organometallics* **2016**, *35*, 1–4.

DOI: 10.1021/jacs.7b05136
J. Am. Chem. Soc. 2017, 139, 8134–8137

9. Silicon and Oxygen's Bond of Affection: An Acyclic Three-Coordinate Silanone and Its Transformation to an Iminosiloxysilylene

Title: "Silicon and Oxygen's Bond of Affection: An Acyclic Three-Coordinate Silanone and Its Transformation to an Iminosiloxysilylene"

Status: Article, published online November 3, 2017

Journal: Journal of the American Chemical Society, 2017, 139 (47), 17193–17198.

Publisher: American Chemical Society

DOI: 10.1021/jacs.7b10634

Authors: Daniel Wendel, Dominik Reiter, Amelie Porzelt, Philipp J. Altmann, Shigeyoshi Inoue, Bernhard Rieger[a]

Content: This publication should be seen as a continuation of the silepin project and focuses on the isolation of a room temperature stable, three-coordinate acyclic silanone, an elusive species that, since the days of organosilicon pioneer Frederic S. Kipping, has fascinated many generations of silicon chemists. In this study, we report on the isolation and full characterization of the first examples of neutral, three-coordinate acyclic imino(silyl)silanones with indefinite stability as solids and lifetimes in solution of up to 2 days. Extensive DFT calculations provided insights into the Si=O bonding and revealed the π-donating NHI and σ-donating silyl groups as important factors for their enhanced stability. Additionally, first reactivity studies of the silanones toward CO_2 and methanol were conducted and different isomerization pathways depending on the silyl substitution pattern were found. For the hypersilyl substituted silanone, a 1,3-silyl migration formed an intermediary disilene, which was trapped as a rare NHC-disilene adduct. For the more stable supersilyl substituted silanone, a selective transformation to the first reported room temperature stable, two-coordinate acyclic *N*,*O*-silylene exhibiting a fascinating siloxy ligand was observed. In summary, this article brings researchers a little closer to the fulfillment of Kipping's original dream of isolable bis(alkyl)silanones and, by isolation of an novel imino(siloxy)silylene, provides new insights and perspectives regarding the synthesis and stabilization modes of two-coordinate acyclic silylenes.

[a]D. Wendel and D. Reiter planned and executed all experiments and co-wrote the manuscript. A. Porzelt designed and performed the theoretical analyses and contributed with fruitful mental input. P. J. Altmann conducted all SC XRD-measurements and managed the processing of the respective data. All work was performed under the supervision of B. Rieger and S. Inoue.

JACS
JOURNAL OF THE AMERICAN CHEMICAL SOCIETY
Article
Cite This: J. Am. Chem. Soc. 2017, 139, 17193-17198
pubs.acs.org/JACS

Silicon and Oxygen's Bond of Affection: An Acyclic Three-Coordinate Silanone and Its Transformation to an Iminosiloxysilylene

Daniel Wendel,[†,‡] Dominik Reiter,[†,§] Amelie Porzelt,[§] Philipp J. Altmann,[⊥] Shigeyoshi Inoue,[*,§] and Bernhard Rieger[*,‡]

[‡]WACKER-Chair of Macromolecular Chemistry, [§]WACKER-Institute of Silicon Chemistry, [⊥]Catalysis Research Center, Technische Universität München, Lichtenbergstraße 4, 85748 Garching bei München, Germany

Supporting Information

ABSTRACT: A long-term dream comes true: An acyclic, neutrally charged silanone at last! Here, we report on the first examples of isolable acyclic, neutral, three-coordinate silanones **2** with indefinite stability as solids and lifetimes in solution of up to 2 days. The electronic properties of the Si═O bond were investigated via DFT calculations and revealed the π-donating *N*-heterocyclic imino (NHI) and σ-donating silyl groups as key factors for their enhanced stability. Besides initial reactivity studies of **2** toward CO_2 and methanol, different isomerization pathways depending on the silyl substitution pattern were found. For **2a** (R = TMS), a 1,3-silyl shift gave an intermediary disilene, which was trapped as unique NHC-disilene adduct **6**. For the more stable silanone **2b** (R = *t*-Bu), a selective transformation to the first reported room temperature stable, acyclic, two-coordinate *N*,*O*-silylene **7** exhibiting a fascinating siloxy ligand was observed. Both compounds were fully characterized experimentally and their bonding features were analyzed by theoretical calculations.

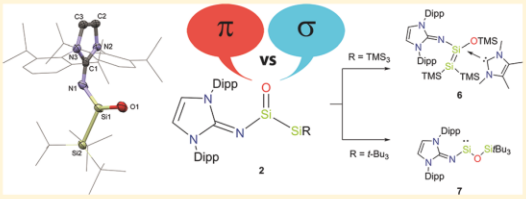

INTRODUCTION

Poly(siloxanes) are some of the most important and widely used inorganic polymers with a broad spectrum of applications ranging from industrial purposes to custom-designed materials of our daily life.[1] Considering today's widespread success, it is quite peculiar that poly(siloxanes) $(R_2SiO)_n$ were discovered by mere accident, when about one century ago organosilicon pioneer Frederic S. Kipping had actually been seeking silicon analogs of ketones ($R_2Si{=}O$).[2] Since then, the truly monomeric $R_2Si{=}O$ unit, generally referred to as silanone, has been one of the most sought-after compounds in modern main group chemistry ("Kipping's dream").[3] Unlike their lighter congeners, silanones possess a highly reactive Si═O double bond, which tends to undergo rapid head-to-tail polymerization to form stable Si−O σ-bonds.[4] This extreme reactivity is mainly attributed to the strong $Si^{\delta+}{-}O^{\delta-}$ polarization as a result of the large difference in electronegativity between both elements and an unfavorable overlap of the interacting silicon and oxygen p_π-orbitals.[5] Therefore, until a few years ago, silanones have been observed only in the gas phase or in argon matrices at low temperatures.[6] However, the recent decade has witnessed several attempts to tame the polarized Si═O double bond by additional coordination to Lewis acids or bases,[7] giving rise to a variety of isolable donor−acceptor[8] or donor-stabilized[9] complexes. A more recent approach abstains from this external perturbation and relies on the basic idea of kinetic and thermodynamic stabilization of the Si═O moiety by only two adjacent ligands (Chart 1).[10] The first impressive breakthrough toward three-coordinate silanones was achieved by Filippou et al., who isolated stable cationic metallosilanone **I**, which may partly be considered as an NHC-adduct of silicon monoxide.[11] Iwamoto and co-workers followed shortly after by reporting transient dialkylsilanone **II** stable at −80 °C.[12] Even more spectacular is the recent success of the group of Kato, who took advantage of two strong π-donors and isolated the first crystalline cyclic silanone **III** with half-life times in solution of up to 5 h at room temperature.[13]

Chart 1. Literature Known Examples of Three-Coordinate Silanones I−III

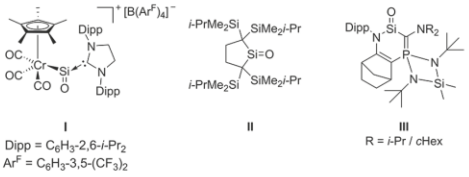

We have previously reported an acyclic iminosilylsilylene, which reversibly inserts into a C═C double bond of its aromatic ligand framework to form silepin **1a** (Scheme 1).[14] This tendency to undergo reductive elimination has been exploited to use **1a** as direct synthetic equivalent of silylene in the activation of small molecules. Continuing this study, we were interested to see whether the *N*-heterocyclic imino (NHI) ligand[15] as single π-donor of the silepin-silylene system may sufficiently stabilize a highly polarized Si═O moiety.

Received: October 6, 2017
Published: November 3, 2017

DOI: 10.1021/jacs.7b10634
J. Am. Chem. Soc. 2017, 139, 17193−17198

Scheme 1. Preparation and Reactivity of Acyclic Three-Coordinate Silanones 2

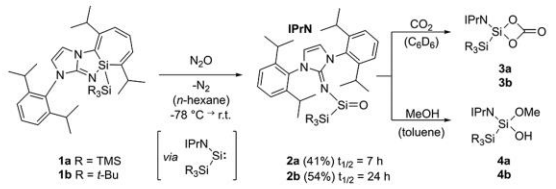

Herein, we present the first examples of acyclic and neutrally charged silanones **2** with a planar three-coordinate Si atom. Furthermore, chemical lifetimes, isomerization pathways, and initial reactivity studies of **2** are discussed in detail.

■ RESULTS AND DISCUSSIONS

Exposure of an *n*-hexane solution of silepin **1** at −78 °C to an atmosphere of N_2O followed by warming to room temperature instantly gave a white precipitate, which was separated by filtration, washed with *n*-hexane and dried in vacuo to give pure silanone **2** in moderate yield (**2a** 41%, **2b** 54%) (Scheme 1). The ^{29}Si NMR spectra of both compounds displayed signals for the central silicon atom at 33.7 ppm for **2a** and 28.8 ppm for **2b** (calc. 33.3 ppm at SMD-B3LYP/6-311+G(2d,2p) level of theory), respectively. Both NMR shifts are in the typical region for three-coordinate silicon compounds, but are considerably high-field shifted in comparison to **I** (169.6 ppm)[11] and **II** (128.4 ppm).[12] They even fall in the same range as cyclic silanone **III** (38.4 ppm)[13] with two π-donating substituents, illustrating the strong donor qualities of a single NHI ligand. The characteristic Si═O stretching vibration was found at 1144 cm^{-1} for both compounds, which is in good agreement with the calculated value ($\nu_{Si=O}$ = 1155 cm^{-1}) and comparable to other Si═O containing structures.[12,16] The UV−vis spectrum of **2b** in toluene revealed an broad absorption peak at 282 nm in the same region as related acyclic three-coordinate germanone (297 nm).[10] Colorless crystals of **2b** were obtained by slow diffusion of Et_2O into a saturated THF solution at −35 °C over several days. Single-crystal X-ray analysis confirmed the monomeric structure of **2b** and exposed the position of the Si═O moiety in a well-protected steric pocket between the two bulky ligands (Figure 1).

The crystal structure revealed a trigonal planar silicon center (sum of bonding angles: 360°) and a Si1−O1 bond length of **2b** (1.537(3) Å), which is slightly longer than that of metallosilanone **I** (1.526 Å)[11] and cyclic silanone **III** (1.533 Å),[13] but generally shorter than those of tetra-coordinate base-stabilized silanones.[8,9] The potent electron donation from the exocyclic nitrogen atom of the NHI ligand to the electron deficient silicon atom is clearly evidenced by a short Si1−N1 bond (1.646(3) Å), for which reason resonance form **2b′** should be denoted (Chart 2). Further, the N1−C1 bond (1.319(4)Å) is elongated and the endocyclic C−N bonds (C1−N2 1.364(5) Å/ C1−N3 1.368(5) Å) are slightly shortened.[17] Combined with a small Si1−N1−C1 angle of merely 131.7(3)° one can assume that the positive charge may be delocalized over the iminato ring as illustrated in structure **2b″**. However, according to the X-ray data, the almost perpendicular assembly of the planar NHC fragment to the N1Si1O1 plane (dihedral angle 89.9(4)°) seems to limit this conjugative effect. To obtain further insights into the bonding properties of **2b**, we performed density functional theory (DFT) calculations at

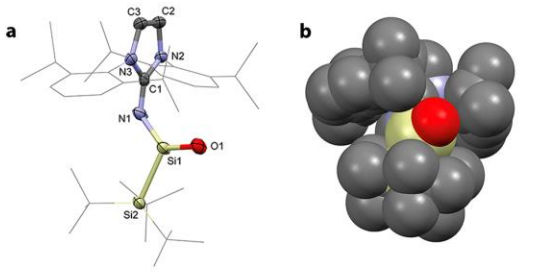

Figure 1. (a) Molecular structure and (b) space filling representation of silanone **2b** in the solid state with ellipsoids set at the 50% probability level (one out of two independent molecules in the asymmetric unit). For clarity, hydrogen atoms are omitted and *t*-Bu as well as Dipp groups are simplified as wireframes. Selected bond lengths (Å) and angles (deg): Si1−O1 1.537(3), Si1−N1 1.646(3), N1−C1 1.319(4), C1−N2 1.364(5), C1−N3 1.368(5), Si1−Si2 2.358(2), N1−Si1−Si2 112.6(1), C1−N1−Si1 131.7(3).

Chart 2. (a) DFT-Calculated HOMO−10 *E* = −7.78 eV and LUMO+4 *E* = −0.41 eV of 2b, (b) Plausible Resonance Forms of 2b and Calculated Smaller Silanones A, B, C, and D Including NPA Charges and Bond Orders (in bold and italics)

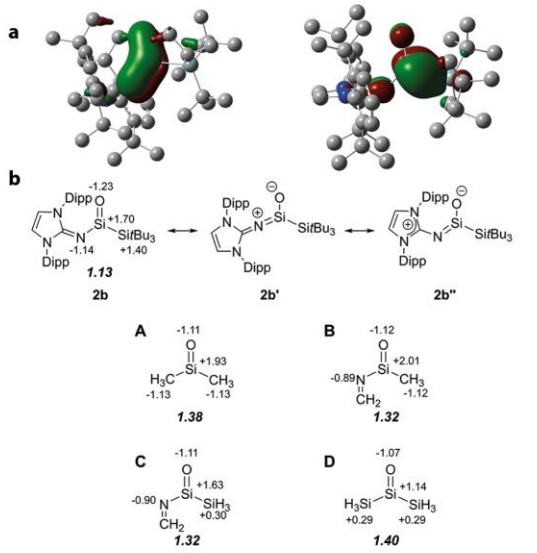

the B3LYP/6-311+G(d) level of theory. The analysis of the Kohn−Sham orbitals (Chart 2a) showed that HOMO−10 represents the Si═O π-bond, which obviously mixes with the nonbonding orbital of the exocyclic nitrogen atom, explaining the observed short Si1−N1 distance. As already extracted from the X-ray data, an expansion of the conjugation to the NHC ring fragment could not be found. Interestingly, the LUMO+4 reveals significant hyperconjugation from the Si−C σ-bond of the silyl group to the π*-bonding orbital of Si═O moiety. Moreover, from NBO analysis (Chart 2b) a decreased Si═O bond order (1.13) and an increased negative charge on the oxygen center (−1.23) compared to those of dimethylsilanone **A** (1.38 and −1.11) were found, illustrating the strong polarization of the Si═O double bond. However, the positive character at Si1 decreases. To explain this effect, we calculated

DOI: 10.1021/jacs.7b10634
J. Am. Chem. Soc. 2017, 139, 17193−17198

the smaller iminoalkyl- **B**, iminosilyl- **C** and disilylsilanone **D** analogs. Here too the trend is visible, that the positive charge at the silicon center is effectively reduced by presumable σ-donation and hyperconjugation of the silyl group.[4b] In compound **2b** this effect fully sets in and Si1 has only a slightly higher positive charge (1.70) than Si2 attached to *t*-Bu groups (1.40). Our analysis proves that besides the kinetical stabilization due to steric encumbrance, especially the π-donor qualities of NHI ligand but as well σ-donor properties of silyl group are key to stabilize acyclic silanone **2b**.

In terms of reactivity, both silanones **2** were directly and quantitatively converted by CO_2 to the respective silicon carbonate complexes **3**, similarly to the reaction of silepin **1a** with carbon dioxide (Scheme 1).[14] Moreover, the reaction of silanones **2** toward methanol was tested. As in carbonyl chemistry, where ketones form hemiketals with alcohols, the corresponding silanol **4** was isolated in good yield (**4a** 71%, **4b** 69%). The ^{29}Si NMR shift of the silicon center of **4a** at −38.6 ppm and **4b** at −46.6 ppm, respectively, clearly displayed the change in coordination number from three to four. The X-ray diffraction analysis of **4a** (Figure 2) verified the presence of a

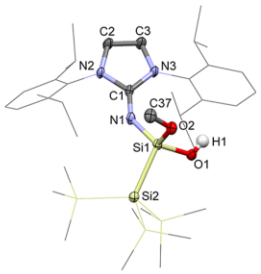

Figure 2. Molecular structure of silanol **4a** in the solid state with ellipsoids set at the 50% probability level. For clarity, hydrogen atoms and cocrystallized solvent molecules are omitted and TMS as well as Dipp groups are simplified as wireframes. Selected bond lengths (Å) and angles (deg): Si1−O1 1.642(2), Si1−O2 1.660(2), Si1−N1 1.680(2), N1−C1 1.278(3), C1−N2 1.394(3), C1−N3 1.396(3), N1−Si1−O1 118.7(1), C1−N1−Si1 142.4(2).

tetra-coordinate silicon center attached to one methoxy and one hydroxyl group. The Si1−O1 bond length of **4a** (1.642(2) Å) is unambiguously distinguishable from the original Si═O bond of **2b**. Interestingly, in this structure, the Si1−N1 bond (1.680(2) Å) is elongated and the N1−C1 bond (1.278(3) Å) slightly shortened in comparison to **2b**, which underlines the disappearance of the former Si═N double-bond character.

A key criterion for storage, handling and reaction design of silanones is their lifetime. Monitoring a C_6D_6 solution of silanone **2a** via ^{1}H NMR spectroscopy showed the full decomposition to an unspecific product mixture within 14 h ($t_{1/2}$ = 7 h). ^{1}H, ^{29}Si and ^{1}H/^{29}Si HMBC NMR data pointed to one major asymmetric product, presumably formed by TMS migration from the hypersilyl group to the Si═O center and subsequent activation of the NHI ligand (see the Supporting Information). Further experiments revealed that its half-life can be extended considerably by using **2a** in CD_3CN solutions ($t_{1/2}$ = 4 days). Consistent with additional Lewis base coordination, the ^{29}Si NMR signal of the Si═O center is shifted from +33.7 ppm to −48.3 ppm. Crystals of tetra-coordinate acetonitrile-silanone adduct **2a** × CD_3CN were isolated and verified the additional solvent coordination (see SI). Still, we were interested to pin down the reactive intermediate in the decomposition process of **2a**. According to literature, a 1,3-silyl migration has been reported for transient cyclic dialkylsilanone **II** to form an intermediary silene.[12] Indeed, we figured out that the same TMS migration can be instantly induced by addition of THF-d_8 to solid **2a**, resulting in a strongly yellow colored solution (Scheme 2). Subsequent NMR

Scheme 2. Isomerization Pathway of Silanone 2a and Trapping of Intermediary Disilene INT

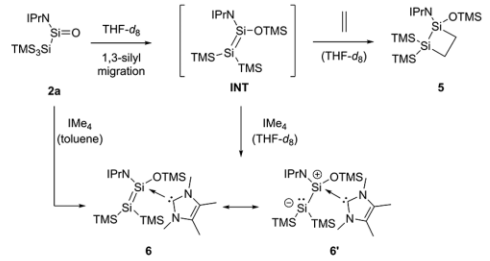

analysis indicated the quantitative formation of the proposed transient disilene **INT**. Strikingly, the different electronic environment at both silicon centers of **INT** due to the asymmetric substitution pattern is already noticeable in the ^{29}Si NMR shifts (−8.0 ppm (*Si*OTMS), − 196.6 ppm (*Si*TMS$_2$)), which suggest a polarized Si═Si double bond with high zwitterionic character. Because of the short lifetime of this species, isolation and full characterization was not possible and so trapping experiments were performed. Exposure of a THF-d_8 solution of **2a**, in situ forming **INT**, to ethylene immediately gave the colorless [2 + 2]-cycloaddition product **5**. 1,2-Disiletane **5** was sufficiently characterized via 2D NMR experiments and matching theoretical NMR shifts. Further, we tried to stabilize **INT** with a strong NHC donor. Reaction of **INT** in THF-d_8 or alternatively directly silanone **2a** in toluene with IMe$_4$ exclusively gave room-temperature-stable NHC-stabilized disilene adduct **6**. The ^{29}Si NMR shifts of **6** (−35.2 ppm (*Si*OTMS), − 174.6 ppm (*Si*TMS$_2$)) are similar to those of intermediary disilene **INT**, especially the latter, illustrating the presence of a highly negatively charged silicon atom, consistent with typical silyl anions.[18]

Orange-red crystals of **6** were isolated from an *n*-hexane solution at −35 °C. Subsequent X-ray analysis confirmed the coordination of the NHC donor to the distorted tetrahedral Si1 center (Figure 3a). The Si1−C28 bond length (1.958(2) Å) is in the range of typical dative NHC-Si bonds,[19] the assumed Si1−Si2 double bond is extremely elongated (2.3297(9) Å), slightly shorter than Si2−Si3 (2.3397(9) Å) and Si2−Si4 (2.3445(9) Å) bond, but beyond the range of classical Si═Si double bonds (2.13−2.31 Å).[20]

Still, compound **6** possesses a typical trans-bent geometry and shows significant pyramidalization, especially at the Si2 center (bent angles θ(Si1) = 42.7° and θ(Si2) = 57.8°). This strong bending underpins the assumption of zwitterionic resonance structure **6′** with a lone pair at Si2, but is distinguishable from a potential Si1−Si2 dative bond as recently discovered for base-stabilized disilene adduct $Me_2EtN \rightarrow SiCl_2 \rightarrow Si(SiCl_3)_2$ with an even larger bent angle ($\theta(Si(SiCl_3)_2$ = 79.1°).[21] Because NHC adducts of multiply bonded silicon compounds are rarely found in literature,[22] we were further interested in the electronic

DOI: 10.1021/jacs.7b10634
J. Am. Chem. Soc. 2017, 139, 17193−17198

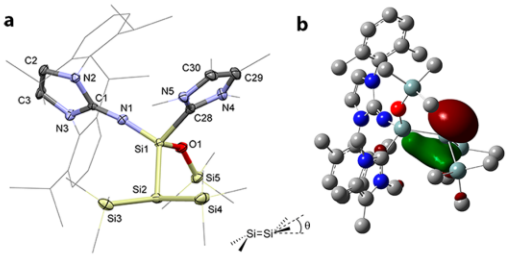

Figure 3. (a) Molecular structure of IMe_4 stabilized disilene adduct **6** in the solid state with ellipsoids set at the 50% probability level (one out of two independent molecules in the asymmetric unit). For clarity, hydrogen atoms and TMS as well as Dipp groups are simplified as wireframes. Selected bond lengths (Å) and angles (deg): Si1−Si2 2.3297(7), Si2−Si3 2.3397(9), Si2−Si4 2.3445(9), Si1−C28 1.958(2), Si1−O1 1.656(2), Si1−N1 1.659(2), N1−C1 1.263(3), C1−N2 1.407(3), C1−N3 1.400(3), C1−N1−Si1 168.9(2). b) DFT-calculated HOMO (−3.54 eV) of **6**.

properties of **6**. DFT calculations indicated that the HOMO (Figure 3b) mainly represents the lone pair at the Si2 atom with only short extensions not only to Si1 but to all surrounding silicon centers. The bond indices (see the Supporting Information) follow the same trend, with a WBI of Si1−Si2 (1.04) only slightly insinuating double bond character compared to Si2−Si3 (0.99) and Si2−Si4 (0.98). Regarding NPA charges, the polarization of Si1 (1.61) and Si2 (−0.60) in comparison to Si3 and Si4 (1.18) come to the same conclusion that the proposed zwitterionic canonical form **6′** is the most fitting representation to describe the electronic nature of this compound.

In strong contrast to the 1,3-silyl migration of **2a**, silanone **2b** shows almost no variations in the ^{29}Si NMR shifts during the solvent change from C_6D_6 to THF-d_8, indicating no observable donor−acceptor interaction between solvent and silanone. Because of replacement of TMS by *t*-Bu groups, silanone **2b** is indefinitely stable as a solid at room temperature, but remarkably forms mixed *N,O*-silylene **7** in C_6D_6 or THF-d_8 solution at ambient conditions within 48 h ($t_{1/2}$ = 24 h) in quantitative yield. This transformation can be accelerated by heating the solution to 60 °C, where full conversion was detected by NMR spectroscopy in less than 1 h (Scheme 3).

Scheme 3. Selective Transformation of Silanone 2b to Acyclic *N,O*-Silylene 7 and Formation of Silirane 8

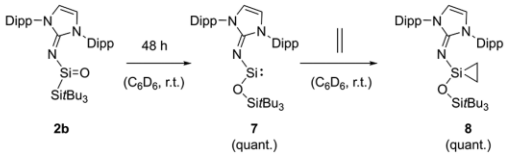

The facile thermal rearrangement is supported by theoretical calculations, which determined that *N,O*-silylene **7** is in fact 28.8 kJ/mol more stable than silanone **2b**. We believe that most likely the oxophilicity of silicon, promoting formation of stable Si−O single bonds, is the driving force of this reaction, which even overcomes the counteracting change of oxidation state from Si(IV) back to less stable Si(II). The ^{29}Si NMR signal of the central silicon atom of silylene **7** at 58.9 ppm (C_6D_6) is high-field shifted compared to other room-temperature-stable two-coordinate diamino (204.6 ppm)[23] and dithiolato silylenes (285.5 ppm).[24]

In particular, the upfield shift in comparison to strongly related in situ generated iminosilylsilylene IPrNSi(II)SiTMS$_3$ (300.0 ppm)[14] suggests additional π-donation by the siloxy ligand. A band for the characteristic $Si_n \rightarrow Si_{3p}$ transition of **7** was observed at 328 nm, which is very close to the theoretically predicted data (HOMO → LUMO 341 nm). X-ray analysis of colorless crystals of **7** revealed a two-coordinate silicon center exhibiting an N1−Si1−O1 angle of 103.56(8)° (Figure 4a).

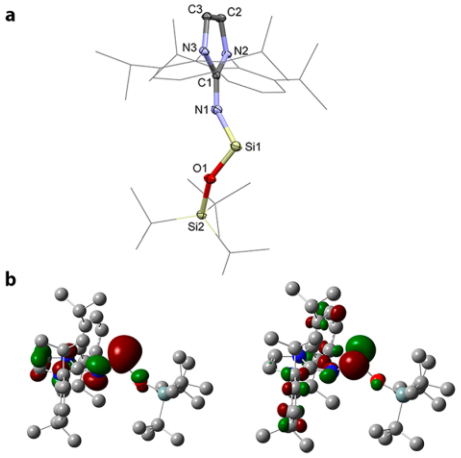

Figure 4. (a) Molecular structure of *N,O*-silylene **7** in the solid state with ellipsoids set at the 50% probability level (one out of two independent molecules in the asymmetric unit). For clarity, hydrogen atoms and *t*-Bu as well as Dipp groups are simplified as wireframes. Selected bond lengths (Å) and angles (deg): Si1−O1 1.643(1), O1−Si2 1.637(1), Si1−N1 1.661(2), N1−C1 1.281(2), C1−N2 1.380(3), C1−N3 1.386(2), N1−Si1−O1 103.56(8), C1−N1−Si1 147.7(2), Si1−O1−Si2 153.2(1). b) DFT-calculated HOMO (left, −5.04 eV) and LUMO (right, −0.71 eV) of **7**.

This angle is clearly wider than for cyclic NHSis (e.g., (CH(*t*-Bu)N)$_2$Si(II) 88.6°),[25] but considerably more compressed than for acyclic DippNTMSSi(II)SiTMS$_3$ (116.91°).[26] The Si1−N1 bond length (1.661(2) Å) is marginally longer than in the parent silanone structure **2b**, illustrating again a partial Si=N double bond character. Surprisingly, regarding potential π-donation by the siloxy group, both Si−O bonds have nearly the same length (Si1−O1 1.643(1) Å, O1−Si2 1.637(1) Å). Therefore, only a minor Si=O double bond character may be suggested. DFT calculations are in line with these findings, the HOMO of *N,O*-silylene **7** exhibits mainly lone pair character (Si_n), the LUMO resembles the empty Si_{3p} orbital with a HOMO−LUMO gap of 4.33 eV (Figure 4b). Both orbitals show only minor contributions from donating N or O atoms. For orbitals lower in energy, some interactions of silicon with nitrogen (HOMO−6), and even lower, minor interactions with oxygen can be found (see SI). The HOMO−LUMO gap is close to that of the acyclic dithiolato silylene by Power et al. (4.23 eV),[24] indicating a similar level of reactivity toward small molecules. Indeed, both silylenes show no sign of reactivity with molecular hydrogen, even if a reaction solution of **7** in H_2 atmosphere (1 bar) is heated to 60 °C for several days.[24] Regarding the activation of ethylene, it is reported that dithiolato silylene reversibly binds the olefin in a dissociation

DOI: 10.1021/jacs.7b10634
J. Am. Chem. Soc. 2017, 139, 17193−17198

equilibrium.[27] In contrast, *N,O*-silylene **7** quantitatively forms the corresponding silirane **8** within 20 min at room temperature with no observable reverse reaction. We believe that this disparity in reactivity is likely caused by reduced steric shielding at the Si(II) center of **7**.[28]

CONCLUSIONS

In summary, we have successfully isolated and fully characterized the first examples of acyclic, neutral, three-coordinate silanones **2** with indefinite stability as solids and lifetimes in solution up to 2 days. DFT calculations provided insight into the Si=O bonding and verified π-donating NHI and σ-donating silyl groups as important factors for their enhanced stability. First reactivity of silanones **2** toward CO_2 and methanol was tested and potential isomerization pathways were discovered. Here, a 1,3-silyl migration of **2a**, gave an intermediary disilene **INT**, which was trapped as 1,2-disiletane **5** in a [2 + 2]-cycloaddition with ethylene. Further, the NHC-disilene adduct **6** was isolated and analyzed by quantum chemical methods. Interestingly, for **2b**, the selective transformation to the first acyclic, two-coordinate *N,O*-silylene **7** was observed. Here, the enormous potential of acyclic silylene **7** to act as transition-metal mimic was demonstrated by successful activation of ethylene under ambient conditions. In total, our work not only continues the fulfillment of Kipping's dream of isolable silanones, but gives first insights into similarities and differences between this novel compound class and well-known carbonyl compounds.

ASSOCIATED CONTENT

Supporting Information

The Supporting Information is available free of charge on the ACS Publications website at DOI: 10.1021/jacs.7b10634.

Experimental details (PDF)

Crystallographic data (CCDC 1577580−1577584) (CIF)

AUTHOR INFORMATION

Corresponding Authors

*E-mail.: rieger@tum.de (B.R.).

*E-mail: s.inoue@tum.de (S.I.).

ORCID

Shigeyoshi Inoue: 0000-0001-6685-6352

Bernhard Rieger: 0000-0002-0023-884X

Author Contributions

†D.W. and D.R. contributed equally.

Notes

The authors declare no competing financial interest.

ACKNOWLEDGMENTS

We are exceptionally grateful to the WACKER Chemie AG and European Research Council (SILION 63794) for financial support. We thank Dr. Samuel Powley, Philipp Pahl, and Martin Machat for revising the manuscript and Dr. Alexander Pöthig for crystallographic advice. We also express our appreciation to the Leibniz Supercomputing Center of the Bavarian Academy of Science and Humanities for provision of computing time.

REFERENCES

(1) Jones, R. G.; Ando, W.; Chojnowski, J. *Silicon-Containing Polymers*; Springer: Dordrecht, The Netherlands, 2000.

(2) Kipping, F. S.; Lloyd, L. L. *J. Chem. Soc., Trans.* **1901**, *79*, 449−459.

(3) Sen, S. S. *Angew. Chem., Int. Ed.* **2014**, *53*, 8820−8822.

(4) (a) Kudo, T.; Nagase, S. *J. Am. Chem. Soc.* **1985**, *107*, 2589−2595. (b) Kimura, M.; Nagase, S. *Chem. Lett.* **2001**, *30*, 1098−1099.

(5) Avakyan, V. G.; Sidorkin, V. F.; Belogolova, E. F.; Guselnikov, S. L.; Gusel'nikov, L. E. *Organometallics* **2006**, *25*, 6007−6013.

(6) Examples of gas-phase and matrix-isolation experiments: (a) Glinski, R. J.; Gole, J. L.; Dixon, D. A. *J. Am. Chem. Soc.* **1985**, *107*, 5891−5894. (b) Withnall, R.; Andrews, L. *J. Am. Chem. Soc.* **1985**, *107*, 2567−2568. (c) Maier, G.; Meudt, A.; Jung, J.; Pacl, H., Matrix Isolation Studies of Silicon Compounds. In *The Chemistry of Organic Silicon Compounds*; John Wiley & Sons: Chichester, U.K., 1998; pp 1143−1185.

(7) Review on silanones and their heavier homologues: Xiong, Y.; Yao, S.; Driess, M. *Angew. Chem., Int. Ed.* **2013**, *52*, 4302−4311.

(8) (a) Yao, S.; Brym, M.; van Wuellen, C.; Driess, M. *Angew. Chem., Int. Ed.* **2007**, *46*, 4159−4162. (b) Xiong, Y.; Yao, S.; Driess, M. *Angew. Chem., Int. Ed.* **2010**, *49*, 6642−6645. (c) Xiong, Y.; Yao, S.; Driess, M. *Dalton Trans.* **2010**, *39*, 9282−9287. (d) Xiong, Y.; Yao, S.; Müller, R.; Kaupp, M.; Driess, M. *J. Am. Chem. Soc.* **2010**, *132*, 6912−6913. (e) Ghadwal, R. S.; Azhakar, R.; Roesky, H. W.; Pröpper, K.; Dittrich, B.; Klein, S.; Frenking, G. *J. Am. Chem. Soc.* **2011**, *133*, 17552−17555. (f) Muraoka, T.; Abe, K.; Haga, Y.; Nakamura, T.; Ueno, K. *J. Am. Chem. Soc.* **2011**, *133*, 15365−15367. (g) Ghadwal, R. S.; Azhakar, R.; Roesky, H. W.; Propper, K.; Dittrich, B.; Goedecke, C.; Frenking, G. *Chem. Commun.* **2012**, *48*, 8186−8188. (h) Rodriguez, R.; Gau, D.; Troadec, T.; Saffon-Merceron, N.; Branchadell, V.; Baceiredo, A.; Kato, T. *Angew. Chem., Int. Ed.* **2013**, *52*, 8980−8983. (i) Muraoka, T.; Abe, K.; Kimura, H.; Haga, Y.; Ueno, K.; Sunada, Y. *Dalton Trans.* **2014**, *43*, 16610−16613. (j) Reyes, M. L.; Troadec, T.; Rodriguez, R.; Baceiredo, A.; Saffon-Merceron, N.; Branchadell, V.; Kato, T. *Chem. - Eur. J.* **2016**, *22*, 10247−10253. (k) Rodriguez, R.; Gau, D.; Saouli, J.; Baceiredo, A.; Saffon-Merceron, N.; Branchadell, V.; Kato, T. *Angew. Chem., Int. Ed.* **2017**, *56*, 3935−3939.

(9) (a) Yao, S.; Xiong, Y.; Brym, M.; Driess, M. *J. Am. Chem. Soc.* **2007**, *129*, 7268−7269. (b) Xiong, Y.; Yao, S.; Driess, M. *J. Am. Chem. Soc.* **2009**, *131*, 7562−7563. (c) Yao, S.; Xiong, Y.; Driess, M. *Chem. - Eur. J.* **2010**, *16*, 1281−1288. (d) Xiong, Y.; Yao, S.; Müller, R.; Kaupp, M.; Driess, M. *Nat. Chem.* **2010**, *2*, 577−580. (e) Epping, J. D.; Yao, S.; Karni, M.; Apeloig, Y.; Driess, M. *J. Am. Chem. Soc.* **2010**, *132*, 5443−5455. (f) Rodriguez, R.; Troadec, T.; Gau, D.; Saffon-Merceron, N.; Hashizume, D.; Miqueu, K.; Sotiropoulos, J.-M.; Baceiredo, A.; Kato, T. *Angew. Chem., Int. Ed.* **2013**, *52*, 4426−4430. (g) Hansen, K.; Szilvási, T.; Blom, B.; Irran, E.; Driess, M. *Chem. - Eur. J.* **2015**, *21*, 18930−18933. (h) Troadec, T.; Lopez Reyes, M.; Rodriguez, R.; Baceiredo, A.; Saffon-Merceron, N.; Branchadell, V.; Kato, T. *J. Am. Chem. Soc.* **2016**, *138*, 2965−2968.

(10) Analog strategy for isolation of acyclic three-coordinate germanone: Li, L.; Fukawa, T.; Matsuo, T.; Hashizume, D.; Fueno, H.; Tanaka, K.; Tamao, K. *Nat. Chem.* **2012**, *4*, 361−365.

(11) Filippou, A. C.; Baars, B.; Chernov, O.; Lebedev, Y. N.; Schnakenburg, G. *Angew. Chem., Int. Ed.* **2014**, *53*, 565−570.

(12) Ishida, S.; Abe, T.; Hirakawa, F.; Kosai, T.; Sato, K.; Kira, M.; Iwamoto, T. *Chem. - Eur. J.* **2015**, *21*, 15100−15103.

(13) Alvarado-Beltran, I.; Rosas-Sánchez, A.; Baceiredo, A.; Saffon-Merceron, N.; Branchadell, V.; Kato, T. *Angew. Chem., Int. Ed.* **2017**, *56*, 10481−10485.

(14) Wendel, D.; Porzelt, A.; Herz, F. A. D.; Sarkar, D.; Jandl, C.; Inoue, S.; Rieger, B. *J. Am. Chem. Soc.* **2017**, *139*, 8134−8137.

(15) Ochiai, T.; Franz, D.; Inoue, S. *Chem. Soc. Rev.* **2016**, *45*, 6327−6344.

(16) Linden, M. M.; Reisenauer, H. P.; Gerbig, D.; Karni, M.; Schäfer, A.; Müller, T.; Apeloig, Y.; Schreiner, P. R. *Angew. Chem., Int. Ed.* **2015**, *54*, 12404−12409.

DOI: 10.1021/jacs.7b10634
J. Am. Chem. Soc. 2017, 139, 17193−17198

(17) Inoue, S.; Leszczynska, K. *Angew. Chem., Int. Ed.* **2012**, *51*, 8589−8593.
(18) Marschner, C. *Eur. J. Inorg. Chem.* **1998**, *1998*, 221−226.
(19) Ahmad, S. U.; Szilvasi, T.; Irran, E.; Inoue, S. *J. Am. Chem. Soc.* **2015**, *137*, 5828−5836.
(20) (a) Weidenbruch, M., In *The Chemistry of Organic Silicon Compounds*, Rappoport, Z., Apeloig, Y., Eds.; John Wiley & Sons: Chichester, U.K., 2001; Vol. 3, pp 391−428. (b) Wendel, D.; Szilvási, T.; Jandl, C.; Inoue, S.; Rieger, B. *J. Am. Chem. Soc.* **2017**, *139*, 9156−9159.
(21) Schweizer, J. I.; Scheibel, M. G.; Diefenbach, M.; Neumeyer, F.; Würtele, C.; Kulminskaya, N.; Linser, R.; Auner, N.; Schneider, S.; Holthausen, M. C. *Angew. Chem., Int. Ed.* **2016**, *55*, 1782−1786.
(22) (a) Yamaguchi, T.; Sekiguchi, A.; Driess, M. *J. Am. Chem. Soc.* **2010**, *132*, 14061−14063. (b) Leszczynska, K.; Abersfelder, K.; Mix, A.; Neumann, B.; Stammler, H.-G.; Cowley, M. J.; Jutzi, P.; Scheschkewitz, D. *Angew. Chem., Int. Ed.* **2012**, *51*, 6785−6788. (c) Yamaguchi, T.; Asay, M.; Sekiguchi, A. *J. Am. Chem. Soc.* **2012**, *134*, 886−889. (d) Cowley, M. J.; Huch, V.; Rzepa, H. S.; Scheschkewitz, D. *Nat. Chem.* **2013**, *5*, 876−879.
(23) Hadlington, T. J.; Abdalla, J. A. B.; Tirfoin, R.; Aldridge, S.; Jones, C. *Chem. Commun.* **2016**, *52*, 1717−1720.
(24) Rekken, B. D.; Brown, T. M.; Fettinger, J. C.; Tuononen, H. M.; Power, P. P. *J. Am. Chem. Soc.* **2012**, *134*, 6504−6507.
(25) Moser, D. F.; Guzei, I. A.; West, R. *Main Group Met. Chem.* **2001**, *24*, 811−812.
(26) Protchenko, A. V.; Schwarz, A. D.; Blake, M. P.; Jones, C.; Kaltsoyannis, N.; Mountford, P.; Aldridge, S. *Angew. Chem., Int. Ed.* **2013**, *52*, 568−571.
(27) Lips, F.; Fettinger, J. C.; Mansikkamaki, A.; Tuononen, H. M.; Power, P. P. *J. Am. Chem. Soc.* **2014**, *136*, 634−637.
(28) Kato, T.; Rosas-Sánchez, A.; Alvarado-Beltran, I.; Baceiredo, A.; Saffon-Merceron, N.; Massou, S.; Hashizume, D.; Branchadell, V. *Angew. Chem.* **2017**, DOI: 10.1002/ange.201710358.

DOI: 10.1021/jacs.7b10634
J. Am. Chem. Soc. 2017, 139, 17193−17198

10. Precise Ammonia Activation and Oxygenation by an Iminodisilene

Title: "Precise Ammonia Activation and Oxygenation by an Iminodisilene"

Status: Draft

Journal: Angewandte Chemie

Publisher: Wiley

DOI:

Authors: Daniel Wendel, Tibor Szilvási, Daniel Henschel, Philipp J. Altmann, Christian Jandl, Shigeyoshi Inoue, Bernhard Rieger[a]

Content: Based on the previous findings and the *trans*-hydrogenation of (*Z*)-imino(silyl)disilene (depicted in Chapter 7), we continued our reactivity study focusing on the activation of ammonia and the behavior of the disilene towards various oxygen-atom transfer agents (O_2, N_2O and CO_2). The underlying motivation and the obtained results shall briefly be presented in this manuscript draft.

[a]D. Wendel planned and executed all experiments and wrote the manuscript. D. Henschel supported this project with additional experimental data. T. Szilvási designed and performed the theoretical analyses and contributed with fruitful mental input. P.J. Altmann and C. Jandl conducted all SC XRD-measurements and managed the processing of the respective data. All work was performed under the supervision of B. Rieger and S. Inoue.

COMMUNICATION WILEY-VCH

Precise Ammonia Activation and Oxygenation by an Iminodisilene

Daniel Wendel,[a] Tibor Szilvási,[d] Daniel Henschel,[a] Philipp J. Altmann,[c] Christian Jandl,[c] Shigeyoshi Inoue*[b] and Bernhard Rieger*[a]

Abstract: The selective activation of NH_3 and CO_2 still remains challenging for sub-valent silicon compounds. Herein, we present the precise splitting of the N–H bond of ammonia by (*Z*)-imino(silyl)disilene **1** to give racemic *trans*-1,2-disilane **2a**. According to DFT calculations, the stereospecific hydroamination follows a similar mechanism as the recently reported *anti*-addition of H_2 to the Si=Si bond of **1**. However, in agreement with theory, also the 1,1-silane **2b** as formal silylene addition product could be obtained under thermodynamic reaction control. Similarly, the cleavage of the labile Si=Si bond of **1** was elucidated in the isolation of silylene–BCF adduct **3**. Furthermore, the exceptional reactivity of **1** toward several oxygenation agents (O_2, N_2O, CO_2) was demonstrated. Beside the *cis*-dioxadisiletane **5-c**, also the *trans*-disilaoxirane **4-t**, a rare silicon analogue of an epoxide, was isolated and fully characterized. Its ring-strain was finally utilized to activate CO_2 and afford the five-membered *trans*-silacycle **6-t**.

The facile activation of ammonia and its transfer to olefines or arenes are considered as two major challenges for present and upcoming generations of chemists.[1] Despite recent spectacular progress in this field,[2] it is mainly the splitting of the strong N–H bond of NH_3 that still poses a significant hurdle for transition metal complexes, owing to the general electrophilicity of the metal center and the resulting preference to form simple coordination complexes with the nitrogen lone pair.[3] Therefore, by successfully accomplishing oxidative addition of ammonia under ambient conditions, in the last two decades a plethora of main group species have emerged as promising candidates to excel *d*-block metal complexes in hydroamination reactions.[4] Regarding low-valent silicon compounds, however, reports of NH_3 activations are still scarcely found. In fact, only three examples of oxidative cleavage of ammonia by cyclic[5] and acyclic silylenes[6] are known. In terms of disilenes, the much more reactive analogues of alkenes, this activation is even limited to only two instances (Scheme 1). Already in 2001, Weidenbruch et al. reported the regioselective addition of NH_3 to both conjugated Si=Si bonds of tetrasilabutadiene **I** to give the respective 1,4-diaminotetrasilane **I'**.[7] This reactivity is quite peculiar, as the structural analogous, uniformly substituted disilene **IIa** exposed to be absolutely inert to this reagent. In this context, Scheschkewitz and coworkers recently isolated the asymmetric disilene **IIb** in which the induced polarization of the Si=Si bond, resulting from the replacement of one Tipp ligand of **IIa** with a 2,4,6-trimethoxyphenyl (TMOP) group, re-enabled the quantitative and regioselective formation of $Tipp_2HSi$–$SiNH_2$(Tipp)TMOP **IIb'** with ammonia.[8]

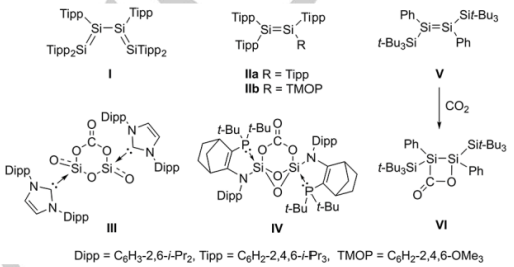

Dipp = C_6H_3-2,6-*i*-Pr_2, Tipp = C_6H_2-2,4,6-*i*-Pr_3, TMOP = C_6H_2-2,4,6-OMe_3

Scheme 1. Reported examples of NH_3 (disilene **I** and **IIb**) and CO_2 activations (products **III**, **IV** and **V**) with multiply bonded silicon compounds.

Another attractive molecule for the metal-free fixation by main group compounds is carbon dioxide. In the last couple of years diverse CO_2 activations involving low-valent silicon complexes have been reported[9], however, its reactivity toward multiply bonded silicon compounds has been explored to a far lesser extent. Notably, it has been demonstrated that NHC-supported Si(0) complex (IPr)Si=Si(IPr) by Robinson et al. could be oxidized by CO_2 to NHC-stabilized silicon-carbon mixed oxide **III**.[10] In a similar fashion, structurally related bis(*μ*-oxo)carbonato silicon complex **IV** was obtained by Baceiredo and coworkers from the stoichiometric reduction of CO_2 to CO using a phosphine-stabilized disilyne.[11] The only example of a reaction of carbon dioxide and a Si=Si bond of a conventional disilene was demonstrated in the formation of oxadisilacyclobutanone **VI** from the respective (*E*)-disilene **V** by the group of Wiberg in 2002, though unambiguous crystallographic data of this product was not presented.[12]

We have previously reported the isolation of (*Z*)-imino(silyl)disilene **1**, the first multiply bonded silicon compound that due to its strongly twisted and bent structure has been shown to stereospecifically add dihydrogen in *trans*-fashion under mild conditions.[13] Continuing this study, we extended the scope to ammonia and the oxygen-donors CO_2, N_2O and O_2. In analogy to the hydrogenation, we herein report the *trans*-hydroamination of **1** to 1,2-disilane **2a** via a similar *anti*-addition pathway. Additionally, dependent on the reaction conditions, also the splitting of the Si=Si bond and the formation of the corresponding 1,1-addition product **2b** was observed and rationalized by in-depth theoretical calculations. Experimentally, the propensity for a facile Si=Si bond cleavage was illustrated by isolation of silylene–BCF adduct **3** upon addition of $B(C_6F_5)_3$ to **1**. Furthermore, the goal of carbon dioxide activation by disilenes

[a] WACKER-Chair of Macromolecular Chemistry
[b] WACKER-Institute of Silicon Chemistry
[c] Catalysis Research Center
Technische Universität München
Lichtenbergstraße 4, 85748 Garching bei München (Germany)
E-mail: s.inoue@tum.de; rieger@tum.de
[d] Department of Chemical and Biological Engineering
University of Wisconsin Madison
1415 Engineering Drive, Madison, Wisconsin 53706-1607 (USA)

Supporting information for this article is given via a link at the end of the document.

was accomplished. Here, for the direct reaction of disilene **1** with CO_2, a mixture of three products could be identified via NMR monitoring experiments at room temperature. Separately conducted investigations with oxidizing agents N_2O and O_2 elucidated two of these unknown compounds as *cis*-dioxadisiletane **5-c** and *trans*-disilaoxirane **4-t**. The synthesis of the latter was finally utilized to identify the remaining product, the unique five-membered silacycle **6-t**.

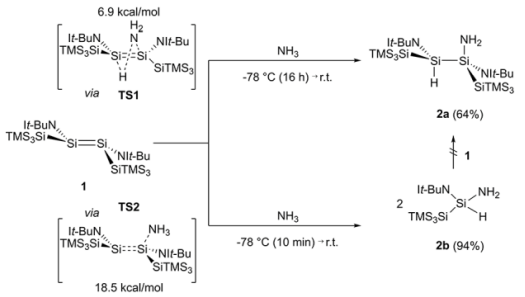

Scheme 2. NH_3 activation by imino(silyl)disilene **1** to selectively afford *trans*-1,2-disilane **2a** or 1,1-silane **2b** and depiction of DFT-calculated transition states (TS1 and TS2).

Exposure of a solution of disilene **1** in *n*-hexane at –78 °C to an excess of dry ammonia gas and stirring this mixture at this low temperature for 16 h led to the full decolorization of the former dark purple solution (Scheme 2). Removal of all volatiles and storage of a concentrated *n*-hexane solution at –35 °C gave 1,2-disilane **2a** as colorless crystals in 64% yield. Interestingly, closer investigations revealed, that if the reaction time at –78 °C is reduced to 10 min or the treatment with NH_3 is conducted directly at room temperature, instead almost exclusively the colorless 1,1-silane **2b**, as formal oxidative addition product of the respective silylene with ammonia, was obtained (yield 94%). Both products were unambiguously identified via multi-nuclear NMR and IR spectroscopy, mass spectrometry and X-ray diffraction. The ^{29}Si NMR shifts of the central silicon atoms of **2a** at –48.6 ppm ($SiNH_2$) and –62.4 ppm (SiH) are distinctly high-field shifted compared to the resonances of 1,2-disilane **IIb'** (–20.9 ppm and –57.1 ppm), most likely as a result of the electron-donating NHI ligand. The ^1J(Si–H) of 174 Hz of **2a**, however, is in fact comparable with the coupling constant of **IIb'** (187 Hz) and as expected much smaller than the one of monomeric silane **2b** (202 Hz). In analogy to the stereospecific hydrogenation, the crystallographic data of **2a** (Figure 1) elucidated a racemic mixture of (*RR*/*SS*)-1,2-disilane with a typical Si–Si single bond length (Si1–Si6 2.3984(6) Å) that is slightly shorter than the one of the respective hydrogen activation product (2.4142(7) Å).[13] Both silanes exhibit short Si–N_{NHI} bond lengths (**2a** Si1–N1 1.6694(15) Å, Si6–N4 1.6605(16) Å; **2b** Si1–N1 1.6350(17) Å) and quite obtuse SiN_{NHI}C angles (**2a** Si1–N1-C1 177.51(14)°, Si6–N4–C21 167.43(15)°; **2b** Si1–N1–C1 177.51(15)°), indicating a substantial π-donation by the exocyclic nitrogen atom of the NHI ligand to the silicon centers. The Si–NH_2 bonds (**2a** Si1–N7 1.7497(18) Å, **2b** Si1–N4 1.702(4) Å) are, however, within the range of typical Si–N bond lengths of related compounds (e.g. **I'** 1.772(3) Å, **IIb'** 1.7237(10) Å).

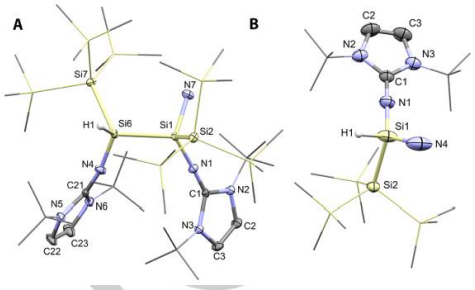

Figure 1. Molecular structures of **2a** and **2b** (one isomer respectively) in the solid state with ellipsoids set at the 50% probability level. Hydrogen atoms are omitted for clarity and TMS- and *t*-Bu-groups are simplified as wireframes. Selected bond lengths (Å) and angles (deg): (**A**) Si1–Si6 2.3984(6), Si1–Si2 2.4250(7), Si6–Si7 2.4182(7), Si1–N1 1.6694(15), Si6–N4 1.6605(16), N1–C1 1.269(2), N4–C21 1.269(2), Si1–N7 1.7497(18), Si1–N1-C1 177.51(14), Si6–N4–C21 167.43(15) (**B**) Si1–Si2 2.3657(10), Si1–N1 1.6350(17), N1–C1 1.277(2), Si1–N4 1.702(4), Si1–N1–C1 177.51(15), Si2–Si1–N1 115.59(7).

To explain the controllable product formation depending on the reaction conditions, we performed DFT calculations at the B3LYP-D3(BJ)/def2-SVP level of theory. In agreement with our reported *trans*-hydrogenation[13], an analog *anti*-transition state (TS1) was found with a low energy barrier (6.9 kcal/mol) (Scheme 2). This activation energy is significantly smaller than the value of the congeneric *anti*-addition of H_2 (15.6 kcal/mol) and hence explains the proceeding of the NH_3 reaction already at –78 °C. In the TS, the synergistic interaction of the σ*-orbital of NH_3 and the HOMO of **1** due to the twisted Si=Si structure facilitates the concerted homolytic cleavage of the N-H bond. Likewise, the LUMO of **1** interacts with the σ-orbital of the N–H bond of ammonia as well as with the lone pair at the nitrogen center (see SI). Notably, in line with our experimental observations, additional calculations located another transition state (TS2), where the interaction of the lone pair at the nitrogen center with the LUMO of **1** is dominating. This weakens the Si=Si double bond, leading to a nucleophilic substitution and subsequent hydroamination that affords two equivalents of 1,1-silane **2b** (see SI). In fact, TS2 is much higher in energy (18.5 kcal/mol), which is in accordance with the observed cleavage of the Si=Si bond and the product formation of **2b** only under thermodynamic reaction control. In this connection, also a potential pathway was considered where **2a** is formed from the insertion of the intermediary silylene into the Si–NH_2 or Si–H bond of **2b**, respectively. However, presumably due to large steric hindrance, the calculated barriers of both pathways (33.7 kcal/mol and 29.2 kcal/mol) are too high to adequately explain the formation of **2a** at low temperatures. To further support the proposed direct hydroamination, in a second experiment we treated two equivalents of **2b** in C_6D_6 with one equivalent of disilene **1**. Monitoring this reaction via ^{1}H NMR spectroscopy did not show any conversion to **2a**, even after one

day at room temperature. Thus, a dissociative pathway via two silylenes seems very unlikely. As a few base-induced disilene dissociations have been reported in literature[14], we were further interested to disclose the apparent silylene character of **1**. However, we followed an alternative strategy and treated disilene **1** with the strong Lewis acid $B(C_6F_3)_3$ in *n*-hexane (Scheme 3). The color of the solution rapidly changed from dark purple to yellow under formation of a fine, yellowish precipitate of silylene–BCF adduct **3** (79% yield). The ^{29}Si NMR spectrum of **3** showed a resonance of the Si(II) center at 161.9 ppm with a ^1J(SiB) of 58.7 Hz, very similar to the data (160.7 ppm, ^1J(SiB) = 53.9 Hz) of closely related IPrN(SiTMS$_3$)Si(II)–BCF adduct (IPrN = (HCNDipp)$_2$C=N).[9b] The X-ray structures of both compounds are also comparable, although the $SiN_{NHI}C$ angle of **3** (Si1–N1–C1 167.53(14)°) is clearly larger than the one of the silylene–borane adduct exhibiting the bulkier NHI ligand (151.10(14)°). Hence, a more pronounced contribution of the 1-sila-2-azallene resonance form **3'** can be assumed.

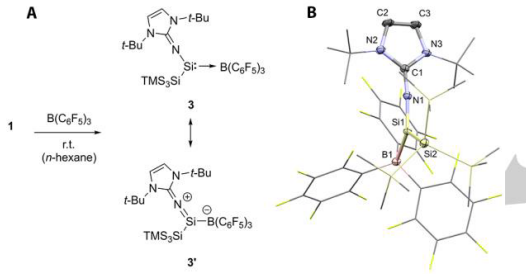

Scheme 3. (**A**) Reaction of **1** with $B(C_6F_5)_3$ to silylene–BCF adduct **3** and representation of zwitterionic resonance form **3'**. (**B**) Molecular structure of **3** in the solid state with ellipsoids set at the 50% probability level. Hydrogen atoms are omitted for clarity and TMS-, $(C_6F_5)_3$- and *t*-Bu-groups are simplified as wireframes. Selected bond lengths (Å) and angles (deg): Si1–B1 2.111(2), Si1–N1 1.6087(17), Si1–Si2 2.3925(7), N1–C1 1.307(2), C1–N2 1.378(2), C1–N3 1.381(2), N1–Si1–Si2 111.61(6), Si2–Si1–B1 126.78(6), B1–Si1–N1 121.50(8), Si1–N1–C1 167.53(14).

After these results, we addressed the CO_2 activation using a Si=Si bond of a disilene (Scheme 4). Treatment of **1** in C_6D_6 with excess carbon dioxide at room temperature, however, gave only a mixture of products. We therefore tried to approach the analysis of this unknown mixture by separate experiments with other common oxygen-atom transfer reagents. Exposure of a solution of **1** in *n*-hexane to molecular oxygen at –78 °C led to full decolorization within seconds and the sole formation of colorless *cis*-dioxadisiletane **5-c** in 80% yield. The retention of the stereochemistry around the Si–Si bond during the formation of **5-c** correlates well with other reported disilene oxygenations using O_2[15] and is further supported by theoretical investigations that predict the *cis*-isomer to be 4.6 kcal/mol more stable than its *trans*-analogue. The comparison of the NMR data of pure **5-c** verified this product as one component of the direct disilene/CO_2 reaction mixture. To elucidate the other products, we tested the behavior of **1** toward N_2O. Exposure of **1** in C_6D_6 to one atmosphere of N_2O at room temperature gave an instant yellow solution that was monitored by ^{1}H and ^{29}Si NMR spectroscopy. As confirmed by matching GIAO-DFT NMR shifts, a mono-oxygenated product, the *cis*-disilaoxirane **4-c**, formed. Interestingly, this compound isomerized quickly (within 4 h) and quantitatively to the thermodynamically more stable *trans*-isomer **4-t** (ΔE = 5.8 kcal/mol), which was isolated as a yellowish solid in 76% yield. In contrast to the oxygenation of Jutzi's (*E*)-disilene [Cp*(TMS)$_2$NSi]$_2$ with N_2O recently reported by Roesky et al., that gave an isolable mixture of *cis*- and *trans*-dioxadisiletanes[16], a second oxygenation step to the *trans*-isomer of **5-c** was only observed upon heating a solution of **4-t** to 50 °C in N_2O atmosphere for 16 hours.

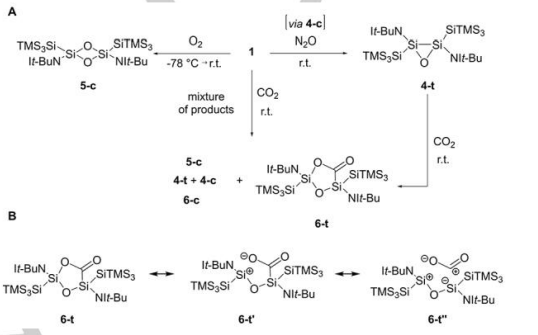

Scheme 4. (**A**) Overview of oxygenation reactions of **1** with O_2, N_2O and CO_2 to afford *trans*-disilaoxirane **4-t**, *cis*-dioxadisiletane **5-c** and five-membered silacycle **6-t**. (**B**) Plausible resonance forms of **6-t**.

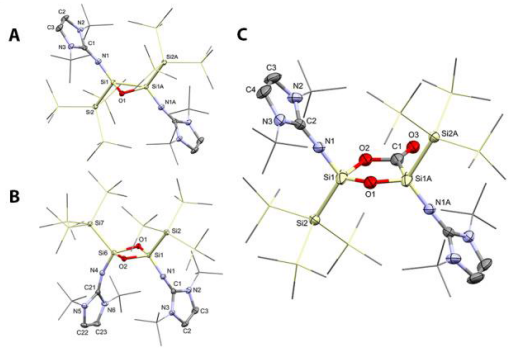

Figure 2. Molecular structures of **4-t** (**A**, one isomer), **5-c** (**B**, one out of two molecules in the asymmetric unit) and **6-t** (**C**, one isomer) in the solid state with ellipsoids set at the 50% probability level. Hydrogen atoms are omitted for clarity and TMS- and *t*-Bu-groups are simplified as wireframes. Selected bond lengths (Å) and angles (deg): (**A**) Si1–Si1A 2.2887(10), Si1–O1 1.742 (2), Si1A–O1 1.757(2), Si1–N1 1.6494(15), Si1–O1–Si1A 81.70(11). (**B**) Si1–Si6 2.4432(8), Si1–O1 1.6990(14), Si1–O2 1.6956(14). Si6–O1 1.6959(14), Si6–O2 1.6879(14), Si1–N1 1.6424(18), Si6–N4 1.6458(17), Si6–O1–Si1 92.05(7), Si1–O2–Si6 92.45(7) (**C**) Si1···Si1A 2.821(3), Si1–O1 1.526(7), Si1A–O1 1.574(6), Si1–N1 1.616(4), Si1A–C1 2.093(11), C1–O3 1.290(13), C1–O2 1.364(11), Si1–O2 1.988(7), Si1–O1–Si1A 131.0(4), O3–C1–O2 111.5(9).

This result agrees with a calculated high energy barrier of 20.4 kcal/mol and a high-lying and sterically protected LUMO of

4-t that hinders the second nucleophilic N_2O attack (see SI). Quite the opposite picture was found for the HOMO with a considerable amount of accessible π-electron density in between the Si–Si bond. As a consequence, treatment of isolated **4-t** with CO_2 led to the selective formation of the respective addition product **6-t**. This novel five-membered silacycle was isolated as colorless crystals in 63% yield and was identified, together with its *cis*-isomer **6-c**, as the remaining product of the direct disilene/CO_2 reaction mixture. Interestingly, X-ray analysis of **6-t** (Figure 2) revealed extremely short bonds for the bridging Si–O moieties (Si1–O1 1.526(7) Å, Si1A–O1 1.574(6) Å), pointing to a distinct double bond character within the disiloxane unit. In contrast, the Si–C and Si–O bonds to the bent CO_2 fragment (Si1A–C1 2.093(11) Å, Si1–O2 1.988(7) Å) are considerably elongated and possess substantial dative nature. Regarding these experimental findings, we propose the zwitterionic resonance forms **6-t'** and **6-t''** as predominant formulation of **6-t**. Quantum chemical calculations agree with this characterization, revealing a charge distribution based on Natural Population Analysis (NPA) with a strongly negatively polarized O2 atom (–0.88) and a highly positively charged Si1 atom (+1.91). Furthermore, Natural Bond Orbital (NBO) analysis gave a similar picture with extremely polarized Si1–O2 (9% versus 91%) and Si1A–C1 (25% versus 75%) bonds illustrating their ionic character.

In summary, our work successfully demonstrates the precise activation of ammonia by (*Z*)-imino(silyl)disilene **1** to afford the *trans*-1,2-disilane **2a** under kinetic and the 1,1-silane **2b** under thermodynamic reaction control. The facile splitting of the Si=Si bond of **1** was further illustrated by isolation of the silylene–BCF adduct **3**. Moreover, the reactivity of **1** was tested toward oxygenation agents N_2O, O_2 and CO_2 leading to novel silacycles, namely disilaoxirane **4-t**, dioxadisiletane **5-c** and five-membered silacycle **6-t** with defined stereochemistry. All reactions were supported by computational calculations. Currently, the utilization of the ring-strain of **4-t** in further activations and experiments regarding potential manipulation reactions at the activated CO_2 moiety of **6-t** are under active investigation in our laboratories.

Acknowledgements

We are grateful to the WACKER Chemie AG for continued financial support. We thank Dominik Reiter, Philipp Frisch and Richard Holzner for revising the paper and Dr. Alexander Pöthig for his advice pertaining to crystallography.

Keywords: ammonia • disilene • main group elements • oxygenation • silicon

[1] J. Haggin, *Chem. Eng. News* **1993**, *71*, 23-27.

[2] Selected examples of transition-metal mediated NH_3 activations: a) G. W. Margulieux, M. J. Bezdek, Z. R. Turner, P. J. Chirik, *J. Am. Chem. Soc.* **2017**, *139*, 6110-6113; b) M. J. Bezdek, S. Guo, P. J. Chirik, *Science* **2016**, *354*, 730-733; c) R. M. Brown, J. Borau Garcia, J. Valjus, C. J. Roberts, H. M. Tuononen, M. Parvez, R. Roesler, *Angew. Chem. Int. Ed.* **2015**, *127*, 6372-6375; d) J. Zhao, A. S. Goldman, J. F. Hartwig, *Science* **2005**, *307*, 1080-1082.

[3] J. Hoover, *Science* **2016**, *354*, 707-708.

[4] Selected examples of NH_3 activations by main group compounds: a) S. Yadav, S. Saha, S. S. Sen, *ChemCatChem* **2016**, *8*, 486-501; b) T. P. Robinson, D. M. De Rosa, S. Aldridge, J. M. Goicoechea, *Angew. Chem. Int. Ed.* **2015**, *54*, 13758-13763; c) S. M. McCarthy, Y.-C. Lin, D. Devarajan, J. W. Chang, H. P. Yennawar, R. M. Rioux, D. H. Ess, A. T. Radosevich, *J. Am. Chem. Soc.* **2014**, *136*, 4640-4650; d) P. P. Power, *Acc. Chem. Res.* **2011**, *44*, 627-637; e) Y. Peng, B. D. Ellis, X. Wang, P. P. Power, *J. Am. Chem. Soc.* **2008**, *130*, 12268-12269; f) G. D. Frey, V. Lavallo, B. Donnadieu, W. W. Schoeller, G. Bertrand, *Science* **2007**, *316*, 439-441; g) Y. Peng, J.-D. Guo, B. D. Ellis, Z. Zhu, J. C. Fettinger, S. Nagase, P. P. Power, *J. Am. Chem. Soc.* **2009**, *131*, 16272-16282; h) Z. Zhu, X. Wang, Y. Peng, H. Lei, J. C. Fettinger, E. Rivard, P. P. Power, *Angew. Chem. Int. Ed.* **2009**, *48*, 2031-2034.

[5] A. Jana, C. Schulzke, H. W. Roesky, *J. Am. Chem. Soc.* **2009**, *131*, 4600-4601.

[6] a) A. V. Protchenko, J. I. Bates, L. M. A. Saleh, M. P. Blake, A. D. Schwarz, E. L. Kolychev, A. L. Thompson, C. Jones, P. Mountford, S. Aldridge, *J. Am. Chem. Soc.* **2016**, 4555–4564; b) T. J. Hadlington, J. A. B. Abdalla, R. Tirfoin, S. Aldridge, C. Jones, *Chem. Commun.* **2016**, *52*, 1717-1720.

[7] S. Boomgaarden, W. Saak, M. Weidenbruch, H. Marsmann, *Z. Anorg. Allg. Chem.* **2001**, *627*, 349-352.

[8] A. Meltzer, M. Majumdar, A. J. P. White, V. Huch, D. Scheschkewitz, *Organometallics* **2013**, *32*, 6844-6850.

[9] Recent examples of CO_2 activations by low-valent silicon compounds: a) T. Kato, R. Rodriguez, I. Alvarado-Beltran, J. Saouli, A. Baceiredo, N. Saffon-Merceron, V. Branchadell, *Angew. Chem. Int. Ed.* **2018**, 10.1002/anie.201709787; b) D. Wendel, A. Porzelt, F. A. D. Herz, D. Sarkar, C. Jandl, S. Inoue, B. Rieger, *J. Am. Chem. Soc.* **2017**, *139*, 8134-8137; c) D. Wendel, D. Reiter, A. Porzelt, P. J. Altmann, S. Inoue, B. Rieger, *J. Am. Chem. Soc.* **2017**, *139*, 17193-17198; d) A. Rosas-Sánchez, I. Alvarado-Beltran, A. Baceiredo, N. Saffon-Merceron, S. Massou, D. Hashizume, V. Branchadell, T. Kato, *Angew. Chem. Int. Ed.* **2017**, *129*, 16132-16136; e) I. Alvarado-Beltran, A. Rosas-Sánchez, A. Baceiredo, N. Saffon-Merceron, V. Branchadell, T. Kato, *Angew. Chem. Int. Ed.* **2017**, *56*, 10481-10485; f) A. Burchert, S. Yao, R. Müller, C. Schattenberg, Y. Xiong, M. Kaupp, M. Driess, *Angew. Chem. Int. Ed.* **2017**, *56*, 1894-1897; g) F. M. Mück, J. A. Baus, M. Nutz, C. Burschka, J. Poater, F. M. Bickelhaupt, R. Tacke, *Chem. Eur. J.* **2015**, *21*, 16665-16672; h) K. Junold, M. Nutz, J. A. Baus, C. Burschka, C. Fonseca Guerra, F. M. Bickelhaupt, R. Tacke, *Chem. Eur. J.* **2014**, *20*, 9319-9329; i) X. Liu, X.-Q. Xiao, Z. Xu, X. Yang, Z. Li, Z. Dong, C. Yan, G. Lai, M. Kira, *Organometallics* **2014**, *33*, 5434-5439.

[10] Y. Wang, M. Chen, Y. Xie, P. Wei, H. F. Schaefer, G. H. Robinson, *J. Am. Chem. Soc.* **2015**, *137*, 8396-8399.

[11] D. Gau, R. Rodriguez, T. Kato, N. Saffon-Merceron, A. de Cózar, F. P. Cossío, A. Baceiredo, *Angew. Chem. Int. Ed.* **2011**, *50*, 1092-1096.

[12] N. Wiberg, W. Niedermayer, K. Polborn, P. Mayer, *Chem. Eur. J.* **2002**, *8*, 2730-2739.

[13] D. Wendel, T. Szilvási, C. Jandl, S. Inoue, B. Rieger, *J. Am. Chem. Soc.* **2017**, *139*, 9156-9159.

[14] a) K. Suzuki, T. Matsuo, D. Hashizume, K. Tamao, *J. Am. Chem. Soc.* **2011**, *133*, 19710-19713; b) N. Takeda, T. Kajiwara, H. Suzuki, R. Okazaki, N. Tokitoh, *Chem. Eur. J.* **2003**, *9*, 3530-3543; c) N. Takeda, H. Suzuki, N. Tokitoh, R. Okazaki, S. Nagase, *J. Am. Chem. Soc.* **1997**, *119*, 1456-1457.

[15] See references within this review: M. Kira, T. Iwamoto, *Adv. Organomet. Chem.* **2006**, *54*, 73-148.

[16] a) B. Maity, D. Koley, *J. Phys. Chem. A* **2017**, *121*, 401-417; b) S. Khan, R. Michel, D. Koley, H. W. Roesky, D. Stalke, *Inorg. Chem.* **2011**, *50*, 10878-10883.

Entry for the Table of Contents (Please choose one layout)

Layout 1:

COMMUNICATION

Precise Activation: The double donor–acceptor type Si=Si bond of a (*Z*)-imino(sily)disilene was exploited to selectively activate ammonia, leading to the *trans*-1,2-disilane under kinetic and the 1,1-silane under thermodynamic control conditions. Furthermore, its reactivity toward Lewis acid $B(C_6F_5)_3$ and the oxygen-atom transfer agents N_2O, O_2 and CO_2 was elucidated.

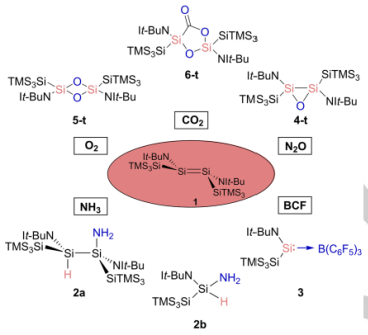

Daniel Wendel,[a] Tibor Szilvási,[d] Daniel Henschel,[a] Philipp J. Altmann,[c] Christian Jandl,[c] Shigeyoshi Inoue[b] and Bernhard Rieger*[a]*

Page No. – Page No.

Precise Ammonia Activation and Oxygenation by an Iminodisilene

11. Summary and Outlook

In 2012, the groups of Jones and Aldridge and separately, the team of P. P. Power discovered the first representatives of room temperature stable, two-coordinate acyclic silylenes (**L9-10**, see Chapter 3.3) – divalent silicon compounds that prior to this seminal work have been considered as absolutely elusive.[63-64] Driven by these extraordinary findings, this thesis sought to expand the number of accessible silylene structures and especially explore their reactivity to better estimate their potential as silicon-based main group catalysts. Initially, with the ulterior motive of a silylene-catalyzed olefin polymerization in mind, the reactivity of literature known amino(silyl)silylene **L-11**, toward ethylene was examined. Different from the dynamic dissociation equilibrium of related bis(thiolato)silylene **L-9** with ethylene (see Chapter 3.3), in our study, only the quantitative conversion of **L-11** to silirane **3** was observed (Scheme 10).

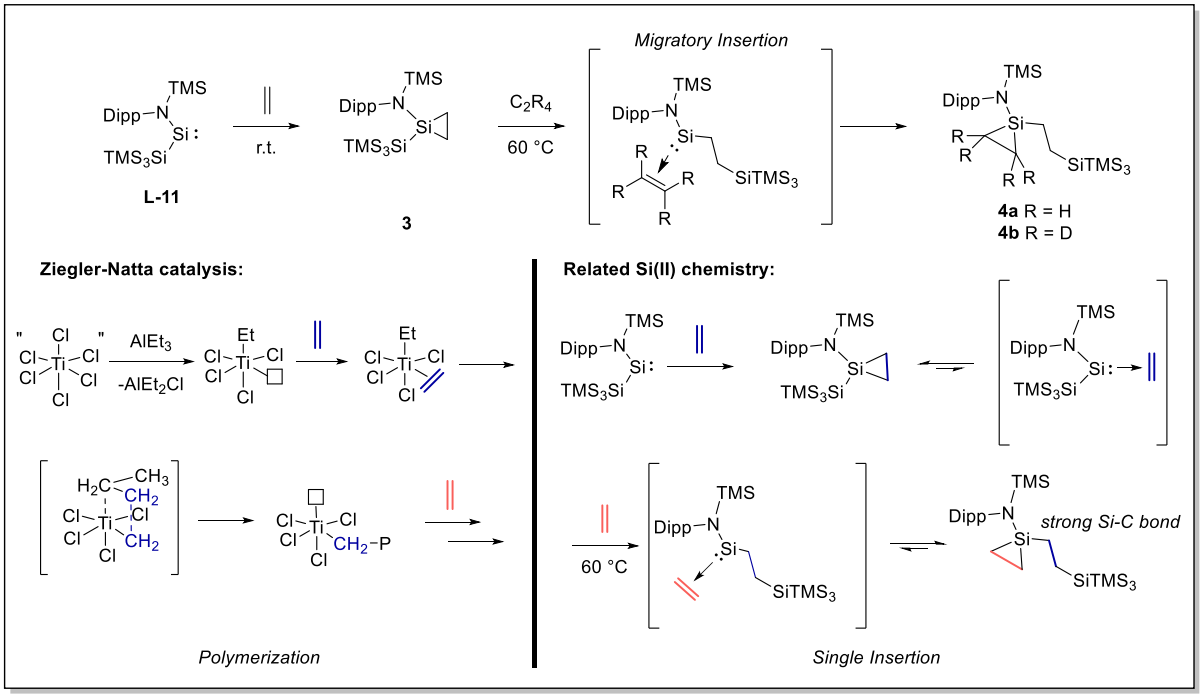

Scheme 10. Reaction pathway of Jones' amino(silyl)silylene **L-11** with ethylene to afford siliranes **4a** and **4b**; Proposed mechanism and comparison to the conventional Ziegler-Natta catalysis.

It was further shown that heating of the reaction solution in ethylene atmosphere to 60 °C triggered the formation of modified silirane **4a**, comprising a second ethylene molecule. Here, NMR experiments with C_2D_4 indicated a migratory insertion pathway of the coordinated ethylene into the Si–Si bond of the ligand framework and subsequent trapping of the

intermediary Si(II) species with deuterated ethylene (silirane **4b**). At first glance, this process seemed reminiscent of the traditional mechanism of the Ziegler-Natta catalysis, however, no second or further insertion steps to extend the alkyl chain were detectable in follow-up experiments, presumably due to the formation of a stable Si–C bond. In total, this study exemplified the general possibility of olefin insertions into labile Si(II)-ligand bonds. However, in order to approach the goal of olefin polymerization *via* the described pathway, aside from finding a solution for the explicit weakening of the intermediary silicon-carbon bond, a chain elimination step has yet to be found.

In addition, the preparation of novel, acyclic sub-valent silicon compounds possessing NHI ligands, preferably silylenes, has been tackled intensively. Following the initial synthesis plan *via* the respective iminotribromosilane (see Chapter 5), the unique (*Z*)-imino(silyl)disilene **2** was isolated as a rare example of a nitrogen-substituted disilene, with a highly *trans*-bent and twisted geometry, including the longest Si=Si bond reported to date (Scheme 11).

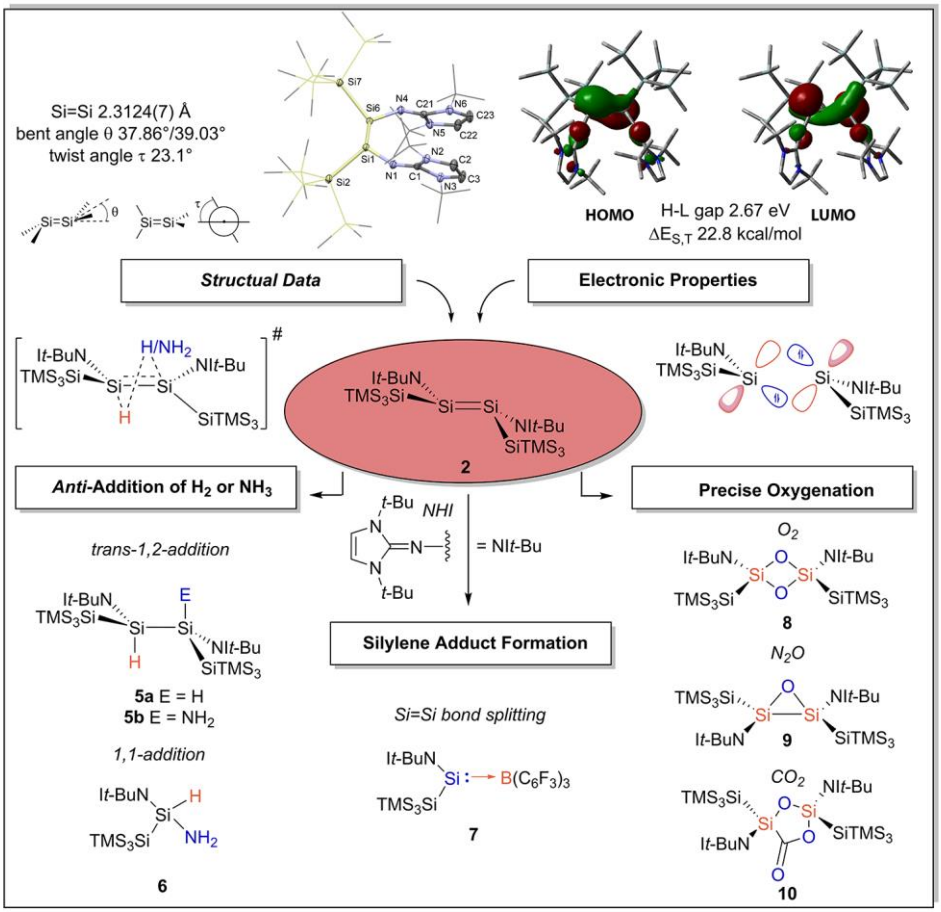

Scheme 11. General overview of structural and electronic properties of (*Z*)-imino(silyl)disilene **2** and its resultant reactivity.

DFT calculations indicated that this highly reactive bond is best described as double donor–acceptor bond between two silylene fragments. This special bonding was further utilized to demonstrate the first hydrogen activation by a multiply bonded silicon compound under ambient conditions. The obtained experimental and theoretical data revealed that, in strong contrast to alkenes, disilene **2** was hydrogenated in *trans*-fashion to 1,2-disilane **5a**, in agreement with a located concerted *anti*-addition pathway that was favored due to the strongly bent and twisted Si=Si structure. Consistently, the same *trans*-stereospecificity was detectable in the activation of ammonia to give 1,2-hydroamination product **5b**. Though here, additionally, the splitting of the Si=Si bond and the formation of the corresponding 1,1-addition product **6** was observed as a result of the interaction of the LUMO of **2** with the nitrogen lone pair of NH_3. It could be verified, that the product selectivity was controlled by precisely adjusting the temperature of the hydroamination process, giving mainly **5b** under kinetic reaction control (–78 °C, 16 h) and **6** under thermodynamic reaction control (–78 °C, only 10 min then r.t.) conditions. As a result of the extremely elongated Si=Si bond, no π-complex or a three-membered metallacycle were obtained in the reaction with the Lewis acid BCF. Instead, the monomeric silylene-BCF adduct **7** with a pronounced sila-aza-allene character was isolated exclusively and fully characterized. Moreover, to gain a deeper insight into the ambiguous reactivity of **2**, its exceptional bonding situation was tested in the activation of oxygen-containing substrates. Dependent on the oxygenation agents (O_2, N_2O and CO_2), several new silacycles **8**-**10** with different ring sizes have been isolated. According to theoretical calculations, all of them were formed as derived products of the direct oxygenation of the Si=Si bond of **2**, thereby excluding any involvement of an intermediary silylene species. The most promising building block seems to be the three-membered *trans*-disilaoxirane ring **9**, a rare silicon analogue of an epoxide, whose ring-strain and labile Si–Si bond may further be used to activate substrates. In this context, the X-ray data of the five-membered silacycle **10**, the formal product of **9** with CO_2, revealed extremely elongated Si–C and Si–O bonds to the loosely bound CO_2 molecule, which may create the possibility to perform manipulation reactions at the activated carbonyl center. In summary, as a result of the counteracting influences of silyl and NHI ligands, the isolated imino(silyl)disilene **2** exhibits exceptional structural and electronic properties that were used to access prior unknown reactivities of disilenes. As a next step towards catalysis, the search for reversibility and potential transfer of the activated substrates to organic molecules has to be intensified.

Following this outcome, the primary goal of the isolation of a two-coordinate acyclic silylene was pursued by increasing the sterical hindrance of the NHI wingtips that would lead to a higher repulsion between both Si centers, and eventually, a monomeric structure. Indeed, by replacement of *t*-Bu with Dipp groups an acyclic imino(silyl)silylene **1a'** was detected, but only at low temperatures (–78 °C) in *in situ* UV-vis and ^{29}Si NMR experiments. Astonishingly, it was demonstrated that above this temperature the Si(II) center of the transient silylene **1a'** quantitatively inserted into the C=C bond of the aromatic ligand framework to form silacycloheptatriene (silepin) **1a** (Scheme 12).

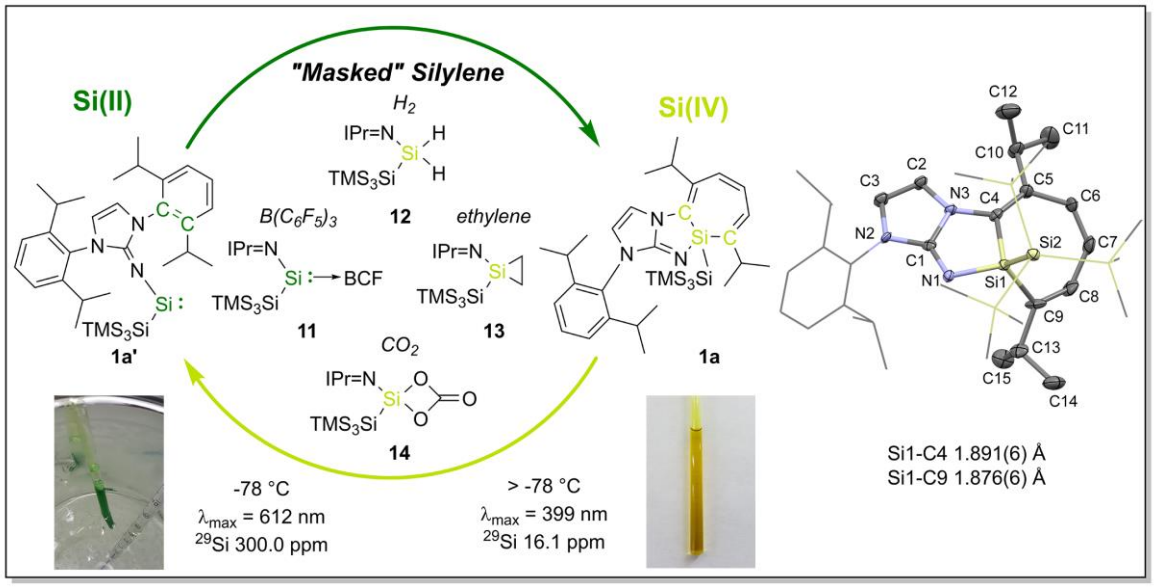

Scheme 12. Summary of imino(silyl)silepin **1a** as "masked" silylene in the activation of small molecules.

According to initial DFT calculations, this facile transformation was likely attributed to a strong interaction of the highly Lewis acidic silylene 3p-orbital with the electron rich π-bond of the proximate phenyl ring, which largely antagonizes the opposing energy-releasing effect of rearomatization during the reverse process. Accordingly, both species were determined to be energetically very narrow (17.3 kJ/mol), which suggested a thermally accessible interconversion. This hypothesis was experimentally verified by detection of silylene **1a'** in additional (HT) UV-vis experiments. In particular the intrinsic Si(II) nature of silepin **1a** was visualized in the isolation of the silylene-borane adduct **11** upon addition of BCF. The unprecedented propensity to undergo facile, intramolecular reductive elimination was further utilized in the investigation of silepin **1a** as a direct "masked" silylene in the activation of small molecules. Exposure of the formal Si(IV) compound **1a** to challenging substrates, such as hydrogen or ethylene, still gave the respective silicon hydride **12** or silirane **13** under mild conditions. Interestingly, carbon dioxide, a notorious target for reactive main group

compounds, was also stoichiometrically reduced to carbon monoxide with the formation of the first monomeric, four-coordinate silicon carbonate complex **14**. As the formation of this compound was presumed to follow a [2+2] cycloaddition of an intermediary transient silanone with a second CO_2 molecule, the focus thereupon shifted to the isolation of such hitherto elusive species.

As expected, a slightly adapted procedure and a simple change of the oxygenation agent from CO_2 to N_2O did the trick and the first precedents of fully neutral, three-coordinate acyclic imino(silyl)silanones **15** were obtained as "bottle-able" white powders with indefinite stability as solids and lifetimes in solution of up to 2 days (Scheme 13).

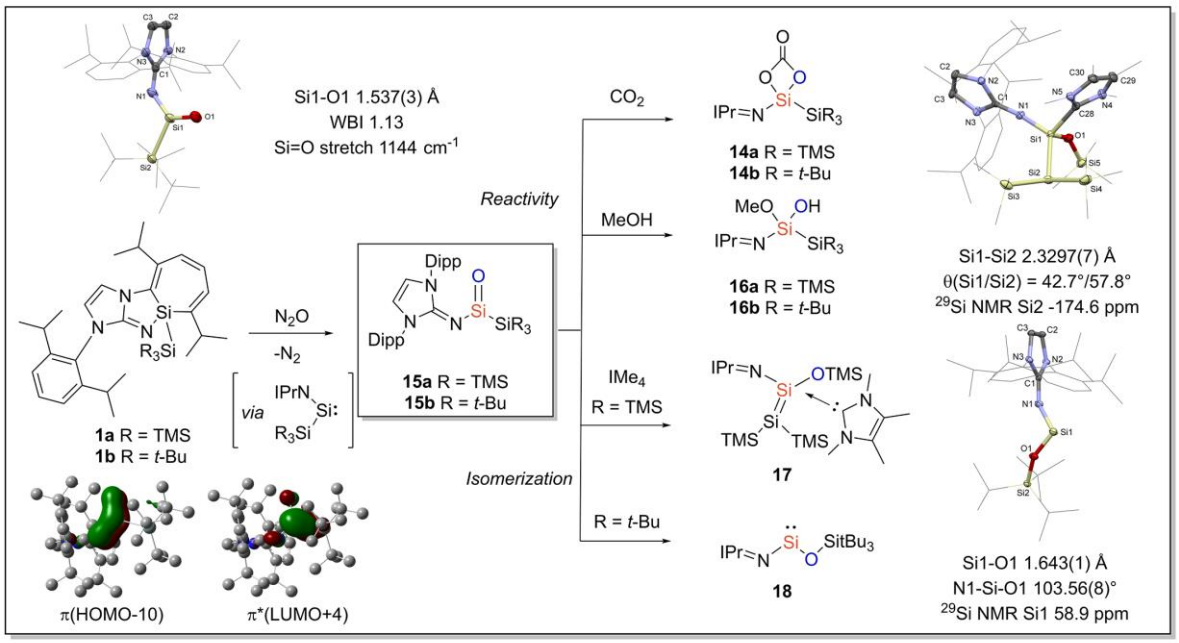

Scheme 13. Formation of imino(silyl)silanones **15** and results of their isomerization and reactivity pathways.

Crystal data analysis of **15b** revealed the presence of an extremely short Si=O bond (1.537(3) Å), which, together with the important stabilization effects of the adjacent NHI and silyl ligands were investigated by in-depth DFT calculations. In particular the mixing of the nonbonding orbital of the exocyclic nitrogen atom with the Si=O π-bond (HOMO-10) and the significant σ-donation and hyperconjugation of the silyl group (LUMO+4) were identified as principal stabilization effects of, the otherwise, highly polarized Si=O moiety. In terms of reactivity, the already mentioned CO_2 activation by the silepin was repeated separately as final proof of the silanone intermediate in this pathway. Moreover, the high reactivity of silanones **15** was tested towards methanol, which instantly gave the respective silanol **16**, in

analogy to the established reaction of ketones with alcohols to hemiketals. Since our long-run objective has been the permanent stabilization of silanones, we were further interested in a detailed investigation of the occurring isomerization processes. For silanone **15a** with a hypersilyl ligand, it was found that an intermediary disilene formed through a 1,3-silyl migration. This intermediate was successfully trapped with IMe_4 as a rare example of an NHC-stabilized disilene **17**, possessing a highly zwitterionic Si=Si bond. For silanone **15b**, the second example of an easy change in the oxidation state of Si(IV) to less stable Si(II) was achieved. Due to the oxophilic nature of silicon and the intrinsic tendency of silicon to form stable σ-bonds with oxygen, a selective rearrangement of **15b** to two-coordinate acyclic *N*,*O*-silylene **18** was discovered. As the first precedent of a siloxy stabilized silylene, this compound is of high interest to provide new insights and perspectives regarding the synthesis, stabilization and reactivity of acyclic two-coordinate silylenes. Due to its oxo-ligand and the structural analogy to the amino(alkoxy)germylene and stannylene derivatives **L-41**, used in the catalytic hydroboration of carbonyl compounds (see Chapter 4.1), finding a similar σ-bond metathesis step of **18** with boranes may pave the way for silylene-based catalysis.

In conclusion, this thesis has succeeded in the implementation of NHI ligands into several novel low-valent silicon compounds with fascinating electronic and structural features, that were not only thoroughly analyzed from both experimental and theoretical point of view, but instantly utilized to demonstrate prior unprecedented reactivities. Strikingly, within this work the first hydrogenation of multiply bonded silicon compounds was discovered. In addition, a new concept using silepins as direct silylene equivalents in the activation of small molecules was developed. Here, as first proof for a viable catalysis based on the Si(II)/Si(IV) redox couple, the elemental step of an mild, intramolecular reductive elimination at a silicon center was presented. Separately, with the first reported examples of room temperature stable three-coordinate, neutral, acyclic silanones, the eagerly-awaited dream of Kipping of isolable silicon analogues of ketones was basically fulfilled, now creating the opportunity to explore the still unknown chemistry of silacarbonyl compounds. Finally, with the extension of the list of accessible two-coordinate acyclic silylenes, the foundation for further investigations of the catalytic potential of this compound class was laid, which will hopefully soon lead to the expected step-change in main group catalysis.

12. Zusammenfassung und Ausblick

Im Jahr 2012 entdeckten die Forschungsgruppen um Prof. Jones und Prof. Aldridge und unabhängig davon das Team von Prof. Power die ersten Vertreter von raumtemperaturstabilen, zweifach koordinierten, acyclischen Silylenen (**L9**-**10**, siehe Kapitel 3.3) – divalente Siliciumverbindungen, die vor diesen bahnbrechenden Arbeiten als absolut instabil und schwer isolierbar galten.[63-64] Von diesen außergewöhnlichen Ergebnissen inspiriert, sollte diese Arbeit versuchen, die Zahl zugänglicher Silylen-Strukturen zu erweitern. Dabei lag der Fokus insbesondere auf der Untersuchung ihrer Reaktivität, um ihr Potenzial als silicium-basierte Hauptgruppenkatalysatoren besser bewerten zu können. Zunächst wurde mit dem Hintergedanken einer silylen-katalysierten Olefinpolymerisation die Reaktivität des literaturbekannten Amino(silyl)silylens **L-11** gegenüber Ethylen analysiert. Im Unterschied zum dynamischen Dissoziationsgleichgewicht des Bis(thiolato)silylens **L-9** mit Ethylen (siehe Kapitel 3.3) wurde in dieser Studie lediglich die quantitative Umsetzung von Silylen **L-11** zu Siliran **3** beobachtet (Schema 14).

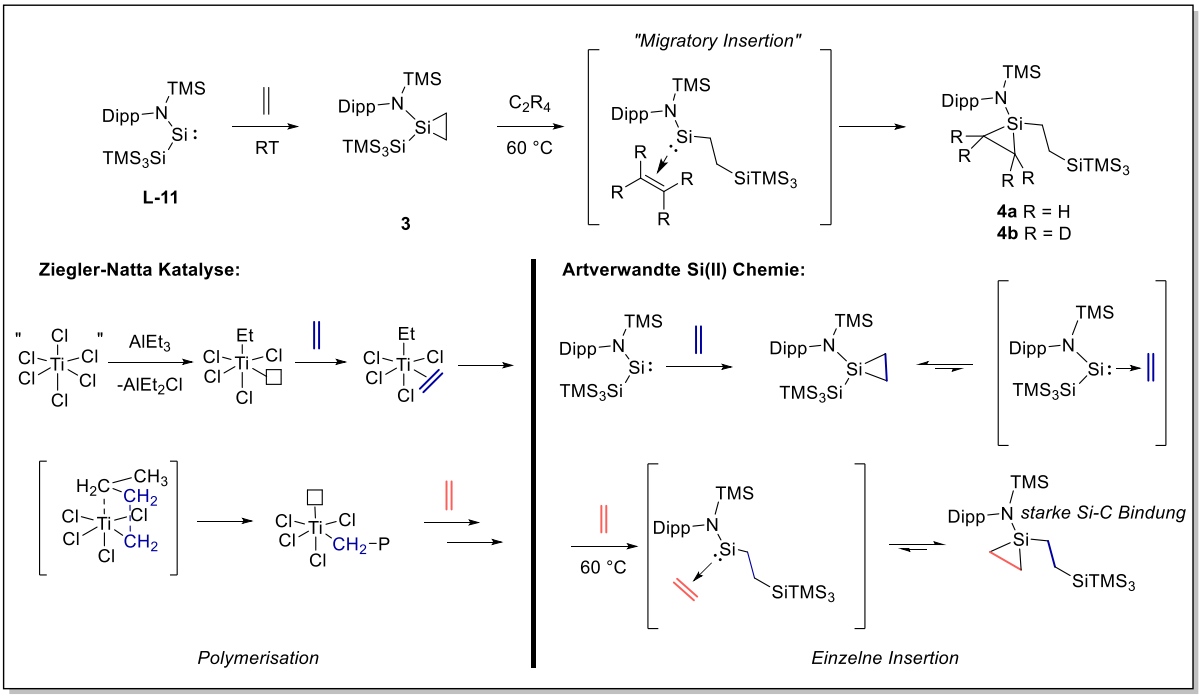

Schema 14. Reaktionspfad des von Jones *et al.* entwickelten Amino(silyl)silylens **L-11** mit Ethylen zu den Siliranen **4a** und **4b**; Postulierter Mechanismus und direkter Vergleich mit dem konventionellen Mechanismus der Ziegler-Natta Katalyse.

Es wurde jedoch gezeigt, dass das Erhitzen der Reaktionslösung auf 60 °C in Ethylen-Atmosphäre die Bildung des modifizierten Silirans **4a**, welches ein zweites Ethylen-Molekül aufweist, auslöst. Hier zeigten weiterführende NMR-Experimente mit C_2D_4, dass der Mechanismus einer „Migratory Insertion“ des koordinierten Ethylens in die Si–Si Bindung des Ligandengerüsts folgt und anschließend die intermediäre Si(II)-Spezies zur Bildung von Siliran **4b** mit deuteriertem Ethylen aus der Lösung abgefangen wird. Auf den ersten Blick scheint dieser Prozess an den traditionellen Mechanismus der Ziegler-Natta-Katalyse zu erinnern, jedoch wurde in Folgeexperimenten, vermutlich durch die Bildung einer äußerst stabilen Si–C Bindung, keine zweite Insertion oder sogar mehrere konsekutive Insertionsschritte zur Verlängerung der Alkylkette nachgewiesen. Dennoch konnte in dieser Studie exemplarisch die generelle Möglichkeit von Olefin-Insertionen in labile Si(II)-Liganden Bindungen aufgezeigt werden. Um trotz dessen dem Ziel einer Olefinpolymerisation über den beschriebenen Reaktionsweg näher zu kommen, muss, neben der Suche nach einer Lösung für die explizite Schwächung der intermediären Silicium-Kohlenstoff Bindung, auch über eine Möglichkeit für einen bislang noch fehlenden Ketteneliminierungsschritt nachgedacht werden.

Darüber hinaus wurde der Darstellung von neuen, acyclischen niedervalenten Siliciumverbindungen, vorzugsweise Silylenen, die durch NHI-Liganden stabilisiert werden, intensiv nachgegangen. Gemäß dem ursprünglichen Syntheseplan, ausgehend vom entsprechenden Iminotribromsilan (siehe Kapitel 5), wurde das außergewöhnliche (*Z*)-Imino(silyl)disilen **2** als seltenes Beispiel eines Stickstoff-substituierten Disilens isoliert, welches eine stark *trans*-gewinkelte und verdrillte Doppelbindungsgeometrie mit der bisher längsten Si=Si Bindung aufweist (Schema 15). DFT-Rechnungen zeigten, dass diese hochreaktive Bindung am besten als doppelte Donor-Akzeptor Bindung zwischen zwei Silylen-Fragmenten beschrieben werden sollte. Diese spezielle Bindungssituation wurde genutzt, um die erste Wasserstoffaktivierung durch eine mehrfach gebundene Siliciumverbindung, die interessanterweise bereits unter Normalbedingungen abläuft, zu demonstrieren. Hierbei belegten die erhaltenen experimentellen und theoretischen Daten, dass Disilen **2**, im starken Gegensatz zu Alkenen, im Sinne einer *trans*-Addition zum 1,2-Disilan **5a** hydriert wurde. Erstaunlicherweise konnte ein direkter, konzertierter *anti*-Additionsweg gefunden werden, der aufgrund der stark pyramidalisierten und verdrillten Si=Si Bindung begünstigt wurde. Die gleiche *trans*-Stereospezifität wurde folglich auch bei der Aktivierung von Ammoniak zum entsprechenden 1,2-Hydroaminierungsprodukt **5b** nachgewiesen. Durch

die zusätzliche Wechselwirkung des LUMO von **2** mit dem freien Stickstoffelektronenpaar von NH_3, wurde hier außerdem eine Spaltung der Si=Si Bindung und die Bildung des entsprechenden 1,1-Additionsproduktes **6** beobachtet.

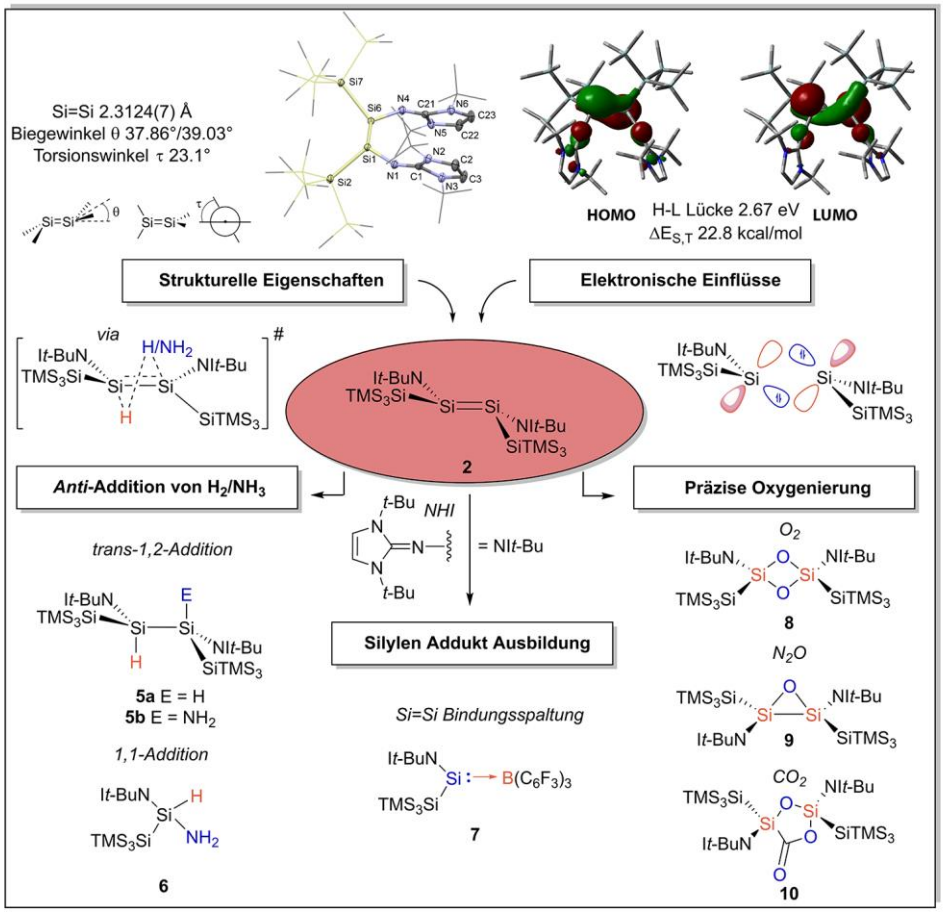

Schema 15. Überblick über die strukturellen und elektronischen Eigenschaften des (*Z*)-Imino(silyl)disilens **2** und die daraus resultierende Reaktivität.

Des Weitern konnte bestätigt werden, dass die Kontrolle der Produktselektivität durch präzise Einstellung der Temperatur während der Hydroaminierungsreaktion möglich ist, wobei hauptsächlich **5b** unter kinetischer Reaktionskontrolle (–78 °C, 16 h) und **6** unter thermodynamischer Reaktionskontrolle (lediglich 10 min bei –78 °C, dann Auftauen auf Raumtemperatur) gebildet wurde. Ferner wurde aufgrund der verlängerten Si=Si Bindung auch kein π-Komplex oder ein potentieller dreigliedriger Metalla-Zyklus bei der Reaktion mit der Lewis-Säure BCF beobachtet. Stattdessen wurde ausschließlich ein monomeres Silylen-BCF Addukt **7** mit ausgeprägtem Sila-aza-allen-Charakter isoliert und vollständig charakterisiert. Um einen tieferen Einblick in die ambivalente Reaktivität von **2** zu erhalten, wurde außerdem diese außergewöhnliche Bindungssituation in der Aktivierung von sauerstoffhaltigen Substraten getestet. In Abhängigkeit von unterschiedlichen

Sauerstoff-Donoren (O_2, N_2O und CO_2) wurden hier mehrere neue Sila-Zyklen **8**-**10** mit unterschiedlichen Ringgrößen isoliert. Nach theoretischen Berechnungen wurden allesamt als Folgeprodukte der direkten Oxygenierung der Si=Si Bindung von **2** gebildet, wodurch jegliche Beteiligung einer intermediären Silylen-Spezies ausgeschlossen wurde. Ein vielversprechender Baustein scheint dabei der dreigliedrige *trans*-Disilaoxiran-Ring **9** zu sein. Hierbei handelt es sich um ein seltenes Silicium-Analogon eines Epoxids, dessen Ringspannung und schwache Si–Si Bindung zur weiteren Aktivierung von Substraten genutzt werden kann. In diesem Zusammenhang zeigten die X-Ray Daten des fünfgliedrigen Sila-Zyklus **10**, des formalen Produkts von **9** mit CO_2, extrem lange Si–C und Si–O Bindungen mit dativem Charakter zum CO_2-Molekül, wodurch die Möglichkeit geschaffen wird, in Zukunft Manipulationsreaktionen am aktivierten Carbonyl-C-Atom durchzuführen. In Summe, weist das isolierte Imino(silyl)disilen **2** aufgrund der elektronisch entgegenwirkenden Einflüsse der Silyl- und NHI-Liganden außergewöhnliche strukturelle und elektronische Eigenschaften auf, die für neuartige, bislang für Disilene unbekannte Reaktivitäten ausgenutzt wurden. Als nächsten Schritt in Richtung Katalyse muss nun die Suche nach reversiblen Reaktionen und potentiellen Übertragungen der aktivierten Substrate auf organische Moleküle intensiviert werden.

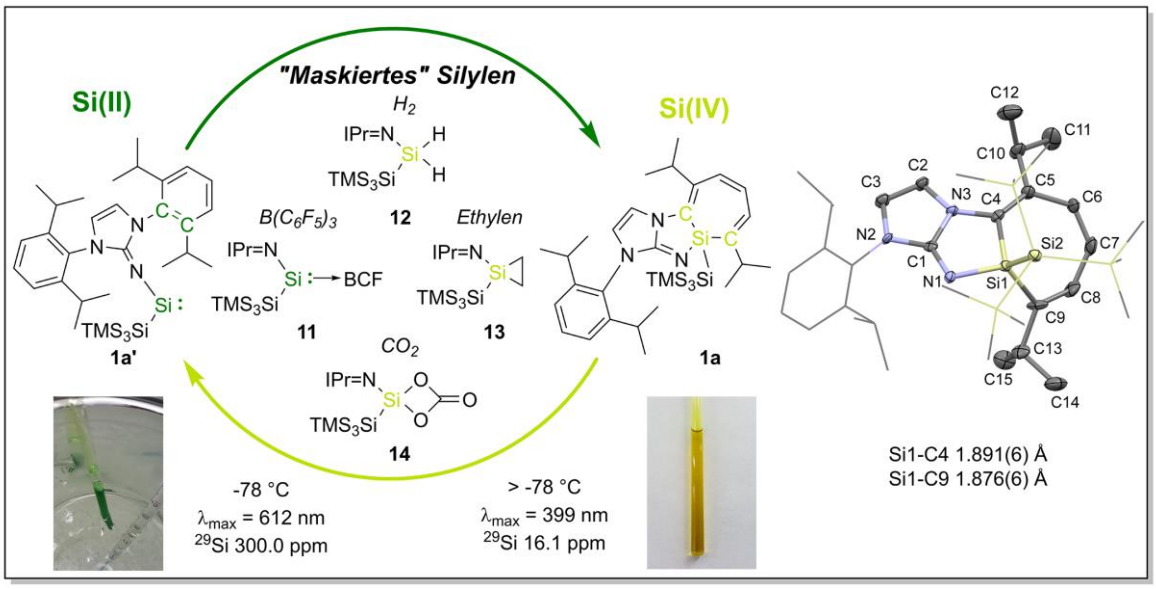

Schema 16. Übersicht der Untersuchungen des Imino(silyl)silepins **1a** als "maskiertes" Silylen für die Aktivierung kleiner Moleküle.

Nach dieser Feststellung wurde das primäre Ziel der Isolierung eines zweifach koordinierten, acyclischen Silylens angestrebt. Hierbei sollte durch Erhöhung des sterischen Anspruchs der NHI-„Wingtips" eine größere Abstoßung zwischen den beiden Si-Zentren erzielt werden, die

schließlich zu einer monomeren Struktur führen sollten. Tatsächlich wurde durch Ersetzen von *tert*-Butyl durch voluminösere Dipp-Gruppen ein acyclisches Imino(silyl)silylen **1a‘** nachgewiesen, jedoch lediglich in *in situ* UV/Vis und ^{29}Si-NMR Experimenten bei niedrigen Temperaturen (–78 °C). Erstaunlicherweise wurde oberhalb dieses Temperaturbereichs festgestellt, dass das Si(II)-Zentrum des transienten Silylens **1a‘** quantitativ in die C=C Bindung des angrenzenden aromatischen Ligandengerüsts insertiert und sich der Silacycloheptatrien (Silepin) **1a** ausbildet (Schema 16). Ersten DFT-Rechnungen zufolge beruht diese begünstigte Transformation sehr wahrscheinlich auf einer starken Wechselwirkung des Lewis-aciden 3p-Orbitals des Silylens mit der elektronenreichen π-Bindung des benachbarten Phenylrings, die sogar den entgegenwirkenden Energie freisetzenden Prozess der Rearomatisierung überwindet. Dementsprechend liegen beide Spezies energetisch sehr eng zusammen (17.3 kJ/mol) – eine Energiedifferenz die auf eine thermisch zugängliche Umwandlung hindeutete. Diese Hypothese wurde experimentell durch den Nachweis von Silylen **1a‘** in weiterführenden (HT) UV-vis Experimenten verifiziert. Insbesondere wurde der intrinsische Si(II)-Charakter des Silepins **1a** bei der Isolierung des Silylen-Boran Addukts **11** nach Zugabe von BCF veranschaulicht. Die Tendenz dieser Verbindung zur intramolekularen reduktiven Eliminierung wurde zudem bei der Untersuchung von Silepin **1a** als "maskiertes" Silylen in der Aktivierung kleiner Moleküle deutlich. Selbst anspruchsvolle Substrate, wie Wasserstoff oder Ethylen, wurden von der formalen Si(IV)-Verbindung **1a** aktiviert und bildeten das entsprechende Hydridosilan **12** oder den Siliran-Ring **13** bereits unter milden Bedingungen. Interessanterweise wurde auch Kohlenstoffdioxid, ein offenkundiges Ziel für reaktive Hauptgruppenverbindungen, unter Darstellung des ersten monomeren, vierfach-koordinierten Siliciumcarbonat-Komplexes **14** stöchiometrisch zu Kohlenstoffmonoxid reduziert. Die Bildung dieser Verbindung wurde der [2+2]-Cycloaddition eines intermediären, transienten Silanons mit einem zweiten CO_2-Molekül zugeschrieben. Daraufhin wurde der Fokus auf die Isolierung einer solchen bislang vollkommen unzugänglichen Spezies gerichtet.

Wie vermutet, gelang durch eine leicht angepasste Synthesevorschrift und dem Wechsel des Oxygenierungsmittels von CO_2 zu N_2O die erste Darstellung komplett neutraler, dreifach-koordinierter, acyclischer Imino(silyl)silanone **15**. Diese wurden als abfüllbare, weiße Pulver isoliert und zeigten unbegrenzte Stabilität in fester Form und eine Lebensdauer in Lösung von bis zu 2 Tagen (Schema 17). Die Einkristallstrukturanalyse von **15b** offenbarte eine extrem kurze Si=O Doppelbindung (1.537(3) Å), die zusammen mit den wichtigen

Stabilisierungseffekten der benachbarten NHI- und Silyl-Liganden durch ausführliche DFT-Rechnungen untersucht wurden. Insbesondere der Überlapp des nichtbindenden Orbitals des exocyclischen Stickstoffatoms mit der Si=O π-Bindung (HOMO-10) sowie die signifikante σ-Donorwirkung und Hyperkonjugation der Silyl-Gruppe (LUMO+4) wurden als Hauptstabilisierungseffekte der ansonsten stark polarisierten Si=O Einheit identifiziert. Hinsichtlich ersten Reaktivitätsstudien wurde die bereits erwähnte CO_2-Aktivierung durch das Silepin, hier separat als finaler Beweis des Silanon-Intermediats, wiederholt.

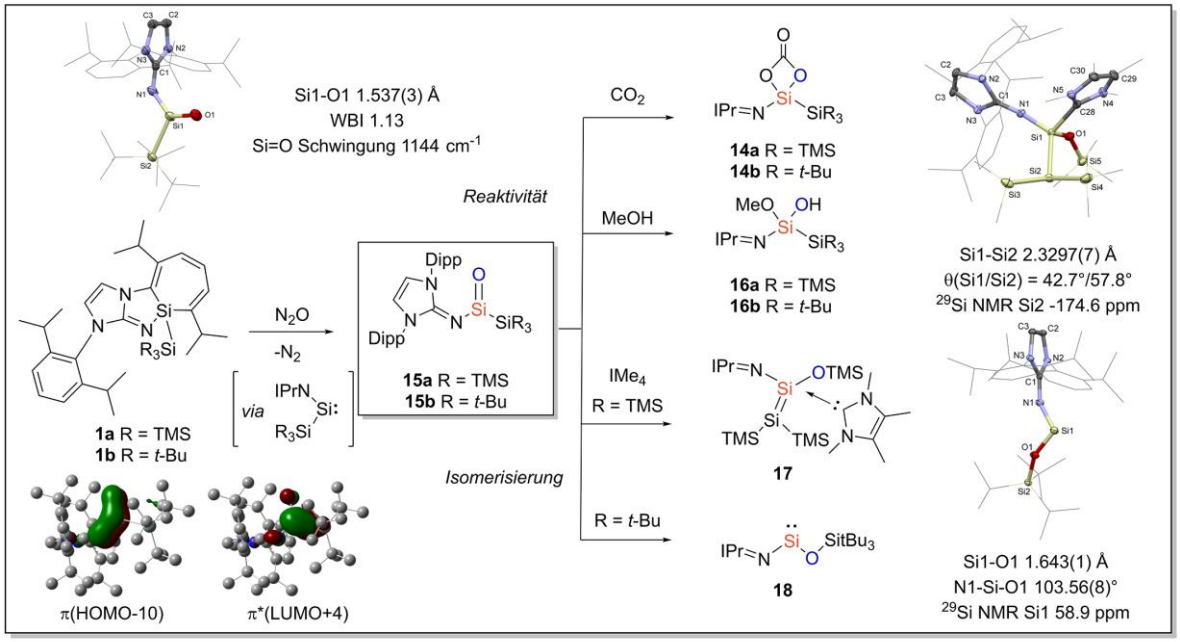

Schema 17. Darstellung der Imino(silyl)silanone **15** und erste Ergebnisse der Isomerisierungsreaktionen und Reaktivitätsstudien.

Darüber hinaus wurde die außergewöhnliche Reaktivität der Silanone **15** gegenüber Methanol getestet, die in Analogie zur etablierten Reaktion von Ketonen mit Alkoholen zu Halbketalen die entsprechende Silanole **16** ergab. Aufgrund unseres langfristigen Ziels – der dauerhaften Stabilisierung von Silanonen – waren wir ferner an einer detaillierten Untersuchung der auftretenden Isomerisierungsvorgänge interessiert. Für das Silanon **15a** mit einem Hypersilyl-Liganden wurde in Lösung ein intermediäres Disilen detektiert, das sich durch eine 1,3-Silylwanderung gebildet hat. Dieses Zwischenprodukt wurde erfolgreich mit IMe_4 als seltenes Beispiel eines NHC-stabilisierten Disilens **17** mit einer stark zwitterionischen Si=Si Bindung abgefangen. Für das Silanon **15b** wurde hingegen, neben den Resultaten des Silepins, das zweite Beispiel eines begünstigten Wechsels der Oxidationsstufe von Si(IV) zur deutlich weniger präferierten Oxidationsstufe Si(II) gefunden. Hier wurde aufgrund der

Oxophilie von Silicium und seiner intrinsischen Neigung stabile σ-Bindungen mit Sauerstoff zu bilden, eine selektive Umlagerung zum zweifach-koordinierten, acyclischen *N,O*-Silylen **18** entdeckt. Um neue Einblicke und Perspektiven hinsichtlich der Synthese, Stabilisierung und Reaktivität von derartigen Silylenen zu erhalten, ist diese Verbindung als erster Präzedenzfall eines siloxy-stabilisierten Silylens von großem Interesse. Aufgrund des Oxo-Liganden und der Strukturverwandtschaft zu den Amino(alkoxy)germylen und -stannylenderivaten **L-41** – die bereits erfolgreich als Katalysatoren bei der Hydroborierung von Carbonylverbindungen getestet wurden (siehe Kapitel 4.1) – könnte das Auffinden einer analogen σ-Bindungsmetathese von **18** mit Boranen, den Weg für eine silylen-basierte Katalyse ebnen.

Zusammenfassend ist es in dieser Dissertation gelungen NHI-Liganden in mehrere neuartige niedervalente Siliciumverbindungen mit faszinierenden elektronischen und strukturellen Eigenschaften zu integrieren. Diese wurden nicht nur experimentell und theoretisch gründlich analysiert, sondern auch direkt eingesetzt, um bislang unbekannte Reaktivitäten zu ermöglichen. Bemerkenswerterweise wurde in dieser Arbeit die erste Hydrierung einer mehrfach gebundenen Siliciumverbindung entdeckt. Darüber hinaus konnte ein neues Konzept entwickelt werden, das Silepine als direkte Silylen-Äquivalente bei der Aktivierung kleiner Moleküle einsetzt. Als erster Beweis für eine potentielle Katalyse auf Basis des Si(II)/Si(IV) Redoxpaares wurde hier der elementare Schritt einer milden, intramolekularen reduktiven Eliminierung an einem Silicium-Zentrum präsentiert. Mit den ersten bekannten Beispielen für raumtemperaturstabile, dreifach-koordinierte, neutrale und acylische Silanone ging zudem der lang ersehnte Traum von F. S. Kipping von isolierbaren Silicium-Analoga von Ketonen in Erfüllung. Diese Errungenschaft bietet nun natürlich die Möglichkeit die noch unberührte Chemie von Sila-Carbonylverbindungen zu erforschen. Abschließend wurde mit der Erweiterung der Liste zugänglicher zweifach-koordinierter, acyclischer Silylene das Fundament für weitere Untersuchungen des katalytischen Potentials dieser Verbindungsklasse gelegt. Diese führen hoffentlich schon bald zu dem erwarteten Durchbruch in der Hauptgruppen-Katalyse.

13. Bibliography

(1) Zecchina, A.; Califano, S., *The Development of Catalysis: A History of Key Processes and Personas in Catalytic Science and Technology*. Wiley: Hoboken, 2017.
(2) Oesper, R. E., *J. Chem. Educ.* **1948**, *25*, 531-532.
(3) Chorkendorff, I.; Niemantsverdriet, J. W., Introduction to Catalysis. In *Concepts of Modern Catalysis and Kinetics*, Wiley: Weinheim, 2005; pp 1-21.
(4) Allied Market Research "Catalyst Market Overview". https://www.alliedmarketresearch.com/catalysts-market (07.01.2018).
(5) (a) van Leeuwen, P. W. N. M., *Homogeneous Catalysis: Understanding the Art*. Springer: Dordrecht, 2006. (b) Falbe, J.; Bahrmann, H., *J. Chem. Educ.* **1984**, *61*, 961-967.
(6) Nakajima, Y.; Shimada, S., *RSC Adv.* **2015**, *5*, 20603-20616.
(7) Wilkins, L. C.; Melen, R. L., *Coord. Chem. Rev.* **2016**, *324*, 123-139.
(8) Periodictable "Abundance in Earth's Crust of the elements". http://periodictable.com/Properties/A/CrustAbundance.an.html (04.01.2018).
(9) Astrobio "Possibility of silicon-based life grows". https://www.astrobio.net/news-exclusive/possibility-silicon-based-life-grows/ (04.01.2018).
(10) Arkles, B., Silicon Compounds, Silanes. In *Kirk-Othmer Encyclopedia of Chemical Technology*, John Wiley & Sons: Hoboken, 2000.
(11) Fischer, R. C.; Power, P. P., *Chem. Rev.* **2010**, *110*, 3877-3923.
(12) (a) Wiberg, N., *Lehrbuch der anorganischen Chemie*. 102. ed.; de Gruyter: Berlin, 2007. (b) Brook, M. A., *Silicon in Organic, Organometallic, and Polymer Chemistry*. 1. ed.; John Wiley & Sons: Hoboken, 2000. (c) Riedel, E.; Janiak, C., *Anorganische Chemie*. de Gruyter: Berlin, 2007.
(13) Janiak, C., *Nichtmetallchemie: Grundlagen und Anwendungen*. Shaker: Aachen, 2012.
(14) Statista "Major countries in silicon production from 2011 to 2016". https://www.statista.com/statistics/268108/world-silicon-production-by-country/ (04.01.2018).
(15) Jones, R. G.; Ando, W.; Chojnowski, J., *Silicon-Containing Polymers*. Springer: Dordrecht, 2000.
(16) Mark, J. E.; Schaefer, D. W.; Lin, G., *The Polysiloxanes*. Oxford University Press: New York, 2015.
(17) Kipping, F. S.; Lloyd, L. L., *J. Chem. Soc.* **1901**, *79*, 449-459.
(18) (a) Avakyan, V. G.; Sidorkin, V. F.; Belogolova, E. F.; Guselnikov, S. L.; Gusel'nikov, L. E., *Organometallics* **2006**, *25*, 6007-6013. (b) Kudo, T.; Nagase, S., *J. Am. Chem. Soc.* **1985**, *107*, 2589-2595.
(19) Thomas, N. R., *Silicon* **2010**, *2*, 187-193.
(20) Burkhard, C. A.; Rochow, E. G.; Booth, H. S.; Hartt, J., *Chem. Rev.* **1947**, *41*, 97-149.
(21) Rücker, C.; Kümmerer, K., *Chem. Rev.* **2015**, *115*, 466-524.
(22) Markets and Markets "Silicone Market worth 18.87 Billion USD by 2022". https://www.marketsandmarkets.com/PressReleases/silicone.asp (04.01.2018).
(23) (a) Gehrhus, B.; Lappert, M. F., *J. Organomet. Chem.* **2001**, *617-618*, 209-223. (b) Hill, N. J.; West, R., *J. Organomet. Chem.* **2004**, *689*, 4165-4183.
(24) West, R.; Fink, M. J.; Michl, J., *Science* **1981**, *214*, 1343-1344.
(25) Rammo, A.; Scheschkewitz, D., *Chem. - Eur. J.*, DOI: 10.1002/chem.201704090.
(26) Milnes, K. K.; Pavelka, L. C.; Baines, K. M., *Chem. Soc. Rev.* **2016**, *45*, 1019-1035.
(27) Lee, V. Y., *Organosilicon Compounds: From Theory to Synthesis to Applications*. Elsevier Science & Technology Books: London, 2017.

(28) Sekiguchi, A.; Kinjo, R.; Ichinohe, M., *Science* **2004**, *305*, 1755-1757.
(29) Wang, Y.; Xie, Y.; Wei, P.; King, R. B.; Schaefer, H. F., III; Schleyer, P. v. R.; Robinson, G. H., *Science* **2008**, *321*, 1069-1071.
(30) Mondal, K. C.; Roesky, H. W.; Schwarzer, M. C.; Frenking, G.; Niepoetter, B.; Wolf, H.; Herbst-Irmer, R.; Stalke, D., *Angew. Chem., Int. Ed.* **2013**, *52*, 2963-2967.
(31) Jutzi, P.; Mix, A.; Rummel, B.; Schoeller, W. W.; Neumann, B.; Stammler, H.-G., *Science* **2004**, *305*, 849-851.
(32) Mizuhata, Y.; Sasamori, T.; Tokitoh, N., *Chem. Rev.* **2009**, *109*, 3479-3511.
(33) Pyykko, P., *Chem. Rev.* **1988**, *88*, 563-594.
(34) Hadlington, T. J., *On the Catalytic Efficacy of Low-Oxidation State Group 14 Complexes*. Springer: Cham, 2017.
(35) Trinquier, G., *J. Am. Chem. Soc.* **1990**, *112*, 2130-2137.
(36) Driess, M.; Grützmacher, H., *Angew. Chem., Int. Ed.* **1996**, *108*, 900-929.
(37) (a) Jutzi, P., *Angew. Chem., Int. Ed.* **1975**, *14*, 232-245. (b) Goubeau, J., *Angew. Chem., Int. Ed.* **1957**, *69*, 77-82.
(38) (a) Goldberg, D. E.; Harris, D. H.; Lappert, M. F.; Thomas, K. M., *J. Chem. Soc., Chem. Commun.* **1976**, 261-262. (b) Yoshifuji, M.; Shima, I.; Inamoto, N.; Hirotsu, K.; Higuchi, T., *J. Am. Chem. Soc.* **1981**, *103*, 4587-4589.
(39) (a) Trinquier, G.; Malrieu, J. P., *J. Am. Chem. Soc.* **1987**, *109*, 5303-15. (b) Carter, E. A.; Goddard, W. A., III, *J. Phys. Chem.* **1986**, *90*, 998-1001.
(40) Power, P. P., *Chem. Rev.* **1999**, *99*, 3463-3504.
(41) (a) Kira, M.; Iwamoto, T., *Adv. Organomet. Chem.* **2006**, *54*, 73-148. (b) Iwamoto, T.; Ishida, S., Multiple Bonds with Silicon: Recent Advances in Synthesis, Structure, and Functions of Stable Disilenes. In *Functional Molecular Silicon Compounds II: Low Oxidation States*, Scheschkewitz, D., Ed.; Springer: Cham, 2014; Vol. 156, pp 125-202.
(42) Grev, R. S.; Schaefer, H. F.; Gaspar, P. P., *J. Am. Chem. Soc.* **1991**, *113*, 5638-5643.
(43) (a) Sekiguchi, A.; Tanaka, T.; Ichinohe, M.; Akiyama, K.; Tero-Kubota, S., *J. Am. Chem. Soc*. **2003**, *125*, 4962-4963. (b) Sekiguchi, A.; Tanaka, T.; Ichinohe, M.; Akiyama, K.; Gaspar, P. P., *J. Am. Chem. Soc.* **2008**, *130*, 426-427.
(44) Pae, D. H.; Xiao, M.; Chiang, M. Y.; Gaspar, P. P., *J. Am. Chem. Soc.* **1991**, *113*, 1281-1288.
(45) (a) Gehrhus, B.; Hitchcock, P. B.; Lappert, M. F., *Z. Anorg. Allg. Chem.* **2005**, *631*, 1383-1386. (b) Sen, S. S.; Jana, A.; Roesky, H. W.; Schulzke, C., *Angew. Chem., Int. Ed.* **2009**, *48*, 8536-8538. (c) Gau, D.; Rodriguez, R.; Kato, T.; Saffon-Merceron, N.; de Cózar, A.; Cossío, F. P.; Baceiredo, A., *Angew. Chem., Int. Ed.* **2011**, *50*, 1092-1096. (d) Wang, W.; Inoue, S.; Yao, S.; Driess, M., *J. Am. Chem. Soc.* **2010**, *132*, 15890-15892.
(46) (a) Blom, B.; Driess, M., Recent Advances in Silylene Chemistry: Small Molecule Activation En-Route Towards Metal-Free Catalysis. In *Functional Molecular Silicon Compounds II: Low Oxidation States*, Scheschkewitz, D., Ed.; Springer: Cham, 2014; Vol. 156, pp 85-123. (b) Rivard, E., Recent Advances in the N-Heterocyclic Carbene-Supported Chemistry of Silicon. In *Functional Molecular Silicon Compounds II: Low Oxidation States*, Scheschkewitz, D., Ed.; Springer: Cham, 2014; Vol. 156, pp 203-227.
(47) Skell, P. S.; Goldstein, E. J., *J. Am. Chem. Soc.* **1964**, *86*, 1442-1443.
(48) Jutzi, P.; Kanne, D.; Kruger, C., *Angew. Chem., Int. Ed.* **1986**, *25*, 164-165.
(49) Kuehler, T.; Jutzi, P., *Adv. Organomet. Chem.* **2003**, *49*, 1-34.
(50) Denk, M.; Lennon, R.; Hayashi, R.; West, R.; Belyakov, A. V.; Verne, H. P.; Haaland, A.; Wagner, M.; Metzler, N., *J. Am. Chem. Soc.* **1994**, *116*, 2691-2692.
(51) (a) Tomasik, A. C.; Mitra, A.; West, R., *Organometallics* **2009**, *28*, 378-381. (b) Zark, P.; Schaefer, A.; Mitra, A.; Haase, D.; Saak, W.; West, R.; Mueller, T., *J. Organomet. Chem.* **2010**, *695*, 398-408.
(52) Kira, M.; Ishida, S.; Iwamoto, T.; Kabuto, C., *J. Am. Chem. Soc.* **1999**, *121*, 9722-9723.

(53) Lee, G.-H.; West, R.; Müller, T., *J. Am. Chem. Soc.* **2003**, *125*, 8114-8115.
(54) Driess, M.; Yao, S.; Brym, M.; Van Wuellen, C.; Lentz, D., *J. Am. Chem. Soc.* **2006**, *128*, 9628-9629.
(55) Yao, S.-L.; Xiong, Y.; Driess, M., *Organometallics* **2011**, *30*, 1748-1767.
(56) Ghadwal, R. S.; Roesky, H. W.; Merkel, S.; Henn, J.; Stalke, D., *Angew. Chem., Int. Ed.* **2009**, *48*, 5683-5686.
(57) (a) Filippou, A. C.; Chernov, O.; Schnakenburg, G., *Angew. Chem., Int. Ed.* **2009**, *48*, 5687-5690. (b) Filippou, A. C.; Lebedev, Y. N.; Chernov, O.; Strassmann, M.; Schnakenburg, G., *Angew. Chem., Int. Ed.* **2013**, *52*, 6974-6978.
(58) Asay, M.; Inoue, S.; Driess, M., *Angew. Chem., Int. Ed.* **2011**, *50*, 9589-9592.
(59) Abe, T.; Tanaka, R.; Ishida, S.; Kira, M.; Iwamoto, T., *J. Am. Chem. Soc.* **2012**, *134*, 20029-20032.
(60) Kosai, T.; Ishida, S.; Iwamoto, T., *Angew. Chem., Int. Ed.* **2016**, *128*, 15783-15787.
(61) (a) Alvarado-Beltran, I.; Baceiredo, A.; Saffon-Merceron, N.; Branchadell, V.; Kato, T., *Angew. Chem., Int. Ed.* **2016**, *55*, 16141-16144. (b) Rosas-Sanchez, A.; Alvarado-Beltran, I.; Baceiredo, A.; Saffon-Merceron, N.; Massou, S.; Branchadell, V.; Kato, T., *Angew. Chem., Int. Ed.* **2017**, *56*, 10549-10554.
(62) (a) Alvarado-Beltran, I.; Rosas-Sánchez, A.; Baceiredo, A.; Saffon-Merceron, N.; Branchadell, V.; Kato, T., *Angew. Chem., Int. Ed.* **2017**, *56*, 10481-10485. (b) Rosas-Sánchez, A.; Alvarado-Beltran, I.; Baceiredo, A.; Saffon-Merceron, N.; Massou, S.; Hashizume, D.; Branchadell, V.; Kato, T., *Angew. Chem., Int. Ed.* **2017**, *129*, 16132-16136.
(63) Protchenko, A. V.; Birjkumar, K. H.; Dange, D.; Schwarz, A. D.; Vidovic, D.; Jones, C.; Kaltsoyannis, N.; Mountford, P.; Aldridge, S., *J. Am. Chem. Soc.* **2012**, *134*, 6500-6503.
(64) Rekken, B. D.; Brown, T. M.; Fettinger, J. C.; Tuononen, H. M.; Power, P. P., *J. Am. Chem. Soc.* **2012**, *134*, 6504-6507.
(65) Driess, M., *Nat. Chem.* **2012**, *4*, 525-526.
(66) Moser, D. F.; Guzei, I. A.; West, R., *Main Group Met. Chem.* **2001**, *24*, 811-812.
(67) Rekken, B. D.; Brown, T. M.; Fettinger, J. C.; Lips, F.; Tuononen, H. M.; Herber, R. H.; Power, P. P., *J. Am. Chem. Soc.* **2013**, *135*, 10134-10148.
(68) Liptrot, D. J.; Power, P. P., *Nat Rev Chem.* **2017**, *1*, 0004.
(69) Holthausen, M. C.; Koch, W.; Apeloig, Y., *J. Am. Chem. Soc.* **1999**, *121*, 2623-2624.
(70) (a) Power, P. P., *Nature* **2010**, *463*, 171-177. (b) Yadav, S.; Saha, S.; Sen, S. S., *ChemCatChem* **2016**, *8*, 486-501.
(71) Lips, F.; Fettinger, J. C.; Mansikkamaki, A.; Tuononen, H. M.; Power, P. P., *J. Am. Chem. Soc.* **2014**, *136*, 634-637.
(72) Lips, F.; Mansikkamaki, A.; Fettinger, J. C.; Tuononen, H. M.; Power, P. P., *Organometallics* **2014**, *33*, 6253-6258.
(73) Protchenko, A. V.; Schwarz, A. D.; Blake, M. P.; Jones, C.; Kaltsoyannis, N.; Mountford, P.; Aldridge, S., *Angew. Chem., Int. Ed.* **2013**, *52*, 568-571.
(74) Chen, P.-h.; Billett, B. A.; Tsukamoto, T.; Dong, G., *ACS Catalysis* **2017**, *7*, 1340-1360.
(75) Wang, Y.; Ma, J., *J. Organomet. Chem.* **2009**, *694*, 2567-2575.
(76) Frey, G. D.; Lavallo, V.; Donnadieu, B.; Schoeller, W. W.; Bertrand, G., *Science* **2007**, *316*, 439-441.
(77) Protchenko, A. V.; Bates, J. I.; Saleh, L. M. A.; Blake, M. P.; Schwarz, A. D.; Kolychev, E. L.; Thompson, A. L.; Jones, C.; Mountford, P.; Aldridge, S., *J. Am. Chem. Soc.* **2016**, 4555–4564.
(78) Hadlington, T. J.; Abdalla, J. A. B.; Tirfoin, R.; Aldridge, S.; Jones, C., *Chem. Commun.* **2016**, *52*, 1717-1720.
(79) Harris, D. H.; Lappert, M. F., *J. Chem. Soc., Chem. Commun.* **1974**, 895-896.
(80) Alder, R. W.; Allen, P. R.; Murray, M.; Orpen, A. G., *Angew. Chem., Int. Ed.* **1996**, *35*, 1121-1123.

(81) Jana, A.; Schulzke, C.; Roesky, H. W., *J. Am. Chem. Soc.* **2009**, *131*, 4600-4601.
(82) (a) Ochiai, T.; Franz, D.; Inoue, S., *Chem. Soc. Rev.* **2016**, *45*, 6327-6344. (b) Wu, X.; Tamm, M., *Coord. Chem. Rev.* **2014**, *260*, 116-138. (c) Trambitas, Alexandra G.; Panda, Tarun K.; Tamm, M., *Z. Anorg. Allg. Chem.* **2010**, *636*, 2156-2171. (d) Kuhn, N.; Goehner, M.; Grathwohl, M.; Wiethoff, J.; Frenking, G.; Chen, Y., *Z. Anorg. Allg. Chem.* **2003**, *629*, 793-802.
(83) Kuhn, N.; Fawzi, R.; Steimann, M.; Wiethoff, J.; Blaeser, D.; Boese, R., *Z. Naturforsch., B: Chem. Sci.* **1995**, *50*, 1779-1784.
(84) (a) Tamm, M.; Beer, S.; Herdtweck, E., *Z. Naturforsch., B: Chem. Sci.* **2004**, *59*, 1497-1504. (b) Tamm, M.; Randoll, S.; Bannenberg, T.; Herdtweck, E., *Chem. Commun.* **2004**, 876-877.
(85) Tamm, M.; Randoll, S.; Herdtweck, E.; Kleigrewe, N.; Kehr, G.; Erker, G.; Rieger, B., *Dalton Trans.* **2006**, 459-467.
(86) Tamm, M.; Petrovic, D.; Randoll, S.; Beer, S.; Bannenberg, T.; Jones, P. G.; Grunenberg, J., *Org. Biomol. Chem.* **2007**, *5*, 523-530.
(87) Back, O.; Donnadieu, B.; von Hopffgarten, M.; Klein, S.; Tonner, R.; Frenking, G.; Bertrand, G., *Chem. Sci.* **2011**, *2*, 858-861.
(88) Kinjo, R.; Donnadieu, B.; Bertrand, G., *Angew. Chem., Int. Ed.* **2010**, *49*, 5930-5933.
(89) Dielmann, F.; Back, O.; Henry-Ellinger, M.; Jerabek, P.; Frenking, G.; Bertrand, G., *Science* **2012**, *337*, 1526-1528.
(90) (a) Back, J.; Park, J.; Kim, Y.; Kang, H.; Kim, Y.; Park, M. J.; Kim, K.; Lee, E., *J. Am. Chem. Soc.* **2017**, *139*, 15300-15303. (b) Eymann, L. Y. M.; Tskhovrebov, A. G.; Sienkiewicz, A.; Bila, J. L.; Živković, I.; Rønnow, H. M.; Wodrich, M. D.; Vannay, L.; Corminboeuf, C.; Pattison, P.; Solari, E.; Scopelliti, R.; Severin, K., *J. Am. Chem. Soc.* **2016**, *138*, 15126-15129.
(91) (a) Lui, M. W.; Paisley, N. R.; McDonald, R.; Ferguson, M. J.; Rivard, E., *Chem. - Eur. J.* **2016**, *22*, 2134-2145. (b) Franz, D.; Irran, E.; Inoue, S., *Dalton Trans.* **2014**, *43*, 4451-4461. (c) Franz, D.; Inoue, S., *Chem. - Asian J.* **2014**, *9*, 2083-2087.
(92) Franz, D.; Irran, E.; Inoue, S., *Angew. Chem., Int. Ed.* **2014**, *53*, 14264-14268.
(93) Franz, D.; Szilvasi, T.; Irran, E.; Inoue, S., *Nat Commun* **2015**, *6*, 10037-10042.
(94) Bag, P.; Ahmad, S. U.; Inoue, S., *Bull. Chem. Soc. Jpn* **2017**, *90*, 255-271.
(95) Ochiai, T.; Franz, D.; Wu, X.-N.; Inoue, S., *Dalton Trans.* **2015**, *44*, 10952-10956.
(96) Ochiai, T.; Franz, D.; Irran, E.; Inoue, S., *Chem. - Eur. J.* **2015**, *21*, 6704-6707.
(97) Ochiai, T.; Szilvási, T.; Franz, D.; Irran, E.; Inoue, S., *Angew. Chem., Int. Ed.* **2016**, *55*, 11619-11624.
(98) Ochiai, T.; Inoue, S., *RSC Adv.* **2017**, *7*, 801-804.
(99) Ochiai, T.; Franz, D.; Wu, X.-N.; Irran, E.; Inoue, S., *Angew. Chem., Int. Ed.* **2016**, *55*, 6983-6987.
(100) Ochiai, T.; Szilvási, T.; Inoue, S., *Molecules* **2016**, *21*, 1155-1167.
(101) Lui, M. W.; Merten, C.; Ferguson, M. J.; McDonald, R.; Xu, Y.; Rivard, E., *Inorg. Chem.* **2015**, *54*, 2040-2049.
(102) Inoue, S.; Leszczynska, K., *Angew. Chem., Int. Ed.* **2012**, *51*, 8589-8593.
(103) Spikes, G. H.; Fettinger, J. C.; Power, P. P., *J. Am. Chem. Soc.* **2005**, *127*, 12232-12233.
(104) (a) Peng, Y.; Brynda, M.; Ellis, B. D.; Fettinger, J. C.; Rivard, E.; Power, P. P., *Chem. Commun.* **2008**, 6042-6044. (b) Li, J.; Schenk, C.; Goedecke, C.; Frenking, G.; Jones, C., *J. Am. Chem. Soc.* **2011**, *133*, 18622-18625. (c) Hadlington, T. J.; Hermann, M.; Li, J.; Frenking, G.; Jones, C., *Angew. Chem., Int. Ed.* **2013**, *52*, 10199-10203.
(105) (a) Peng, Y.; Ellis, B. D.; Wang, X.; Power, P. P., *J. Am. Chem. Soc.* **2008**, *130*, 12268-12269. (b) Peng, Y.; Guo, J.-D.; Ellis, B. D.; Zhu, Z.; Fettinger, J. C.; Nagase, S.; Power, P. P., *J. Am. Chem. Soc.* **2009**, *131*, 16272-16282.

(106) Welch, G. C.; San Juan, R. R.; Masuda, J. D.; Stephan, D. W., *Science* **2006**, *314*, 1124-1126.
(107) (a) Stephan, D. W., *Acc. Chem. Res.* **2015**, *48*, 306-316. (b) Stephan, D. W.; Erker, G., *Angew. Chem., Int. Ed.* **2015**, *54*, 6400-6441.
(108) (a) Sumerin, V.; Schulz, F.; Nieger, M.; Leskelä, M.; Repo, T.; Rieger, B., *Angew. Chem., Int. Ed.* **2008**, *47*, 6001-6003. (b) Chase, P. A.; Welch, G. C.; Jurca, T.; Stephan, D. W., *Angew. Chem., Int. Ed.* **2007**, *46*, 8050-8053.
(109) Mahdi, T.; Stephan, D. W., *J. Am. Chem. Soc.* **2014**, *136*, 15809-15812.
(110) Chernichenko, K.; Madarász, Á.; Pápai, I.; Nieger, M.; Leskelä, M.; Repo, T., *Nat. Chem.* **2013**, *5*, 718-723.
(111) Ghattas, G.; Chen, D.; Pan, F.; Klankermayer, J., *Dalton Trans.* **2012**, *41*, 9026-9028.
(112) Berkefeld, A.; Piers, W. E.; Parvez, M., *J. Am. Chem. Soc.* **2010**, *132*, 10660-10661.
(113) Zhang, Y.; Miyake, G. M.; Chen, E. Y. X., *Angew. Chem., Int. Ed.* **2010**, *49*, 10158-10162.
(114) Penafiel, J.; Maron, L.; Harder, S., *Angew. Chem., Int. Ed.* **2015**, *54*, 201-206.
(115) Klare, H. F. T.; Oestreich, M., *Dalton Trans.* **2010**, *39*, 9176-9184.
(116) (a) Swamy, V. S. V. S. N.; Bisai, M. K.; Das, T.; Sen, S. S., *Chem. Commun.* **2017**, *53*, 6910-6913. (b) Bisai, M. K.; Pahar, S.; Das, T.; Vanka, K.; Sen, S. S., *Dalton Trans.* **2017**, *46*, 2420-2424. (c) Liberman-Martin, A. L.; Bergman, R. G.; Tilley, T. D., *J. Am. Chem. Soc.* **2015**, *137*, 5328-5331.
(117) Jana, A.; Tavcar, G.; Roesky, H. W.; John, M., *Dalton Trans.* **2010**, *39*, 9487-9489.
(118) Tan, G.; Wang, W.; Blom, B.; Driess, M., *Dalton Trans.* **2014**, *43*, 6006-6011.
(119) Siwatch, R. K.; Nagendran, S., *Chem. - Eur. J.* **2014**, *20*, 13551-13556.
(120) Leszczyńska, K.; Mix, A.; Berger, R. J. F.; Rummel, B.; Neumann, B.; Stammler, H.-G.; Jutzi, P., *Angew. Chem., Int. Ed.* **2011**, *50*, 6843-6846.
(121) Jutzi, P., *Chem. - Eur. J.* **2014**, *20*, 9192-9207.
(122) Hadlington, T. J.; Hermann, M.; Frenking, G.; Jones, C., *J. Am. Chem. Soc.* **2014**, *136*, 3028-3031.
(123) Hadlington, T. J.; Kefalidis, C. E.; Maron, L.; Jones, C., *ACS Catalysis* **2017**, *7*, 1853-1859.
(124) Schmedake, T. A.; Haaf, M.; Apeloig, Y.; Müller, T.; Bukalov, S.; West, R., *J. Am. Chem. Soc.* **1999**, *121*, 9479-9480.
(125) Jutzi, P.; Eikenberg, D.; Moehrke, A.; Neumann, B.; Stammler, H.-G., *Organometallics* **1996**, *15*, 753-9.

14. Appendix

14.1 Supporting Information Chapter 6

Reactivity of an Acyclic Silylsilylene toward Ethylene: Migratory Insertion into the Si-Si Bond

Daniel Wendel,[†] Wolfgang Eisenreich,[‡] Christian Jandl,[§] Alexander Pöthig,[§] and Bernhard Rieger*[,†]

[†]WACKER-Lehrstuhl für Makromolekulare Chemie and [‡]Lehrstuhl für Biochemie, Technische Universität München, Lichtenbergstraße 4, 85747 Garching bei München, Germany

[§]Zentralinstitut für Katalyseforschung, Technische Universität München, Ernst-Otto-Fischer Straße 1, 85747 Garching bei München, Germany

Supporting Information

Total: S22 pages

1. Experimental procedures and NMR spectra

A) General Methods and Instrumentation

All manipulations were carried out under argon atmosphere using standard Schlenk or glovebox techniques. Glassware was heat dried under vacuum prior to use. Unless otherwise stated, all chemicals were purchased from Sigma-Aldrich or ABCR and used as received. Hexane and benzene were refluxed over sodium/ benzophenone, distilled and deoxygenated prior to use. Deuterated benzene (C_6D_6) was obtained from Deutero Deutschland GmbH and was dried over 3 Å molecular sieve. All NMR samples were prepared under argon in J. Young PTFE tubes. Acyclic silylsilylene Si{NDipp($SiMe_3$)}{Si($SiMe_3$)$_3$} (**II**) was synthesized according to the procedure described in literature.[S1] Ethylene (99.95% by Westfalen AG) was purified by passage through a column filled with BASF catalyst (R3-11)/ molecular sieve 3-4 Å. Ethylene-d_4 was purchased from Sigma-Aldrich and used as received. 2,3-Dimethyl-1,3-butadiene was dried over CaH_2 and distilled prior to use. NMR spectra were recorded on a Bruker AV-500C or AV-500 spectrometer at ambient temperature (300 K). ^{1}H, ^{13}C and ^{29}Si NMR spectroscopic chemical shifts δ are reported in ppm relative to tetramethylsilane. δ(^{1}H) is calibrated to the residual proton signal, δ(^{13}C) to the carbon signal. δ(^{29}Si) is referenced to the signal of tetramethylsilane (TMS) (δ = 0 ppm) as external standard. Elemental analyses were measured at the Laboratory for Microanalysis at the Institute of Inorganic Chemistry at the Technische Universität München. Mass spectra (MS-CI) were recorded on a double focusing Finnigan MAT 90 mass spectrometer (isobutene, 150 eV).

B) Synthesis and characterization of new compounds

Si{CH$_2$-CH$_2$}{NDipp(SiMe$_3$)}{Si(SiMe$_3$)$_3$} (1)

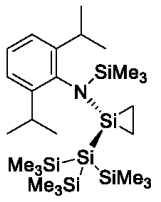

1

$C_{26}H_{57}NSi_6$
552.26 g/mol

NMR-scale kinetic study

For preliminary kinetic investigations a Young-NMR tube filled with silylsilylene **II** (10 mg, 19 µmol) in 0.5 mL C_6D_6 was exposed to ethylene gas (0.5 bar) via a glass cap at room temperature. The characteristic bright purple color vanished within seconds, resulting in a clear colorless solution. Subsequent NMR analysis confirmed the completion of the reaction with full conversion to **1**.

Scaled-up synthesis

A pressurizable schlenk flask filled with silylsilylene **II** (100 mg, 0.19 mmol) in 3 mL hexane was exposed to ethylene gas (0.5 bar) at room temperature. The characteristic bright purple color vanished immediately, resulting in a clear colorless solution. Slow removal of all volatiles *in vacuo* led to colorless needles of **1** (89 mg, 0.16 mmol, 84%) suitable for single crystal x-ray analysis.

^{1}H NMR (C_6D_6, 500 MHz): δ = 7.04 (s, 3H, Ar*H*), 3.48 (h, 2H, ^3J = 6.8 Hz, C*H*Me$_2$), 1.35 (d, 6H, ^3J = 6.8 Hz, CH*Me*$_2$), 1.21 (d, 6H, ^3J = 6.8 Hz, CH*Me*$_2$), 0.94 – 0.89 (m, 2H, Si{C*H*$_2$C*H*$_2$}), 0.39 – 0.36 (m, 2H, Si{C*H*$_2$C*H*$_2$}), 0.34 (s, 27H, Si(Si*Me*$_3$)$_3$), 0.22 (s, 9H, N(Si*Me*$_3$)).

^{13}C{^{1}H} NMR (C_6D_6, 126 MHz): δ = 146.7 (*o-C* of Ar), 143.1 (*ipso-C* of Ar), 125.3 (*p-C* of Ar), 124.5 (*m-C* of Ar), 28.0 (*C*HMe$_2$), 26.0 (CH*Me*$_2$), 25.1 (CH*Me*$_2$), 4.1 (Si{*C*H$_2$*C*H$_2$}), 4.0 (SiSi*Me*$_3$), 3.3 (NSi*Me*$_3$).

^{29}Si{^{1}H} NMR (C_6D_6, 99 MHz): δ = 8.18 (N*Si*Me$_3$), -8.44 (Si*Si*Me$_3$), -80.76 (central *Si*), -118.94 (*Si*SiMe$_3$).

MS-CI (150 eV): m/z (%) = 552 (100) [M$^+$], 524 (32), 496 (40).

EA experimental (calculated): C 55.13 (56.55), H 10.40 (10.40), N 2.66 (2.54) %.

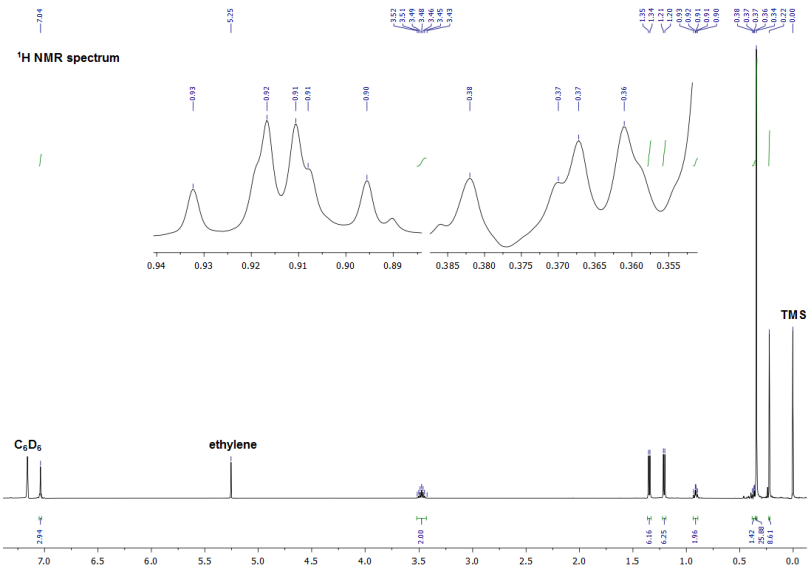

Figure S1. ^{1}H NMR spectrum of compound **1** (C_6D_6, ethylene excess).

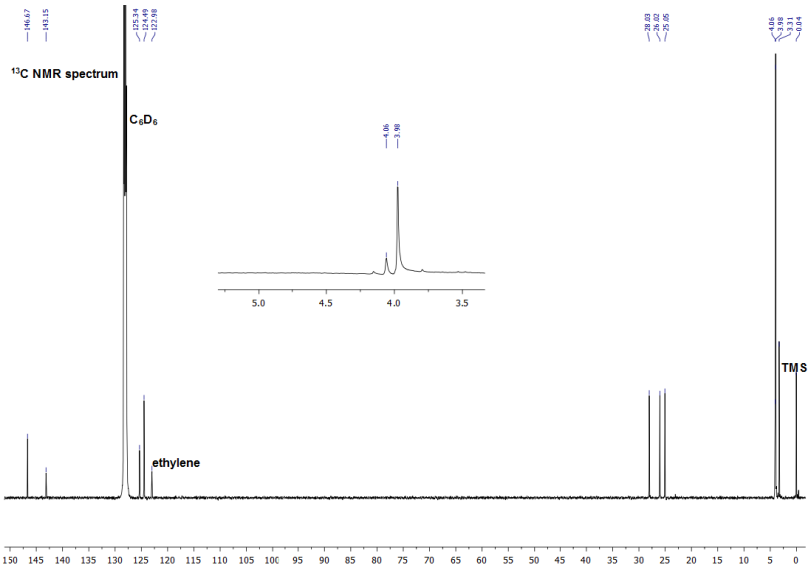

Figure S2. ^{13}C NMR spectrum of compound **1** (C_6D_6, ethylene excess).

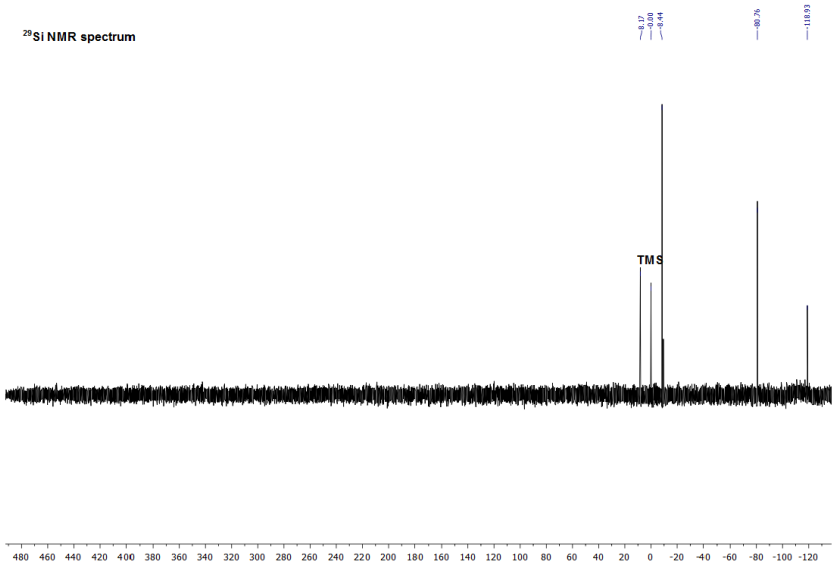

Figure S3. ^{29}Si NMR spectrum of compound **(1)** (C_6D_6, ethylene excess).

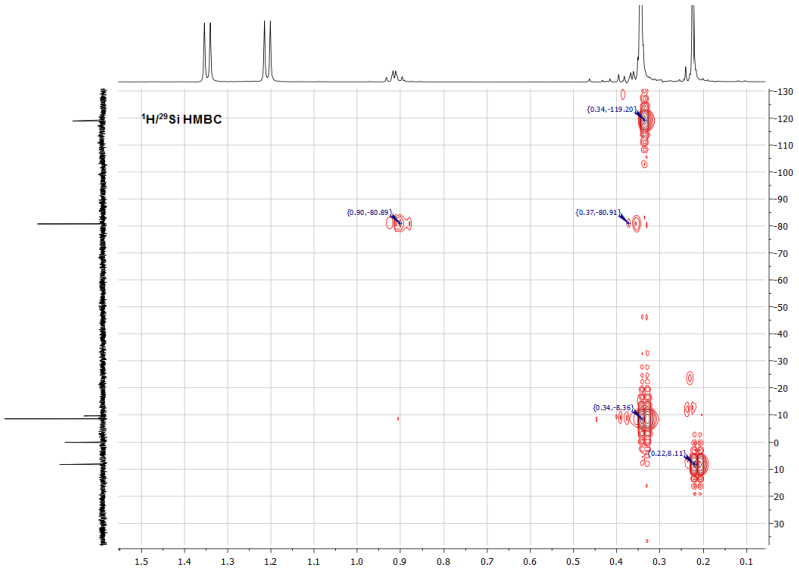

Figure S4. ^{1}H/^{29}Si-HMBC NMR spectrum of compound **1** (C_6D_6, ethylene excess).

Si{CH$_2$-CH$_2$}{NDipp(SiMe$_3$)}{CH$_2$-CH$_2$-Si(SiMe$_3$)$_3$} (2a)

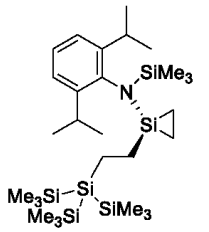

$C_{28}H_{61}NSi_6$
580.31 g/mol

2a

NMR-scale kinetic study

A Young-NMR tube filled with silylsilylene **II** (8 mg, 15 µmol) in 0.5 mL C_6D_6 was exposed to ethylene gas (0.5 bar) via a glass cap at room temperature. The clear colorless solution was heated to 60 °C for three days while the progress of the reaction was monitored via NMR spectroscopy. After this period of time full conversion to compound **2a** was determined.

Scaled-up synthesis

A pressurizable schlenk flask filled with silylsilylene **II** (43 mg, 82 µmol) in 3 mL benzene was exposed to ethylene gas (0.5 bar) at room temperature. The clear colorless solution was heated to 60 °C for three days. Afterwards slow removal of all volatiles *in vacuo* gave the modified silirane **2a** (37 mg, 64 mmol, 78%) as colorless star-shaped needles, which were suitable for single crystal x-ray analysis.

^{1}H NMR (C_6D_6, 500 MHz): δ = 7.09 – 7.01 (m, 3H, Ar*H*), 3.61 (h, 2H, ^3J = 6.8 Hz, C*H*Me$_2$), 1.32 (d, 6H, ^3J = 6.8 Hz, CH*Me*$_2$), 1.21 (d, 6H, ^3J = 6.8 Hz, CH*Me*$_2$), 1.18 – 1.13 (m, 2H, {CH$_2$CH$_2$}SiC*H*$_2$), 1.00 – 0.95 (m, 2H, *J* = Si{C*H*$_2$C*H*$_2$}), 0.80 – 0.76 (m, 2H, Si{C*H*$_2$C*H*$_2$}), 0.75 – 0.71 (m, 2H, (SiMe$_3$)$_3$SiC*H*$_2$), 0.20 (s, 27H, Si(Si*Me*$_3$)$_3$), 0.19 (s, 9H, N(Si*Me*$_3$)).

^{13}C{^{1}H} NMR (C_6D_6, 126 MHz): δ = 147.1 (*o*-*C* of Ar), 141.0 (*ipso*-*C* of Ar), 125.7 (*p*-*C* of Ar), 124.3 (*m*-*C* of Ar), 28.1 (*C*HMe$_2$), 25.4 (CH*Me*$_2$), 24.9 (CH*Me*$_2$), 10.1 ({CH$_2$CH$_2$}Si*C*H$_2$), 2.1 (NSi*Me*$_3$), 1.4 (SiSi*Me*$_3$), 1.0 ((SiMe$_3$)$_3$Si*C*H$_2$), -2.1 (Si{*C*H$_2$*C*H$_2$}).

^{29}Si{^{1}H} NMR (C_6D_6, 99 MHz): δ = 6.90 (N*Si*Me$_3$), -12.92 (Si*Si*Me$_3$), -51.88 (central *Si*), -76.47 (*Si*SiMe$_3$).

MS-CI (150 eV): m/z (%) = 580 (73) [M$^+$], 374 (70), 318 (62), 304 (100), 247 (62).

EA experimental (calculated): C 57.03 (57.95), H 10.55 (10.60), N 2.66 (2.41) %.

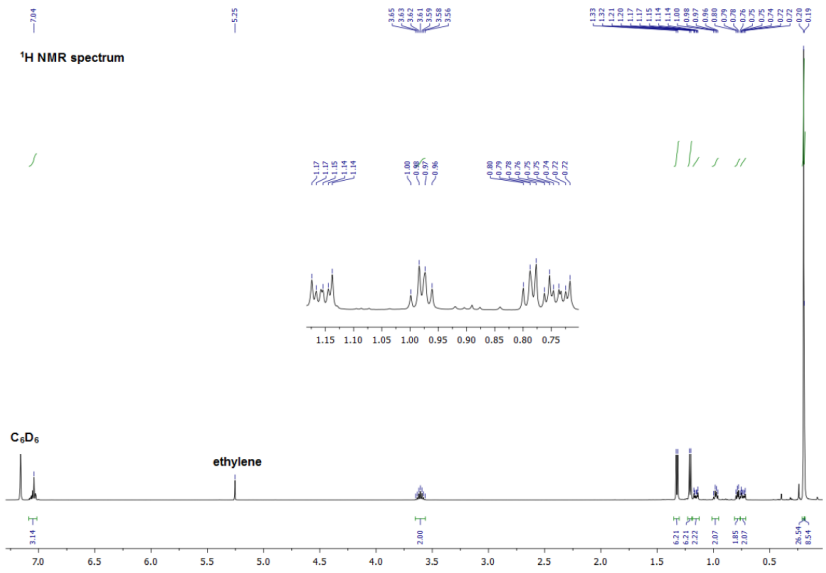

Figure S5. ^{1}H NMR spectrum of compound **2a** (C_6D_6, ethylene excess).

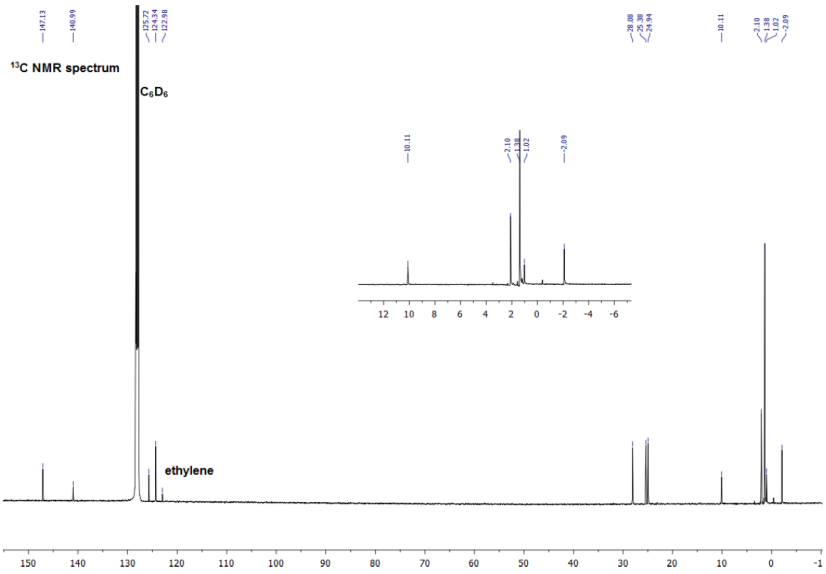

Figure S6. ^{13}C NMR spectrum of compound **2a** (C_6D_6, ethylene excess).

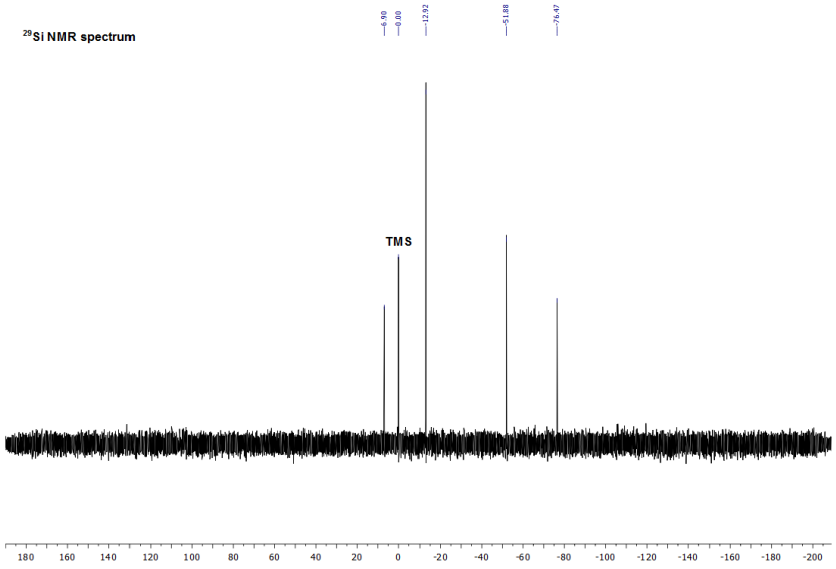

Figure S7. ^{29}Si NMR spectrum of compound **2a** (C_6D_6, ethylene excess).

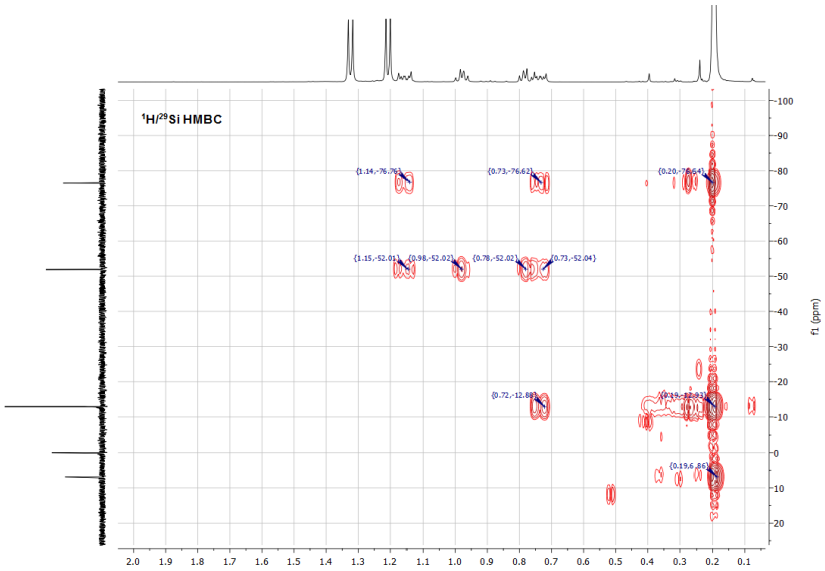

Figure S8. ^{1}H/ ^{29}Si-HMBC NMR spectrum of compound **2a** (C_6D_6, ethylene excess).

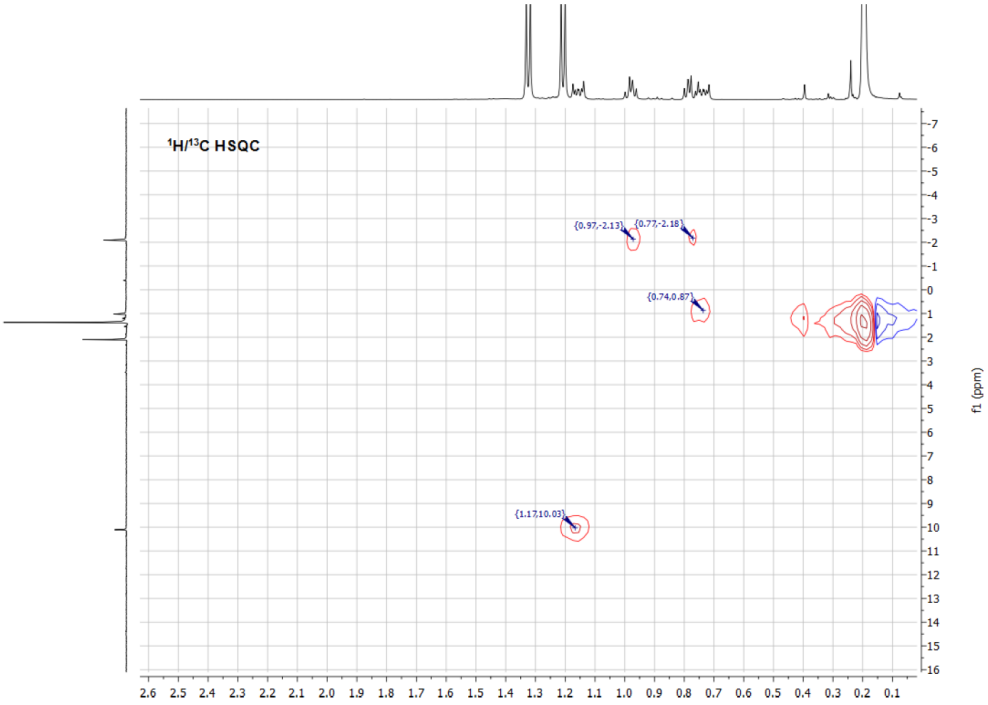

Figure S9. ^{1}H/ ^{13}C-HSQC NMR spectrum of compound **2a** (C_6D_6, ethylene excess).

Si{CD_2-CD_2}{NDipp($SiMe_3$)}{CH_2-CH_2-Si($SiMe_3$)$_3$} (2b)

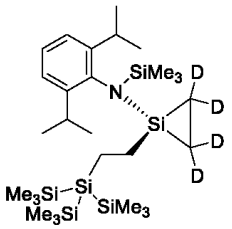

2b

$C_{28}H_{57}D_4NSi_6$
584.34 g/mol

NMR-scale mechanistic study

A Young-NMR tube filled with silirane **1** (9 mg, 14 µmol) in 0.5 mL C_6D_6 was exposed to C_2D_4 gas (0.5 bar) via a glass cap at room temperature. The clear colorless solution was heated to 60 °C for three days while the progress of the reaction was monitored via NMR spectroscopy. Product **2b** was not isolated, its structure was determined by comparison of the ^{1}H NMR data with the fully characterized non-deuterated equivalent **2a**.

^{1}H NMR (C_6D_6, 500 MHz): δ = 7.09 – 7.01 (m, 3H, Ar*H*), 3.61 (h, 2H, ^3J = 6.8 Hz, C*H*Me$_2$), 1.32 (d, 6H, ^3J = 6.8 Hz, CH*Me*$_2$), 1.21 (d, 6H, ^3J = 6.8 Hz, CH*Me*$_2$), 1.18 – 1.13 (m, 2H, {CD_2CD_2}SiCH_2), 0.75 – 0.71 (m, 2H, ($SiMe_3$)$_3$SiCH_2), 0.20 (s, 27H, Si(Si*Me*$_3$)$_3$), 0.19 (s, 9H, N(Si*Me*$_3$)).

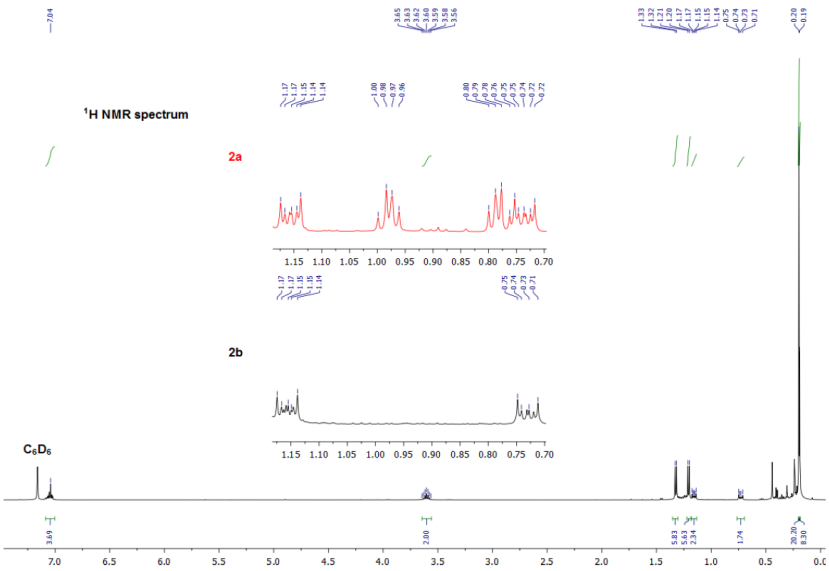

Figure S10. ^{1}H NMR spectrum of compound **2b** in comparison with **2a**.

Si{CH$_2$-CH$_3$C=CCH$_3$-CH$_2$}{NDipp(SiMe$_3$)}{Si(SiMe$_3$)$_3$} (3)

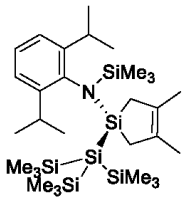

$C_{30}H_{63}NSi_6$
606.35 g/mol

3

NMR-scale kinetic study

A solution of silylsilylene **II** (13 mg, 25 µmol, 1.0 eq) in 0.3 mL C_6D_6 was added to a Young-NMR tube filled with 2,3-dimethyl-1,3-butadiene (4.0 mg, 0.04 mmol, 2.0 eq) in 0.4 mL C_6D_6. The characteristic bright purple solution slowly decolorized resulting in a clear colorless solution after three days at room temperature. The progress of the reaction was monitored via NMR spectroscopy. After full conversion all volatiles were removed *in vacuo* to give silacyclopentene **3** (12 mg, 20 µmol, 80%) as a colorless, air stable solid. Single crystals for x-ray analysis were obtained by slow evaporation of a hexane solution.

^{1}H NMR (C_6D_6, 500 MHz): δ = 7.10 – 7.01 (m, 3H, Ar*H*), 3.48 (h, 2H, ^3J = 6.8 Hz, C*H*Me$_2$), 1.74 – 1.60 (m, 4H, C*H*$_2$-CH$_3$C=CCH$_3$-C*H*$_2$), 1.53 (s, 6H, CH$_2$-C*H*$_3$C=CC*H*$_3$-CH$_2$), 1.25 (d, 6H, ^3J = 6.8 Hz, CH*Me*$_2$), 1.18 (d, 6H, ^3J = 6.8 Hz, CH*Me*$_2$), 0.41 (s, 27H, Si(Si*Me*$_3$)$_3$), 0.23 (s, 9H, N(Si*Me*$_3$)).

^{13}C{^{1}H} NMR (C_6D_6, 126 MHz): δ = 147.4 (*o-C* of Ar), 143.8 (*ipso-C* of Ar), 125.3 (*p-C* of Ar), 131.8 (Si{CH$_2$-CH$_3$*C*=*C*CH$_3$-CH$_2$}), 124.3 (*m-C* of Ar), 31.7 (Si{*C*H$_2$-CH$_3$C=CCH$_3$-*C*H$_2$}), 28.1 (*C*HMe$_2$), 25.4 (CH*Me*$_2$), 25.2 (CH*Me*$_2$), 19.4 (Si{CH$_2$-*C*H$_3$C=C*C*H$_3$-CH$_2$}), 4.6 (SiSi*Me*$_3$), 3.7 (NSi*Me*$_3$).

^{29}Si{^{1}H} NMR (C_6D_6, 99 MHz): δ = 7.71 (central *Si*) 6.59 (N*Si*Me$_3$), -8.82 (Si*Si*Me$_3$), -123.31 (*Si*SiMe$_3$).

MS-CI (150 eV): $^m/_z$ (%) = 606 (13) [M$^+$], 358 (100), 247 (17).

EA experimental (calculated): C 57.71 (59.43), H 10.53 (10.47), N 2.36 (2.31) %.

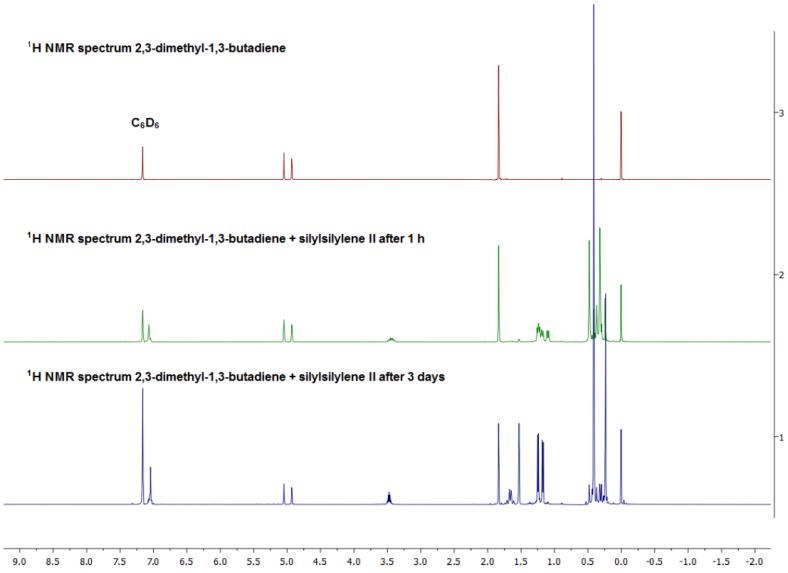

Figure S11. Reaction progress monitored by ^{1}H-NMR spectroscopy (C_6D_6, excess of 2,3-dimethyl-1,3-butadiene).

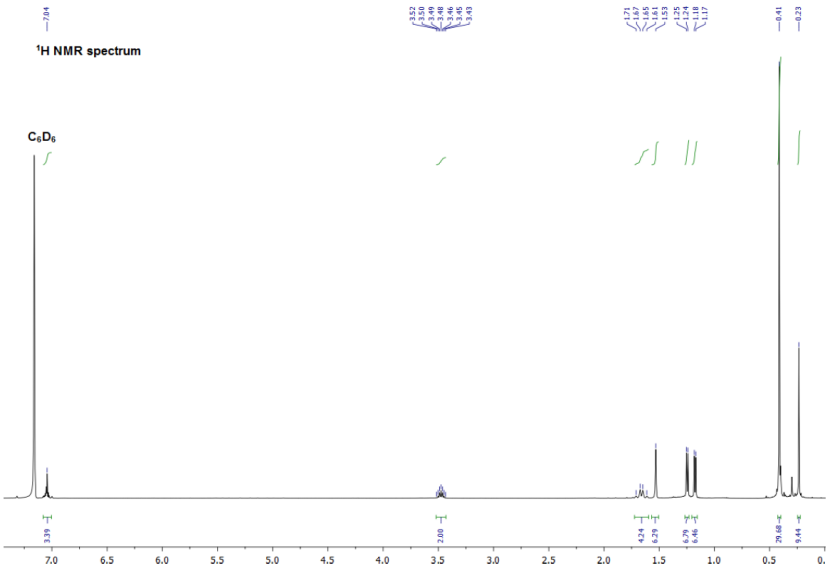

Figure S12. ^{1}H NMR spectrum of compound **3** (C_6D_6).

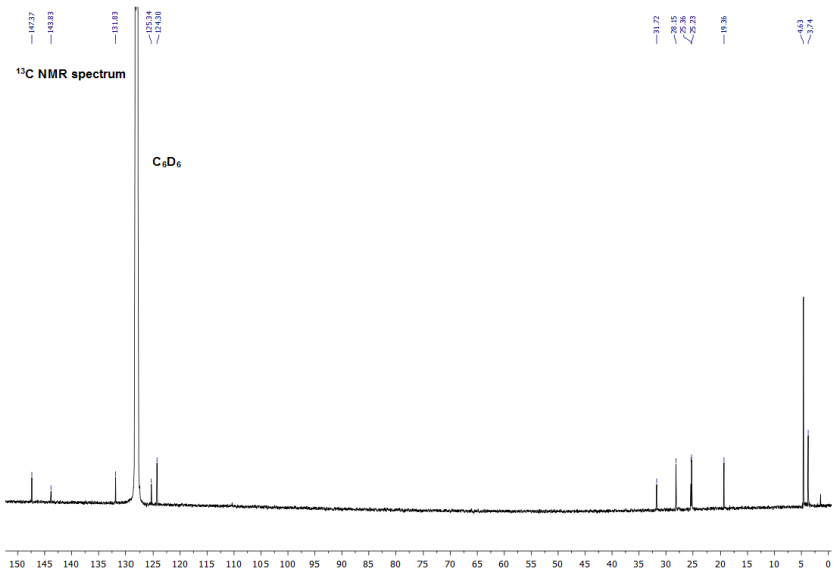

Figure S13. ^{13}C NMR spectrum of compound **3** (C_6D_6).

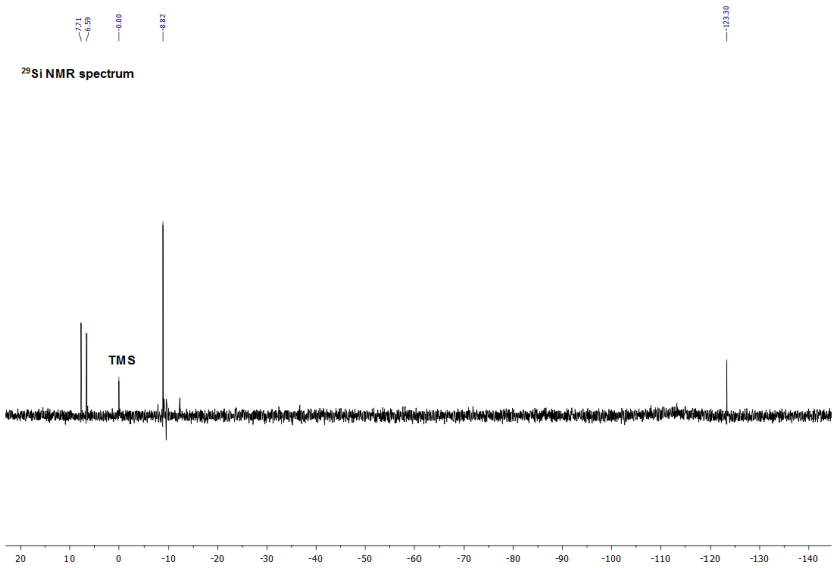

Figure S14. ^{29}Si NMR spectrum of compound **3** (C_6D_6).

2. X-ray Crystallographic Data

General:

Data were collected on an X-ray single crystal diffractometer equipped with a CCD detector (APEX II, κ–CCD), a rotating anode FR591 and a Montel mirror optic by using the SMART software package.[S2] The measurements were performed on single crystals coated with perfluorinated ether. The crystals were fixed on the top of a glass fiber and transferred to the diffractometer. Crystals were frozen under a stream of cold nitrogen. A matrix scan was used to determine the initial lattice parameters. Reflections were merged and corrected for Lorenz and polarization effects, scan speed, and background using SAINT.[S3] Absorption corrections, including odd and even ordered spherical harmonics were performed using SADABS.[S3] Space group assignments were based upon systematic absences, *E* statistics, and successful refinement of the structures. Structures were solved by direct methods with the aid of successive difference Fourier maps,[S4] and were refined against all data using the APEX 2 software[S2] in conjunction with SHELXL-97 or SHELXL-2014[S5] and SHELXLE[S6]. Methyl hydrogen atoms were refined as part of rigid rotating groups, with a C–H distance of 0.98 Å and $U_{iso(H)} = 1.5 \cdot U_{eq(C)}$. Other H atoms were placed in calculated positions and refined using a riding model, with methylene and aromatic C–H distances of 0.99 and 0.95 Å, respectively, and $U_{iso(H)} = 1.2 \cdot U_{eq(C)}$. Non-hydrogen atoms were refined with anisotropic displacement parameters. Full-matrix least-squares refinements were carried out by minimizing $\Sigma w(F_o^2 - F_c^2)^2$ with SHELXL-97[S5] weighting scheme. Neutral atom scattering factors for all atoms and anomalous dispersion corrections for the non-hydrogen atoms were taken from *International Tables for Crystallography*.[S7] Images of the molecular structure in the single crystal were generated with PLATON.[S8]

Compound 1 (CCDC 1424204)

Diffractometer operator C. Jandl
scanspeed 10 s per frame
dx 35 mm
3450 frames measured in 8 data sets
phi-scans with delta_phi = 0.5
omega-scans with delta_omega = 0.5

Table S1: Crystal data of compound ***1***

$C_{26}H_{57}NSi_6$	$F(000)$ = 608
M_r = 552.27	
Triclinic, *P*	D_x = 1.070 Mg m^{-3}
Hall symbol: -P 1	Melting point: unknown
a = 9.8837 (6) Å	Mo $K\alpha$ radiation, λ = 0.71073 Å
b = 12.1135 (8) Å	Cell parameters from 9955 reflections
c = 15.9823 (10) Å	θ = 2.5–28.4°
α = 101.921 (3)°	μ = 0.26 mm^{-1}
β = 90.777 (3)°	T = 123 K
γ = 112.977 (3)°	Fragment, colourless
V = 1714.24 (19) Å^3	0.28 × 0.19 × 0.15 mm
Z = 2	

Table S2: Data collection of compound ***1***

Bruker APEX-II CCD diffractometer	8501 independent reflections
Radiation source: rotating anode FR591	7260 reflections with i > 2σ(i)
MONTEL optic monochromator	R_{int} = 0.043
Detector resolution: 16 pixels mm^{-1}	θ_{max} = 28.3°, θ_{min} = 1.9°
phi– and ω–rotation scans	h = –13 13
Absorption correction: multi-scan *SADABS*, Bruker, 2008b	k = –16 16
T_{min} = 0.678, T_{max} = 0.746	l = –21 21

S16

63371 measured reflections

Table S3: Refinement of compound ***1***

Refinement on F^2	Secondary atom site location: difference Fourier map
Least-squares matrix: full	Hydrogen site location: inferred from neighbouring sites
$R[F^2 > 2\sigma(F^2)]$ = 0.038	H-atom parameters constrained
$wR(F^2)$ = 0.104	$W = 1/[\Sigma^2(FO^2) + (0.0513P)^2 + 0.8045P]$ WHERE $P = (FO^2 + 2FC^2)/3$
S = 1.05	$(\Delta/\sigma)_{max} \leq 0.001$
8501 reflections	$\Delta\rho_{max}$ = 0.84 e Å^{-3}
314 parameters	$\Delta\rho_{min}$ = −0.40 e Å^{-3}
0 restraints	Extinction correction: none
0 constraints	Extinction coefficient: -
Primary atom site location: structure-invariant direct methods	

Compound 2a (CCDC 1424205)

Diffractometer operator C. Jandl
scanspeed 10 s per frame
dx 40 mm
3149 frames measured in 7 data sets
phi-scans with delta_phi = 0.5
omega-scans with delta_omega = 0.5

Table S4: Crystal data of compound ***2a***

$C_{28}H_{61}NSi_6$

M_r = 580.32	D_x = 1.027 Mg m^{-3}
Monoclinic, $P2_1/c$	Melting point: unknown
Hall symbol: -P 2ybc	Mo $K\alpha$ radiation, λ = 0.71073 Å
a = 13.0454 (5) Å	Cell parameters from 9952 reflections
b = 14.7163 (6) Å	θ = 2.4–30.3°
c = 19.9536 (8) Å	μ = 0.24 mm^{-1}
β = 101.566 (2)°	T = 100 K
V = 3752.9 (3) Å^3	Fragment, colourless
Z = 4	0.33 × 0.25 × 0.17 mm
F(000) = 1280	

Table 5: Data collection of compound ***2a***

Bruker APEX-II CCD diffractometer	9327 independent reflections
Radiation source: rotating anode FR591	7833 reflections with i > 2σ(i)
MONTEL optic monochromator	R_{int} = 0.045
Detector resolution: 16 pixels mm^{-1}	θ_{max} = 28.3°, θ_{min} = 1.7°
phi– and ω–rotation scans	h = –17 17
Absorption correction: multi-scan *SADABS*, Bruker, 2008b	k = –19 19
T_{min} = 0.690, T_{max} = 0.746	l = –26 26
97085 measured reflections	

Table S6: Refinement of compound ***2a***

Refinement on F^2	Secondary atom site location: difference Fourier map
Least-squares matrix: full	Hydrogen site location: inferred from neighbouring sites
$R[F^2 > 2\sigma(F^2)] = 0.030$	H-atom parameters constrained
$wR(F^2) = 0.082$	$W = 1/[\Sigma^2(FO^2) + (0.0392P)^2 + 1.2737P]$ WHERE $P = (FO^2 + 2FC^2)/3$
$S = 1.04$	$(\Delta/\sigma)_{max} = 0.002$
9327 reflections	$\Delta\rho_{max} = 0.41$ e Å^{-3}
332 parameters	$\Delta\rho_{min} = -0.24$ e Å^{-3}
0 restraints	Extinction correction: none
0 constraints	Extinction coefficient: -
Primary atom site location: structure-invariant direct methods	

Compound 3 (CCDC 1424206)

Diffractometer operator C. Jandl
scanspeed 10 s per frame
dx 40 mm
4341 frames measured in 9 data sets
phi-scans with delta_phi = 0.5
omega-scans with delta_omega = 0.5

Table S7: Crystal data of compound ***3***

$C_{30}H_{63}NSi_6$	$F(000)$ = 668
M_r = 606.35	
Triclinic, *P*	D_x = 1.039 Mg m^{-3}
Hall symbol: -P 1	Melting point: unknown
a = 9.5649 (10) Å	Mo $K\alpha$ radiation, λ = 0.71073 Å
b = 12.2744 (13) Å	Cell parameters from 9497 reflections
c = 18.351 (2) Å	θ = 2.3–27.1°
α = 74.859 (5)°	μ = 0.23 mm^{-1}
β = 88.531 (6)°	T = 100 K
γ = 69.141 (5)°	Needle, colourless
V = 1938.0 (4) Å^3	0.45 × 0.17 × 0.12 mm
Z = 2	

Table S8: Data collection of compound ***3***

Bruker APEX-II CCD diffractometer	7582 independent reflections
Radiation source: rotating anode FR591	6504 reflections with i > 2σ(i)
MONTEL optic monochromator	R_{int} = 0.035
Detector resolution: 16 pixels mm^{-1}	θ_{max} = 26.0°, θ_{min} = 1.8°
phi– and ω–rotation scans	h = –11 11
Absorption correction: multi-scan *SADABS*, Bruker, 2008b	k = –15 15
T_{min} = 0.697, T_{max} = 0.746	l = –22 22

62102 measured reflections

Table S9: Refinement of compound ***3***

Refinement on F^2	Secondary atom site location: difference Fourier map
Least-squares matrix: full	Hydrogen site location: inferred from neighbouring sites
$R[F^2 > 2\sigma(F^2)]$ = 0.035	H-atom parameters constrained
$wR(F^2)$ = 0.088	$W = 1/[\Sigma^2(FO^2) + (0.036P)^2 + 1.3183P]$ WHERE $P = (FO^2 + 2FC^2)/3$
S = 1.04	$(\Delta/\sigma)_{max}$ = 0.001
7582 reflections	$\Delta\rho_{max}$ = 0.70 e Å^{-3}
352 parameters	$\Delta\rho_{min}$ = −0.37 e Å^{-3}
0 restraints	Extinction correction: none
0 constraints	Extinction coefficient: -
Primary atom site location: structure-invariant direct methods	

3. References

(S1) Protchenko, A. V.; Schwarz, A. D.; Blake, M. P.; Jones, C.; Kaltsoyannis, N.; Mountford, P.; Aldridge, S., *Angew. Chem. Int. Ed. Engl.* **2013,** *52*, 568-71.
(S2) *APEX* suite of crystallographic software. *APEX* 2 Version 2013.4. Bruker AXS Inc., Madison, Wisconsin, USA (2013).
(S3) *SAINT*, Version 8.27b and *SADABS* Version 2012/1. Bruker AXS Inc., Madison, Wisconsin, USA (2012).
(S4) Sheldrick, G. M. "**SHELXS-97**", Program for Crystal Structure Solution, Göttingen, (1997).
(S5) Sheldrick, G. M. "**SHELXL-97**", University of Göttingen, Göttingen, Germany, (1998). *or* Sheldrick, G. M. "**SHELXL-2014**", University of Göttingen, Göttingen, Germany, (2014).
(S6) Huebschle, C. B., Sheldrick, G. M. & Dittrich, B. "**SHELXLE**", *J. Appl. Cryst.* **2011**, *44*, 1281-1284.
(S7) International Tables for Crystallography, Vol. C, Tables 6.1.1.4 (pp. 500-502), 4.2.6.8 (pp. 219-222), and 4.2.4.2 (pp. 193-199), Wilson, A. J. C., Ed., Kluwer Academic Publishers, Dordrecht, The Netherlands, 1992.
(S8) Spek, A. L. "**PLATON**", A Multipurpose Crystallographic Tool, Utrecht University, Utrecht, The Netherlands, (2011).

14.2 Supporting Information Chapter 7

Twist of a Silicon–Silicon Double Bond: Selective *Anti*-Addition of Hydrogen to an Iminodisilene

Daniel Wendel,[†] Tibor Szilvási,[§] Christian Jandl,[‡] Shigeyoshi Inoue[*,∥] and Bernhard Rieger[*,†]

[†]WACKER-Chair of Macromolecular Chemistry, [∥]WACKER-Institute of Silicon Chemistry, [‡]Catalysis Research Center, Technische Universität München, Lichtenbergstraße 4, 85748 Garching bei München, Germany.

[§]Department of Chemical and Biological Engineering, University of Wisconsin Madison, 1415 Engineering Drive, Madison, Wisconsin 53706-1607, USA.

*s.inoue@tum.de; rieger@tum.de

Supporting Information

Total: S54 pages

1. Experimental Procedures

A) General Methods and Instrumentation

All manipulations were carried out under argon atmosphere using standard Schlenk or glovebox techniques. Glassware was heat-dried under vacuum prior to use. Unless otherwise stated, all chemicals were purchased from Sigma-Aldrich or ABCR and used as received. *n*-Hexane and toluene were refluxed over Sodium/benzophenone, distilled and deoxygenated prior to use. Deuterated benzene (C_6D_6) and toluene (C_7D_8) were obtained from Deutero Deutschland GmbH and were dried over 3 Å molecular sieves. All NMR samples were prepared under argon in J. Young PTFE tubes. I*t*-BuNTMS and $KSiTMS_3$ were synthesized according to procedures described in literature[S1-2]. Hydrogen (5.0) and deuterium gas (2.0) were purchased from Westfalen AG and used as received. NMR spectra were recorded on Bruker AV-500C, AV-500 or DRX-400 spectrometers at ambient temperature (300 K), unless otherwise stated. ^{1}H, ^{13}C and ^{29}Si NMR spectroscopic chemical shifts δ are reported in ppm relative to tetramethylsilane. $\delta(^{1}H)$ and $\delta(^{13}C)$ were referenced internally to the relevant residual solvent resonances. $\delta(^{29}Si)$ was referenced to the signal of tetramethylsilane (TMS) (δ = 0 ppm) as external standard. Elemental analyses (EA) were conducted with a EURO EA (HEKA tech) instrument equipped with a CHNS combustion analyzer. Mass spectra (MS-CI) were recorded on a double focusing Finnigan MAT 90 mass spectrometer (isobutene, 150 eV). Variable Temperature (VT) UV-Vis spectra were taken on an Agilent Cary 60 spectrophotometer connected to a UnispeKs CoolSpeK cryostat (Unisoku Scientific Instruments Co.). ATR-FTIR spectra were recorded on a Perkin Elmer FTIR spectrometer (diamond ATR, Spectrum Two; located inside an argon-filled glovebox) in a range of 400 – 4000 cm^{-1}. Melting Points (T_m) were determined in sealed glass capillaries under inert gas by a Büchi M-565.

B) Synthesis and Characterization of New Compounds

Synthesis of I*t*-BuNSiBr$_3$ (1)

This compound was prepared in analog fashion to the synthesis of IPrNSiBr$_3$ by Rivard et al.[S3]. A solution of SiBr$_4$ (5.20 g, 14.9 mmol, 1.00 eq) in toluene (10 mL) was added to I*t*-BuNTMS (4.00 g, 14.9 mmol, 1.00 eq) in toluene (40 mL) in a pressurizable Schlenk flask (Teflon capped, thick-walled). The resulting colorless solution was heated to 130 °C overnight to give a slightly cloudy mixture. The precipitate was allowed to settle and the mother liquor was isolated by filtration. Removal of all volatiles afforded pure tribromoiminosilane **1** (6.10 g, 13.2 mmol, 89%) as a white powder. Crystals suitable for single crystal X-ray analysis were obtained by cooling (-35 °C) a concentrated solution of **1** in toluene.

^{1}H NMR (500 MHz, C_6D_6, r.t.): δ = 5.94 (s, 2H, C*H*-N), 1.36 (s, 18H, CC*H*$_3$).

^{13}C NMR (126 MHz, C_6D_6, r.t.): δ = 140.5 (*C*=N), 109.4 (*C*H-N), 56.6 (*C*CH$_3$), 28.5 (CC*H*$_3$).

^{29}Si NMR (99 MHz, C_6D_6, r.t.): δ = -125.5 (*Si*Br$_3$).

MS-CI (150 eV): m/z (%) = 462 $[M]^+$ (100), 381 $[M-Br]^+$ (90).

EA experimental (calculated): C 28.43 (28.59), H 4.31 (4.36), N 8.93 (9.09) %.

M_p: 153.3 °C (color change to brownish).

Synthesis of I*t*-BuN(SiTMS$_3$)Si=Si(SiTMS$_3$)N*t*-Bu (2)

A solution of KSiTMS$_3$ (624 mg, 2.18 mmol, 2.00 eq) in *n*-hexane (10 mL) was added to tribromosilane **1** (504 mg, 1.09 mmol, 1.00 eq) in toluene (5 mL) at -78 °C. The color immediately changed into dark purple with formation of a white precipitate. After stirring the solution for 20 min, the solvent was removed *in vacuo*. The obtained residue is extracted with *n*-hexane (3 × 10 mL) and filtered with a microfiber glass filter. The solution is concentrated and cooled to -35 °C for 3 days to yield disilene **2** (327 mg, 0.347 mmol, 64%) as dark purple to brown crystals suitable for single crystal X-ray analysis. Depending on the crystallization conditions some batches contained small amounts of oily co-product TMS$_3$SiBr (^{29}Si NMR δ = -12.8 and -24.1 ppm)[S4]. Isolated disilene **2** is stable as a solid (-35 °C), but decomposes in benzene or *n*-hexane solution within one or two weeks at ambient temperatures to give a red oil.

^{1}H NMR (500 MHz, C$_7$D$_8$, r.t.): δ = 5.98 (s, 4H, C*H*-N), 1.42 (s, 36H, CC*H*$_3$), 0.50 (s, 54H, Si*TMS*$_3$).

^{13}C NMR (126 MHz, C$_7$D$_8$, r.t.): δ = 143.7 (*C*=N), 108.5 (*C*H-N), 55.5 (*C*CH$_3$), 30.6 (C*C*H$_3$), 5.0 (Si*TMS*$_3$).

^{29}Si NMR (80 MHz, C$_7$D$_8$, -78 °C): δ = 72.0 (*Si*=*Si*), -9.3 (*TMS*$_3$), -123.3 (*Si*TMS$_3$).

The ^{29}Si NMR spectrum was measured at -78 °C because of the very weak intensity of the Si=Si signal (bs, 71.0 ppm, C$_7$D$_8$, r.t.) at room temperature, presumably due to the biradical character of **2** (see Figure S5). Similar behavior has been observed for related tetrakis(di-tert-butylmethylsilyl)disilene[S5]. Neither additional signal sets for the (*E*)-isomer of **2** nor a respective iminosilylene were observable at -78 °C or room temperature.

MS could not be obtained for **2** due to its extreme air and moisture sensitivity.

EA experimental (calculated): C 50.32 (51.11), H 9.99 (10.08), N 8.56 (8.94) %.

M$_p$: 129.9°C (color change to dark red, sticky oil).

IR (cm^{-1}): 2971 (w), 2945 (w), 2892 (w), 1645 (m), 1581 (m), 1403 (w), 1361 (w), 1222 (m), 953 (w), 824 (s), 677 (m), 621 (m), 515 (w).

Figure S1. Dark purple iminodisilene **2** as crystals and in solution (C_6D_6).

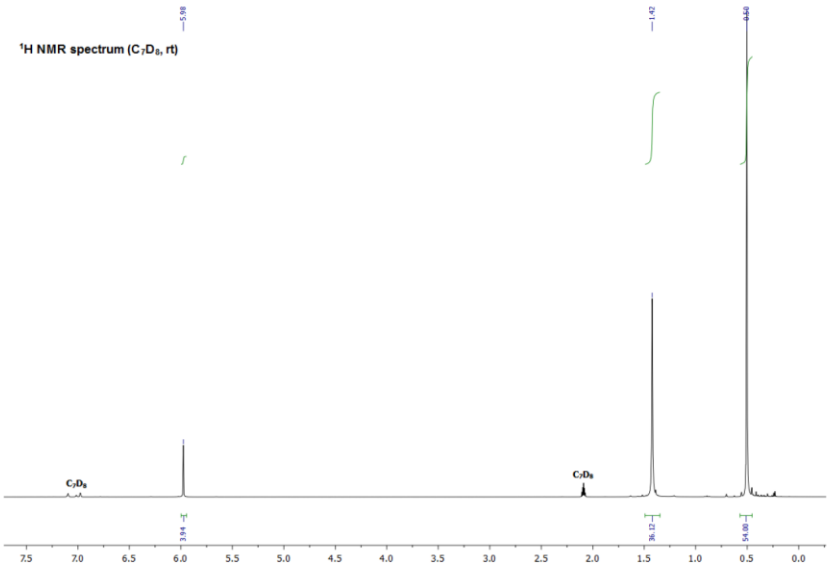

Figure S2. ^{1}H NMR spectrum of compound **2** (C_7D_8, r.t.).

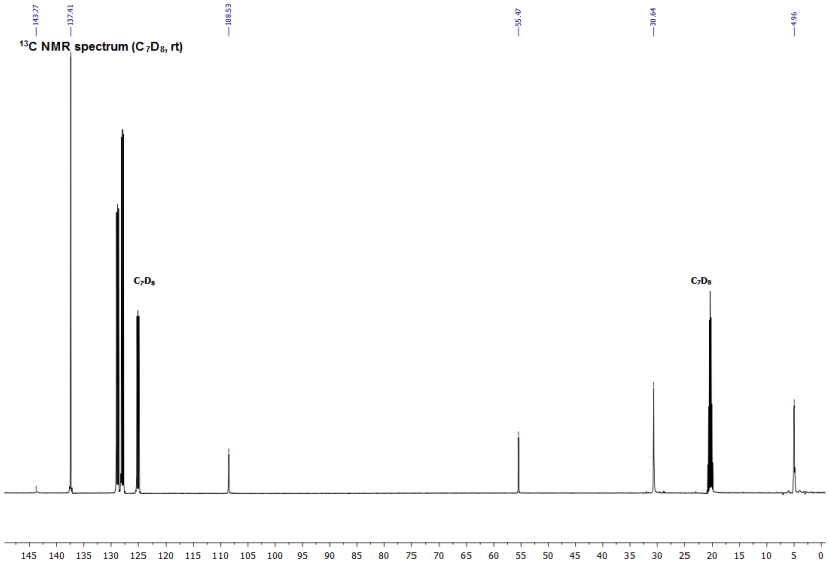

Figure S3. ^{13}C NMR spectrum of compound **2** (C_7D_8, r.t.).

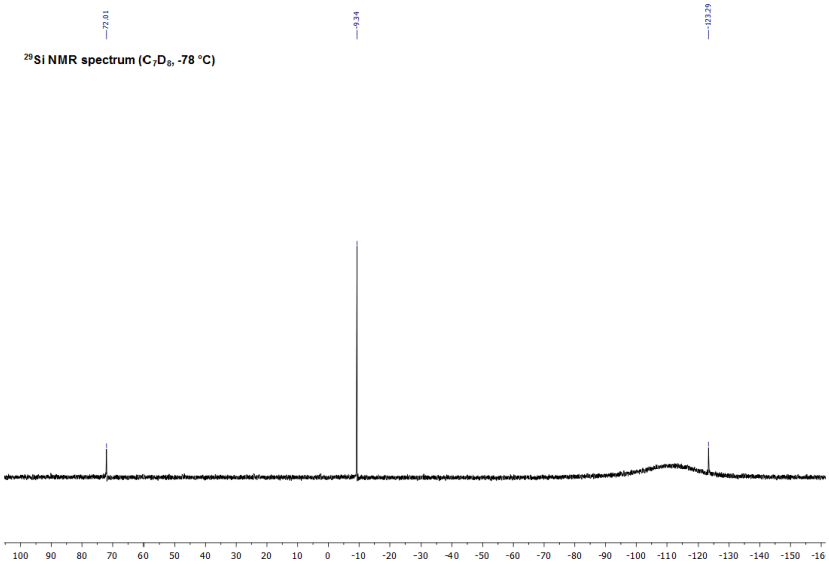

Figure S4. ^{29}Si NMR spectrum of compound **2** (C_7D_8, -78 °C).

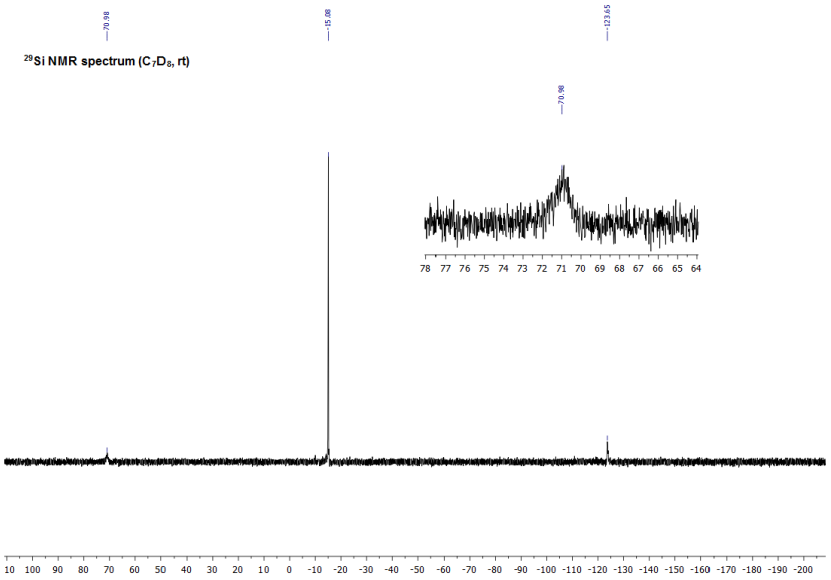

Figure S5. ^{29}Si NMR spectrum of compound **2** (C_7D_8, r.t.).

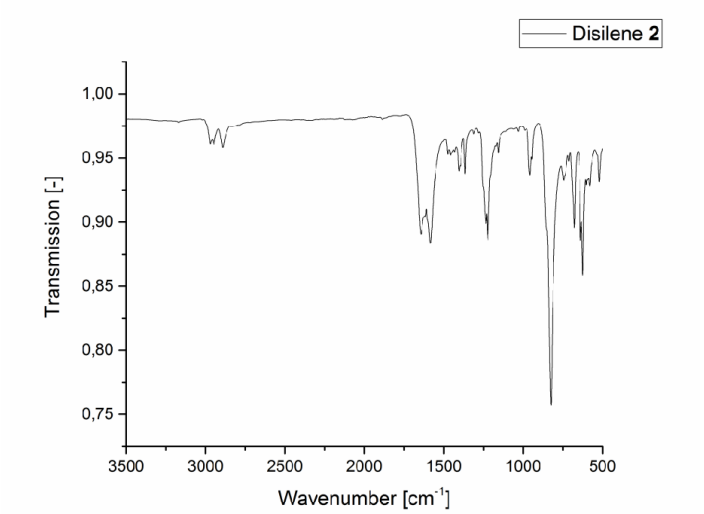

Figure S6. IR-spectrum of compound **2**.

Variable Temperature (VT) UV-Vis Spectroscopy

We performed variable temperature (VT) UV-Vis spectroscopy (see Figure S7) from -80 °C to 50 °C to verify a potential dynamic equilibrium between disilene and silylene. A $2.5*10^{-3}$ M solution of **2** in hexane (1 cm schlenk square quartz cell) was freshly prepared for this measurement.

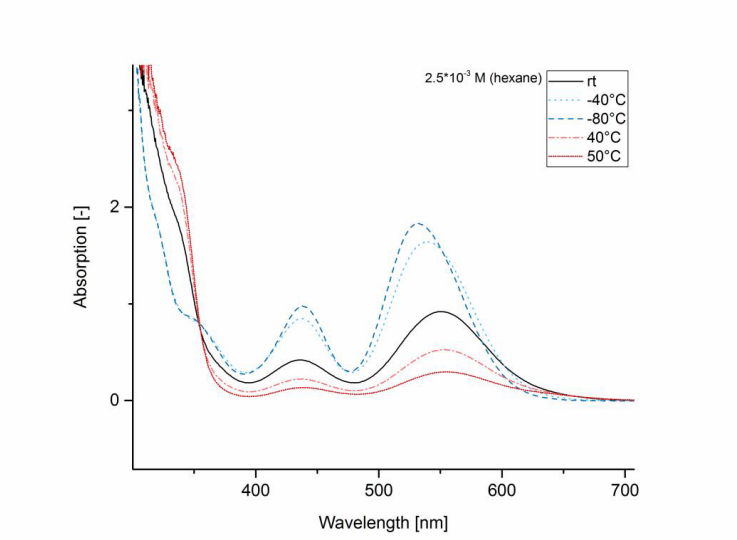

Figure S7. Variable Temperature (VT) UV-Vis spectra of compound **2** (2.5×10^{-3}M in *n*-hexane); λ_{max} (r.t.) = 551 nm (π→π*), 435 nm (HOMO→LUMO+1).

The spectrum of **2** at room temperature displayed two characteristic peaks, a large one at 551 nm, assigned to the π→π* transition (theo. 518 nm), and a smaller one at 435 nm, belonging to the HOMO→LUMO+1 transition (theo. 425 nm) of the disilene. At low temperatures the π→π* transition is blue- and the HOMO→LUMO+1 transition is red-shifted with an increase of intensity of both assigned peaks. Simultaneously, a distinct decrease of a broad shoulder at 330 nm is visible. This process is completely reversible and higher temperature led to the exact opposite picture with a clear growth of the mentioned shoulder. Though, cooling back from 50 °C to the initial position at room temperature did not yield the same curve, indicating an accelerated decomposition process at elevated temperatures, which presumably involves dissociation to two highly reactive silylene fragments. Theoretical calculations predict two major peaks at 317 and 286 nm and a minor one at 659 nm for the n→3p transition of the iminosilylsilylene I*t*-BuNSi(II)SiTMS$_3$. Regarding the theoretical data, the former two peaks might be brought in line with

the rising shoulder at 330 nm, the latter is presumably suppressed by the broad, very intense signal of the π→π* transition of the disilene. This observation is in contrast with the ^{29}Si NMR experiments, where only **2** is present both at -78 °C and room temperature, which clearly excludes a dissociation equilibrium in this temperature range. Similar temperature-dependent UV-VIS data have been found for cyclic alkylaminosilylene by Iwamoto *et al.*. Here, at very low temperatures the formation of head-to-head dimers (disilene with an extremely long Si=Si bond) has been proposed[S6].

Even though no distinct experimental proof is presented, the facile dissociation of **2** is supported theoretically by a dissociation Gibbs free energy of (7.9 kcal/mol), which is much less than the bond-dissociation energy (BDE) of the Si=Si bond (19.2 kcal/mol) of a 1,2-dibromodisilene investigated by Tamao et al previously. Here, an equilibrium was not directly observed spectroscopically, but upon addition of a strong Lewis base a dissociation to the respective bromosilylene was detected[S7].

Synthesis of I*t*-BuN(SiTMS$_3$)HSi-SiH(SiTMS$_3$)N*t*-Bu (3a)

A pressurizable Schlenk flask filled with disilene **2** (100 mg, 0.106 mmol) in *n*-hexane (5 mL) was exposed to hydrogen gas (1 bar) at room temperature. The characteristic dark purple color vanished within 10 min, resulting in a clear colorless solution. Slow removal of all volatiles *in vacuo* led to colorless crystals of disilane **3a** (93 mg, 0.099 mmol, 95%) suitable for single crystal X-ray analysis.

^{1}H NMR (500 MHz, C_6D_6, r.t.): δ = 6.17 (s, ^1J (Si-H) = 146 Hz, ^2J (SiSi-H) = 21.4 Hz, ^2J (TMS$_3$SiSi-H) = 13.7 Hz, ^3J (H-SiSi-H) = 1.8 Hz, 2H, Si*H*), 6.03 (d, ^3J = 3.3 Hz, 2H, C*H*-N), 5.99 (d, ^3J = 3.3 Hz, 2H, C*H*-N), 1.48 (s, 18H, CC*H*$_3$), 1.44 (s, 18H, CC*H*$_3$), 0.50 (s, 54H, Si*TMS*$_3$).

^{13}C NMR (126 MHz, C_6D_6, r.t.): δ = 141.5 (*C*=N), 108.2 (*C*H-N), 107.8 (*C*H-N), 55.3 (*C*CH$_3$), 54.9 (*C*CH$_3$), 30.9 (C*C*H$_3$), 30.7 (C*C*H$_3$), 4.8 (Si*TMS*$_3$).

^{29}Si NMR (99 MHz, C_6D_6, r.t.): δ = -9.5 (*TMS*$_3$), -62.4 (d, ^1J (Si-H) = 146 Hz, H*Si*-*Si*H,), -126.1 (*Si*TMS$_3$).

MS-CI (150 eV): m/z (%) = 470 [M -SiHSiTMS$_3$N*t*-Bu]$^+$ (100).

EA experimental (calculated): C 51.64 (51.00), H 10.36 (10.27), N 8.07 (8.92) %.

M$_p$: 204.0 °C (color change to red, sticky oil).

IR (cm^{-1}): 2956 (w), 2930 (w), 2888 (w), 2023 (w, Si-H), 1998 (w, Si-H), 1626 (m), 1596 (m), 1417 (w), 1373 (w), 1226 (m), 956 (w), 830 (s), 740 (w), 687 (m), 618 (m), 528 (w).

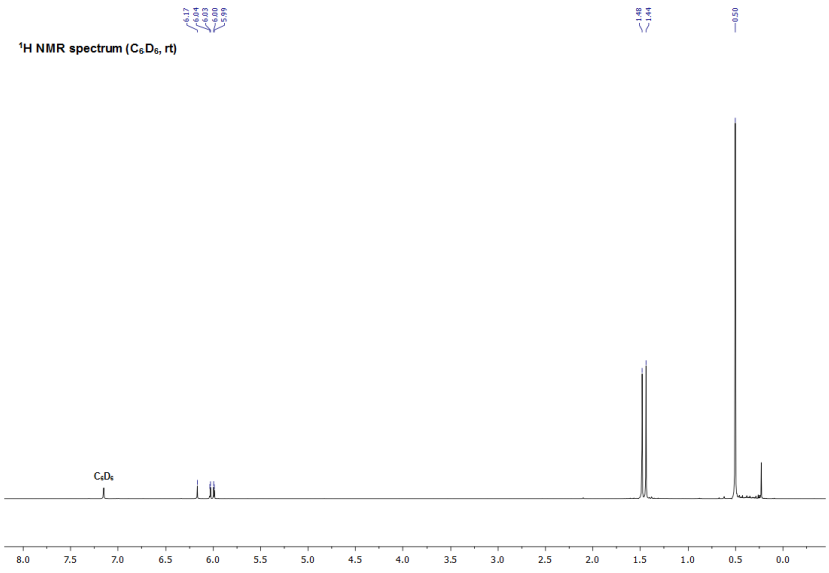

Figure S8. ^{1}H NMR spectrum of compound **3a** (C_6D_6, r.t.).

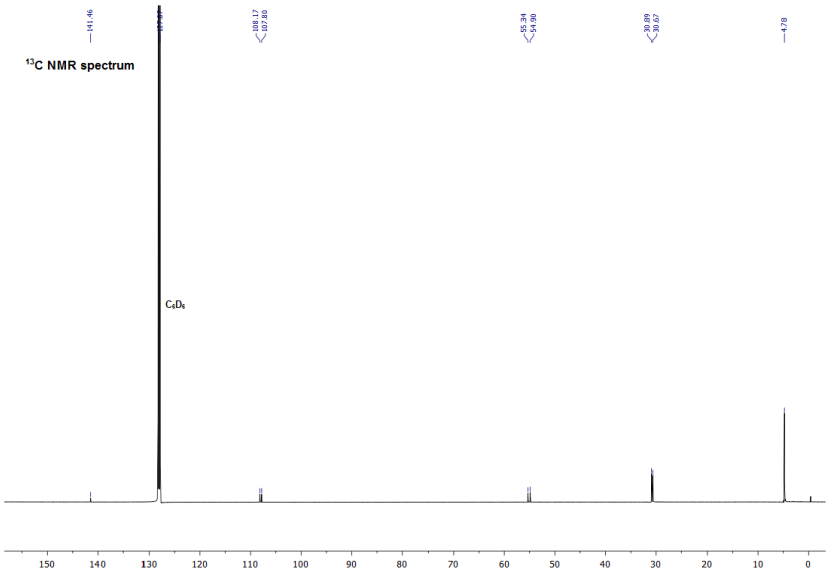

Figure S9. ^{13}C NMR spectrum of compound **3a** (C_6D_6, r.t.).

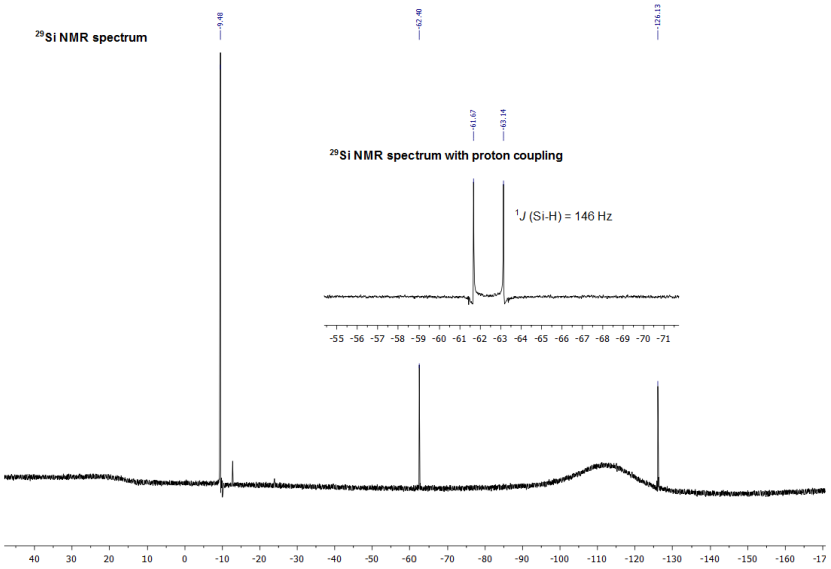

Figure S10. ^{29}Si NMR spectrum of compound **3a** (C_6D_6, r.t.).

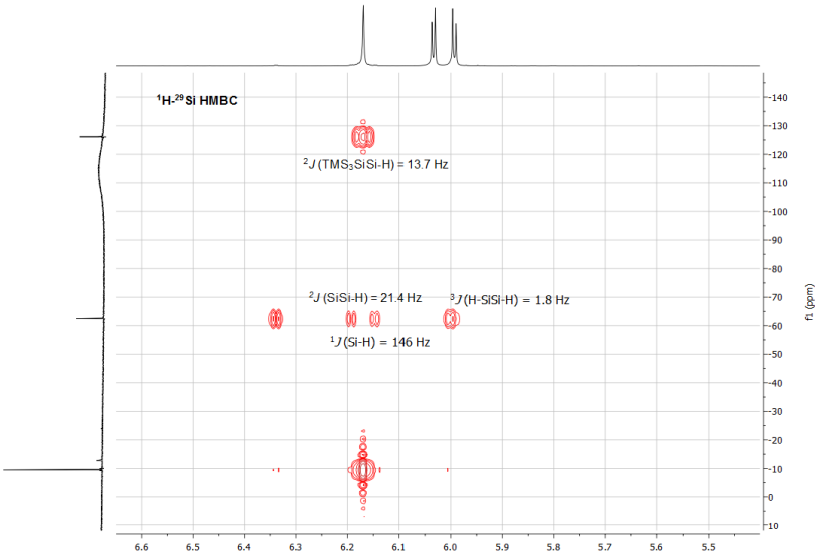

Figure S11. ^{1}H-^{29}Si HMBC NMR spectrum of compound **3a** (C_6D_6, r.t.).

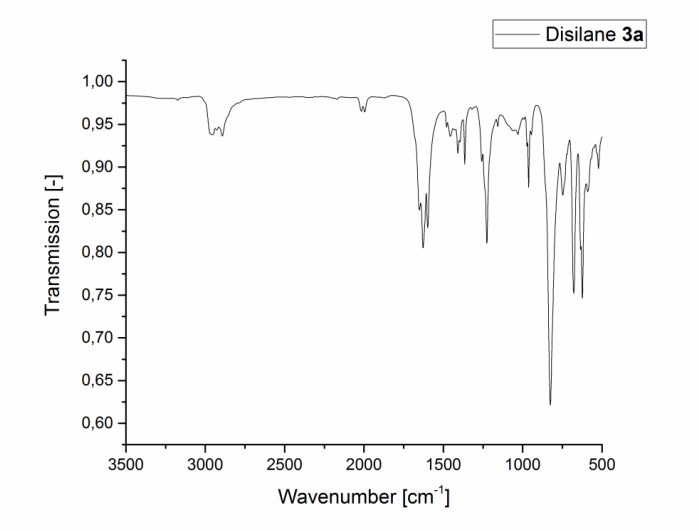

Figure S12. IR-spectrum of compound **3a**.

NMR experiments:

To determine the product selectivity of this reaction, the synthesis was repeated in a J. Young PTFE tube (C_6D_6) and monitored via ^{1}H NMR spectroscopy. At room temperature the complete conversion of **2** to the single product *racemic*-**3a** was verified within 10 min. To further exclude a mechanism that follows a dissociation/silylene hydrogenation/Si-H insertion pathway, we conducted a second NMR experiment, where the disilene **2** solution (toluene-d_8) was pressurized with 1 bar H_2 at -78 °C and subsequently monitored via NMR spectroscopy at this temperature. A slow conversion solely to **3a** was detected when the solution was warmed up to -20 °C with a reasonable extension of reaction time to approximately 4 h (Figure S13). At all times only disilene **2** and direct hydrogenation product **3a** were present and no intermediary iminosilylsilylene I*t*-BuNSi(II)SiTMS$_3$ or monomeric silane I*t*-BuNSiH$_2$SiTMS$_3$ were detectable. In analogy to the room temperature experiment no *meso*-disilane was observed. In a third NMR experiment, the reaction of disilene **2** (1 eq, C_6D_6) with *t*-Bu$_2$SiH$_2$ (2 eq) was carried out to re-enact an insertion of a potential dissociated I*t*-BuNSi(II)SiTMS$_3$ into a Si-H bond of a comparable R_2SiH_2 compound. Monitoring this reaction via ^{1}H NMR spectroscopy did not show any conversion to the respective disilane I*t*-BuNSiTMS$_3$HSiSiH*t*-Bu$_2$ even after one day at room temperature.

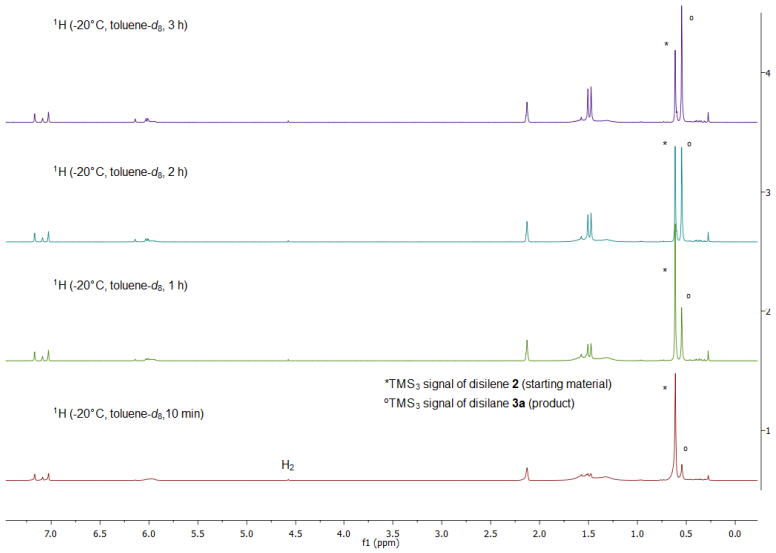

Figure S13: NMR study of hydrogenation of disilene **2** with 1 bar H_2 at -20 °C in toluene-d_8.

Synthesis of I*t*-BuN(SiTMS$_3$)DSi-SiD(SiTMS$_3$)N*t*-Bu (3b)

A Young-NMR tube filled with disilene **2** (10.6 mg, 11.3 µmol) in 0.5 mL C_6D_6 was exposed to D_2 gas (0.5 bar) via a glass cap at room temperature. The characteristic dark purple color vanished within 10 min, resulting in a clear colorless solution. Product **3b** was not isolated, its structure was determined by comparison of the NMR data with the fully characterized non-deuterated equivalent **3a**.

^{1}H NMR (500 MHz, C_6D_6, r.t.): δ = 6.03 (d, ^3J = 3.3 Hz, 2H, C*H*-N), 5.99 (d, ^3J = 3.3 Hz, 2H, C*H*-N), 1.48 (s, 18H, CC*H*$_3$), 1.44 (s, 18H, CC*H*$_3$), 0.50 (s, 54H, Si*TMS*$_3$).

^{13}C NMR (126 MHz, C_6D_6, r.t.): δ = 141.5 (*C*=N), 108.2 (*C*H-N), 107.8 (*C*H-N), 55.3 (*C*CH$_3$), 54.9 (*C*CH$_3$), 30.9 (CC*H*$_3$), 30.7 (CC*H*$_3$), 4.8 (Si*TMS*$_3$).

^{29}Si NMR (99 MHz, C_6D_6, r.t.): δ = -9.5 (*TMS*$_3$), -62.8 (t, ^1J (Si-D) = 25 Hz, D*Si*-*Si*D,), -126.1 (*Si*TMS$_3$).

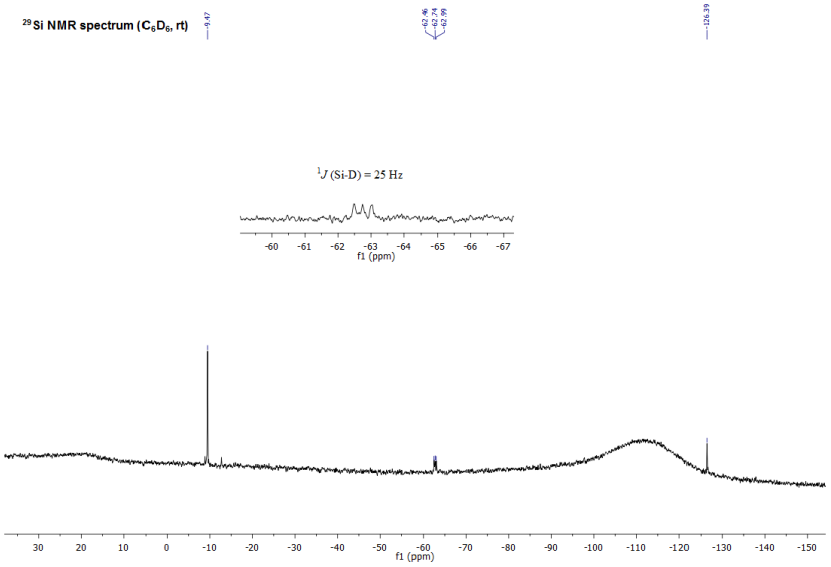

Figure S14. ^{29}Si NMR spectrum of compound **3b** (C_6D_6, r.t.).

2. X-ray Crystallographic Data

General:

Data were collected on a single crystal X-ray diffractometer equipped with a CCD detector (APEX II, κ-CCD), a fine-focus sealed tube with MoK_α radiation (λ = 0.71073 Å) and a Triumph monochromator using the APEX II software package (**1**,**2**) or with a CMOS detector (APEX III, κ-CMOS), an IMS microsource with MoK_α radiation (λ = 0.71073 Å) and a Helios optic using the APEX III software package (**3a**)[S8-9]. The crystals were fixed on the top of glass fiber or a kapton micro sampler with perfluorinated ether, transferred to the diffractometer and frozen under a stream of cold nitrogen. A matrix scan was used to determine the initial lattice parameters. For **1** twin domains related by the twin law -1 0 0 0 -1 0 -0.305 -0.032 1 were identified using CELL_NOW[S10]. Both were integrated and refinement was carried out against a HKLF 5 dataset created by TWINABS containing all observed data[S11]. The final refinement afforded a ratio of the two domains of 0.494:0.506. Reflections were merged and corrected for Lorentz and polarization effects, scan speed, and background using SAINT[S12]. Absorption corrections, including odd and even ordered spherical harmonics were performed using SADABS (**2**,**3a**) or TWINABS (**1**)[S11-12]. Space group assignments were based upon systematic absences, *E* statistics, and successful refinement of the structures. Structures were solved using SHELXT with the aid of successive difference Fourier maps, and were refined against all data using the APEX III software in conjunction with SHELXL-2014 and SHELXLE[S9, S13-15]. Hydrogen atoms were calculated in ideal positions as follows: Methyl hydrogen atoms were refined as part of rigid rotating groups, with a C–H distance of 0.98 Å and $U_{iso(H)} = 1.5 \cdot U_{eq(C)}$. Other H atoms were placed in calculated positions and refined using a riding model with methylene and aromatic C–H distances of 0.99 Å and 0.95 Å, respectively, other C–H distances of 1.00 Å and $U_{iso(H)} = 1.2 \cdot U_{eq(C)}$. In case of **3a** the two hydrogen atoms on the former Si-Si double bond were refined freely in proof of their presence and therefore the addition of H_2. Non-hydrogen atoms were refined with anisotropic displacement parameters. Full-matrix least-squares refinements were carried out by minimizing $\Sigma w(F_o^2-F_c^2)^2$ with the SHELXL weighting scheme[S14]. Neutral atom scattering factors for all atoms and anomalous dispersion corrections for the non-hydrogen atoms were taken from *International Tables for Crystallography*[S16]. Images were created with Mercury (main article) or PLATON (SI)[S17-18].

Compound **1** (CCDC 1538753)

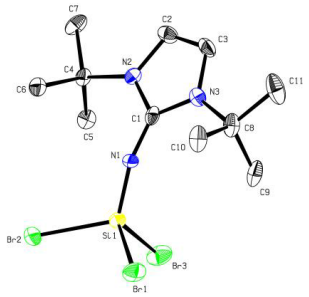

Figure S15. Molecular structure of iminotribromosilane **1**.

Table S1. Crystallographic data of **1**.

Diffractometer operator C. Jandl
scanspeed 5 s per frame
dx 80 mm
10456 frames measured in 29 data sets
phi-scans with delta_phi = 0.5
omega-scans with delta_omega = 0.5

Crystal data

$C_{11}H_{20}Br_3N_3Si$	$F(000)$ = 1808
M_r = 462.09	
Triclinic, *P*	D_x = 1.784 Mg m^{-3}
Hall symbol: -P 1	Melting point: - K
a = 11.0798 (4) Å	Mo *K*α radiation, λ = 0.71073 Å
b = 16.3858 (7) Å	Cell parameters from 9913 reflections
c = 19.5188 (9) Å	θ = 2.4–26.4°
α = 88.435 (2)°	μ = 7.10 mm^{-1}
β = 84.999 (2)°	*T* = 100 K
γ = 77.037 (2)°	Fragment, colorless
V = 3440.1 (3) Å^3	0.55 × 0.39 × 0.25 mm
Z = 8	

Data collection

Apex II CCD diffractometer	16228 independent reflections
Radiation source: fine-focus sealed tube	13931 reflections with $I > 2\sigma(I)$
Triumph monochromator	R_{int} = ?
Detector resolution: 16 pixels mm^{-1}	θ_{max} = 25.4°, θ_{min} = 1.3°
phi– and ω–rotation scans	h = –13 13
Absorption correction: multi-scan TWINABS 2012/1	k = –19 19
T_{min} = 0.400, T_{max} = 0.745	l = 0 23
16228 measured reflections	

Refinement

Refinement on F^2	Secondary atom site location: difference Fourier map
Least-squares matrix: full	Hydrogen site location: inferred from neighbouring sites
$R[F^2 > 2\sigma(F^2)]$ = 0.043	H-atom parameters constrained
$wR(F^2)$ = 0.105	W = 1/[$\Sigma^2(FO^2) + (0.041P)^2 + 16.2822P$] WHERE $P = (FO^2 + 2FC^2)/3$
S = 1.05	$(\Delta/\sigma)_{max}$ = 0.002
16228 reflections	$\Delta\rho_{max}$ = 0.95 e Å^{-3}
674 parameters	$\Delta\rho_{min}$ = –0.98 e Å^{-3}
0 restraints	Extinction correction: none
- constraints	Extinction coefficient: -
Primary atom site location: intrinsic phasing	

Compound **2** (CCDC 1538755)

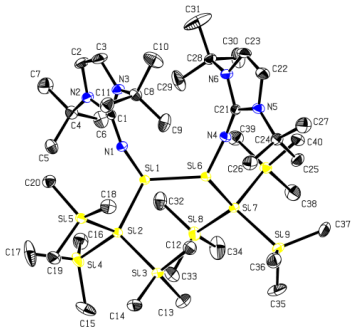

Figure S16. Molecular structure of disilene **2**.

Table S2. Crystallographic data of **2**.

Diffractometer operator C. Jandl
scanspeed 20 s per frame
dx 50 mm
3880 frames measured in 6 data sets
phi-scans with delta_phi = 0.5
omega-scans with delta_omega = 0.5

Crystal data

$C_{40}H_{94}N_6Si_{10}$

M_r = 940.11

Monoclinic, $P2_1/n$

Hall symbol: -P 2yn

a = 10.2224 (2) Å

b = 24.6439 (4) Å

c = 23.6839 (4) Å

β = 95.701 (1)°

V = 5936.93 (18) Å^3

Z = 4

F(000) = 2064

D_x = 1.052 Mg m^{-3}

Melting point: - K

Mo $K\alpha$ radiation, λ = 0.71073 Å

Cell parameters from 9690 reflections

θ = 2.2–26.3°

μ = 0.25 mm^{-1}

T = 100 K

Fragment, red-brown

0.24 × 0.23 × 0.10 mm

Data collection

Apex II CCD diffractometer	11697 independent reflections
Radiation source: fine-focus sealed tube	9341 reflections with $I > 2\sigma(I)$
Triumph monochromator	R_{int} = 0.061
Detector resolution: 16 pixels mm^{-1}	θ_{max} = 26.0°, θ_{min} = 1.7°
phi– and ω–rotation scans	h = −12 12
Absorption correction: multi-scan *SADABS* 2014/5	k = −30 30
T_{min} = 0.642, T_{max} = 0.742	l = −29 29
141559 measured reflections	

Refinement

Refinement on F^2	Secondary atom site location: difference Fourier map
Least-squares matrix: full	Hydrogen site location: inferred from neighbouring sites
$R[F^2 > 2\sigma(F^2)]$ = 0.038	H-atom parameters constrained
$wR(F^2)$ = 0.090	W = 1/[$\Sigma^2(FO^2)$ + (0.0343P)^2 + 3.336P] WHERE P = (FO^2 + 2FC^2)/3
S = 1.02	$(\Delta/\sigma)_{max}$ = 0.005
11697 reflections	$\Delta\rho_{max}$ = 0.38 e Å^{-3}
535 parameters	$\Delta\rho_{min}$ = −0.25 e Å^{-3}
0 restraints	Extinction correction: none
- constraints	Extinction coefficient: -
Primary atom site location: intrinsic phasing	

Compound **3a** (CCDC 1538754)

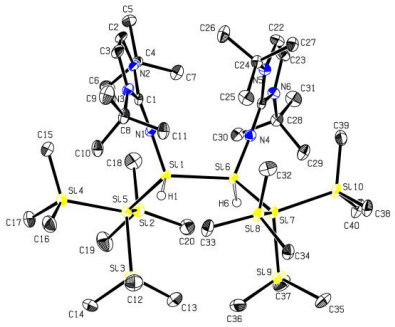

Figure S17. Molecular structure of disilane **3a**.

Table S3. Crystallographic data of **3a**.

Diffractometer operator C. Jandl
scanspeed 60 s per frame
dx 45 mm
981 frames measured in 4 data sets
phi-scans with delta_phi = 0.5
omega-scans with delta_omega = 0.5

Crystal data

$C_{40}H_{96}N_6Si_{10}$

M_r = 942.13	D_x = 1.059 Mg m^{-3}
Monoclinic, $P2_1/c$	Melting point: - K
Hall symbol: -P 2ybc	Mo $K\alpha$ radiation, λ = 0.71073 Å
a = 20.3289 (13) Å	Cell parameters from 9725 reflections
b = 13.9624 (9) Å	θ = 2.6–26.1°
c = 22.7699 (16) Å	μ = 0.25 mm^{-1}
β = 113.931 (2)°	T = 100 K
V = 5907.4 (7) Å^3	Fragment, colorless
Z = 4	0.52 × 0.17 × 0.16 mm
F(000) = 2072	

Data collection

Bruker Photon CMOS diffractometer	11190 independent reflections
Radiation source: IMS microsource	9950 reflections with $I > 2\sigma(I)$
Helios optic monochromator	R_{int} = 0.046
Detector resolution: 16 pixels mm^{-1}	θ_{max} = 25.7°, θ_{min} = 2.2°
phi– and ω–rotation scans	h = –24 24
Absorption correction: multi-scan *SADABS* 2014/5	k = –17 17
T_{min} = 0.669, T_{max} = 0.745	l = –27 27
87418 measured reflections	

Refinement

Refinement on F^2	Secondary atom site location: difference Fourier map
Least-squares matrix: full	Hydrogen site location: mixed
$R[F^2 > 2\sigma(F^2)]$ = 0.036	H atoms treated by a mixture of independent and constrained refinement
$wR(F^2)$ = 0.086	W = 1/[$\Sigma^2(FO^2)$ + (0.0054P)^2 + 7.486P] WHERE P = (FO^2 + 2FC^2)/3
S = 1.10	$(\Delta/\sigma)_{max}$ = 0.001
11190 reflections	$\Delta\rho_{max}$ = 0.45 e Å^{-3}
543 parameters	$\Delta\rho_{min}$ = –0.44 e Å^{-3}
0 restraints	Extinction correction: none
- constraints	Extinction coefficient: -
Primary atom site location: intrinsic phasing	

3. Computational Calculations

We performed ab initio calculations at CCSD(T)/cc-pVTZ and CASPT2(6,6)/cc-pVTZ level[S19] for the H_2 activation process of parent disilene to find a fairly accurate Density Functional Theory-based method for the production calculations for compound **2**. We found that B3LYP functional[S20-22] with Def2-TZVP basis set[S23] yielded satisfactory results in agreement with previous calculations[S24-26]. Therefore all reported calculations regarding parent disilene (Si_2H_4) were carried out at B3LYP/def2-TZVP level of theory. For computational reasons, all geometry optimization calculations related to compound **2** were carried out using def2-SVP basis set for all atoms except the disilene Si=Si moiety with the connected four atoms and the reacting H_2 molecule for which def2-TZVP basis set was employed for higher accuracy. This methodology resulted in very similar metric parameters to the crystallographic results. For example the calculated Si=Si bond length was 2.309 Å which is in very good agreement with the experimental 2.3124(7) Å. To obtain more reliable energies related to compound **2**, using the optimized geometries single point calculations were carried out with larger def2-TZVPP basis set applied on all atoms with B3LYP density functional. It was shown that dispersion interaction could be important even for small reactants[S27] thus we used Grimme's DFT-D3 empirical dispersion correction scheme without damping function in all calculation[S28]. At the end of all geometry optimization, harmonic vibrational frequency calculation was employed to verify the nature of the obtained optimum; zero imaginary frequency implied local minimum while one imaginary frequency referred to transition state. For all three transition states, Intrinsic Reaction Coordinate (IRC) calculations and subsequent optimizations were executed to confirm the corresponding minima. IRC calculations revealed for *syn*- and *anti*-addition a direct one-step reaction where the transition state connected the initial disilene (**2**) with the *cis*- and *trans*-product, respectively. For the stepwise mechanism, IRC calculation verified that the proton can freely migrate and standard optimization proved that it can migrate to *cis*- and *trans*-product as well.

For TD-DFT calculations we used the previously optimized geometries and the same B3LYP functional and basis set that we used for the optimization to calculate the optical transitions. Free energy corrections were calculated at 298 K and 1 atm using the method we applied for optimization.

Natural Resonance Theory (NRT) analysis was carried out using the previously optimized geometry of **2**, but owing to computational reasons we removed the bulky *tert*-butyl and silyl ligand and replaced them with hydrogen. Hydrogen positions were determined to follow the direction of the bond between the remaining central moiety and the bulky ligands while the distance was set to 1.1 and 1.55 Å in case of N-H and Si-H bonds, respectively. NRT analysis of this model compound could not yield any covalent

resonance structures. However, NRT could determine the resonance structures of the silylene moiety (half of the model compound), thus we concluded that the bonding between the formal Si=Si could be the problem. Explicit inclusion of logical resonance structures did not yield covalent reference structures for the model structure as well. To reconcile these results and the formally double bond character we think two very weak donor-acceptor bonds can be formed between both silylene moieties. This also in agreement with the very small dissociation free energy of **2** and previous theoretical results related to tetraaminodisilenes[S29].

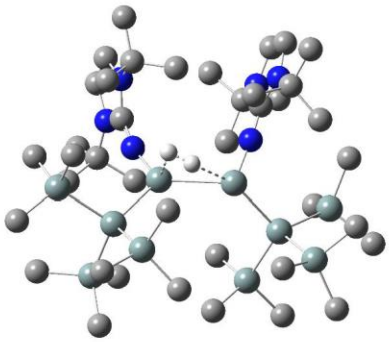

Figure S18. *Syn*-addition transition state of compound **2**. Hydrogens except the reacting H_2 molecule are omitted for clarity. White, blue, tan, and gray colors refer to H, N, Si, and C atoms, respectively.

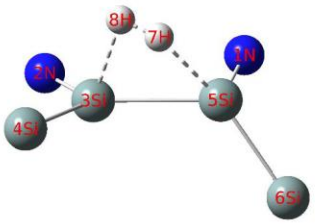

Figure S19. The reaction center during the *syn*-addition transition state of compound **2**. White, blue, and tan colors refer to H, N, and Si atoms, respectively. Selected bond lengths (Å), and angles (deg): 3Si-5Si 2.640, 3Si-8H 2.014, 5Si-7H 2.024, 8H-7H 0.899, 5Si-3Si-8H 70.96, 3Si-5Si-7H 54.83, 3Si-8H-7H 90.73, 5Si-7H-8H 136.78.

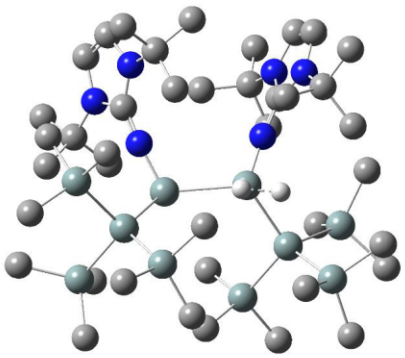

Figure S20. *Stepwise*-addition transition state of compound **2**. Hydrogens except the reacting H_2 molecule are omitted for clarity. White, blue, tan, and gray colors refer to H, N, Si, and C atoms, respectively.

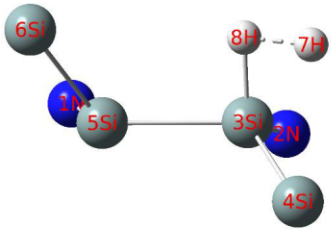

Figure S21. The reaction center during the *stepwise*-addition transition state of compound **2**. White, blue, and tan colors refer to H, N, and Si atoms, respectively. Selected bond lengths (Å), and angles (deg): 3Si-5Si 2.541, 3Si-8H 1.547, 3Si-7H 1.892, 8H-7H 1.202, 5Si-3Si-8H 89.59, 3Si-8H-7H 86.02, 3Si-7H-8H 54.66.

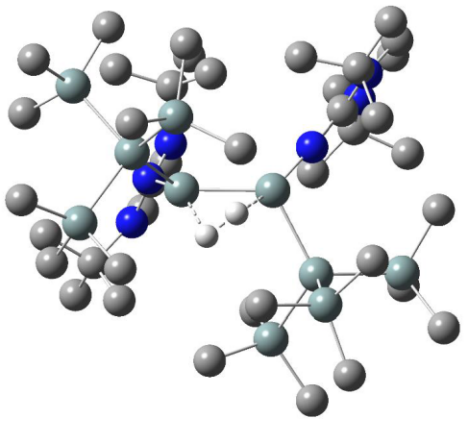

Figure S22. *Anti*-addition transition state of compound **2**. Hydrogens except the reacting H_2 molecule are omitted for clarity. White, blue, tan, and gray colors refer to H, N, Si, and C atoms, respectively.

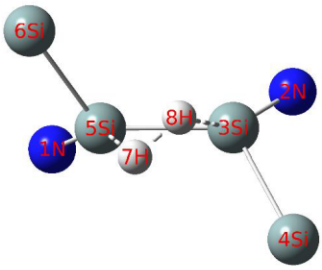

Figure S23. The reaction center during the *anti*-addition transition state of compound **2**. White, blue, and tan colors refer to H, N, and Si atoms, respectively. Selected bond lengths (Å), and angles (deg): 3Si-5Si 2.332, 3Si-8H 1.864, 5Si-7H 1.872, 8H-7H 1.046, 5Si-3Si-8H 65.14, 3Si-5Si-7H 66.24, 3Si-8H-7H 102.67, 5Si-7H-8H 99.68.

To further analyze the staggering effect of ligands on the Si=Si double bond we carried out a series of constrained optimizations, where we fixed one H-Si=Si-H dihedral angle (Figure S24). The fully optimized structure has H-Si=Si-H dihedral angle of 34.9° which is defined as zero energy level (green cross). As we increased the dihedral angle, the energy increased monotonically. We also calculated the logically analog Si-Si=Si-Si dihedral angle of **2** (82.0°), in good agreement with the experimental 78.1°. 82.0° is labelled with a red cross in Figure S24, corresponding to 4.1 kcal/mol on the figure. We also measured the same dihedral angle in the *anti*-addition transition state which gave 117.8° (yellow cross in Figure S24 at 12.6 kcal/mol). Based on these calculations, we can conclude that the ligand induced rotation of the Si=Si double bond considerably promotes *anti*-addition. In case of the parent disilene, this preorganization can cover ~1/3 of the energy investment which is needed to rotate the Si=Si bond to the

anti-addition transition state. It is also important to note that this is in contrast to the *syn*-addition, where planarization is restricted by the bulky ligands for **2** (see manuscript).

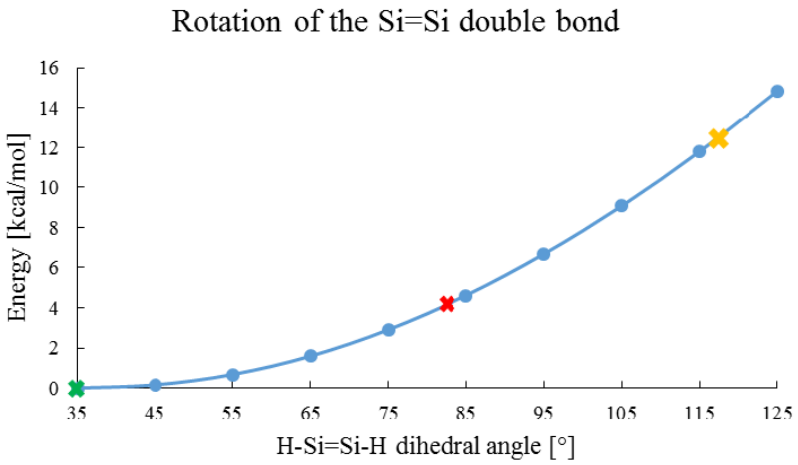

Figure S24. Rotation of the Si=Si double bond in parent disilene (Si_2H_4) in the function of a H-Si=Si-H dihedral angle. Blue dots are calculated using constrained optimization. Fully optimized structure lays at 34.9° (green cross) with 0.0 kcal/mol. In **2**, the logically analog Si-Si=Si-Si has 82.0° (red cross at 4.1 kcal/mol) while in the *trans*-addition transition state Si-Si=Si-Si has 117.8° (yellow cross at 12.6 kcal/mol).

We were also interested in the HOMO and LUMO orbitals of the parent disilene with different H-Si=Si-H dihedral angles. Figure S25-27 show the HOMO and LUMO orbitals of the parent disilene at fully relaxed (34.9°), at 82.0° (corresponds to the relaxed value of **2**) and at 117.8° (corresponds to the *trans*-addition transition state value of **2**), respectively. In the fully relaxed structure, HOMO and LUMO orbitals correspond to usual π-π* orbitals with some asymmetry in the atomic contributions of each sign of the orbitals, which is the consequence of the bent structure. At 82.0° the asymmetry is increased compared to the fully relaxed structure, which is not surprising because the structure is now more bent. However, LUMO shows some characteristic difference compared to the fully relaxed structure. There is a new, extended lobe in the middle of the Si-Si bond which is not present in the fully relaxed case. This is the result of the mixing of the σ and π Si-orbitals in the LUMO. This is important because in the *anti*-addition this new feature of the LUMO can interact with the σ-orbital of the H_2 molecule and thus this is responsible for the activation process. At 117.8° there is no qualitatively new feature in the orbitals compared to the previous 82.0° state, therefore we can conclude that the staggering effect of the bulky ligands already effectively changed the orbital shapes to be favorable for *anti*-addition.

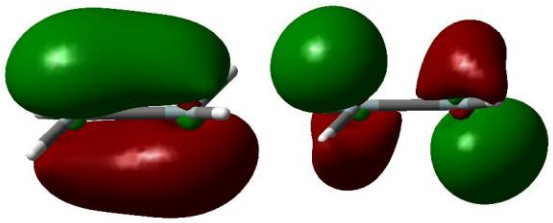

Figure S25. DFT calculated HOMO (-5.94 eV) and LUMO (-2.30 eV) of parent disilene Si_2H_4 in its fully relaxed structure.

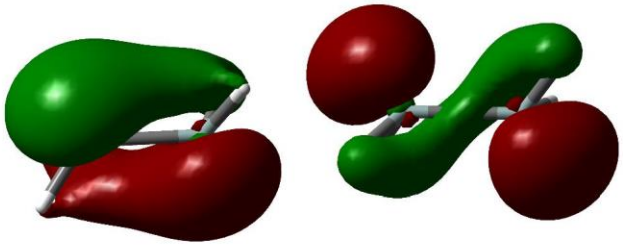

Figure S26. DFT calculated HOMO (-6.23 eV) and LUMO (-3.01 eV) of parent disilene Si_2H_4 with constrained H-Si=Si-H dihedral angle at 82.0°.

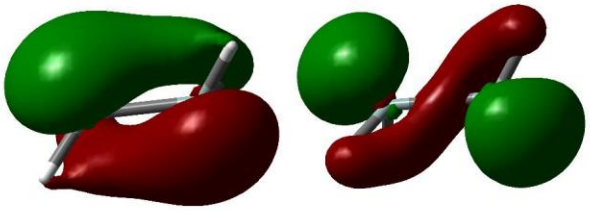

Figure S27. DFT calculated HOMO (-6.29 eV) and LUMO (-3.33 eV) of parent disilene Si_2H_4 with constrained H-Si=Si-H dihedral angle at 117.8°.

S28

The explicit cartesian coordinates (S29-S53) of all calculated structures were removed due to space-saving issues, but the data is available free of charge at the ACS publications homepage.

4. References

(S1) Tamm, M.; Beer, S.; Herdtweck, E., *Z. Naturforsch., B: Chem. Sci.* **2004**, *59*, 1497-1504.
(S2) Marschner, C., *Eur. J. Inorg. Chem.* **1998**, 221-226.
(S3) Lui, M. W.; Merten, C.; Ferguson, M. J.; McDonald, R.; Xu, Y.; Rivard, E., *Inorg. Chem.* **2015**, *54*, 2040-2049.
(S4) Protchenko, A. V.; Schwarz, A. D.; Blake, M. P.; Jones, C.; Kaltsoyannis, N.; Mountford, P.; Aldridge, S., *Angew. Chem. Int. Ed.* **2013**, *52*, 568-71.
(S5) Sekiguchi, A.; Inoue, S.; Ichinohe, M.; Arai, Y., *J. Am. Chem. Soc.* **2004**, *126*, 9626-9629.
(S6) Kosai, T.; Ishida, S.; Iwamoto, T., *Angew. Chem.* **2016**, *128*, 15783-15787.
(S7) Suzuki, K.; Matsuo, T.; Hashizume, D.; Tamao, K., *J. Am. Chem. Soc.* **2011**, *133*, 19710-19713.
(S8) *APEX suite of crystallographic software*, APEX 2 Version 2014-9.0; Bruker AXS Inc.: Madison, Wisconsin, USA, **2014**.
(S9) *APEX suite of crystallographic software*, APEX 3 Version 2015-5.2; Bruker AXS Inc.: Madison, Wisconsin, USA, **2015**.
(S10) Sheldrick, G. M., *CELL_NOW*, University of Göttingen, Germany, **2008**.
(S11) Sheldrick, G. M., *TWINABS*, University of Göttingen, Germany, **2002**.
(S12) *SAINT*, Version 8.34A and *SADABS*, Version 2014/5; Bruker AXS Inc.: Madison, Wisconsin, USA, **2014**.
(S13) Sheldrick, G. M., *Acta Crystallogr., Sect. A* **2015**, *71*, 3–8.
(S14) Sheldrick G. M., *Acta Crystallogr., Sect. C* **2015**, *71*, 3–8.
(S15) Huebschle, C. B.; Sheldrick, G. M.; Dittrich, B., *J. Appl. Cryst.* **2011**, *44*, 1281–1284.
(S16) Wilson, A. J. C. (Ed.) *International Tables for Crystallography, Vol. C*, Tables 6.1.1.4 (pp. 500-502), 4.2.6.8 (pp. 219-222), and 4.2.4.2 (pp. 193-199); Kluwer Academic Publishers: Dordrecht, The Netherlands, **1992**.
(S17) Macrae, C. F.; Edgington, P. R.; McCabe, P., Pidcock E.; Shields, G. P.; Taylor, R.; Towler, M.; van de Streek, J., *J. Appl. Cryst.* **2006**, *39*, 453–457.
(S18) Spek, A. L., *Acta Crystallogr., Sect. D* **2009**, *65*, 148-155.
(S19) Dunning, T. H., *J. Chem. Phys.* **1989**, *90*, 1007-1023.
(S20) Becke, A. D., *J. Chem. Phys.* **1993,** *98*, 5648-5652.
(S21) Vosko, S. H.; Wilk, L.; Nusair, M., *Can. J. Phys.* **1980**, *58*, 1200-1211.
(S22) Lee, C.; Yang, W.; Parr, R. G., *Phys. Rev. B* **1988**, *37*, 785-789.
(S23) Weigend, F.; Ahlrichs, R., *Phys. Chem. Chem. Phys.* **2005**, *7*, 3297-3305.
(S24) Sakai, S., *The Journal of Physical Chemistry A* **1997**, *101*, 1140-1146.
(S25) Nyíri, K.; Szilvási, T.; Veszprémi, T., *Dalton Trans.* **2010**, *39*, 9347–9352.
(S26) Szilvási, T.; Nyíri, K.; Veszprémi, T., *Organometallics* **2011**, *30*, 5344–5351.
(S27) Szilvási, T.; Veszprémi, T., *Dalton Trans.* **2011**, 40, 7193–7200.
(S28) Grimme, S.; Antony, J.; Ehrlich, S.; Krieg, H., *J. Chem. Phys.* **2010**, *132*, 154104.
(S29) Takahashi, M.; Tsutsui, S.; Sakamoto, K.; Kira, M.; Müller, T.; Apeloig, Y., *J. Am. Chem. Soc.* **2001**, *123*, 347-348.

14.3 Supporting Information Chapter 8

From Si(II) to Si(IV) and Back – Reversible Intramolecular Carbon–Carbon Bond Activation by an Acyclic Iminosilylene

Daniel Wendel,[†] Amelie Porzelt,[‖] Fabian A. D. Herz,[†] Debotra Sarkar,[‖] Christian Jandl,[‡] Shigeyoshi Inoue[*,‖] and Bernhard Rieger[*,†]

[†]WACKER-Chair of Macromolecular Chemistry, [‖]WACKER-Institute of Silicon Chemistry, [‡]Catalysis Research Center, Technische Universität München, Lichtenbergstraße 4, 85748 Garching bei München, Germany.

*s.inoue@tum.de; rieger@tum.de

Supporting Information

Total: S40 pages

1. Experimental Procedures

A) General Methods and Instrumentation

All manipulations were carried out under argon atmosphere using standard Schlenk or glovebox techniques. Glassware was heat-dried under vacuum prior to use. Unless otherwise stated, all chemicals were purchased from Sigma-Aldrich or ABCR and used as received. *n*-Hexane and toluene were refluxed over sodium/benzophenone, distilled and deoxygenated prior to use. Deuterated benzene (C_6D_6) and toluene (C_7D_8) were obtained from Deutero Deutschland GmbH and were dried over 3 Å molecular sieves. All NMR samples were prepared under argon in J. Young PTFE tubes. $IPrNSiBr_3$ and $KSiTMS_3$ were synthesized according to procedures described in literature.[S1-2] Carbon dioxide (5.0), hydrogen (5.0) and ethylene (3.5) were purchased from Westfalen AG and used as received. NMR spectra were recorded on Bruker AV-500C, AV-500 or DRX-400 spectrometers at ambient temperature (300 K), unless otherwise stated. ^{1}H, ^{13}C and ^{29}Si NMR spectroscopic chemical shifts δ are reported in ppm relative to tetramethylsilane. $\delta(^{1}H)$ and $\delta(^{13}C)$ were referenced internally to the relevant residual solvent resonances. $\delta(^{29}Si)$ was referenced to the signal of tetramethylsilane (TMS) ($\delta = 0$ ppm) as external standard. Elemental analyses (EA) were conducted with a EURO EA (HEKA tech) instrument equipped with a CHNS combustion analyzer. Mass spectra (MS-CI) were recorded on a double focusing Finnigan MAT 90 mass spectrometer (isobutene, 150 eV). Variable Temperature (VT) UV-Vis spectra were taken on an Agilent Cary 60 spectrophotometer connected to a UnispeKs CoolSpeK cryostat (Unisoku Scientific Instruments Co.). ATR-FTIR spectra were recorded on a Perkin Elmer FTIR spectrometer (diamond ATR, Spectrum Two; located inside an argon-filled glovebox) in a range of 400 – 4000 cm^{-1}. Melting Points (T_m) were determined in sealed glass capillaries under inert gas by a Büchi M-565.

B) Synthesis and Characterization of New Compounds

Spectroscopic Evidence of IPrNSi(II)SiTMS$_3$ (1)

Low-temperature NMR experiment:

A J. Young PTFE tube was filled with IPrNSiBr$_3$ (26.1 mg, 38.9 µmol, 1.00 eq) and KSiTMS$_3$ (22.3 mg, 77.8 µmol, 2.00 eq), precooled to -78 °C, and C_7D_8 (0.5 mL) was condensed into the tube. The suspension was mixed rapidly until a light green color (Figure S1) was observed. A ^{29}Si NMR spectrum was immediately measured at -78 °C. Minor temperature changes directly led to a yellow solution and formation of silepin **2**. For comparison, a separate ^{29}Si NMR spectrum of the final silepin **2** and TMS$_3$SiBr mixture (prepared at room temperature) was recorded at the same temperature (Figure S2).

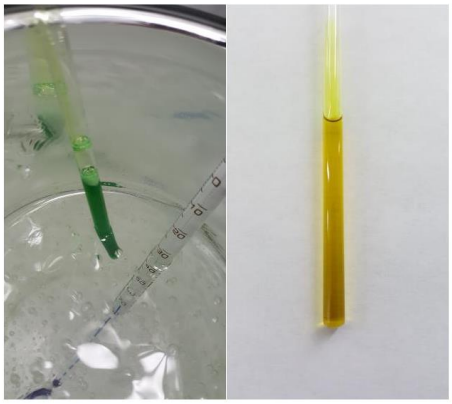

Figure S1. (Left) *In situ* detection of iminosilylene **1**. (Right) Solution after insertion into the C=C bond to form silepin **2**.

Iminosilylsilylene (1)

^{29}Si NMR (80 MHz, C_7D_8, -78 °C): δ = 300.0 ppm (*central Si*), -4.3 ppm (Si*TMS*$_3$), not observed due to low concentration (*Si*TMS$_3$).

Silepin (2)

^{29}Si NMR (80 MHz, C_7D_8, -78 °C): δ = 16.3 ppm (*central Si*), -9.5 ppm (Si*TMS*$_3$), -138.2 (*Si*TMS$_3$).

TMS_3SiBr

^{29}Si NMR (80 MHz, C_7D_8, -78 °C): δ = -12.2 ppm (Si*TMS*$_3$), -24.5 (*Si*TMS$_3$).[S3]

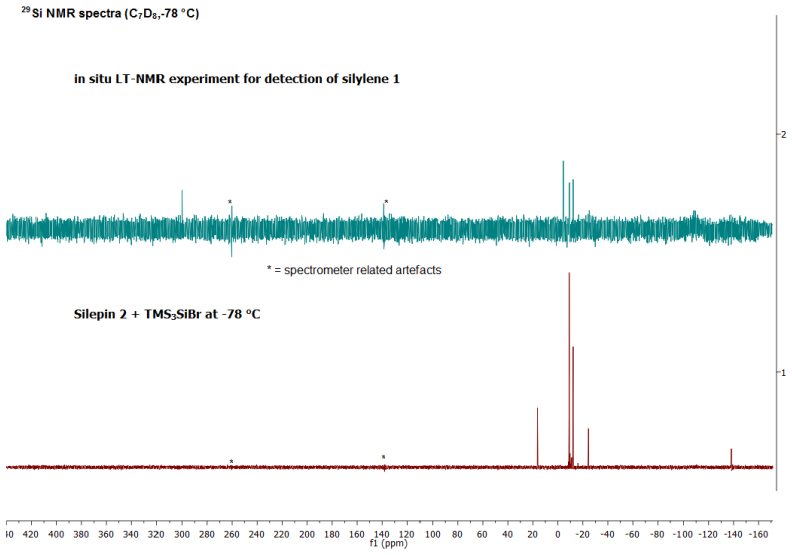

Figure S2: ^{29}Si NMR spectra (C_7D_8, -78 °C) (Top) *In situ* detection of iminosilylene **1** (Bottom) Silepin **2** and TMS_3SiBr at -78 °C.

Variable Temperature (VT) UV-Vis Measurement:

We performed Variable Temperature (VT) UV-Vis spectroscopy from -70 °C to +20 °C with a highly concentrated reaction solution to observe the characteristic n→3p transition of *in situ* generated iminosilylene **1**. A 1 cm Schlenk square quartz cell was filled with IPrNSiBr$_3$ (13.0 mg, 19.4 µmol, 1.00 eq) and KSiTMS$_3$ (11.1 mg, 38.8 µmol, 2.00 eq), precooled to -78 °C, and toluene (4.0 mL) was slowly condensed into the cuvette. The suspension was mixed directly before placing it into the UV-Vis spectrometer at -70°C. The temperature was increased at intervals of approximately 10 min (total 60 min). A small band for the characteristic n→3p transition of **1** was observed at 612 nm (-70 °C) (calculated value 609 nm, c.f. Table S1), decreasing rapidly upon warming up the solution to room temperature (Figure S3).

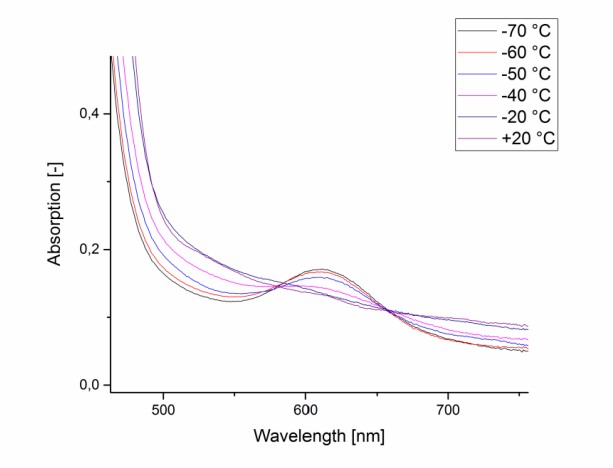

Figure S3. UV-Vis spectrum of *in situ* generated iminosilylene **1** at low temperatures λ_{max} (toluene, -70 °C) = 612 nm (n→3p).

To verify a potential equilibrium between **1** and **2** at elevated temperatures, two separate experiments with varied concentrations of silepin **2**/TMS$_3$SiBr mixtures were carried out. First, the focus was set on the detection of **1** with a highly concentrated solution of **2**. Here a 1 cm Schlenk square quartz cell was filled with IPrNSiBr$_3$ (23.1 mg, 34.5 µmol, 1.00 eq) and KSiTMS$_3$ (19.8 mg, 69.0 µmol, 2.00 eq) and toluene (4.0 mL) was added (9.4×10^{-3} M). The intensive yellow solution was heated from +25 °C to 100 °C. At higher temperatures the same small, but characteristic, band of **1** (at 617 nm at 100 °C) was observed, clearly indicating partial formation of iminosilylene **1** (Figure S4). Lowering the temperature again shifted the equilibrium back to silepin **2**.

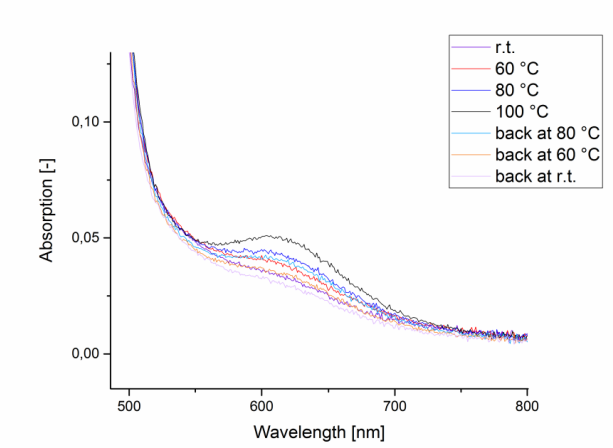

Figure S4. UV-Vis spectrum of a highly concentrated silepin **2**/TMS_3SiBr mixture (9.4×10^{-3} M; focus on silylene formation) at different temperatures λ_{max} (toluene, 100 °C) = 617 nm (n→3p).

Separately, in a second experiment, the decrease of **2** as function of temperature was monitored with a less concentrated silepin **2**/TMS_3SiBr mixture (2.9×10^{-4} M). Here, the reversible reduction of the characteristic silepin signal at 399 nm (calculated value 432 nm, c.f. Table S2) further supports the existence of an equilibrium between **1** and **2** at elevated temperatures (Figure S5).

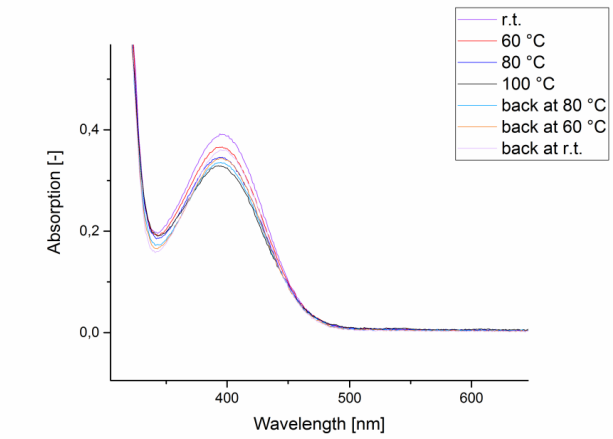

Figure S5. UV-Vis spectrum of a low concentrated silepin **2**/TMS_3SiBr mixture (2.9×10^{-4} M; focus on decrease of silepin) at different temperatures λ_{max} (toluene, r.t.) = 399 nm.

Synthesis of Silepin (2)

A solution of $KSiTMS_3$ (1.28 g, 4.46 mmol, 2.00 eq) in toluene (20 mL) was added to $IPrNSiBr_3$ (1.49 g, 2.23 mmol, 1.00 eq) in toluene (20 mL) at room temperature. The color rapidly changed to light green (approx. 1 sec) and then immediately to yellow with formation of a white precipitate. After stirring the solution for 20 min, the solvent was removed *in vacuo*. The obtained residue was extracted with *n*-hexane (3 × 10 mL) and filtered through a microfiber glass filter. The solution was concentrated and cooled to -35 °C for 3 months to yield pure silepin **2** (91 mg, 0.13 mmol, 6%) as yellow crystals suitable for single crystal X-ray analysis. For reactivity studies, **2**/TMS_3SiBr mixtures were prepared in analogous fashion, since separation of both compounds by crystallization or sublimation was low yielding. Compound **2** is stable at room temperature for months both as a solid and in solution (*n*-hexane or toluene) even in the presence of TMS_3SiBr.

^{1}H NMR (500 MHz, C_6D_6, r.t.): δ = 7.20 (m, 2H, *m*-C*H*-Ar), 7.10 (dd, *J* = 7.4, 1.8 Hz, 1H, *p*-C*H*-Ar), 6.67 (d, *J* = 3.0 Hz, 1H, C*H*-N), 6.59 (d, *J* = 12.8 Hz, 1H, C*H*-Ar), 6.44 (dd, *J* = 6.3, 1.1 Hz, 1H, C*H*-Ar), 6.37 (dd, *J* = 12.8, 6.3 Hz, 1H, C*H*-Ar), 5.88 (d, *J* = 3.0 Hz, 1H, C*H*-N), 3.30 (hept, *J* = 6.8 Hz, 1H, C*H*), 3.15 – 3.08 (m, 2H, C*H*), 3.01 (hept, *J* = 6.8 Hz, 1H, C*H*), 1.42 (d, *J* = 6.8 Hz, 3H, CH_3), 1.34 (d, *J* = 6.8 Hz, 3H, CH_3), 1.33 (d, *J* = 6.8 Hz, 3H, CH_3), 1.23 (d, *J* = 6.8 Hz, 6H, CH_3), 1.20 (d, *J* = 6.8 Hz, 3H, CH_3), 1.08 (d, *J* = 6.8 Hz, 3H, CH_3), 0.93 (d, *J* = 6.8 Hz, 6H, CH_3), 0.32 (s, 27H, Si*TMS*$_3$).

^{13}C NMR (126 MHz, C_6D_6, r.t.): δ = 156.6 (*C*-Ar), 148.1 (*C*-Ar), 147.1 (*C*-Ar), 146.9 (N-*C*-N), 133.7 (*C*-Ar), 131.8 (*C*-Ar), 130.6 (*C*H-Ar), 129.5 (*C*H-Ar), 128.8 (*C*H-Ar), 128.5 (*C*H-Ar), 124.3 (*C*H-Ar), 123.9 (*C*H-Ar), 117.6 (*C*H-N), 109.8 (*C*H-N), 33.0 (*C*H), 29.3 (*C*H), 28.8 (*C*H), 28.6 (*C*H), 26.0 (*C*H_3), 25.2 (*C*H_3), 24.6 (*C*H_3), 23.9 (*C*H_3), 23.8 (*C*H_3), 23.5 (*C*H_3), 22.7 (*C*H_3), 21.4 (*C*H_3), 3.3 (Si*TMS*$_3$).

^{29}Si NMR (99 MHz, C_6D_6, r.t.): δ = 16.1 (*central Si*), -9.6 (*TMS*$_3$), -135.5 (*Si*TMS_3).

MS-CI (150 eV): m/z (%) = 677 $[M]^+$ (100).

EA experimental (calculated): C 63.91 (63.74), H 9.47 (9.36), N 5.81 (6.19) %.

M_p: 99.2 °C (color change from yellow to light green).

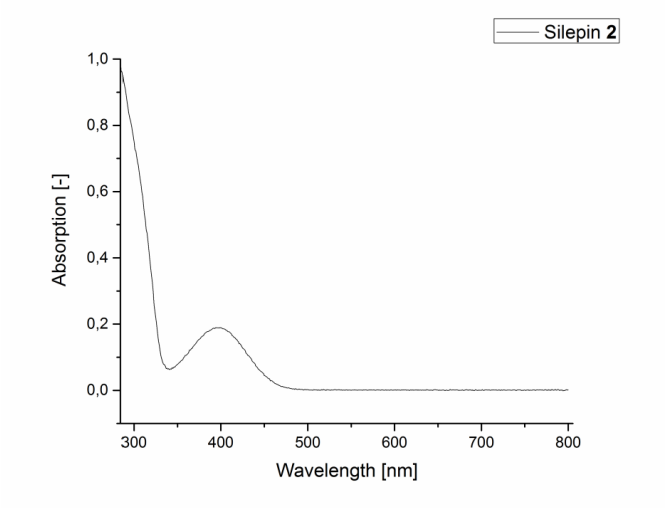

Figure S6. UV-Vis spectrum of silepin **2** λ_{max} (r.t., toluene, 3.0×10^{-4} M) = 305, 399 nm.

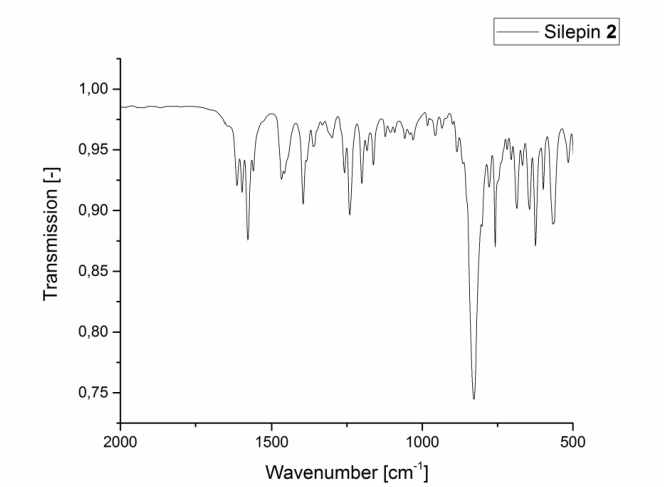

Figure S7: IR spectrum of silepin **2** (cm^{-1}): 1614 (w), 1595 (w), 1577 (m), 1456 (w), 1387 (w), 1240 (m), 1193 (w), 830 (s), 751 (m), 687 (m), 649 (m), 628 (m), 557 (w).

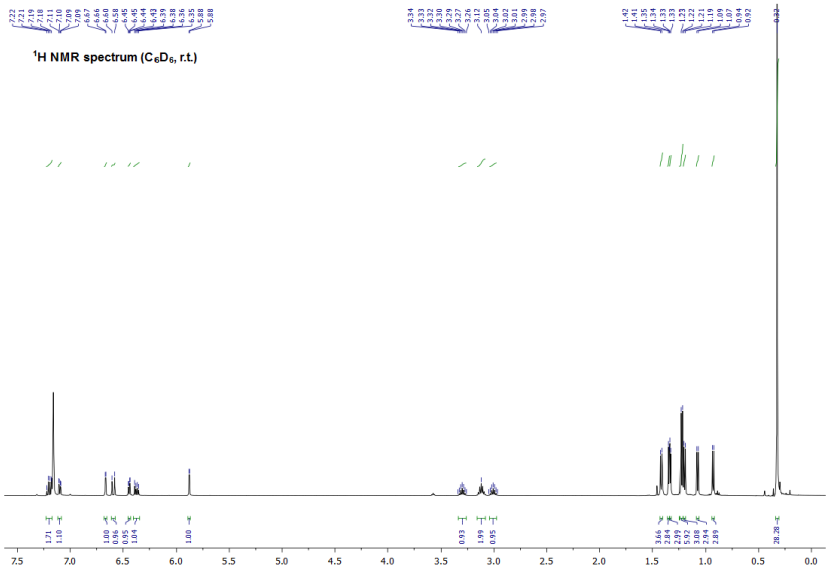

Figure S8: ^{1}H NMR spectrum of silepin **2** (C_6D_6, r.t.).

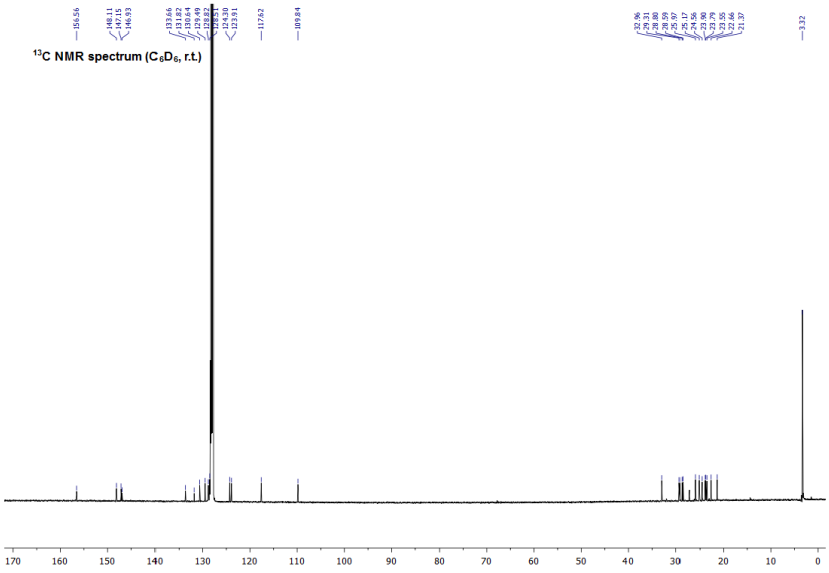

Figure S9: ^{13}C NMR spectrum of silepin **2** (C_6D_6, r.t.).

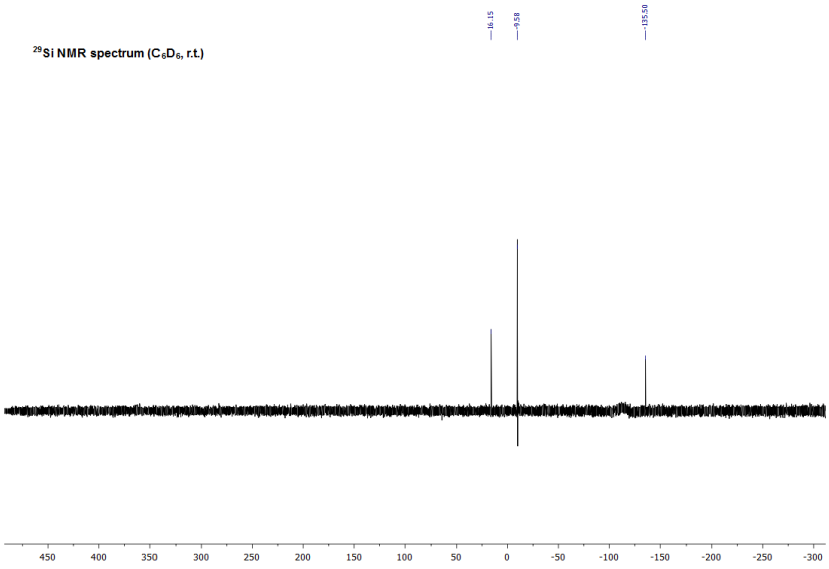

Figure S10: ^{29}Si NMR spectrum of silepin **2** (C_6D_6, r.t.).

Synthesis of IPrNSi(II)SiTMS$_3$-B(C$_6$F$_5$)$_3$ (3)

A solution of KSiTMS$_3$ (112 mg, 0.39 mmol, 2.00 eq) in toluene (3 mL) was added to IPrNSiBr$_3$ (130 mg, 0.19 mmol, 1.00 eq) in toluene (2 mL) at room temperature. The color rapidly changed to light green (approx. 1 sec) and then immediately to yellow with formation of a white precipitate. After stirring the solution for 20 min, the solvent was removed *in vacuo*. The obtained residue was extracted with *n*-hexane (3 × 3 mL) and filtered through a microfiber glass filter. B(C$_6$F$_5$)$_3$ (99.7 mg, 0.19 mmol, 1.00 eq) in hexane (5 mL) was added and the mixture was stirred for 20 min. The yellow solution was concentrated and cooled to -35 °C for 16 h to yield silylene-BCF adduct **3** (103 mg, 0.08 mmol, 45%) as yellow crystals suitable for single crystal X-ray analysis. Compound **3** is stable as a solid, but decomposes in C$_6$D$_6$ at room temperature within a day (unspecific formation of several products).

^{1}H NMR (500 MHz, C$_6$D$_6$, r.t.): δ = 7.21 – 7.17 (m, 2H, *p*-C*H*-Ar), 7.09 (dd, *J* = 7.8, 1.3 Hz, 2H, *m*-C*H*-Ar), 6.85 (dd, *J* = 7.8, 1.3 Hz, 2H, *m*-C*H*-Ar), 6.01 (s, 2H, C*H*-N), 3.03 (hept, *J* = 6.8 Hz, 2H, C*H*), 2.97 (hept, *J* = 6.8 Hz, 2H, C*H*), 1.31 (d, *J* = 6.8 Hz, 6H, C*H*$_3$), 0.91 (d, *J* = 6.8 Hz, 6H, C*H*$_3$), 0.88 (d, *J* = 6.8 Hz, 6H, C*H*$_3$), 0.78 (d, *J* = 6.8 Hz, 6H, C*H*$_3$), 0.03 (s, 27H, Si*TMS*$_3$).

^{13}C NMR (126 MHz, C$_6$D$_6$, r.t.): δ = 150.0 (*C*-F), 149.2 (N-*C*-N), 148.2 (*C*-F), 147.6 (*C*-Ar), 146.2 (*C*-Ar), 141.3 (*C*-F), 139.3 (*C*-F), 138.7 (*C*-F), 136.8 (*C*-F), 133.4 (*C*-Ar), 130.6 (*C*H-Ar), 125.0 (*C*H-Ar), 124.6 (*C*H-Ar), 118.0 (*C*H-N), 28.8 (*C*H), 28.5 (*C*H), 26.5 (*C*H$_3$), 26.2 (*C*H$_3$), 23.3 (*C*H$_3$), 22.3 (*C*H$_3$), 3.6 (Si*TMS*$_3$).

^{29}Si NMR (99 MHz, C$_6$D$_6$, r.t.): δ = 160.7 (q, $^1J_{SiB}$ = 53.9 Hz, *central Si*), -7.7 (*TMS*$_3$), -112.4 (*Si*TMS$_3$).

^{11}B NMR (96 MHz, C$_6$D$_6$, r.t.): δ = -15.1.

^{19}F NMR (471 MHz, C$_6$D$_6$, r.t.): δ = -123.8, -157.9, -162.3.

MS-CI (150 eV): m/z (%) = 801 [M-IPr]$^+$ (100), 787 [M-NIPr]$^+$ (15).

EA experimental (calculated): C 53.05 (54.59), H 5.36 (5.33), N 3.40 (3.53) %.

M$_p$: 149.5 °C (color change from yellow to orange-red).

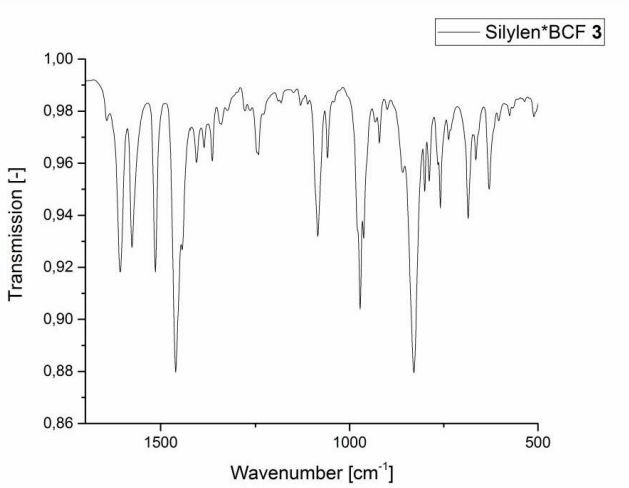

Figure S11: IR spectrum of silylene-BCF adduct **3** (cm^{-1}): 1611 (m), 1575 (w), 1515 (w), 11459 (s), 1402 (w), 1365 (w) 1241 (w), 1086 (w), 1056 (w), 968 (s), 836 (s), 759 (m), 679 (m), 630 (m).

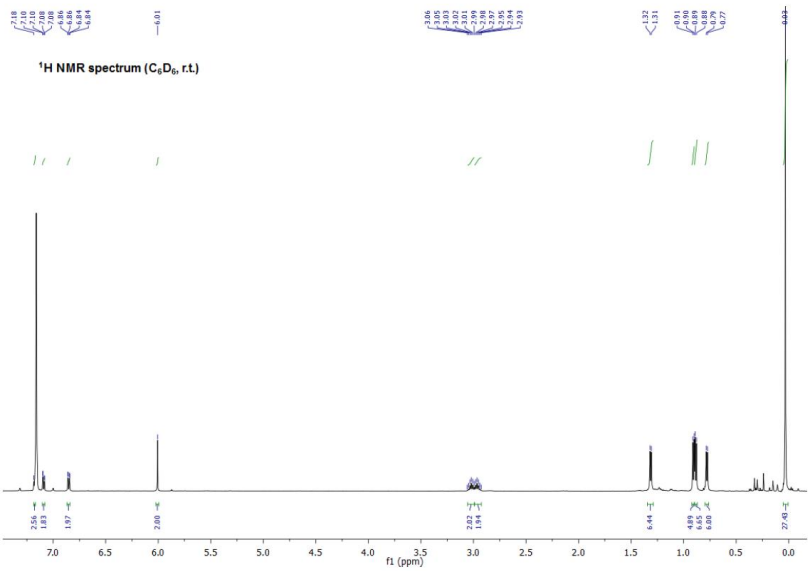

Figure S12: ^1H NMR spectrum of silylene-BCF adduct **3** (C_6D_6, r.t.).

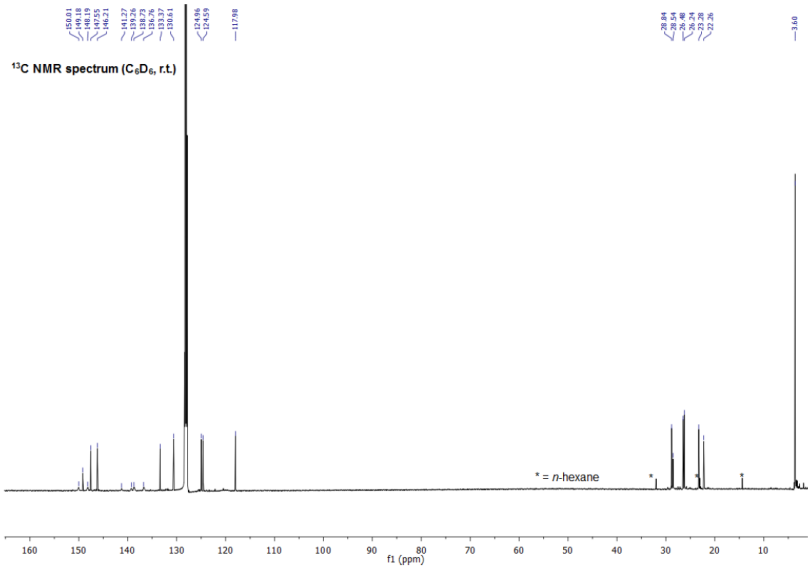

Figure S13: ^{13}C NMR spectrum silylene-BCF adduct **3** (C_6D_6, r.t.).

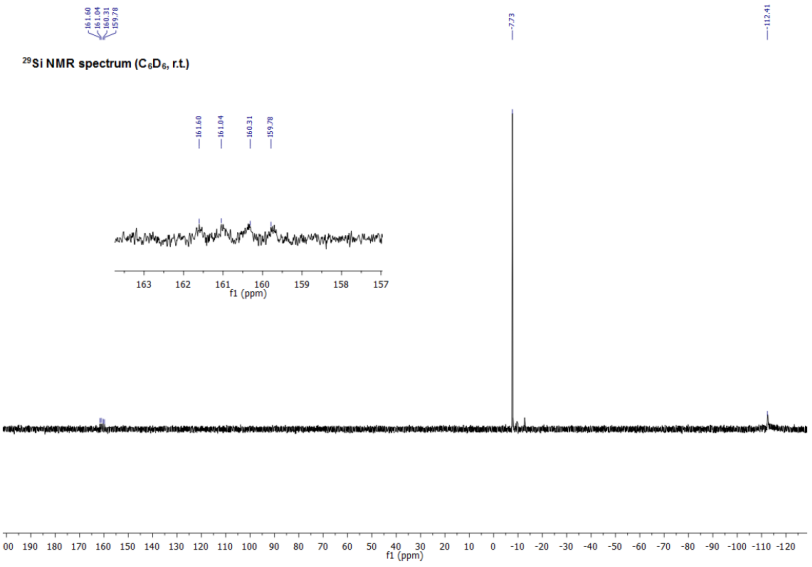

Figure S14: ^{29}Si NMR spectrum of silylene-BCF adduct **3** (C_6D_6, r.t.).

Synthesis of IPrNSi(O_2C=O)SiTMS$_3$ (4)

A solution of KSiTMS$_3$ (228 mg, 0.79 mmol, 2.00 eq) in toluene (3 mL) was added to IPrNSiBr$_3$ (267 mg, 0.39 mmol, 1.00 eq) in toluene (2 mL) at room temperature. The color rapidly changed to light green (approx. 1 sec) and then immediately to yellow with formation of a white precipitate. After stirring the solution for 20 min, the solvent was removed *in vacuo*. The obtained residue was extracted with *n*-hexane (3 × 3 mL) and filtered through a microfiber glass filter into a pressurizable Schlenk flask. The solution was exposed to CO_2 gas (1 bar) and stirred for 1 h. Removal of all volatiles and crystallization in *n*-hexane at -35 °C for 16 h gave carbonato silane **4** (173 mg, 0.23 mmol, 60%) as colorless crystals suitable for single crystal X-ray analysis. Compound **4** is completely stable as a solid and in solution at room temperature.

^{1}H NMR (500 MHz, C_6D_6, r.t.): δ = 7.30 – 7.26 (m, 2H, *p*-C*H*-Ar), 7.19 – 7.16 (m, 4H, *m*-C*H*-Ar), 5.93 (s, 2H, C*H*-N), 2.95 (hept, *J* = 6.9 Hz, 4H, C*H*), 1.47 (d, *J* = 6.9 Hz, 12H, CH_3), 1.08 (d, *J* = 6.9 Hz, 12H, CH_3), 0.18 (s, 27H, Si*TMS*$_3$).

^{13}C NMR (126 MHz, C_6D_6, r.t.): δ = 150.4 (O_2C=O), 146.7 (*C*-Ar), 145.6 (N-*C*-N), 133.2 (*C*-Ar), 130.7 (*C*H-Ar), 124.8 (*C*H-Ar), 116.0 (*C*H-N), 29.2 (*C*H), 25.2 (*C*H$_3$), 23.2 (*C*H$_3$), 2.5 (Si*TMS*$_3$).

^{29}Si NMR (99 MHz, C_6D_6, r.t.): δ = -35.0 (*central Si*), -9.8 (*TMS*$_3$), -134.3 (*Si*TMS$_3$).

MS-CI (150 eV): m/z (%) = 693 [M-CO_2]$^+$ (100), 403 [IPr=N]$^+$ (65).

EA experimental (calculated): C 59.21 (60.19), H 8.58 (8.60), N 5.64 (5.69) %.

M_p: 161.8 °C (gas formation, sticky colorless oil).

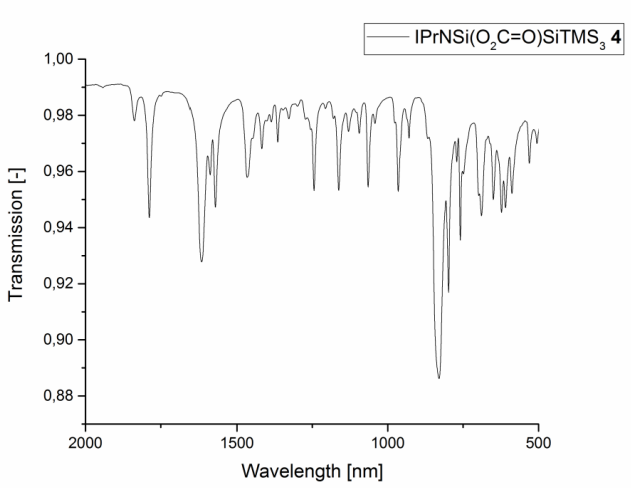

Figure S15: IR spectrum of IPrNSi(O_2C=O)$SiTMS_3$ **4** (cm^{-1}):1838 (w), 1789 (s), 1620 (s), 1569 (m), 1465 (m), 1418 (w), 1359 (w), 1242 (m), 1159 (m), 1061 (m), 963 (m), 934 (w), 826 (s), 793 (s), 755 (m), 687 (m), 649 (m), 618 (m), 591 (m).

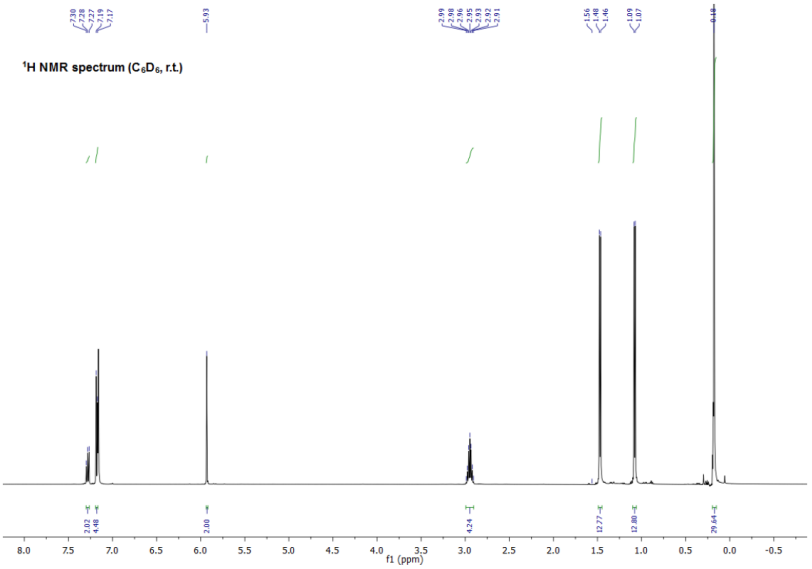

Figure S16: ^{1}H NMR spectrum of IPrNSi(O_2C=O)$SiTMS_3$ **4** (C_6D_6, r.t.).

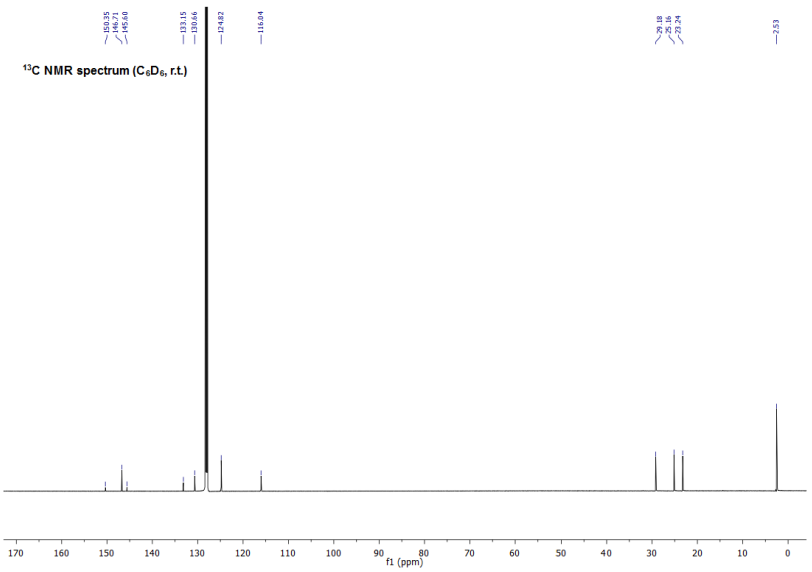

Figure S17: ^{13}C NMR spectrum IPrNSi(O_2C=O)$SiTMS_3$ **4** (C_6D_6, r.t.).

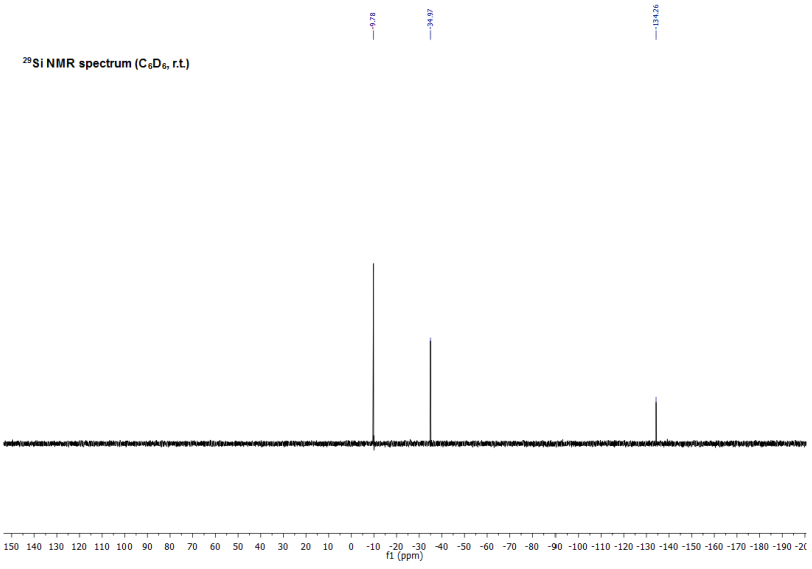

Figure S18: ^{29}Si NMR spectrum of IPrNSi(O_2C=O)$SiTMS_3$ **4** (C_6D_6, r.t.).

NMR Studies on the Reactivity of Silepin 2 towards Ethylene and Hydrogen

A solution of $KSiTMS_3$ (10.7 mg, 37.3 µmol, 2.00 eq) in C_6D_6 (0.4 mL) was added to $IPrNSiBr_3$ (12.6 mg, 18.7 µmol, 1.00 eq) in C_6D_6 (0.3 mL) at room temperature. The color rapidly changed to light green (approx. 1 sec) and then immediately to yellow with formation of a white precipitate. After 5 min, the solution was filtered into a J. Young PTFE tube and exposed to ethylene or hydrogen gas (1 bar). With ethylene, monitoring the reaction at room temperature showed silirane **5** as sole product after 2 h reaction time. For the activation of hydrogen the respective solution was heated to 50 °C for 2 days (reaction at r.t. very slow) to fully convert silepin **2** to silane **6**. Due to their similar solubility, both compounds could not be separated from TMS_3SiBr (^{29}Si NMR δ = -12.7, -23.9 ppm) and further characterized.

IPrNSi(CH_2CH_2)$SiTMS_3$ (5)

^{1}H NMR (500 MHz, C_6D_6, r.t.): δ = 7.24 (dd, J = 8.3, 7.1 Hz, 2H, *p*-C*H*-Ar), 7.16 – 7.14 (m, 4H, *m*-C*H*-Ar), 5.88 (s, 2H, C*H*-N), 3.15 (hept, J = 6.9 Hz, 4H, C*H*), 1.47 (d, J = 6.9 Hz, 12H, CH_3), 1.13 (d, J = 6.9 Hz, 12H, CH_3), 0.24 (s, 27H, Si*TMS*$_3$), 0.00 – -0.04 (m, 4H, CH_2CH_2).

^{13}C NMR (126 MHz, C_6D_6, r.t.): δ = 147.6 (*C*-Ar), 142.2 (N-*C*-N), 135.2 (*C*-Ar), 129.7 (*C*H-Ar), 123.0 (*C*H-Ar), 115.0 (*C*H-N), 28.9 (*C*H), 25.2 (*C*H$_3$), 23.6 (*C*H$_3$), 2.9 (Si*TMS*$_3$), 2.0 (*C*H$_2$*C*H$_2$).

^{29}Si NMR (99 MHz, C_6D_6, r.t.): δ = -100.9 (*central Si*), -10.0 (*TMS*$_3$), -129.9 (*Si*TMS$_3$).

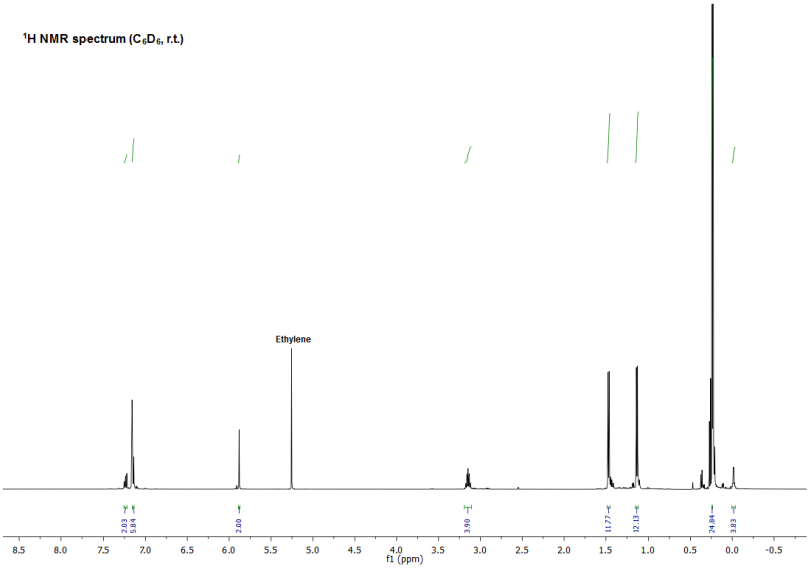

Figure S19: ^{1}H NMR spectrum of silirane **5** (C_6D_6, r.t.).

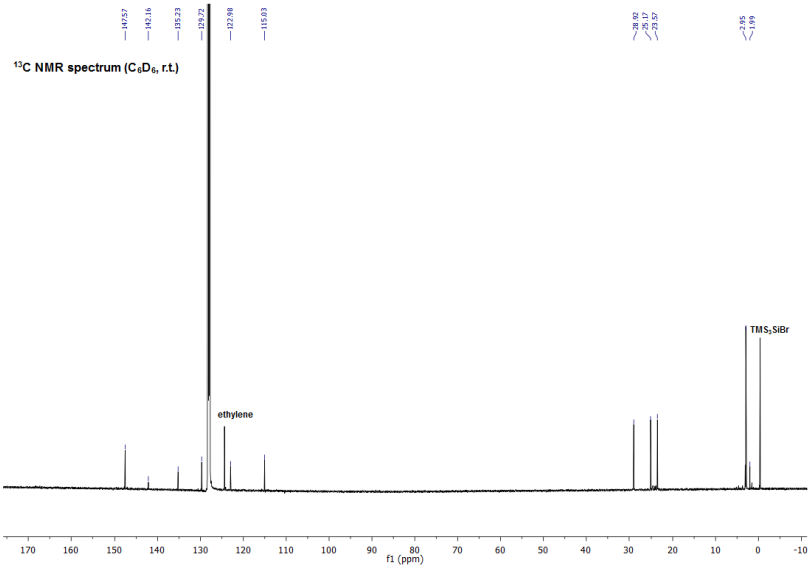

Figure S20: ^{13}C NMR spectrum of silirane **5** (C_6D_6, r.t.).

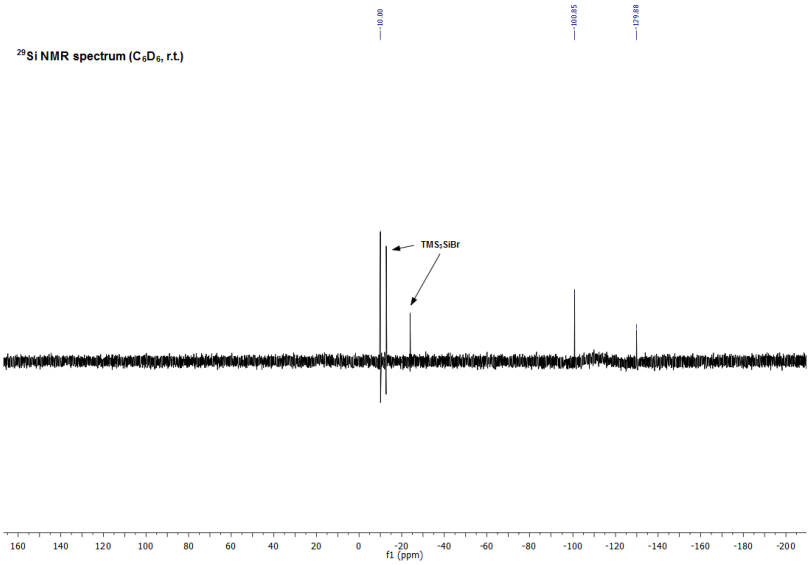

Figure S21: ^{29}Si NMR spectrum of silirane **5** (C_6D_6, r.t.).

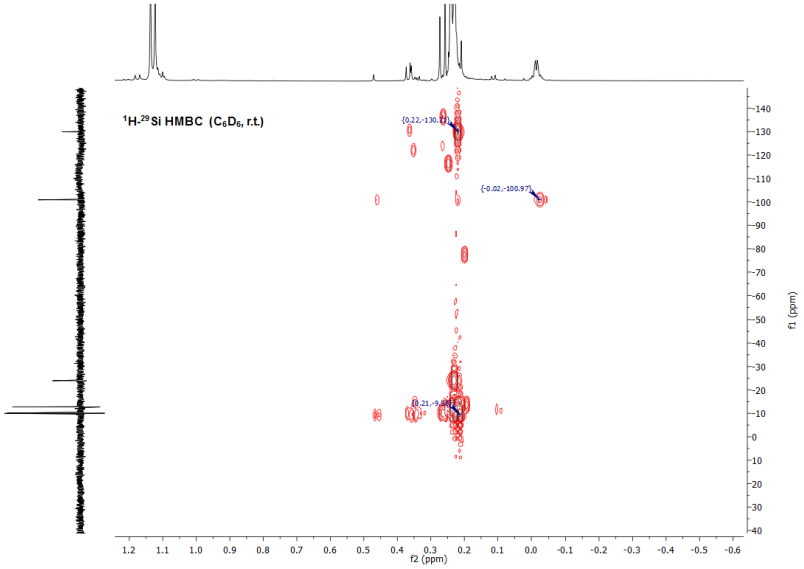

Figure S22: ^{1}H-^{29}Si HMBC of silirane **5** (C_6D_6, r.t.).

IPrNSiH$_2$SiTMS$_3$ (6)

^{1}H NMR (500 MHz, C_6D_6, r.t.): δ = 7.26 – 7.21 (m, 2H, *p*-C*H*-Ar), 7.14 – 7.11 (m, 4H, *m*-C*H*-Ar), 5.90 (s, 2H, C*H*-N), 4.82 (s, 2H, $^1J_{SiH}$ = 189 Hz, Si*H*$_2$), 3.15 (hept, *J* = 6.9 Hz, 4H, C*H*), 1.45 (d, *J* = 6.9 Hz, 12H, C*H*$_3$), 1.18 (d, *J* = 6.9 Hz, 12H, C*H*$_3$), 0.20 (s, 27H, Si*TMS*$_3$).

^{13}C NMR (126 MHz, C_6D_6, r.t.): δ = 148.1 (*C*-Ar), 146.4 (N-*C*-N), 134.7 (*C*-Ar), 129.8 (*C*H-Ar), 124.0 (*C*H-Ar), 114.8 (*C*H-N), 29.1 (*C*H), 24.8 (*C*H$_3$), 23.4 (*C*H$_3$), 2.7 (Si*TMS*$_3$).

^{29}Si NMR (99 MHz, C_6D_6, r.t.): δ = -60.7 (t, $^1J_{SiH}$ = 189 Hz, *central Si*), -9.7 (*TMS*$_3$), -137.1 (*Si*TMS$_3$).

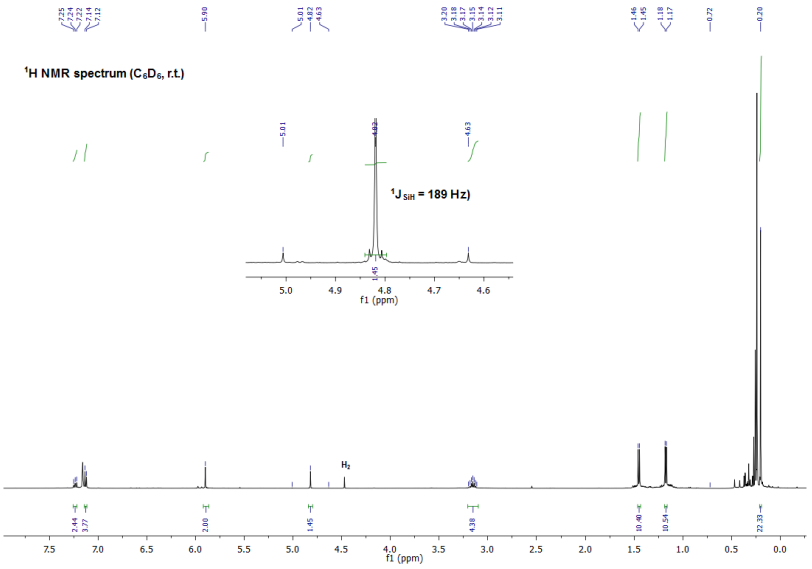

Figure S23: ^{1}H NMR spectrum of IPrNSiH$_2$SiTMS$_3$ **6** (C_6D_6, r.t.).

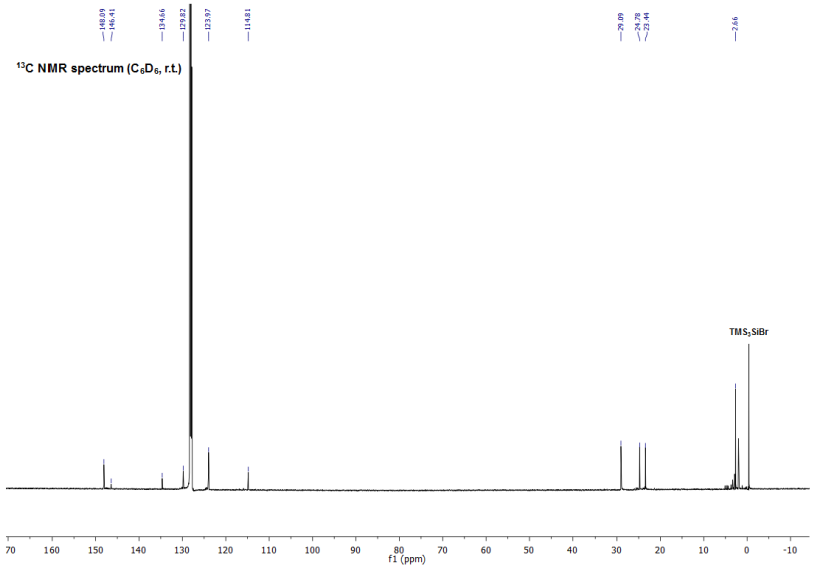

Figure S24: ^{13}C NMR spectrum of IPrNSiH$_2$SiTMS$_3$ **6** (C_6D_6, r.t.).

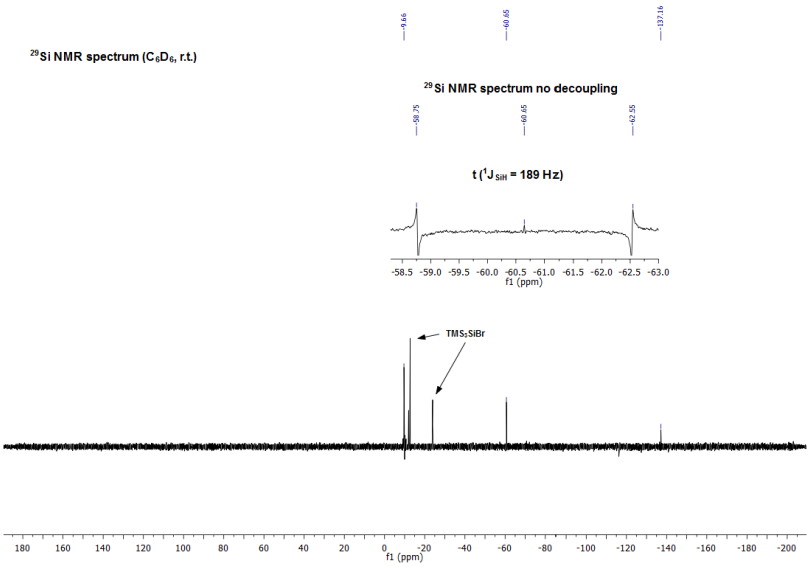

Figure S25: ^{29}Si NMR spectrum of IPrNSiH$_2$SiTMS$_3$ **6** (C_6D_6, r.t.).

2. X-ray Crystallographic Data

General:

Data were collected on a single crystal X-ray diffractometer equipped with a CMOS detector (APEX III, κ-CMOS), an IMS microsource with MoK_α radiation (λ = 0.71073 Å) and a Helios optic using the APEX III software package.[S4] The crystals were fixed on the top of a Kapton micro sampler with perfluorinated ether, transferred to the diffractometer and frozen under a stream of cold nitrogen. A matrix scan was used to determine the initial lattice parameters. Reflections were merged and corrected for Lorentz and polarization effects, scan speed, and background using SAINT.[S5] Absorption corrections, including odd and even ordered spherical harmonics were performed using SADABS.[S5] Space group assignments were based upon systematic absences, *E* statistics, and successful refinement of the structures. Structures were solved using SHELXT with the aid of successive difference Fourier maps, and were refined against all data using SHELXL-2014 in conjunction with SHELXLE.[S6-8] Hydrogen atoms were calculated in ideal positions as follows: methyl hydrogen atoms were refined as part of rigid rotating groups, with a C–H distance of 0.98 Å and $U_{iso(H)} = 1.5 \cdot U_{eq(C)}$. Other H atoms were placed in calculated positions and refined using a riding model with methylene and aromatic C–H distances of 0.99 Å and 0.95 Å, respectively, with other C–H distances of 1.00 Å and $U_{iso(H)} = 1.2 \cdot U_{eq(C)}$. Non-hydrogen atoms were refined with anisotropic displacement parameters. Full-matrix least-squares refinements were carried out by minimizing $\Sigma w(F_o^2 - F_c^2)^2$ with the SHELXL weighting scheme.[S7] Neutral atom scattering factors for all atoms and anomalous dispersion corrections for the non-hydrogen atoms were taken from *International Tables for Crystallography*.[S9] A split layer refinement was used to treat disordered groups and additional SIMU, DELU and SAME restraints were employed to stabilize the refinement of the layers. **2** contains disordered benzene on special positions which was treated as a diffuse contribution to the overall scattering without specific atom positions using the PLATON/SQUEEZE procedure.[S10] Images were created with Mercury (main article) and PLATON (SI).[S11-12]

Compound **2** (CCDC 1547492)

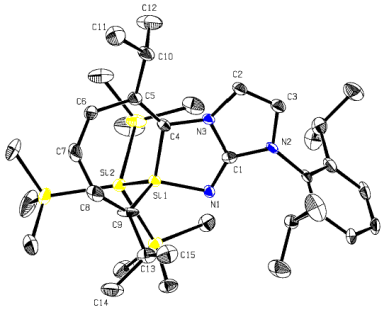

Diffractometer operator C. Jandl
scanspeed 60 s per frame
dx 50 mm
3647 frames measured in 14 data sets
phi-scans with delta_phi = 0.5
omega-scans with delta_omega = 0.5
shutterless mode

Crystal data

$C_{36}H_{63}N_3Si_5$	$F(000)$ = 1480
M_r = 678.34	
Triclinic, *P*	D_x = 1.050 Mg m^{-3}
Hall symbol: -P 1	Melting point: - K
a = 12.015 (17) Å	Mo $K\alpha$ radiation, λ = 0.71073 Å
b = 16.37 (2) Å	Cell parameters from 9466 reflections
c = 22.31 (3) Å	θ = 2.4–26.1°
α = 77.90 (2)°	μ = 0.19 mm^{-1}
β = 88.71 (4)°	T = 100 K
γ = 89.63 (3)°	Fragment, yellow
V = 4290 (10) Å^3	0.22 × 0.15 × 0.12 mm
Z = 4	

Data collection

Bruker Photon CMOS diffractometer	15686 independent reflections
Radiation source: IMS microsource	13200 reflections with i > 2σ(i)
Helios optic monochromator	R_{int} = 0.076
Detector resolution: 16 pixels mm^{-1}	θ_{max} = 25.4°, θ_{min} = 2.2°
phi– and ω–rotation scans	h = –14 14
Absorption correction: multi-scan *SADABS* 2014/5	k = –19 19
T_{min} = 0.681, T_{max} = 0.745	l = –26 26
185048 measured reflections	

Refinement

Refinement on F^2	Secondary atom site location: difference Fourier map
Least-squares matrix: full	Hydrogen site location: inferred from neighbouring sites
$R[F^2 > 2\sigma(F^2)]$ = 0.098	H-atom parameters constrained
$wR(F^2)$ = 0.245	W = 1/[$\Sigma^2(FO^2)$ + (0.0745P)^2 + 27.1114P] WHERE P = (FO^2 + 2FC^2)/3
S = 1.15	$(\Delta/\sigma)_{max}$ < 0.001
15686 reflections	$\Delta\rho_{max}$ = 1.85 e Å^{-3}
858 parameters	$\Delta\rho_{min}$ = –0.47 e Å^{-3}
69 restraints	Extinction correction: none
- constraints	Extinction coefficient: -
Primary atom site location: intrinsic phasing	

Compound **3** (CCDC 1548491)

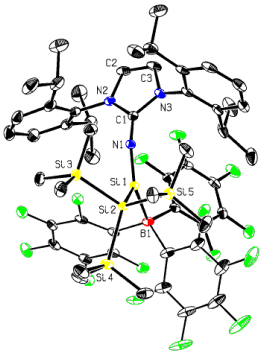

Diffractometer operator C. Jandl
scanspeed 20 s per frame
dx 50 mm
2471 frames measured in 8 data sets
phi-scans with delta_phi = 0.5
omega-scans with delta_omega = 0.5
shutterless mode

Crystal data

$C_{54}H_{63}BF_{15}N_3Si_5 \cdot 0.5(C_6H_{14})$

M_r = 1233.42	D_x = 1.321 Mg m^{-3}
Monoclinic, $P2_1/n$	Melting point: - K
Hall symbol: -P 2yn	Mo $K\alpha$ radiation, λ = 0.71073 Å
a = 12.8285 (6) Å	Cell parameters from 9313 reflections
b = 22.1079 (9) Å	θ = 2.5–26.1°
c = 21.9560 (11) Å	μ = 0.20 mm^{-1}
β = 95.129 (2)°	T = 100 K
V = 6202.0 (5) Å^3	Fragment, yellow
Z = 4	0.24 × 0.12 × 0.10 mm
F(000) = 2572	

Data collection

Bruker Photon CMOS diffractometer	11356 independent reflections
Radiation source: IMS microsource	9472 reflections with $I > 2\sigma(I)$
Helios optic monochromator	R_{int} = 0.056
Detector resolution: 16 pixels mm^{-1}	θ_{max} = 25.4°, θ_{min} = 2.4°
phi– and ω–rotation scans	h = –15 15
Absorption correction: multi-scan *SADABS* 2014/5	k = –25 26
T_{min} = 0.723, T_{max} = 0.745	l = –26 26
173455 measured reflections	

Refinement

Refinement on F^2	Secondary atom site location: difference Fourier map
Least-squares matrix: full	Hydrogen site location: inferred from neighbouring sites
$R[F^2 > 2\sigma(F^2)]$ = 0.040	H-atom parameters constrained
$wR(F^2)$ = 0.087	$W = 1/[\Sigma^2(FO^2) + (0.0268P)^2 + 5.981P]$ WHERE $P = (FO^2 + 2FC^2)/3$
S = 1.08	$(\Delta/\sigma)_{max}$ = 0.001
11356 reflections	$\Delta\rho_{max}$ = 0.30 e Å^{-3}
942 parameters	$\Delta\rho_{min}$ = –0.26 e Å^{-3}
852 restraints	Extinction correction: none
- constraints	Extinction coefficient: -
Primary atom site location: intrinsic phasing	

Compound **4** (CCDC 1547490)

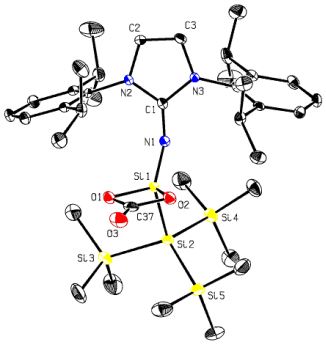

Diffractometer operator C. Jandl
scanspeed 10 s per frame
dx 50 mm
1926 frames measured in 10 data sets
phi-scans with delta_phi = 0.5
omega-scans with delta_omega = 0.5
shutterless mode

Crystal data

$C_{37}H_{63}N_3O_3Si_5$

M_r = 738.35	D_x = 1.105 Mg m^{-3}
Monoclinic, $P2_1/n$	Melting point: - K
Hall symbol: -P 2yn	Mo $K\alpha$ radiation, λ = 0.71073 Å
a = 10.2747 (4) Å	Cell parameters from 9977 reflections
b = 18.4172 (8) Å	θ = 2.3–25.9°
c = 23.9282 (10) Å	μ = 0.20 mm^{-1}
β = 101.484 (1)°	T = 100 K
V = 4437.3 (3) Å^3	Fragment, colorless
Z = 4	0.27 × 0.20 × 0.11 mm
F(000) = 1600	

Data collection

Bruker Photon CMOS diffractometer	8438 independent reflections

Radiation source: IMS microsource	6412 reflections with $I > 2\sigma(I)$
Helios optic monochromator	R_{int} = 0.098
Detector resolution: 16 pixels mm^{-1}	θ_{max} = 25.7°, θ_{min} = 2.2°
phi– and ω–rotation scans	h = –12 12
Absorption correction: multi-scan *SADABS* 2014/5	k = –22 22
T_{min} = 0.698, T_{max} = 0.745	l = –29 29
94623 measured reflections	

Refinement

Refinement on F^2	Secondary atom site location: difference Fourier map
Least-squares matrix: full	Hydrogen site location: inferred from neighbouring sites
$R[F^2 > 2\sigma(F^2)]$ = 0.052	H-atom parameters constrained
$wR(F^2)$ = 0.105	$W = 1/[\Sigma^2(FO^2) + (0.0347P)^2 + 3.8732P]$ WHERE $P = (FO^2 + 2FC^2)/3$
S = 1.08	$(\Delta/\sigma)_{max} \leq 0.001$
8438 reflections	$\Delta\rho_{max}$ = 0.34 e Å^{-3}
450 parameters	$\Delta\rho_{min}$ = –0.33 e Å^{-3}
0 restraints	Extinction correction: none
- constraints	Extinction coefficient: -
Primary atom site location: intrinsic phasing	

3. Computational Calculations

A) General

All calculations were performed at the B3LYP[S13-S15]/6-311+G(d,p) level of theory using Gaussian 09[S16]. The geometry of compounds **1** and **2** were optimized but, due to the size of the system, frequency calculations were only performed on the reduced system **1'**(Dipp groups replaced by phenyl groups), assessing the nature of stationary points found. To verify this approximation, important structural data of silylene **1** and **1'** and silepin **2** and **2'** were compared (Table S3). TD-DFT calculations were performed on the optimized structure of **1** revealing the HOMO-LUMO gap, whereas the singlet triplet gap was calculated from the reduced structures (^{1}**1'**singlet, ^{3}**1'** triplet).

B) Theoretical Investigations

Conversion of silylene 1' to silepin 2'

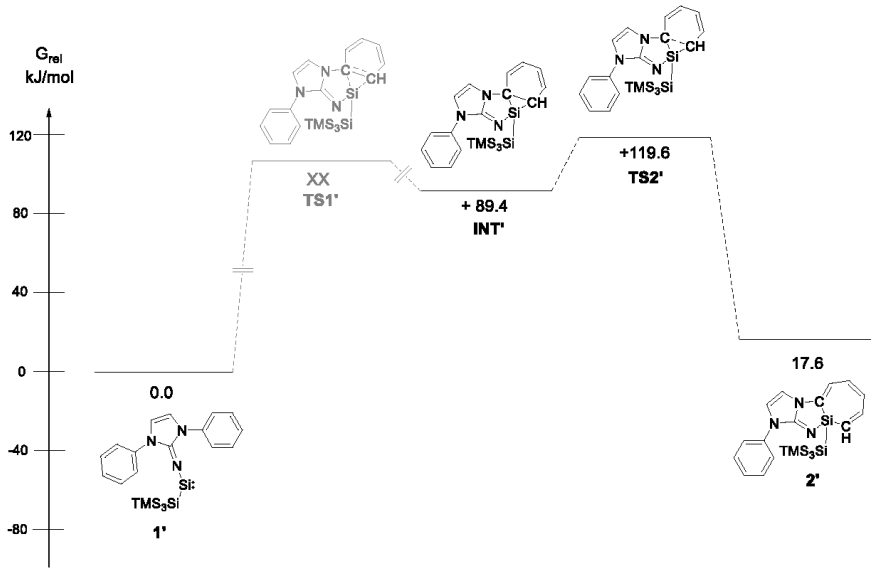

Figure S26. Energy profile for the pathway from silylene **1'** to silepin **2'** via an intermediate ground state **INT'**.

Due to the small energy difference between silylene **1'** and silepin **2'** of only 17.6 kJ/mol, we took a closer look at the mechanism of this transformation. It proceeds *via* approach of the silylene Si atom to the C=C bond of the imino ligand (**TS1'**), the formation of an intermediate silirane **INT'**, followed by the cleavage of the C-C bond *via* **TS2'** to obtain silepin **2'**, as proposed by Suzuki *et al.* for the intermolecular case.[S17] Similar to the suggestions by Kira et al. we believe that in **TS1'** mainly the 3p-orbital of the highly acidic silicon center interacts with π HOMO of the nearby phenyl ring.[S18] Despite great effort to elucidate the entire mechanism, we were not able to determine **TS1'** as the potential energy surface seems to be quite flat in this case. However **INT'** and **TS2'** were determined, providing low barriers and thus enabling a thermally accessible interconversion.

TD-DFT calculations of silylene 1 and silepine 2

Table S1. Excerpt of the TD-DFT calculations of **1**.

Wavelength [nm]	MO contributions	f
609.31	**HOMO→LUMO**	**0.0020**
414.31	HOMO→LUMO+1	0.0006
395.74	HOMO→LUMO+2	0.0011
391.36	HOMO→LUMO+4	0.0011
389.60	HOMO→LUMO+3	0.0004
346.77	HOMO→LUMO+5	0.0043

The calculated transition for the "forbidden" n (HOMO)→3p (LUMO) transition of **1** at 609.31 nm possesses low oscillator strength, matching the experimental value of 612 nm and its low intensity in the spectrum. HOMO and LUMO of **1** are depicted in Figure S27. As comparison we measured the UV-VIS spectrum of strongly related DippNTMSSi(II)TMS_3[S3]. Here as well a highly concentrated solution (1×10^{-3} mol/l, *n*-hexane, r.t.) gave a similar low intensity transition band at 532 nm (ε = 92 M^{-1} cm^{-1}).

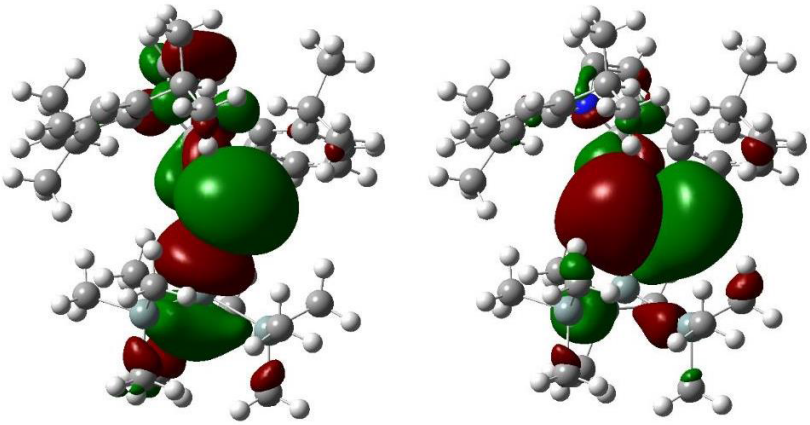

Figure S27. Representations of HOMO (-4.37 eV) and LUMO (-1.41 eV) of **1**.

Table S2: Excerpt of the TD-DFT calculation of **2**.

Wavelength [nm]	MO contributions	f
432.76	**HOMO→LUMO**	**0.0534**
326.41	HOMO-1→LUMO HOMO→LUMO+1 HOMO→LUMO+3	0.0133
321.37	HOMO→LUMO+2 HOMO→LUMO+3	0.0091
317.64	HOMO-1→LUMO HOMO→LUMO+1 HOMO→LUMO+2 HOMO→LUMO+3	0.0289
307.53	HOMO-1→LUMO HOMO→LUMO+3 HOMO→LUMO+4	0.0617
295.25	HOMO→LUMO+3 HOMO→LUMO+4 HOMO→LUMO+5	0.0083

Comparison of calculated and experimental structures

Table S3. Comparison of selected bond length (r) and angels (a) of calculated and experimental structures.

	1	**1'**	**2**	**2'**	**2** crystal data
r(N_{Imine}Si)	1.689	1.675	1.766	1.772	1.755
r(SiSi)	2.460	2.458	2.399	2.381	2.346
r(CN_{Imine})	1.286	1.270	1.286	1.284	1.275
r(SiC4)	-	-	1.913	1.909	1.897
r(SiC9)	-	-	1.879	1.860	1.878
a(N_{Imine}SiSi)	108.042°	103.455°	108.625°	108.026°	109.297°

C) Calculated structures

Table S4. Cartesian coordinated (x,y,z) for the optimized structure of **1**.

Si	0.653985	0.119976	-1.295552
Si	2.813262	-0.035934	-0.128060
N	-0.574424	0.000939	-0.141839
Si	2.971636	-0.973138	2.048335
Si	4.066342	-1.387475	-1.650898
Si	3.777287	2.147135	-0.164668
C	-1.850205	0.031462	0.014519
C	4.688035	-0.731352	2.831144
C	2.636678	-2.842186	1.976339
C	1.704080	-0.176305	3.214028
C	4.365475	-0.485842	-3.297159
C	3.107332	-2.979364	-2.053283
C	5.761521	-1.905898	-0.962780
C	5.671439	2.097972	-0.017371
C	3.348325	3.060109	-1.774806
C	3.121615	3.209017	1.269297
N	-2.723286	-1.054401	0.108480

The explicit cartesian coordinates (S32-S39) of all calculated structures were removed due to space-saving issues, but the data is available free of charge at the ACS publications homepage.

4. References

(S1) Lui, M. W.; Merten, C.; Ferguson, M. J.; McDonald, R.; Xu, Y.; Rivard, E., *Inorg. Chem.* **2015**, *54*, 2040-2049.

(S2) Marschner, C., *Eur. J. Inorg. Chem.* **1998**, 221-226.

(S3) Protchenko, A. V.; Schwarz, A. D.; Blake, M. P.; Jones, C.; Kaltsoyannis, N.; Mountford, P.; Aldridge, S., *Angew. Chem. Int. Ed.* **2013**, *52*, 568-71.

(S4) *APEX suite of crystallographic software*, APEX 3 Version 2015-5.2; Bruker AXS Inc.: Madison, Wisconsin, USA, **2015**.

(S5) *SAINT*, Version 8.34A and *SADABS*, Version 2014/5; Bruker AXS Inc.: Madison, Wisconsin, USA, **2014**.

(S6) Sheldrick, G. M., *Acta Crystallogr., Sect. A* **2015**, *71*, 3–8.

(S7) Sheldrick G. M., *Acta Crystallogr., Sect. C* **2015**, *71*, 3–8.

(S8) Huebschle, C. B.; Sheldrick, G. M.; Dittrich, B., *J. Appl. Cryst.* **2011**, *44*, 1281–1284.

(S9) Wilson, A. J. C. (Ed.) *International Tables for Crystallography, Vol. C*, Tables 6.1.1.4 (pp. 500-502), 4.2.6.8 (pp. 219-222), and 4.2.4.2 (pp. 193-199); Kluwer Academic Publishers: Dordrecht, The Netherlands, 1992.

(S10) Spek, A. L., *Acta Crystallogr., Sect. C* **2015**, *71*, 9–18.

(S11) Macrae, C. F.; Edgington, P. R.; McCabe, P., Pidcock E.; Shields, G. P.; Taylor, R.; Towler, M.; van de Streek, J., *J. Appl. Cryst.* **2006**, *39*, 453–457.

(S12) Spek, A. L., *Acta Crystallogr., Sect. D* **2009**, *65*, 148-155.

(S13) Becke, A. D., *J. Chem. Phys.* **1993**, *98*, 5648-5652.

(S14) Vosko, S. H.; Wilk, L., Nusair, M., *Can. J. Phys.* **1980**, *58*, 1200-1211.

(S15) Lee, C.; Yang, W.; Parr, R. G., *Phys. Rev. B* **1988**, *37*, 785-789.

(S16) Gaussian 09, Revision E.01, M. J. Frisch, G. W. Trucks, H. B. Schlegel, G. E. Scuseria, M. A. Robb, J. R. Cheeseman, G. Scalmani, V. Barone, G. A. Petersson, H. Nakatsuji, X. Li, M. Caricato, A. Marenich, J. Bloino, B. G. Janesko, R. Gomperts, B. Mennucci, H. P. Hratchian, J. V. Ortiz, A. F. Izmaylov, J. L. Sonnenberg, D. Williams-Young, F. Ding, F. Lipparini, F. Egidi, J. Goings, B. Peng, A. Petrone, T. Henderson, D. Ranasinghe, V. G. Zakrzewski, J. Gao, N. Rega, G. Zheng, W. Liang, M. Hada, M. Ehara, K. Toyota, R. Fukuda, J. Hasegawa, M. Ishida, T. Nakajima, Y. Honda, O. Kitao, H. Nakai, T. Vreven, K. Throssell, J. A. Montgomery, Jr., J. E. Peralta, F. Ogliaro, M. Bearpark, J. J. Heyd, E. Brothers, K. N. Kudin, V. N. Staroverov, T. Keith, R. Kobayashi, J. Normand, K. Raghavachari, A. Rendell, J. C. Burant, S. S. Iyengar, J. Tomasi, M. Cossi, J. M. Millam, M. Klene, C. Adamo, R. Cammi, J. W. Ochterski, R. L. Martin, K. Morokuma, O. Farkas, J. B. Foresman, and D. J. Fox, Gaussian, Inc., Wallingford CT, **2016**.

(S17) Suzuki, H.; Tokitoh, N.; Okazaki, R., *J. Am. Chem. Soc.* **1994**, *116*, 11572-11573.

(S18) Kira, M.; Ishida, S.; Iwamoto, T.; Kabuto, C., *J. Am. Chem. Soc.* **2002**, *124*, 3830-3831.

14.4 Supporting Information Chapter 9

Silicon and Oxygen's Bond of Affection: An Acyclic Three-Coordinate Silanone and Its Transformation to an Iminosiloxysilylene

Daniel Wendel,[†,‡] Dominik Reiter,[†,§] Amelie Porzelt,[§] Philipp J. Altmann,[⊥] Shigeyoshi Inoue[*,§] and Bernhard Rieger[*,‡]

[‡]WACKER-Chair of Macromolecular Chemistry, [§]WACKER-Institute of Silicon Chemistry, [⊥]Catalysis Research Center, Technische Universität München, Lichtenbergstraße 4, 85748 Garching bei München, Germany

*s.inoue@tum.de; rieger@tum.de

Supporting Information

Total: S65 pages

1. Experimental Procedures

A) General Methods and Instrumentation

All manipulations were carried out under argon atmosphere using standard Schlenk or glovebox techniques. Glassware was heat-dried under vacuum prior to use. Unless otherwise stated, all chemicals were purchased from Sigma-Aldrich or ABCR and used as received. Benzene, Et_2O, *n*-hexane, THF and toluene were refluxed over sodium/benzophenone, acetonitrile over CaH_2 and methanol over magnesium, distilled and deoxygenated prior to use. Deuterated benzene (C_6D_6), THF (THF-d_8) and acetonitrile (CD_3CN) were obtained from Deutero Deutschland GmbH and were dried over 3 Å molecular sieves. All NMR samples were prepared under argon in J. Young PTFE tubes. Silepin **1a**, IPrNSiBr$_3$, IMe$_4$ and NaSi*t*-Bu$_3$(THF$_2$) were synthesized according to procedures described in literature.[S1-4] Dinitrogen monoxide (5.0), carbon dioxide (5.0), hydrogen (5.0) and ethylene (3.5) were purchased from Westfalen AG and used as received. NMR spectra were recorded on Bruker AV-500C, AV-500 or DRX-400 spectrometers at ambient temperature (300 K), unless otherwise stated. ^{1}H, ^{13}C and ^{29}Si NMR spectroscopic chemical shifts δ are reported in ppm relative to tetramethylsilane. δ(^{1}H) and δ(^{13}C) were referenced internally to the relevant residual solvent resonances. δ(^{29}Si) was referenced to the signal of tetramethylsilane (TMS) (δ = 0 ppm) as external standard. Elemental analyses (EA) were conducted with a EURO EA (HEKA tech) instrument equipped with a CHNS combustion analyzer. Mass spectra (MS-CI) were recorded on a double focusing Finnigan MAT 90 mass spectrometer (isobutene, 150 eV). UV-Vis spectra were taken on an Agilent Cary 60 spectrophotometer. ATR-FTIR spectra were recorded on a Perkin Elmer FTIR spectrometer (diamond ATR, Spectrum Two; located inside an argon-filled glovebox) in a range of 400 – 4000 cm^{-1}. Melting Points (M_p) were determined in sealed glass capillaries under inert gas by a Büchi M-565 melting point apparatus.

B) Synthesis and Characterization of New Compounds

Synthesis of Silepin (Si*t*-Bu$_3$ Substituted) (1b)

An analogue procedure as for the preparation of SiTMS$_3$ substituted silepin **1a** was applied.[S1] A solution of NaSi*t*-Bu$_3$(THF$_2$) (134 mg, 0.18 mmol, 2.00 eq) in toluene (2 mL) was added to IPrNSiBr$_3$ (123 mg, 0.36 mmol, 1.00 eq) in toluene (2 mL) at room temperature. The color rapidly changed to light green (approx. 1 sec) and then immediately to yellow with formation of a white precipitate. After stirring the solution for 20 min, the solvent was removed *in vacuo*. The obtained residue was extracted with *n*-hexane (3 × 5 mL) and filtered through a microfiber glass filter. For further studies, mixtures of **1b**/*t*-Bu$_3$SiBr were prepared in analogue fashion, since attempts to separate both products by fractional crystallization or sublimation were unsuccessful.

^{1}H NMR (500 MHz, C$_6$D$_6$, r.t.): δ = 7.19 – 7.00 (m, 3H, *p*-/*m*-C*H*-Ar), 6.70 (d, *J* = 2.9 Hz, 1H, C*H*-N), 6.63 (d, *J* = 6.5 Hz, 1H, C*H*-Ar), 6.49 (d, *J* = 12.9 Hz, 1H, C*H*-Ar), 6.37 (dd, *J* = 12.9, 6.5 Hz, 1H, C*H*-Ar), 5.88 (d, *J* = 2.9 Hz, 1H, C*H*-N), 3.39 (hept, *J* = 6.8 Hz, 1H, C*H*), 3.22 (hept, *J* = 6.8 Hz, 1H, C*H*), 3.12 (hept, *J* = 6.8 Hz, 1H, C*H*), 3.05 (hept, *J* = 6.8 Hz, 1H, C*H*) 1.35 (d, *J* = 6.8 Hz, 6H, C*H*$_3$), 1.31 (d, *J* = 6.8 Hz, 6H, C*H*$_3$), 1.25 (s, 27H, Si*t*-*Bu*$_3$), 1.21 (d, *J* = 6.8 Hz, 3H, C*H*$_3$), 1.20 (d, *J* = 6.8 Hz, 3H, C*H*$_3$), 1.09 (d, *J* = 6.8 Hz, 3H, C*H*$_3$), 0.93 (d, *J* = 6.8 Hz, 3H, C*H*$_3$).

^{29}Si NMR (99 MHz, C$_6$D$_6$, r.t.): δ = 11.6 (*central Si*), 7.8 (*Si*t-Bu$_3$).

The obtained NMR and UV-VIS data of **1b** are in accordance with the one of SiTMS$_3$ substituted silepin **1a**.[S1]

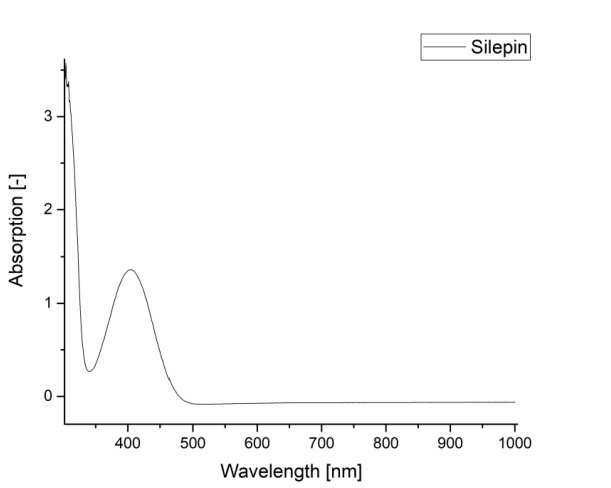

Figure S1. UV-Vis spectrum of silepin **1b**/*t*-Bu$_3$SiBr mixture λ_{max} (r.t., hexane, 8.0×10^{-4} M) = 405 nm.

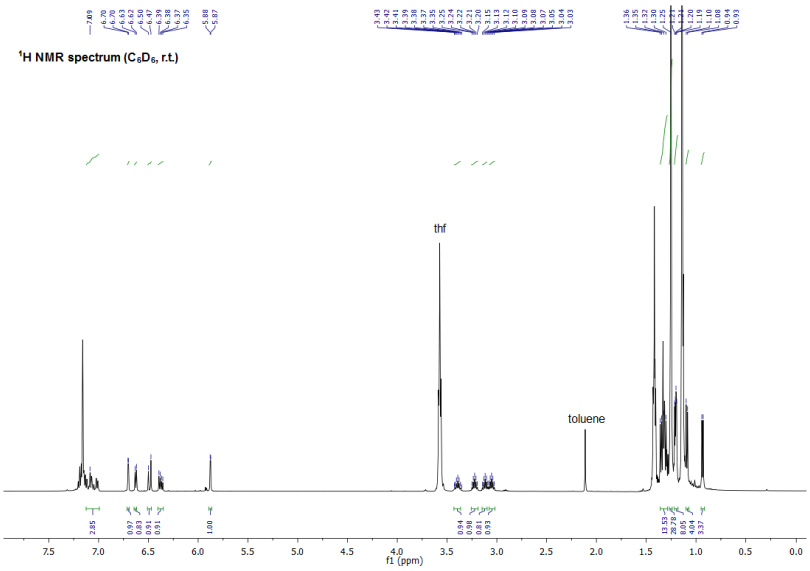

Figure S2: ^{1}H NMR spectrum of silepin **1b**/*t*-Bu_3SiBr mixture (C_6D_6, r.t.).

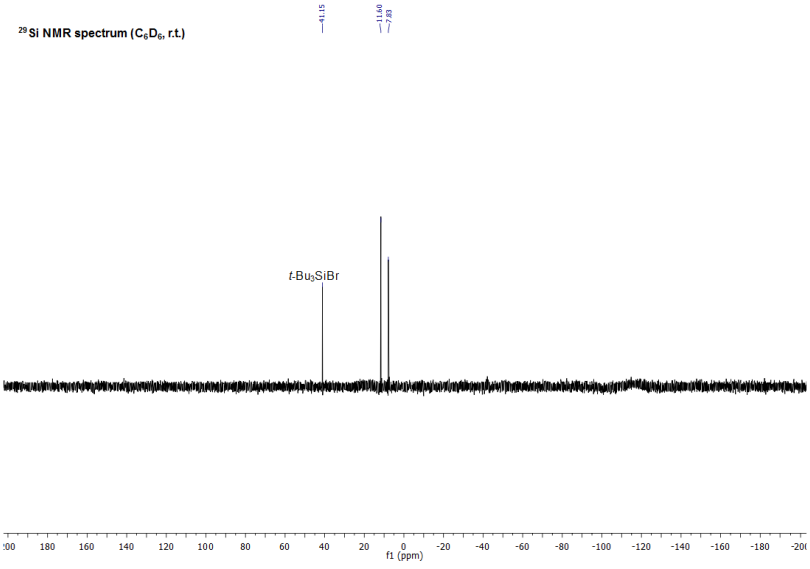

Figure S3: ^{29}Si NMR spectrum of silepin **1b**/*t*-Bu_3SiBr mixture (C_6D_6, r.t.).

Synthesis of Silanone (SiTMS$_3$ Substituted) (2a)

A solution of KSiTMS$_3$ (726 mg, 2.53 mmol, 2.00 eq) in toluene (20 mL) was added to IPrNSiBr$_3$ (849 mg, 1.27 mmol, 1.00 eq) in toluene (20 mL) at room temperature. The color rapidly changed to light green (approx. 1 sec) and then immediately to yellow with formation of a white precipitate. After stirring the solution for 20 min, the solvent was removed *in vacuo*. The obtained residue was extracted with *n*-hexane (3 × 15 mL) and filtered through a microfiber glass filter. The yellow solution was concentrated, cooled to –78 °C and exposed to N_2O (1 bar). While warming up the solution to room temperature, a fine white precipitate forms, which is immediately separated *via* filtration, washed with *n*-hexane and dried *in vacuo* to give pure silanone **2a** (484 mg, 0.51 mmol, 41%) as a white powder. Attempts to crystallize the donor-free silanone **2a** failed in several solvents (e.g. toluene, monofluorobenzene, difluorobenzene or diethylether), however crystallization in acetonitrile at –35 °C yielded single crystals of tetra-coordinate acetonitrile-stabilized silanone **2a** × CD_3CN. The coordination of one acetonitrile molecule to the silicon center of **2a** was additionally verified *via* NMR spectroscopy (see below). Silanone **2a** is indefinitely stable as a solid at –35 °C, but decomposes in C_6D_6 at room temperature within 14 h ($t_{1/2}$ = 7 h). Still, the half-life time of silanone **2a** can be extended considerably by using **2a** × CD_3CN solutions ($t_{1/2}$ = 4 d).

Compound 2a:

^{1}H NMR (500 MHz, C_6D_6, r.t.): δ = 7.34 – 7.05 (m, 6H, C*H*-Ar), 6.08 (s, 2H, C*H*-N), 3.19 (hept, *J* = 6.8 Hz, 4H, C*H*), 1.51 (d, *J* = 6.8 Hz, 12H, CH_3), 1.12 (d, *J* = 6.8 Hz, 12H, CH_3), 0.22 (s, 27H, Si*TMS*$_3$).

^{13}C NMR (126 MHz, C_6D_6, r.t.): δ = 148.8 (N-*C*-N), 147.7 (*C*-Ar), 133.1 (*C*-Ar), 130.2 (*C*H-Ar), 124.3 (*C*H-Ar), 115.7 (*C*H-N), 29.1 (*C*H), 25.4 (*C*H$_3$), 23.8 (*C*H$_3$), 2.5 (Si*TMS*$_3$).

^{29}Si NMR (99 MHz, C_6D_6, r.t.): δ = 33.7 (*central Si*), -9.6 (*TMS*$_3$), -130.6 (*Si*TMS$_3$).

MS-CI (150 eV): m/z (%) = 693 $[M]^+$ (8), 711 $[M+H_2O]^+$ (5).

Reproducible EA could not be obtained for compound **2a** due to its extreme air and moisture sensitivity.

M_p: 111.0 °C (decomposition, color change from colorless to yellow).

Compound 2a × CD_3CN:

^{1}H NMR (500 MHz, CD_3CN, r.t.): δ = 7.46 – 7.38 (m, 2H, *p*-C*H*-Ar), 7.38 – 7.23 (m, 4H, *m*-C*H*-Ar), 6.56 (s, 2H, C*H*-N), 3.01 (overlapping hept, *J* = 6.8 Hz, 4H, C*H*), 1.35 (d, *J* = 6.8 Hz, 6H, CH_3), 1.32 (d, *J* = 6.8 Hz, 6H, CH_3) 1.18 (d, *J* = 6.8 Hz, 6H, CH_3) 1.14 (d, *J* = 6.8 Hz, 6H, CH_3), -0.04 (s, 27H, Si*TMS*$_3$).

^{29}Si NMR (99 MHz, CD_3CN, r.t.): δ = -10.9 (*TMS*$_3$), -48.3 (*central Si*), -133.6 (*Si*TMS$_3$).

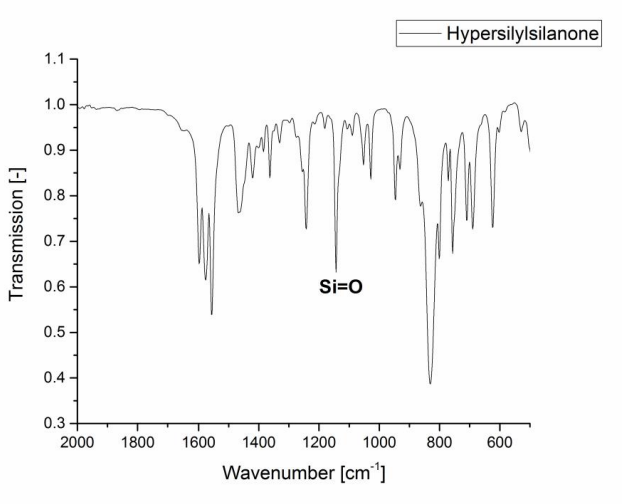

Figure S4: IR spectrum of silanone **2a** (cm^{-1}): 1598 (m), 1577 (m), 1552 (s), 1456 (m), 1420 (w), 1244 (m), 1144 (m, Si=O), 1053 (w), 1023 (w), 944 (w), 825 (s), 751 (m), 721 (m), 685 (m), 622 (m).

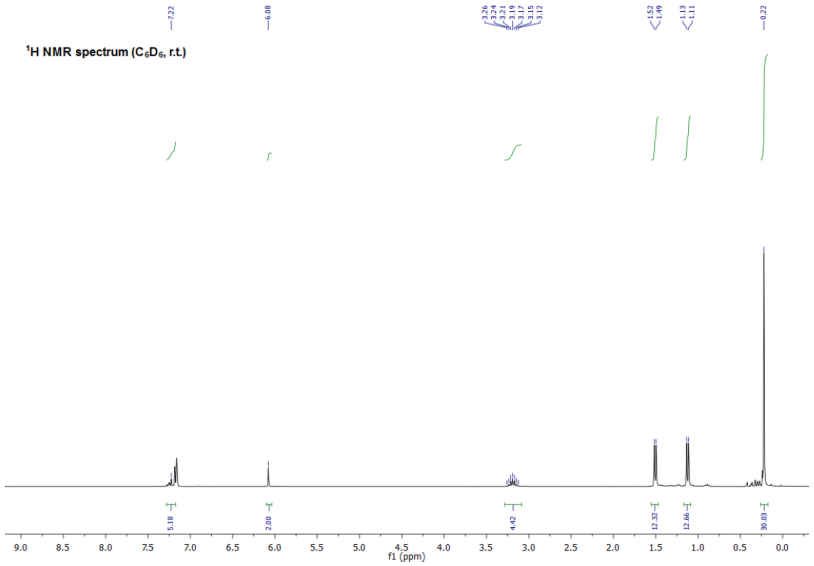

Figure S5: ^{1}H NMR spectrum of silanone **2a** (C_6D_6, r.t.).

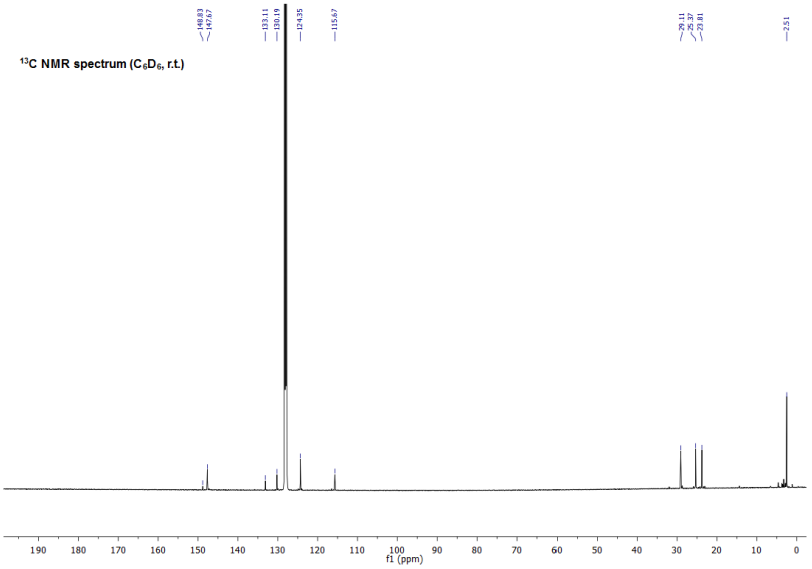

Figure S6: ^{13}C NMR spectrum of silanone **2a** (C_6D_6, r.t.).

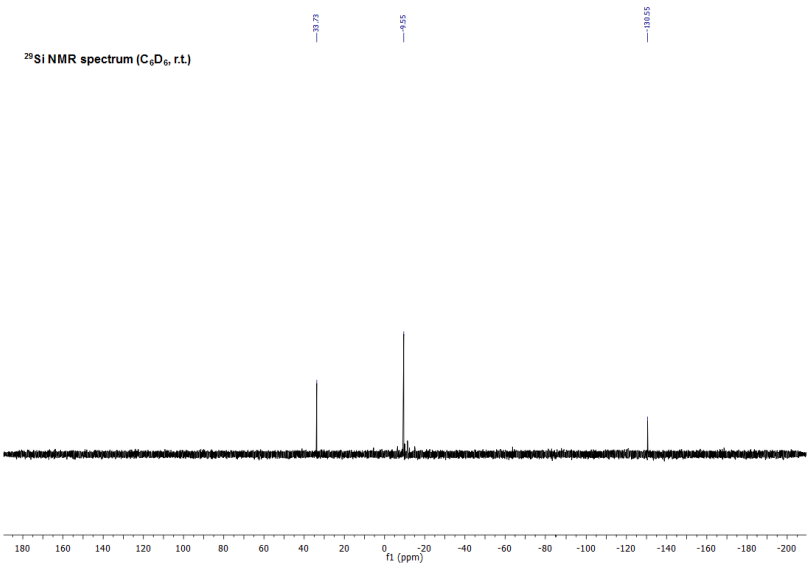

Figure S7: ^{29}Si NMR spectrum of silanone **2a** (C_6D_6, r.t.).

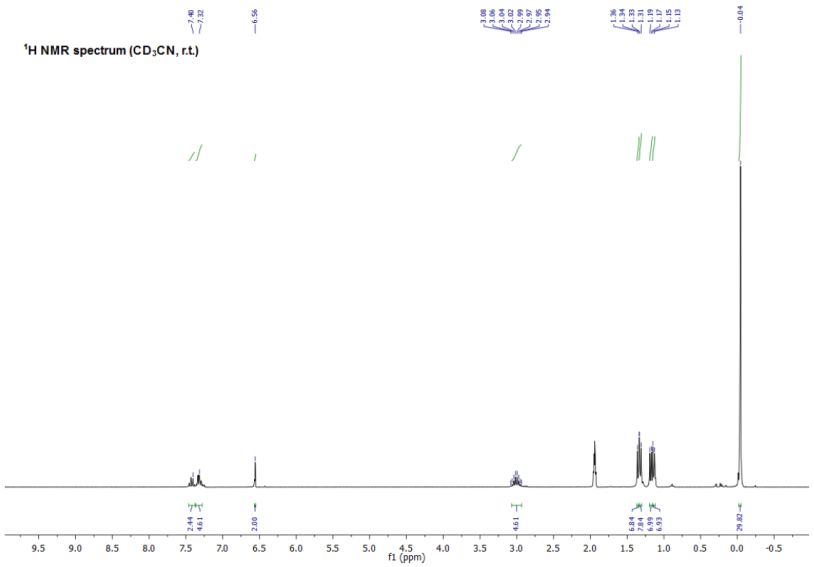

Figure S8: ^{1}H NMR spectrum of tetra-coordinate silanone **2a** × CD_3CN (CD_3CN, r.t.).

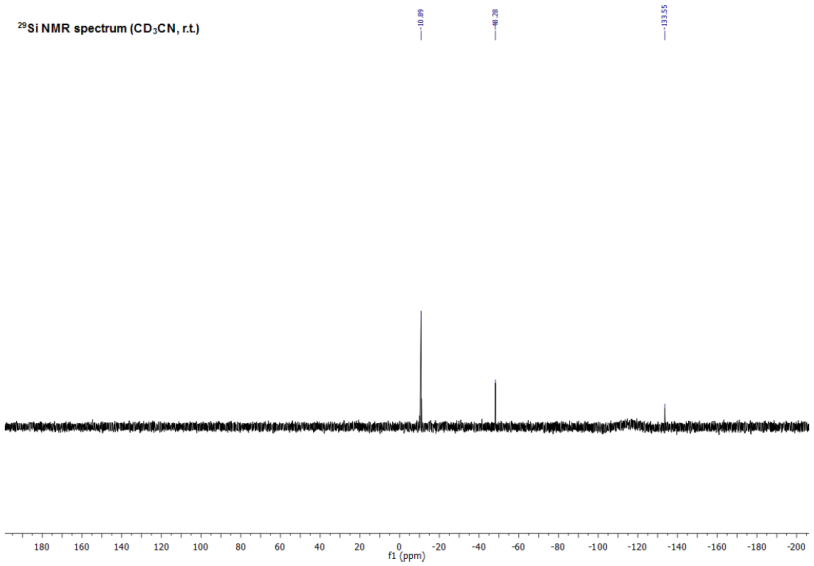

Figure S9: ^{29}Si NMR spectrum of tetra-coordinate silanone **2a** × CD_3CN (CD_3CN, r.t.).

Decomposition of Silanone 2a

In general, the decomposition process of **2a** in C_6D_6 is rather unspecific and led to several unidentified compounds within 14 h. However, according to the obtained ^{1}H, ^{29}Si and $^{1}H/^{29}Si$ HMBC NMR data one major asymmetric product was identified, presumably formed by TMS migration from the hypersilyl group to the Si=O center and subsequent activation of the NHI ligand (see Figure S11 and Figure S12). A comparable 1,3-silyl migration has been reported for Kira's transient cyclic dialkylsilanone to form an intermediary silene.[S5] For silanone **2a** the identical decomposition pathway leads to transient disilene **INT** (see Figure S10), which probably due to the strong donation of NHI and OTMS group possesses a highly polarized Si=Si bond. Therefore also a zwitterionic resonance form **INT'** should be considered. We propose, that this highly reactive intermediate is capable to intra- or intermolecularly activate the NHI ligand. Although currently specific details are unclear, this reaction seems very likely, since a similar NHI activation has been observed in literature.[S2]

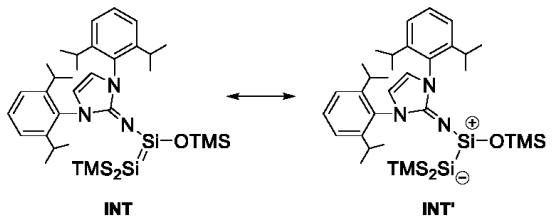

Figure S10: Proposed intermediate **INT** in the decomposition process of silanone **2a** formed by 1,3-silyl migration to the Si=O center.

Moreover, we figured out that the same 1,3-silyl migration can be instantly induced by addition of THF-d_8 to solid **2a**, resulting in a strongly yellow colored solution. Subsequent NMR analysis indicated the quantitative formation of the proposed transient disilene **INT** (NMR data see below). By comparing the NMR shifts of **INT** with the theoretical data (Table S13), exclusively the ^{29}Si NMR shift of the positively polarized Si^{+} atom showed a strong deviation (Δ67.5 ppm). We therefore believe that (very similar to compound **6**) a THF molecule can act as potential donor and coordinate to the silicon center, forming **INT** × THF. This species is highly reactive and decomposed in analogue fashion to **2a** in C_6D_6 within a few hours. All attempts to isolate and crystallize **INT** × THF failed, however trapping experiments with ethylene led to the corresponding [2+2]-cycloaddition product **5**. Further, by using a stronger external NHC donor the IMe_4 stabilized zwitterionic disilene **6** was isolated (for details see compound **5** and **6**).

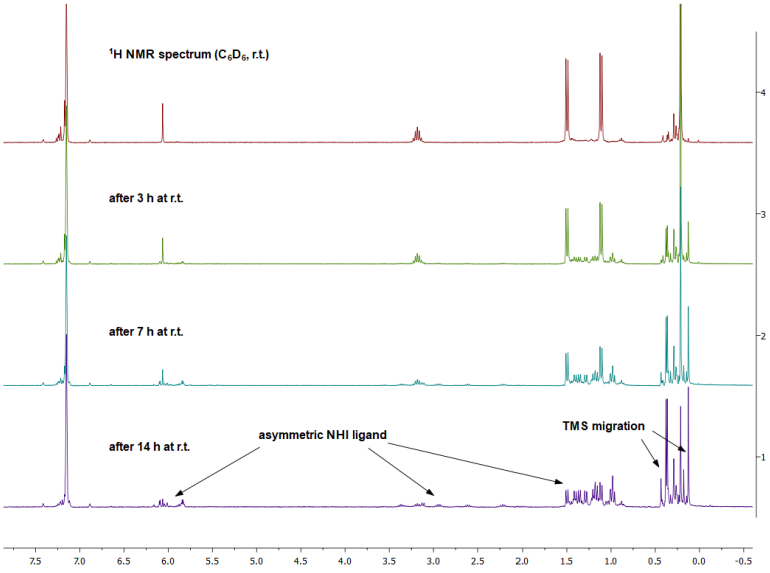

Figure S11: ^{1}H NMR spectra of the decomposition process of silanone **2a** after 3, 7 and 14 h in solution (C_6D_6, r.t.).

Figure S12: ^{1}H/^{29}Si HMBC NMR spectrum of the decomposition mixture of silanone **2a** after 14 h in solution (C_6D_6, r.t.).

NMR data of transient disilene INT (THF-d_8 induced TMS migration):

^{1}H NMR (500 MHz, THF-d_8, r.t.): δ = 7.39 – 7.35 (m, 4H, *m*-C*H*-Ar), 7.30 – 7.27 (m, 2H, *o*-C*H*-Ar), 6.56 (s, 2H, C*H*-N), 3.16 (hept, *J* = 6.8 Hz, 4H, C*H*), 1.41 (d, *J* = 6.8 Hz, 12H, CH_3), 1.16 (d, *J* = 6.8 Hz, 12H, CH_3), 0.01 (s, 18H, Si*TMS*$_2$), -0.11 (s, 9H, O*TMS*).

^{13}C NMR (126 MHz, THF-d_8, r.t.): δ =, 148.7 (*C*-Ar), 143.0 (N-*C*-N), 136.1 (*C*-Ar), 130.3 (*C*H-Ar), 125.1 (*C*H-Ar), 117.0 (*C*H-N), 29.4 (*C*H), 25.9 (*C*H$_3$), 24.4 (*C*H$_3$), 7.4 (Si*TMS*$_2$), 3.4 (O*TMS*).

^{29}Si NMR (99 MHz, THF-d_8, r.t.): δ = 4.3 (O*TMS*), -7.2 (Si*TMS*$_2$), -8.0 (*Si*OTMS), -196.6 (*Si*TMS$_2$).

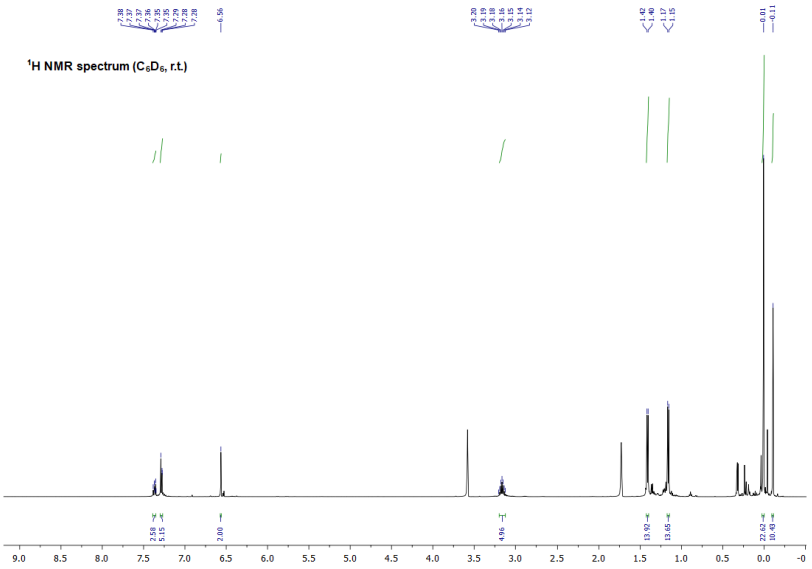

Figure S13: ^{1}H NMR spectrum of transient disilene **INT** (THF-d_8, r.t.).

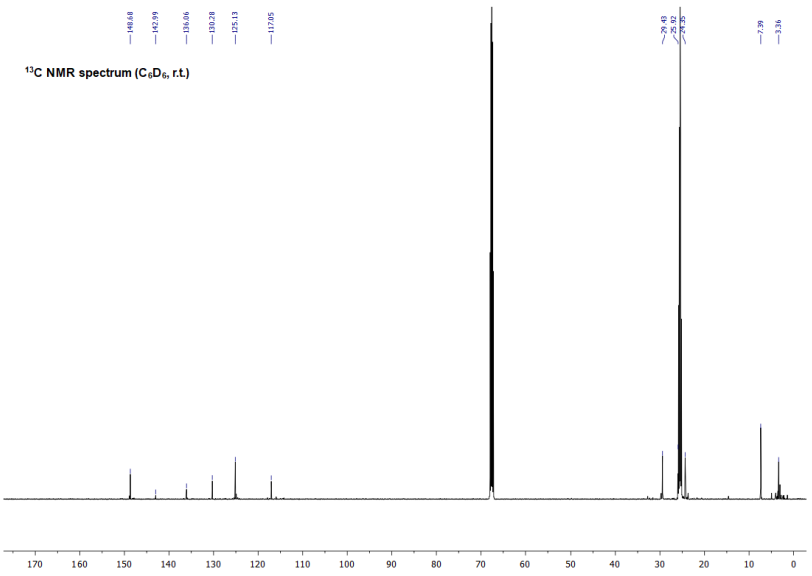

Figure S14: ^{13}C NMR spectrum of transient disilene **INT** (THF-d_8, r.t.).

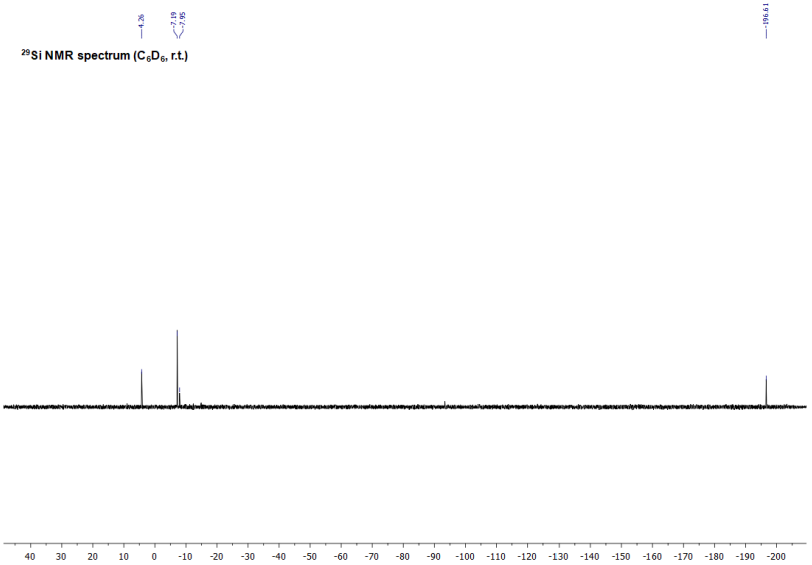

Figure S15: ^{29}Si NMR spectrum of transient disilene **INT** (THF-d_8, r.t.).

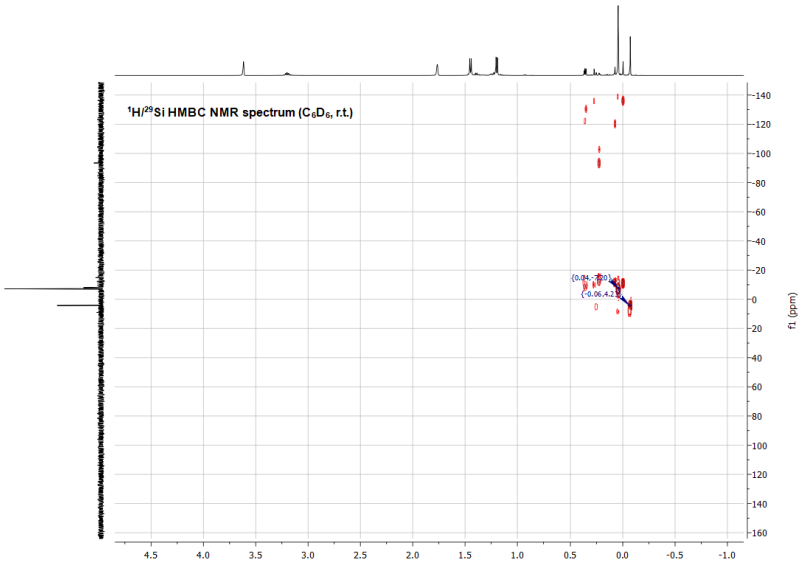

Figure S16: ^{1}H/^{29}Si HMBC NMR spectrum of transient disilene **INT** (THF-d_8, r.t.).

Synthesis of Silanone (Si*t*-Bu$_3$ Substituted) (2b)

A solution of NaSi*t*-Bu$_3$(THF$_2$) (1.09 g, 2.98 mmol, 2.00 eq) in benzene (20 mL) was added to IPrNSiBr$_3$ (1.00 g, 1.49 mmol, 1.00 eq) in benzene (20 mL) at room temperature. The color rapidly changed to light green (approx. 1 sec) and then immediately to yellow with formation of a white precipitate. After stirring the solution for 20 min, the solvent was removed *in vacuo*. The obtained residue was extracted with *n*-hexane (3 × 20 mL) and filtered through a microfiber glass filter. The yellow solution was concentrated, cooled to –78 °C and exposed to N_2O (1 bar). While warming up the solution to room temperature, a fine white precipitate forms, which is immediately separated *via* filtration, washed with *n*-hexane and dried *in vacuo* to give pure silanone **2b** (521 mg, 0.81 mmol, 54%) as a white powder. Colorless crystals of **2b** suitable for single crystal X-ray analysis were obtained by slow diffusion of Et_2O into a saturated THF solution at –35 °C for several days. Compound **2b** is indefinitely stable as a solid at r.t. (no changes after 1 month), but quantitatively forms *N*,*O*-silylene **7** in C_6D_6 or THF-d_8 at room temperature within 48 h ($t_{1/2}$ = 24 h).

Compound 2b:

^{1}H NMR (500 MHz, C_6D_6, r.t.): δ = 7.25 – 7.19 (m, 2H, *p*-C*H*-Ar), 7.16 – 7.11 (m, 4H, *m*-C*H*-Ar), 6.11 (s, 2H, C*H*-N), 3.17 (hept, *J* = 6.8 Hz, 4H, C*H*), 1.49 (d, *J* = 6.8 Hz, 12H, CH_3), 1.13 (s, 27H, Si*t*-*Bu*$_3$), 1.12 (d, *J* = 6.8 Hz, 12H, CH_3).

^{13}C NMR (126 MHz, C_6D_6, r.t.): δ = 148.4 (N-*C*-N), 147.6 (*C*-Ar), 133.2 (*C*-Ar), 130.2 (*C*H-Ar), 124.3 (*C*H-Ar), 115.7 (*C*H-N), 31.8 (C(*C*H$_3$)$_3$), 29.1 (*C*H), 25.5 (*C*H$_3$), 23.4 (*C*H$_3$), 23.1 (*C*(CH$_3$)$_3$).

^{29}Si NMR (99 MHz, C_6D_6, r.t.): δ = 28.8 (*central Si*), 13.7 (Si*t*-Bu$_3$).

^{29}Si NMR (99 MHz, THF-d_8, r.t.): δ = 26.2 (*central Si*), 13.0 (Si*t*-Bu$_3$).

EA experimental (calculated): C 72.32 (72.50), H 9.97 (9.83), N 6.45 (6.50) %.

M_p: 126.5 °C (decomposition, color change from colorless to yellowish).

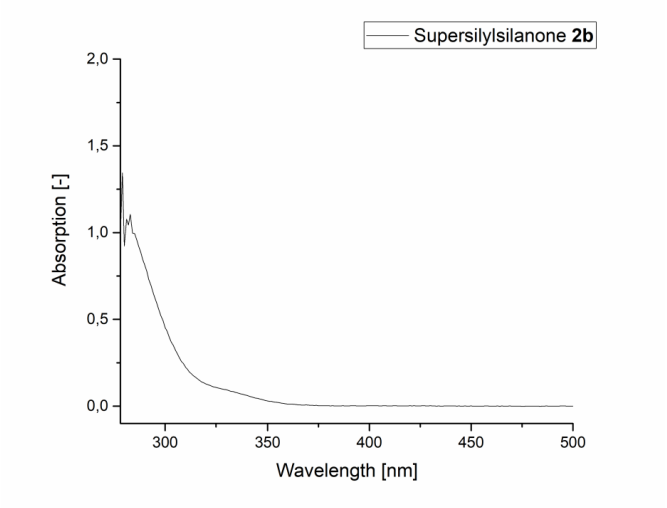

Figure S17. UV-Vis spectrum of silanone **2b** λ_{max} (r.t., toluene, 4.0×10^{-4} M) = 282 nm.

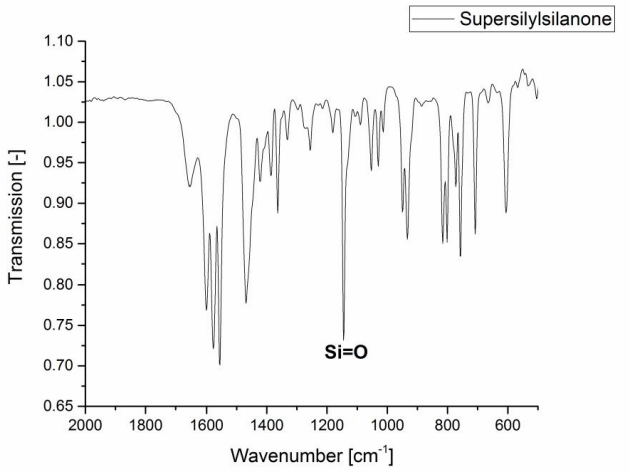

Figure S18: IR spectrum of silanone **2b** (cm^{-1}): 1649 (w), 1599 (m), 1577 (m), 1550 (s), 1463 (m), 1359 (w), 1144 (s, Si=O), 1051 (w), 1029 (w), 945 (w), 936 (m), 808 (m), 755 (m), 705 (m), 606 (m).

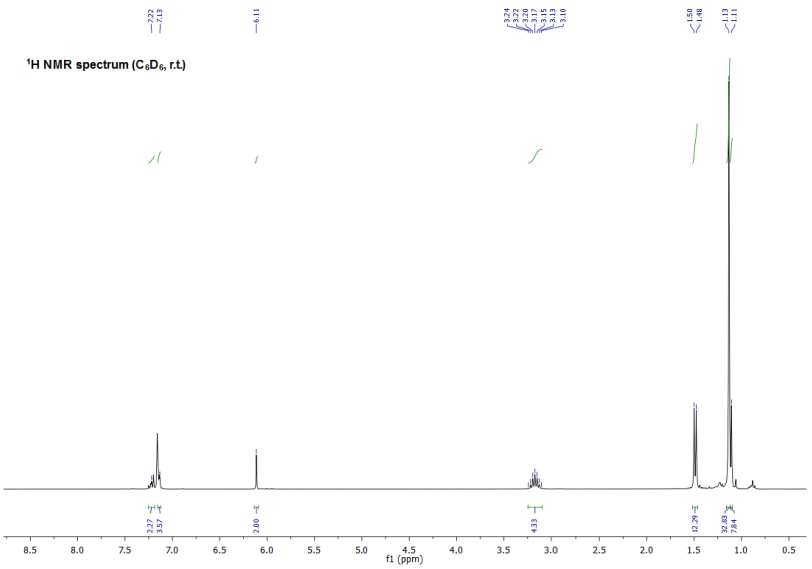

Figure S19: ^{1}H NMR spectrum of silanone **2b** (C_6D_6, r.t.).

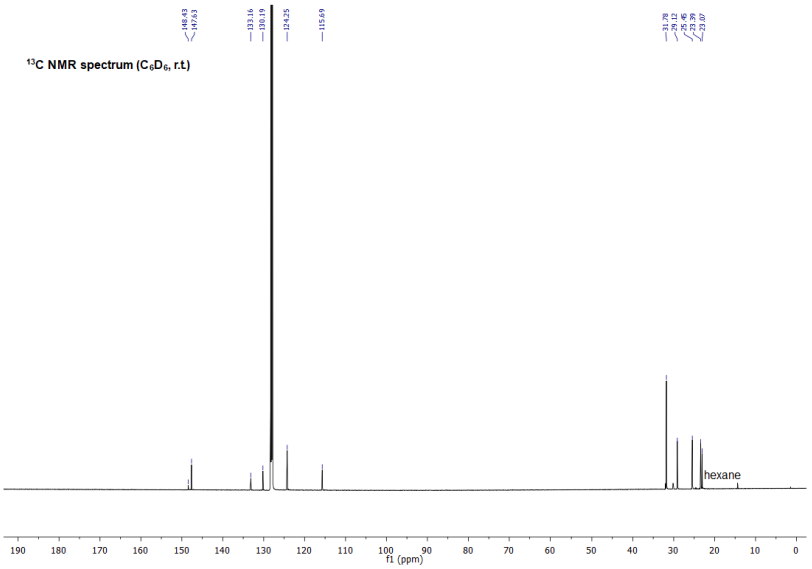

Figure S20: ^{13}C NMR spectrum of silanone **2b** (C_6D_6, r.t.).

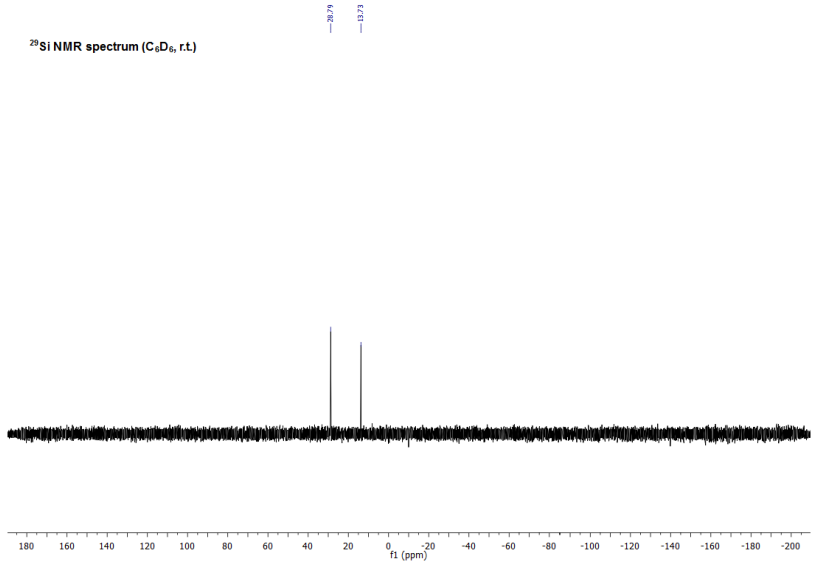

Figure S21: ^{29}Si NMR spectrum of silanone **2b** (C_6D_6, r.t.).

Synthesis of IPrNSi(O_2C=O)SiR_3 (R = TMS 3a, R = *t*-Bu 3b)

Similarly to the reaction of silepin **1a** with CO_2[S1], both silanones **2** can be directly converted with CO_2 to the respective silicon carbonate complexes **3**. Generally, a solution of **2** in C_6D_6 (0.5 mL) was exposed to CO_2 gas (1 bar) at room temperature in a J. Young PTFE tube. Monitoring the reaction *via* NMR spectroscopy showed the direct and quantitative formation of silicon carbonate complexes **3**.

Compound 3a:

The NMR shifts of this reaction product are identical to the published data.[S1]

^{1}H NMR (500 MHz, C_6D_6, r.t.): δ = 7.30 – 7.26 (m, 2H, *p*-C*H*-Ar), 7.19 – 7.16 (m, 4H, *m*-C*H*-Ar), 5.93 (s, 2H, C*H*-N), 2.95 (hept, *J* = 6.9 Hz, 4H, C*H*), 1.47 (d, *J* = 6.9 Hz, 12H, CH_3), 1.08 (d, *J* = 6.9 Hz, 12H, CH_3), 0.18 (s, 27H, Si*TMS*$_3$).

^{13}C NMR (126 MHz, C_6D_6, r.t.): δ = 150.4 (O_2C=O), 146.7 (*C*-Ar), 145.6 (N-*C*-N), 133.2 (*C*-Ar), 130.7 (*C*H-Ar), 124.8 (*C*H-Ar), 116.0 (*C*H-N), 29.2 (*C*H), 25.2 (*C*H$_3$), 23.2 (*C*H$_3$), 2.5 (Si*TMS*$_3$).

^{29}Si NMR (99 MHz, C_6D_6, r.t.): δ = -9.8 (*TMS*$_3$), -35.0 (*central Si*), -134.3 (*Si*TMS$_3$).

Compound 3b:

^{1}H NMR (500 MHz, C_6D_6, r.t.): δ = 7.33 – 7.26 (m, 2H, *p*-C*H*-Ar), 7.22 – 7.16 (m, 4H, *m*-C*H*-Ar), 5.97 (s, 2H, C*H*-N), 2.96 (hept, *J* = 6.9 Hz, 4H, C*H*), 1.45 (d, *J* = 6.9 Hz, 12H, CH_3), 1.08 (d, *J* = 6.9 Hz, 12H, CH_3), 1.05 (s, 27H, Si*t-Bu*$_3$).

^{13}C NMR (126 MHz, C_6D_6, r.t.): δ = 150.7 (O_2C=O), 146.8 (*C*-Ar), 145.5 (N-*C*-N), 133.3 (*C*-Ar), 130.6 (*C*H-Ar), 124.7 (*C*H-Ar), 116.2 (*C*H-N), 31.4 (C(*C*H$_3$)$_3$), 29.2 (*C*H), 25.4 (*C*H$_3$), 22.7 (*C*(CH$_3$)$_3$), 22.6 (*C*H$_3$).

^{29}Si NMR (99 MHz, C_6D_6, r.t.): δ = 5.5 (Si*t*-Bu$_3$), -43.0 (*central Si*).

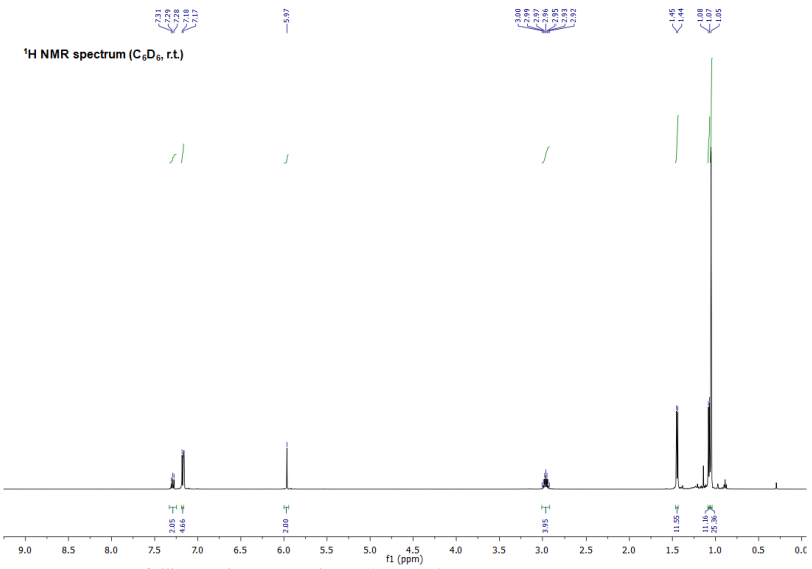

Figure S22: ^{1}H NMR spectrum of silicon carbonate complex **3b** (C_6D_6, r.t.).

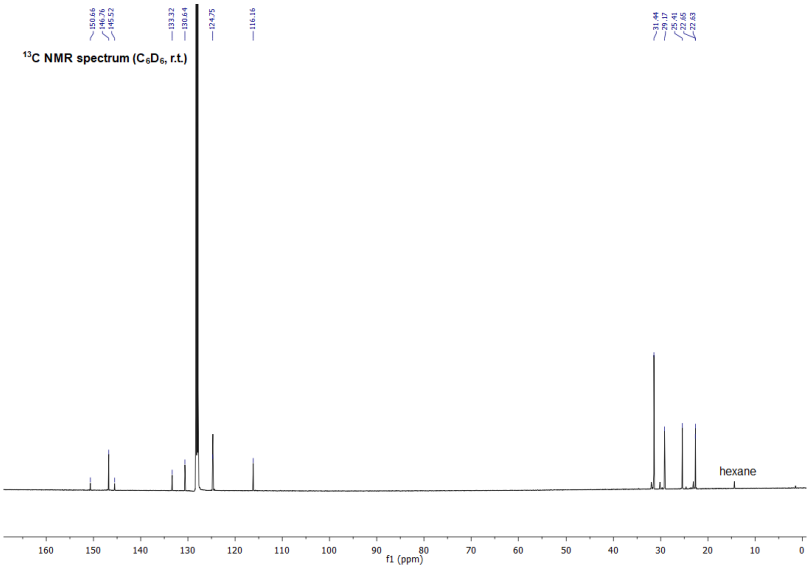

Figure S23: ^{13}C NMR spectrum of silicon carbonate complex **3b** (C_6D_6, r.t.).

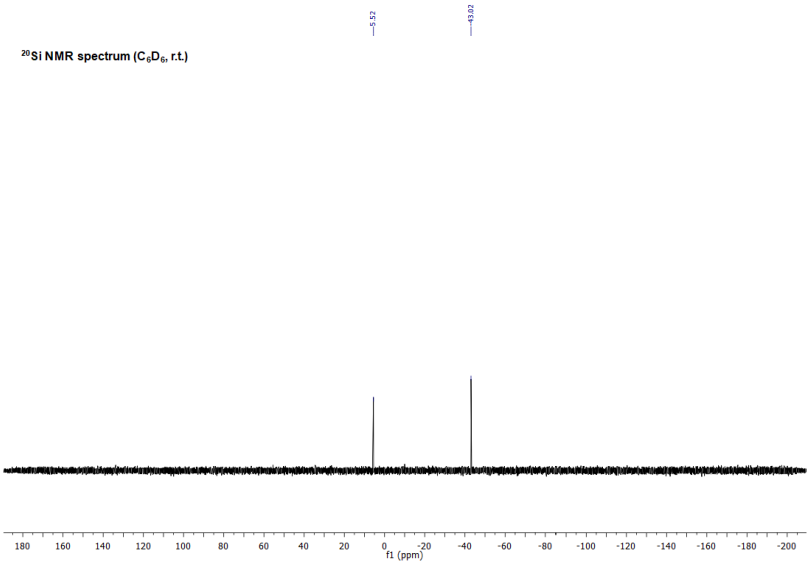

Figure S24: ^{29}Si NMR spectrum of silicon carbonate complex **3b** (C_6D_6, r.t.).

Synthesis of IPrNSi(OMe)(OH)SiR$_3$ (R = TMS 4a, R = *t*-Bu 4b)

To a yellowish solution of **2a** (35 mg, 50.4 µmol, 1.00 eq) in toluene (2 mL) were added a few drops of methanol (dried and degassed). The solution immediately turned colorless and was stirred for additional 20 min. Removal of all volatiles and crystallization in toluene/*n*-hexane at -35 °C for 2 days gave compound **4a** (26 mg, 35.7 µmol, 71%) as colorless crystals suitable for single crystal X-ray analysis. The analogue procedure was repeated for the preparation of compound **4b** (69%). For the synthesis of **4a**, also acetonitrile solutions of tetra-coordinate silanone **2a** × CD_3CN were used successfully.

Compound 4a:

^{1}H NMR (500 MHz, C_6D_6, r.t.): δ = 7.15 – 7.09 (m, 6H, C*H*-Ar), 5.94 (s, 2H, C*H*-N), 3.41 (s, 3H, OMe), 3.17 (overlapping hept, *J* = 6.9 Hz, 4H, C*H*), 1.45 (d, *J* = 6.9 Hz, 6H, CH_3), 1.42 (d, *J* = 6.9 Hz, 6H, CH_3) 1.13 (d, *J* = 6.9 Hz, 6H, CH_3), 1.11 (d, *J* = 6.9 Hz, 6H, CH_3), 0.28 (s, 27H, Si*TMS*$_3$).

^{13}C NMR (126 MHz, C_6D_6, r.t.): δ = 148.1 (*C*-Ar), 148.1 (*C*-Ar), 143.7 (N-*C*-N), 134.8 (*C*-Ar), 129.9 (*C*H-Ar), 124.4 (*C*H-Ar), 124.1 (*C*H-Ar), 114.9 (*C*H-N), 49.6 (O*C*H$_3$), 29.2 (*C*H), 28.9 (*C*H), 25.5 (*C*H$_3$), 25.2 (*C*H$_3$), 23.1 (*C*H$_3$), 23.0 (*C*H$_3$), 3.1 (Si*TMS*$_3$).

^{29}Si NMR (99 MHz, C_6D_6, r.t.): δ = -10.6 (*TMS*$_3$), -38.6 (*central Si*), -137.6 (*Si*TMS$_3$).

EA experimental (calculated): C 60.07 (61.18), H 9.21 (9.30), N 5.64 (5.78) %.

Compound 4b:

^{1}H NMR (500 MHz, C_6D_6, r.t.): δ = 7.18 – 7.14 (m, 2H, *m*-C*H*-Ar), 7.12 – 7.07 (m, 4H, *p*-C*H*-Ar) 5.96 (s, 2H, C*H*-N), 3.45 (s, 3H, OMe), 3.22 (hept, *J* = 6.9 Hz, 2H, C*H*), 3.11 (hept, *J* = 6.9 Hz, 2H, C*H*) 1.38 (d, *J* = 6.9 Hz, 12H, CH_3), 1.23 (s, 27H, Si*t-Bu*$_3$). 1.11 (d, *J* = 6.9 Hz, 6H, CH_3) 1.10 (d, *J* = 6.9 Hz, 6H, CH_3).

^{13}C NMR (126 MHz, C_6D_6, r.t.): δ = 148.0 (*C*-Ar), 147.9 (*C*-Ar), 143.2 (N-*C*-N), 134.9 (*C*-Ar), 129.9 (*C*H-Ar), 124.3 (*C*H-Ar), 124.1 (*C*H-Ar), 115.0 (*C*H-N), 49.7 (O*C*H$_3$), 31.9 (C(*C*H$_3$)$_3$), 28.9 (*C*H), 28.8 (*C*H), 25.7 (*C*H$_3$), 25.5 (*C*H$_3$), 22.7 (*C*H$_3$), 22.5 (*C*(CH$_3$)$_3$), 22.4 (*C*H$_3$).

^{29}Si NMR (99 MHz, C_6D_6, r.t.): δ = 1.2 (Si*t*-Bu$_3$), -46.6 (*central Si*).

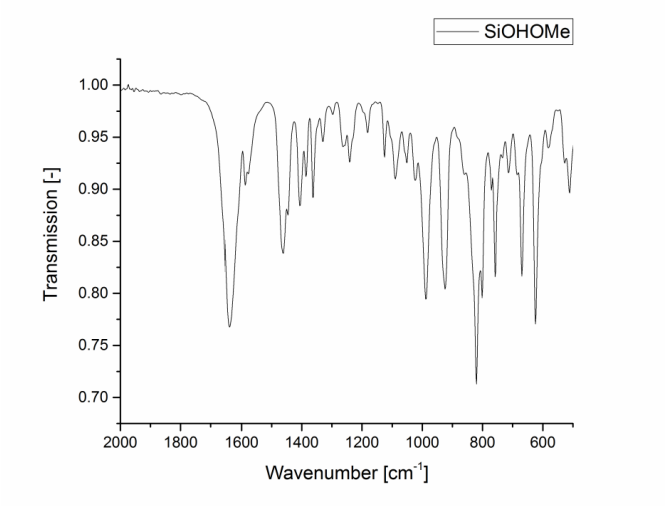

Figure S25: IR spectrum of compound **4a** (cm^{-1}): 1635 (s), 1584 (w), 1463 (m), 1403 (w), 1361 (w), 1237 (w), 1093 (w), 985 (s), 925 (s), 824 (s), 757 (m), 666 (m), 624 (s).

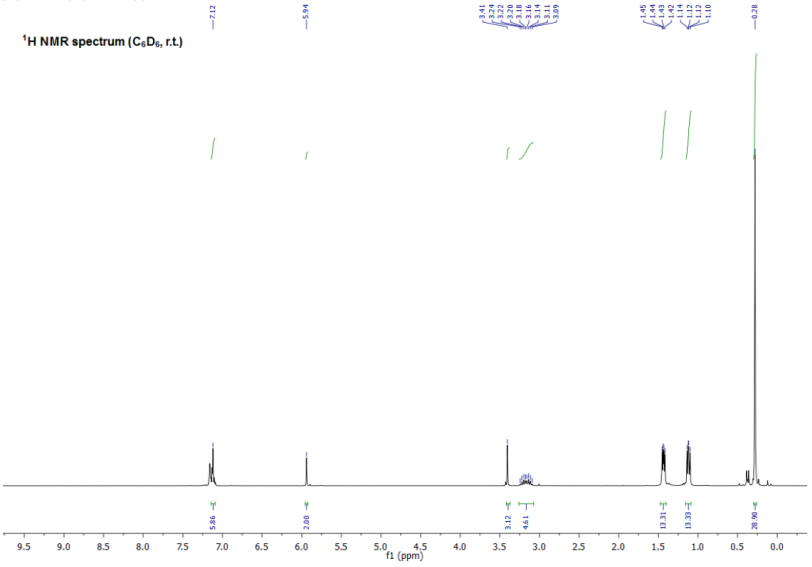

Figure S26: ^{1}H NMR spectrum of compound **4a** (C_6D_6, r.t.).

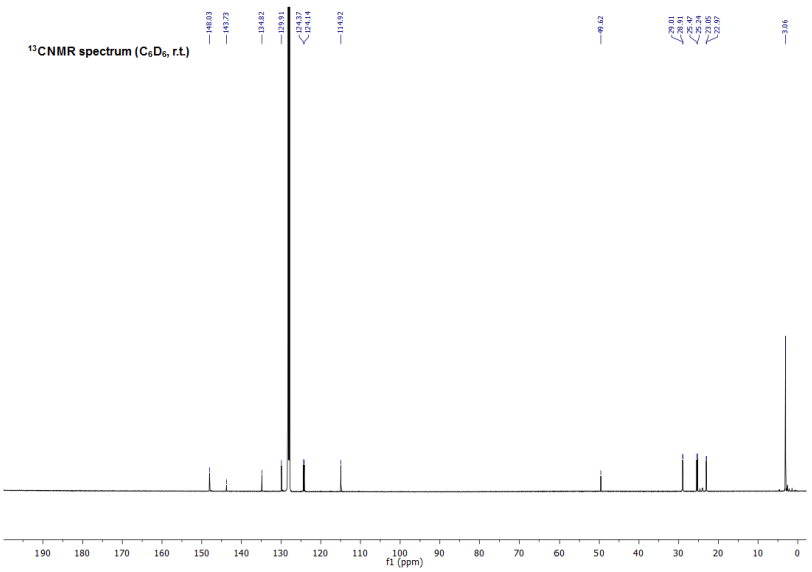

Figure S27: ^{13}C NMR spectrum of compound **4a** (C_6D_6, r.t.).

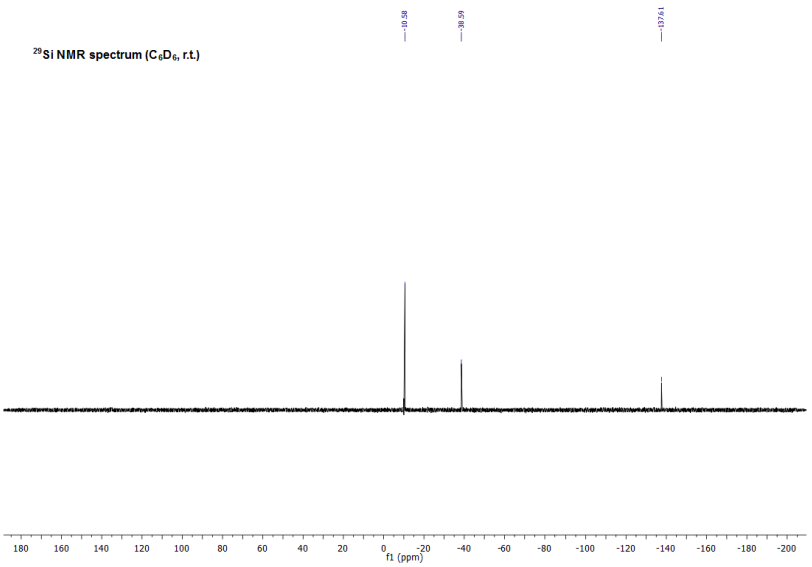

Figure S28: ^{29}Si NMR spectrum of compound **4a** (C_6D_6, r.t.).

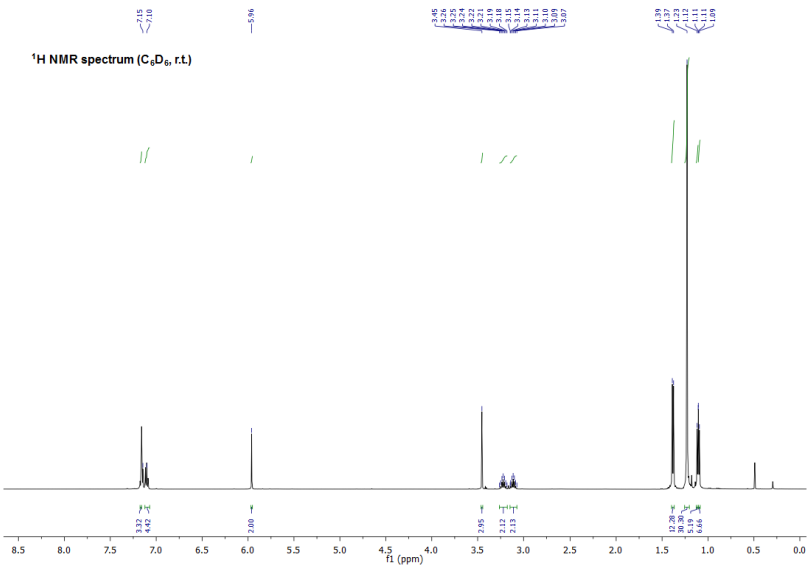

Figure S29: ^{1}H NMR spectrum of compound **4b** (C_6D_6, r.t.).

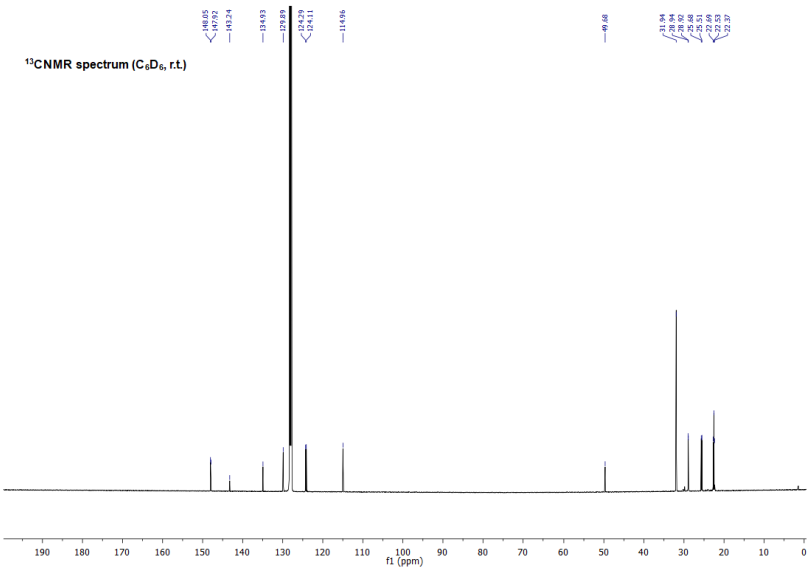

Figure S30: ^{13}C NMR spectrum of compound **4b** (C_6D_6, r.t.).

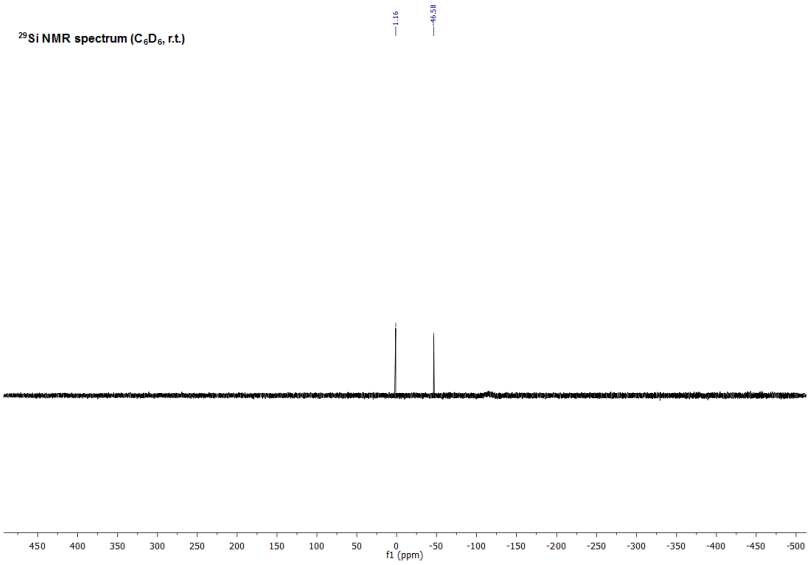

Figure S31: ^{29}Si NMR spectrum of compound **4b** (C_6D_6, r.t.).

Trapping Experiments of Transient Disilene INT with Ethylene and IMe_4

Synthesis of IPrNTMSOSi(CH_2CH_2)SiTMS_2 (5)

A J. Young PTFE tube was loaded with solid silanone **2a** (14 mg, 20.2 µmol, 1.00 eq), addition of THF-d_8 (0.5 mL) instantly formed a strongly yellow colored solution of transient disilene **INT** (NMR data see above). Subsequently, the solution was exposed to ethylene gas (1 bar) and monitored *via* NMR spectroscopy. After 10 min the yellow color faded completely and full conversion to 1,2-disilacyclobutane **5** was detected (structure verified *via* 2D NMR experiments and matching theoretical NMR shifts). In a second experiment, the slow decomposition of **2a** in C_6D_6 was repeated in ethylene atmosphere, here as well the formation of 1,2-disiletane **5** was observed.

^{1}H NMR (500 MHz, THF-d_8, r.t.): δ = 7.35 – 7.30 (m, 2H, *m*-C*H*-Ar), 7.27 – 7.23 (m, 4H, *m*-C*H*-Ar), 6.55 (s, 2H, C*H*-N), 3.20 (hept, *J* = 6.9 Hz, 2H, C*H*), 3.12 (hept, *J* = 6.9 Hz, 2H, C*H*), 1.32 (d, *J* = 6.9 Hz, 12H, CH_3), 1.30 (d, *J* = 6.9 Hz, 6H, CH_3) 1.21 (d, *J* = 6.9 Hz, 6H, CH_3), 1.15 (d, *J* = 6.9 Hz, 6H, CH_3), 0.99 – 0.94 (m, 2H, Si(CH_2CH$_2$)Si), 0.50 – 0.41 (m, 2H, Si(CH$_2$CH_2)Si), 0.39 – 0.36 (m, 1H, Si(CH_2CH$_2$)Si), 0.06 (s, 9H, Si*TMS*$_2$), -0.07 (s, 9H, Si*TMS*$_2$) -0.11 (s, 9H, O*TMS*).

^{13}C NMR (126 MHz, THF-d_8, r.t.): δ = 148.3 (*C*-Ar), 148.1 (*C*-Ar), 143.1 (N-*C*-N), 135.7 (*C*-Ar), 130.0 (*C*H-Ar), 125.0 (*C*H-Ar), 124.9 (*C*H-Ar), 116.1 (*C*H-N), 31.1 (Si(*C*H$_2$CH$_2$)Si), 29.5 (*C*H), 24.5 (*C*H$_3$), 24.0 (*C*H$_3$), 3.2 (O*TMS*), 1.6 (Si*TMS*$_2$), 1.5 (Si*TMS*$_2$),-0.3 (Si(CH$_2$*C*H$_2$)Si).

^{29}Si NMR (99 MHz, THF-d_8, r.t.): δ = 4.3 (O*TMS*), -14.6 (Si*TMS*$_2$), -14.8 (Si*TMS*$_2$), -35.7 (*Si*OTMS), -39.8 (*Si*TMS$_2$).

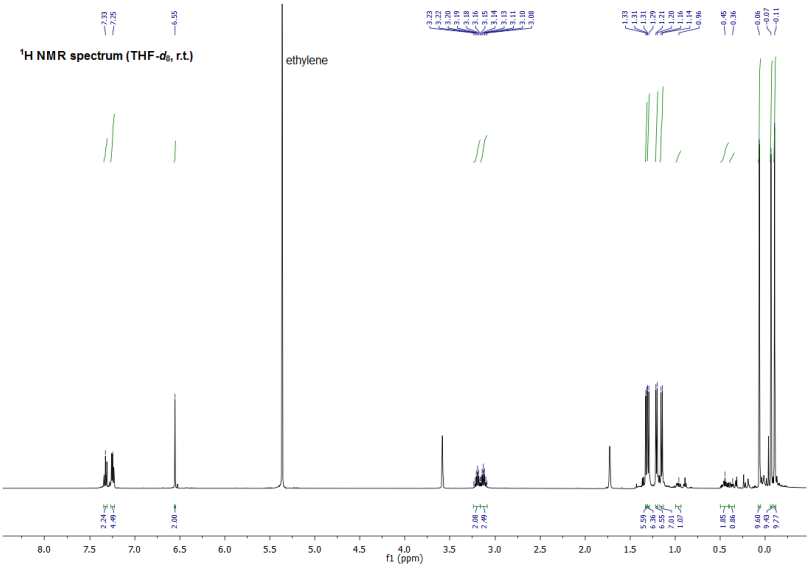

Figure S32: ^{1}H NMR spectrum of 1,2-disiletane **5** (THF-d_8, r.t.).

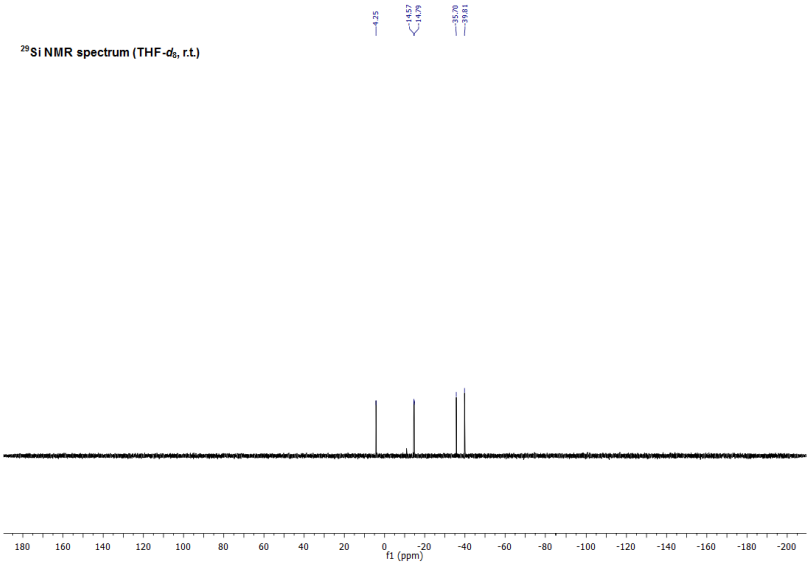

Figure S33: ^{29}Si NMR spectrum of 1,2-disiletane **5** (THF-d_8, r.t.)

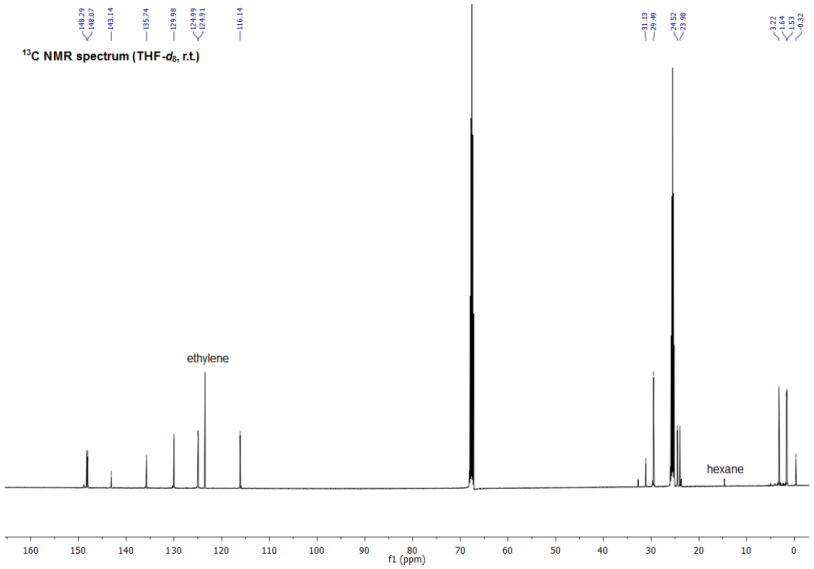

Figure S34: ^{13}C NMR spectrum of 1,2-disiletane **5** (THF-d_8, r.t.)

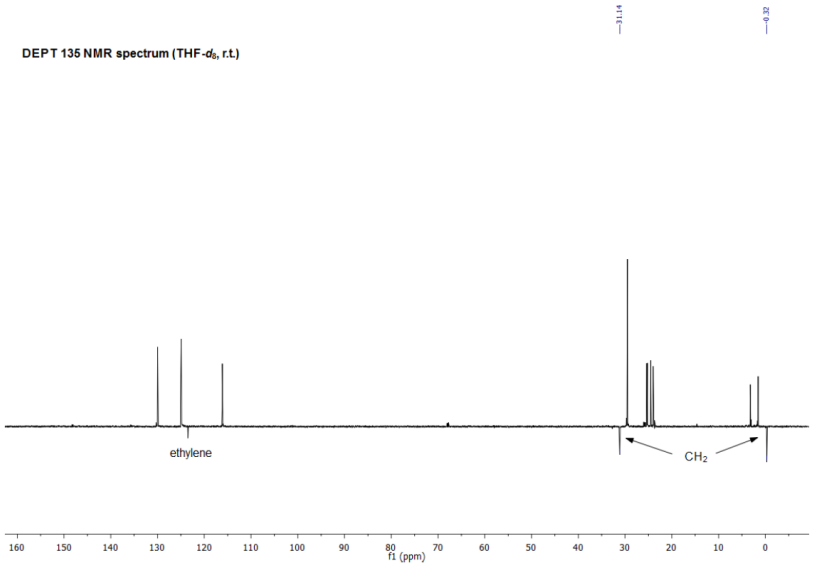

Figure S35: DEPT 135 NMR spectrum of 1,2-disiletane **5** (THF-d_8, r.t.)

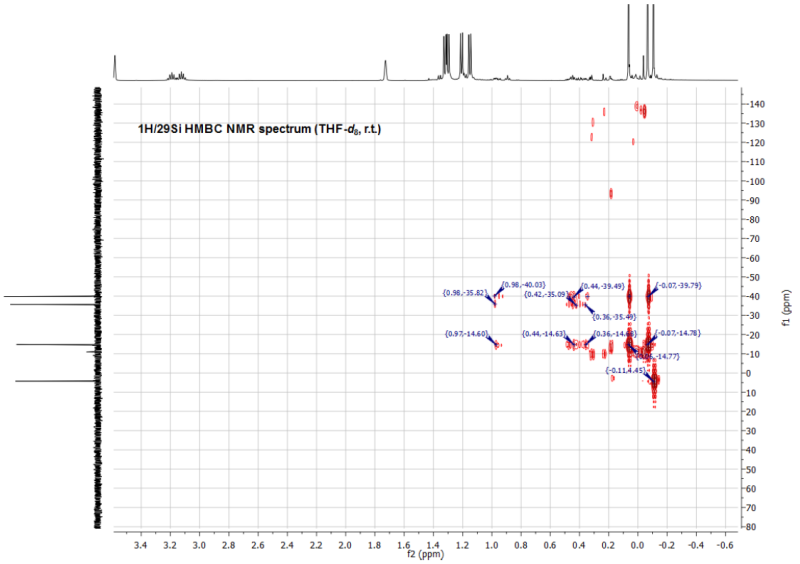

Figure S36: $^{1}H/^{29}Si$ HMBC NMR spectrum of 1,2-disiletane **5** (THF-d_8, r.t.)

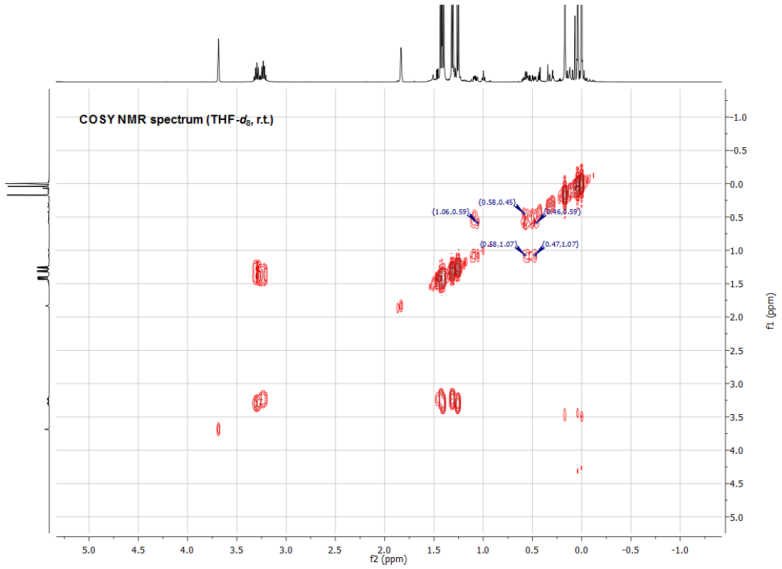

Figure S37: COSY NMR spectrum of 1,2-disiletane **5** (THF-d_8, r.t.)

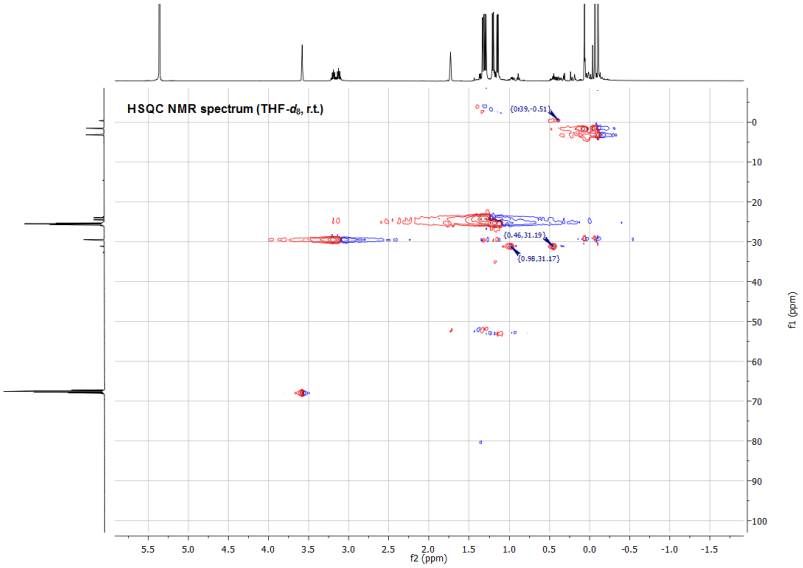

Figure S38: HSQC NMR spectrum of 1,2-disiletane **5** (THF-d_8, r.t.)

Synthesis of IMe$_4$ Stabilized Zwitterionic Disilene (6)

To a yellowish toluene (2 mL) solution of **2a** (29 mg, 41.9 µmol, 1.00 eq) was added IMe$_4$ (5.2 mg, 41.9 µmol, 1.00 eq) in toluene (1 mL). The solution immediately turned orange-red and was stirred additional 20 min. Removal of all volatiles and crystallization from *n*-hexane at -35 °C for 1 day gave IMe$_4$ stabilized zwitterionic disilene **6** (20 mg, 24.4 µmol, 58%) as orange-red crystals suitable for single crystal X-ray analysis. Compound **6** is permanently stable as a solid and in C_6D_6 solution at room temperature. Alternatively, intermediary disilene **INT** can also be trapped, by first inducing the 1,3-silyl migration of silanone **2a** with THF, followed by the addition of IMe$_4$.

^{1}H NMR (500 MHz, C_6D_6, r.t.): δ = 7.22 – 7.13 (m, 4H, *m*-C*H*-Ar), 6.98 – 6.93 (m, 2H, *p*-C*H*-Ar), 5.91 (s, 2H, C*H*-N), 3.44 (hept, *J* = 6.9 Hz, 2H, C*H*), 3.13 (s, 6H, IMe$_4$-NC*H*$_3$), 3.09 (hept, *J* = 6.9 Hz, 2H, C*H*), 1.40 (d, *J* = 6.9 Hz, 12H, C*H*$_3$), 1.34 (s, 6H, IMe$_4$-C*H*$_3$), 1.12 (d, *J* = 6.9 Hz, 6H, C*H*$_3$), 1.08 (d, *J* = 6.9 Hz, 6H, C*H*$_3$), 0.42 (s, 18H, Si*TMS*$_2$), 0.28 (s, 9H, O*TMS*).

^{13}C NMR (126 MHz, C_6D_6, r.t.): δ = 156.3 (IMe$_4$-N-*C*-N), 148.3 (*C*-Ar), 148.2 (*C*-Ar), 140.2 (N-*C*-N), 135.9 (*C*-Ar), 129.2 (*C*H-Ar), 124.8 (*C*H-Ar), 124.3 (*C*H-Ar), 124.2 (IMe$_4$-*C*=*C*), 115.3 (*C*H-N), 33.2 (IMe$_4$-NCH$_3$), 28.7 (*C*H), 28.4 (*C*H), 25.7 (*C*H$_3$), 24.5 (*C*H$_3$), 22.0 (*C*H$_3$), 7.9 (IMe$_4$-C*C*H$_3$), 7.2 (Si*TMS*$_2$), 4.8 (O*TMS*).

^{29}Si NMR (99 MHz, C_6D_6, r.t.): δ = 6.1 (O*TMS*), -7.1 (Si*TMS*$_2$), -35.2 (*Si*OTMS), -174.6 (*Si*TMS$_2$).

EA experimental (calculated): C 62.37 (63.10), H 9.16 (9.24), N 8.06 (8.56) %.

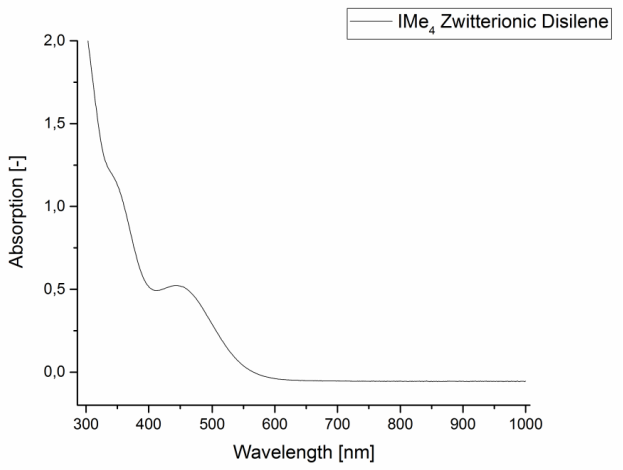

Figure S39. UV-Vis spectrum of IMe$_4$ stabilized zwitterionic disilene **6** λ_{max} (r.t., toluene, 4.0×10^{-4} M) = 342, 449 nm.

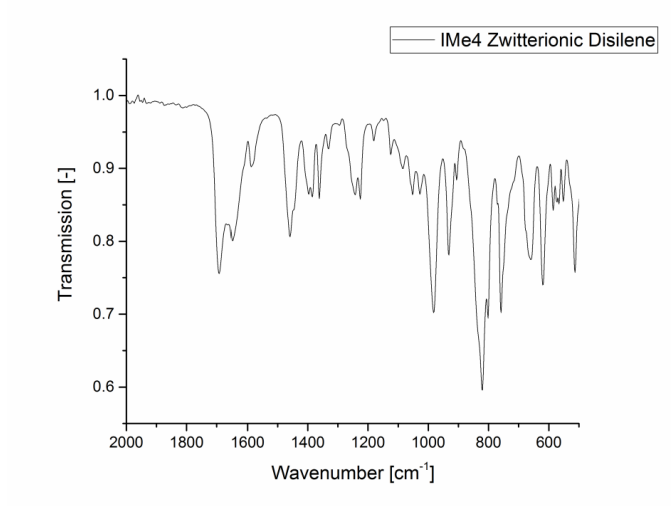

Figure S40: IR spectrum of IMe_4 stabilized zwitterionic disilene **6** (cm^{-1}): 1690 (m), 1641 (m), 1586 (s), 1454 (m), 1401 (s), 1229 (s), 978 (m), 929 (m), 832 (s), 751 (m), 662 (m), 615 (m).

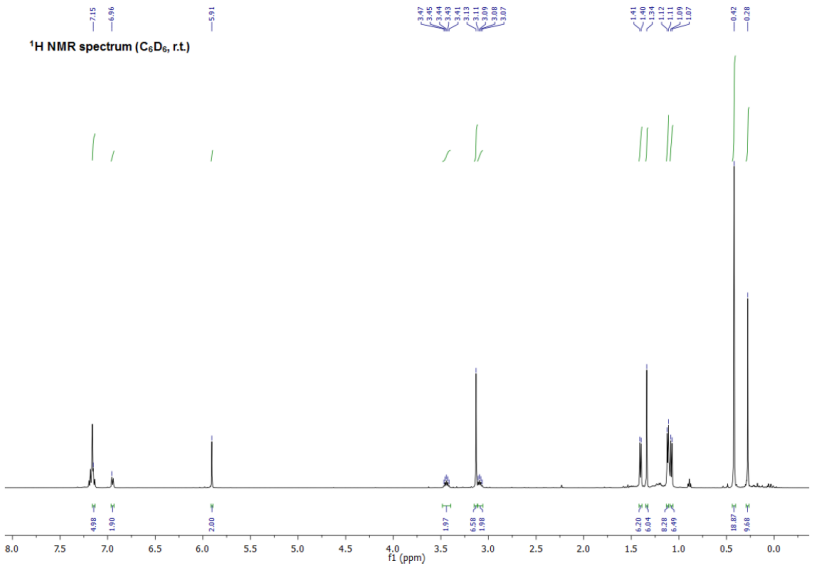

Figure S41: ^1H NMR spectrum of IMe_4 stabilized zwitterionic disilene **6** (C_6D_6, r.t.).

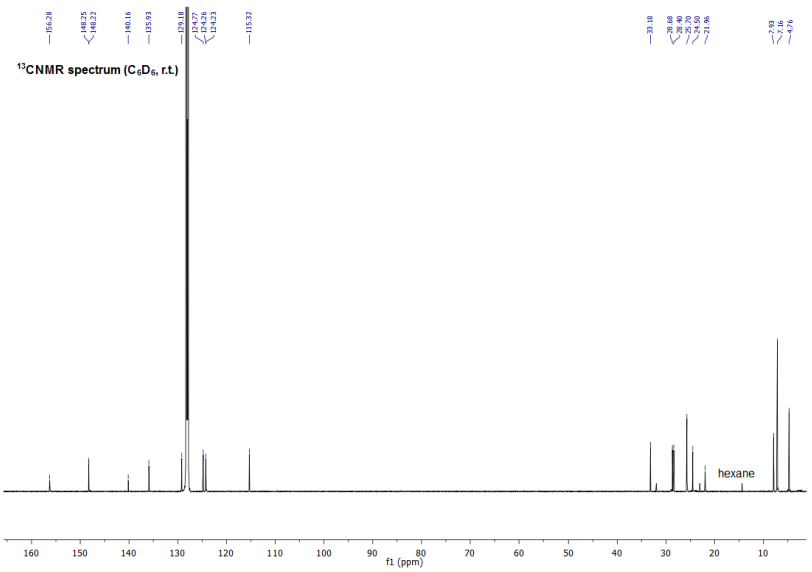

Figure S42: ^{13}C NMR spectrum of IMe$_4$ stabilized zwitterionic disilene **6** (C_6D_6, r.t.).

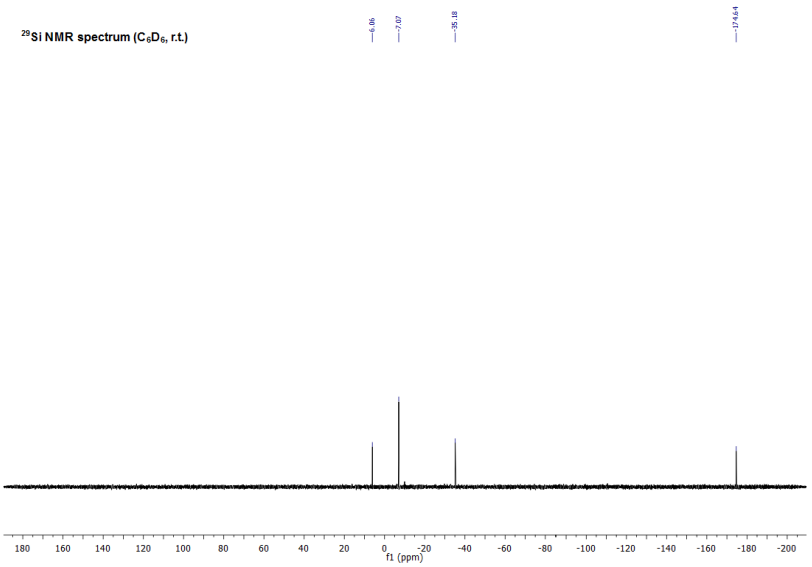

Figure S43: ^{29}Si NMR spectrum of IMe$_4$ stabilized zwitterionic disilene **6** (C_6D_6, r.t.).

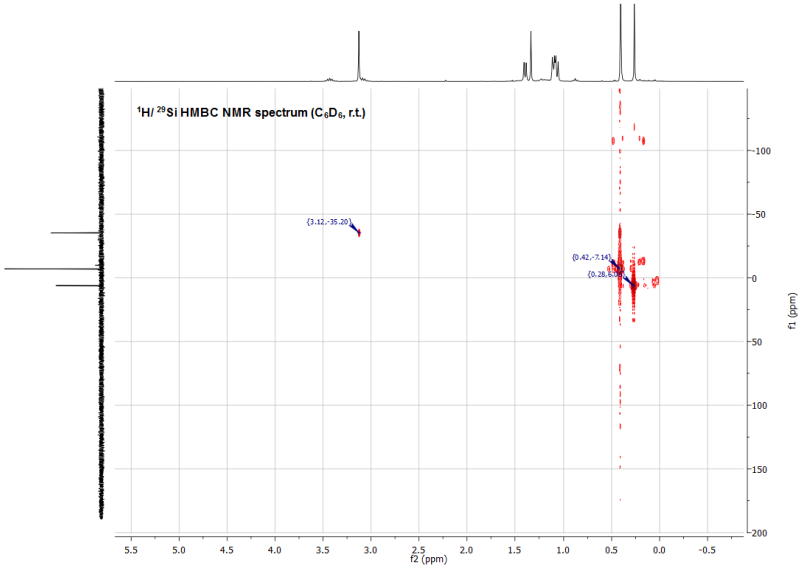

Figure S44: ^{1}H/^{29}Si HMBC NMR spectrum of IMe_4 stabilized zwitterionic disilene **6** (C_6D_6, r.t.).

Synthesis of IPrNSi(II)OSi*t*-Bu$_3$ (7)

As already stated, silanone **2b** quantitatively forms *N*,*O*-silylene **7** in C_6D_6 or THF-d_8 at room temperature within 48 h ($t_{1/2}$ = 24 h). By heating the solution to 60 °C, this transformation can be accelerated and full conversion was detected by NMR spectroscopy in less than 1 h. Hence, a solution of **2b** (100 mg, 155 µmol, 1.00 eq) in toluene (5 mL) was heated to 60 °C for 1 h. Removal of all volatiles gave *N*,*O*-silylene **7** as colorless solid (100 mg, 155 µmol, quantitative yield). Crystals suitable for single crystal X-ray analysis were obtained by cooling a concentrated *n*-hexane solution of **7** at -35 °C for several days. *N*,*O*-Silylene **7** is completely stable as a solid and in solution at room temperature.

^{1}H NMR (500 MHz, C_6D_6, r.t.): δ = 7.24 – 7.17 (m, 2H, *p*-C*H*-Ar), 7.15 – 7.09 (m, 4H, *m*-C*H*-Ar), 5.99 (s, 2H, C*H*-N), 3.10 (hept, *J* = 6.8 Hz, 4H, C*H*), 1.46 (d, *J* = 6.8 Hz, 12H, CH_3), 1.17 (d, *J* = 6.8 Hz, 12H, CH_3), 1.07 (s, 27H, Si*t-Bu$_3$*).

^{13}C NMR (126 MHz, C_6D_6, r.t.): δ =, 147.7 (*C*-Ar), 146.6 (N-*C*-N) 133.5 (*C*-Ar), 129.9 (*C*H-Ar), 124.0 (*C*H-Ar), 114.9 (*C*H-N), 30.3 (C(*C*H$_3$)$_3$), 29.1 (*C*H), 24.6 (*C*H$_3$), 23.8 (*C*H$_3$), 22.8 (*C*(CH$_3$)$_3$).

^{29}Si NMR (99 MHz, C_6D_6, r.t.): δ = 58.9 (*central Si*), 4.4 (Si*t*-Bu$_3$).

EA experimental (calculated): C 71.92 (72.50), H 10.02 (9.83), N 6.31 (6.50) %.

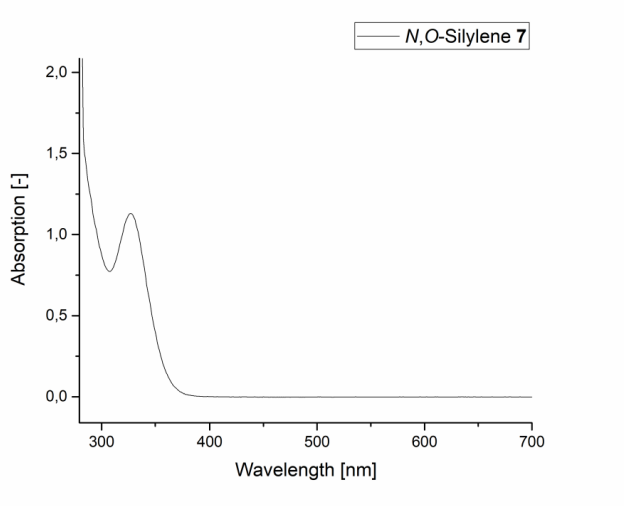

Figure S45. UV-Vis spectrum of *N*,*O*-silylene **7** λ_{max} (r.t., toluene, 8.0×10^{-4} M) = 328 nm.

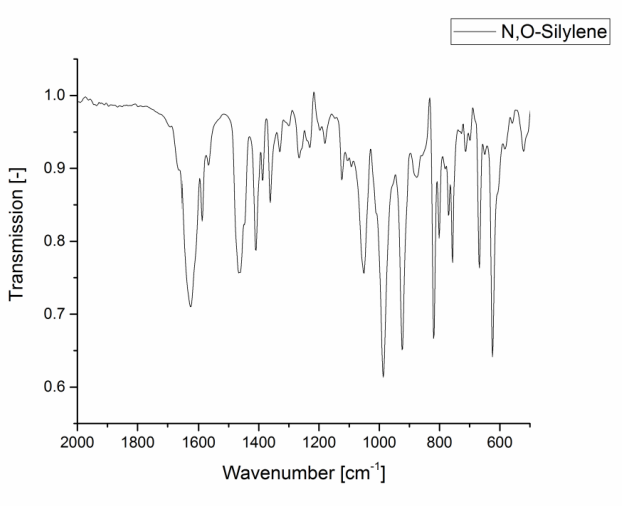

Figure S46: IR spectrum of *N,O*-silylene **7** (cm^{-1}): 1624 (s), 1459 (m), 1405 (m), 1365 (s), 1049 (m), 980 (s), 917 (s), 819 (s), 758 (m), 666 (m), 621 (s).

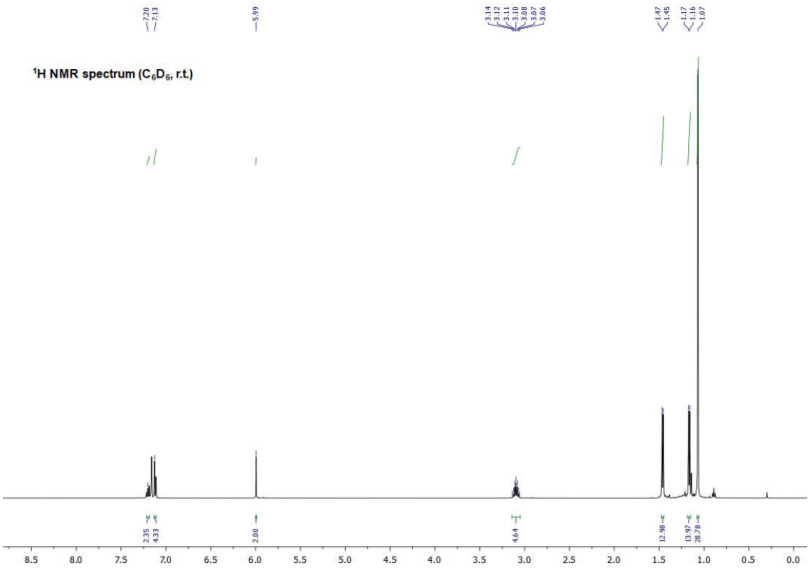

Figure S47: ^{1}H NMR spectrum of *N,O*-silylene **7** (C_6D_6, r.t.).

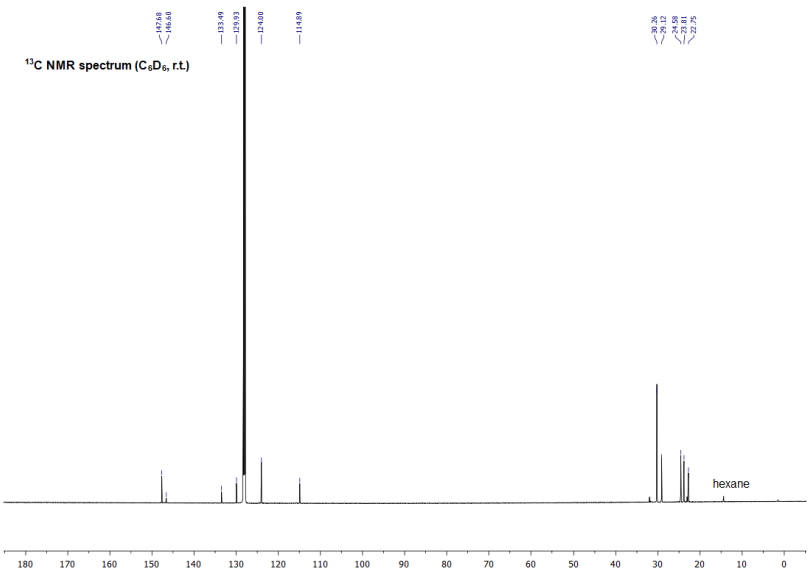

Figure S48: ^{13}C NMR spectrum of *N,O*-silylene **7** (C_6D_6, r.t.).

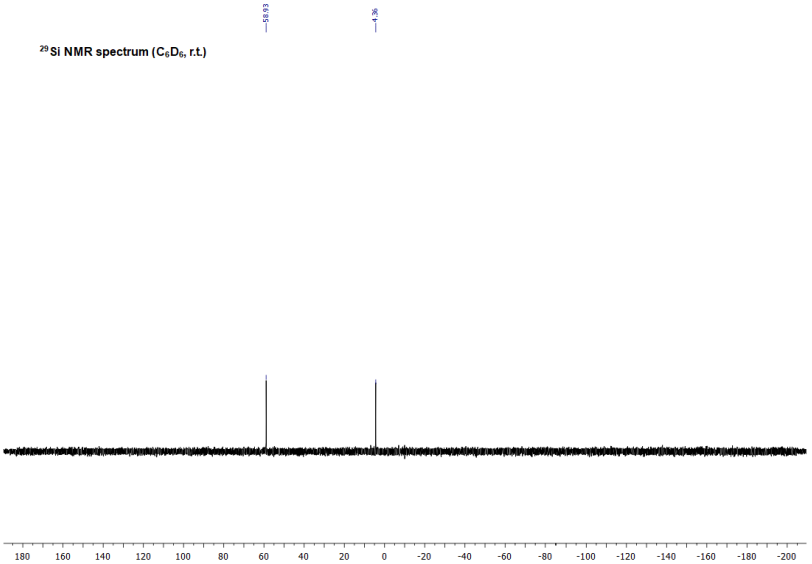

Figure S49: ^{29}Si NMR spectrum of *N,O*-silylene **7** (C_6D_6, r.t.).

NMR Studies on the Reactivity of *N*,*O*-Silylene 7 towards Ethylene and Hydrogen

Synthesis of IPrNSi(CH$_2$CH$_2$)OSi*t*-Bu$_3$ (8)

A C_6D_6 (0.5 mL) solution of *N*,*O*-silylene **7** (15 mg, 23.2 µmol, 1.00 eq) in a J. Young PTFE tube was exposed to ethylene or hydrogen gas (1 bar), respectively. With ethylene, monitoring the reaction at room temperature showed silirane **8** as sole product after 20 min reaction time. Removal of all volatiles gave compound **8** as a colorless sticky solid (15.7 mg, 23.2 µmol, quantitative yield). Compound **8** is completely stable as a solid and in solution at room temperature. For hydrogen, no activation was observed even after heating the reaction solution to 60 °C for several days.

^{1}H NMR (500 MHz, C_6D_6, r.t.): δ = 7.26 – 7.21 (m, 2H, *p*-C*H*-Ar), 7.14 – 7.11 (m, 4H, *m*-C*H*-Ar), 5.94 (s, 2H, C*H*-N), 3.15 (hept, *J* = 6.8 Hz, 4H, C*H*), 1.40 (d, *J* = 6.8 Hz, 12H, C*H*$_3$), 1.15 (d, *J* = 6.8 Hz, 12H, C*H*$_3$), 1.07 (s, 27H, Si*t-Bu*$_3$), 0.91 – 0.85 (m, 2H, Si*(CH*$_2$-C*H*$_2$), 0.03 – -0.03 (m, 2H, Si*(CH*$_2$-C*H*$_2$).

^{13}C NMR (126 MHz, C_6D_6, r.t.): δ = 147.5 (*C*-Ar), 142.7 (N-*C*-N), 134.5 (*C*-Ar), 129.8 (*C*H-Ar), 123.0 (*C*H-Ar), 114.6 (*C*H-N), 30.2 (C(*C*H$_3$)$_3$), 29.0 (*C*H), 24.7 (*C*H$_3$), 23.4 (*C*H$_3$), 23.1 (*C*(CH$_3$)$_3$), 4.8 (*C*H$_2$*C*H$_2$).

^{29}Si NMR (99 MHz, C_6D_6, r.t.): δ = 3.4 (Si*t*-Bu$_3$), -75.0 (*central Si*).

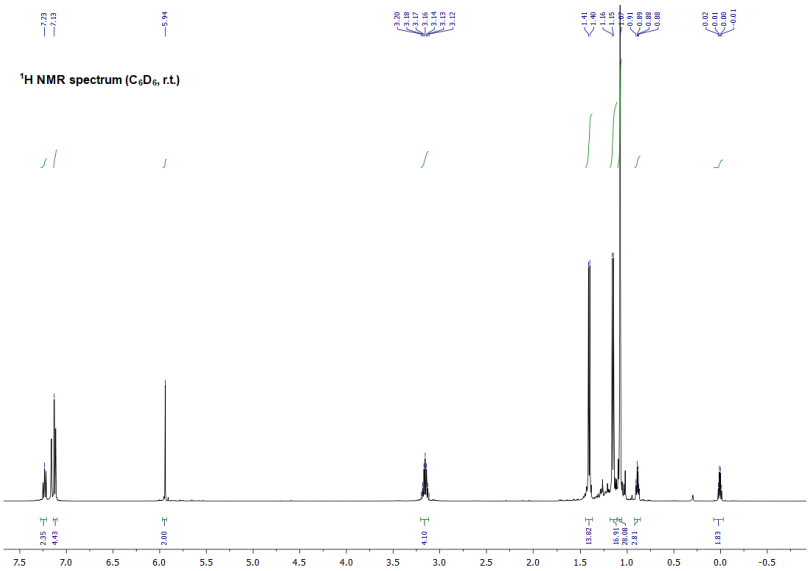

Figure S50: ^{1}H NMR spectrum of silirane **8** (C_6D_6, r.t.).

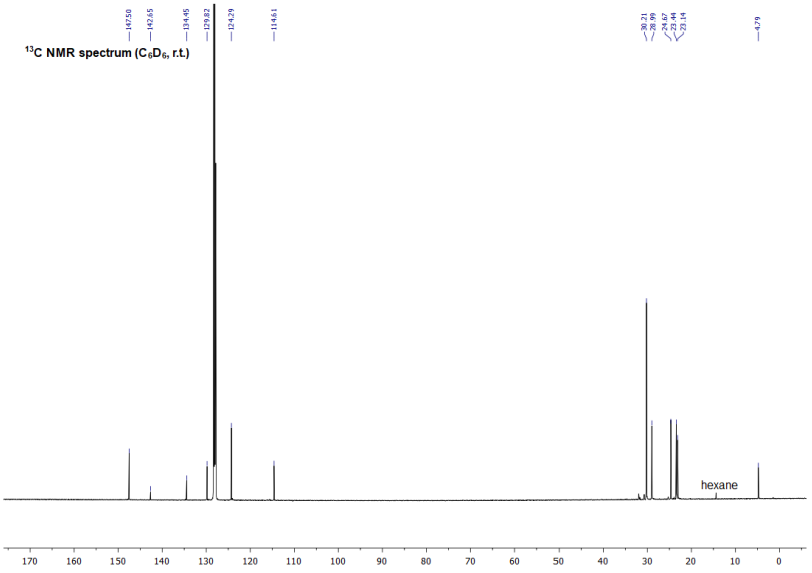

Figure S51: ^{13}C NMR spectrum of silirane **8** (C_6D_6, r.t.).

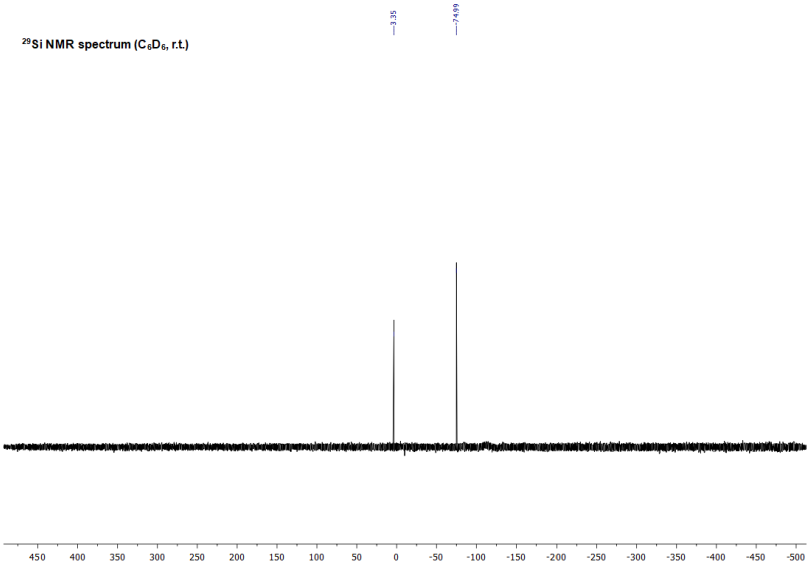

Figure S52: ^{29}Si NMR spectrum of silirane **8** (C_6D_6, r.t.).

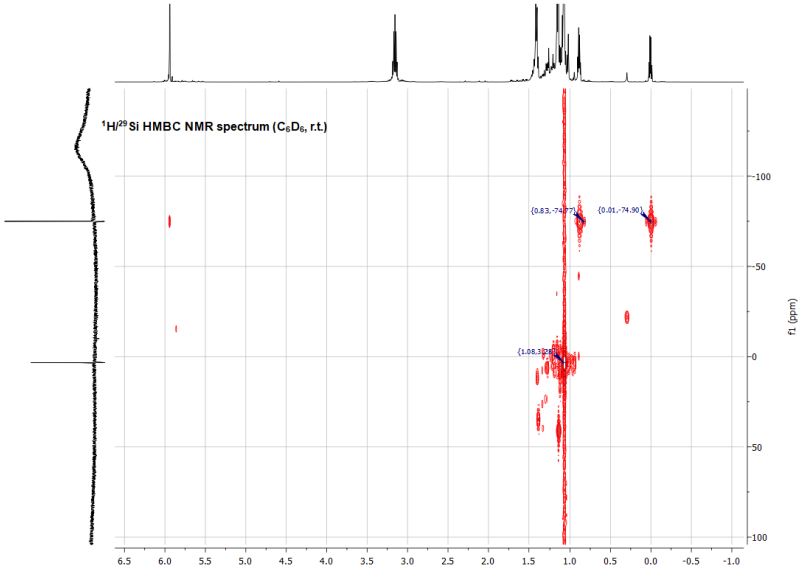

Figure S53: ^{1}H/^{29}Si HMBC NMR spectrum of silirane **8** (C_6D_6, r.t.).

2. X-ray Crystallographic Data

A) General information

The X-ray intensity data of **2a** × **CD_3CN**, **4a**, **6** and **7** were collected on an X-ray single crystal diffractometer equipped with a CMOS detector (Bruker Photon-100), an IMS microsource with MoKα radiation (λ = 0.71073 Å) and a Helios mirror optic by using the APEX III software package.[S6] The X-ray intensity data of **2b** were collected on an X-ray single crystal diffractometer equipped with a CMOS detector (Bruker Photon-100), a rotating anode (Bruker TXS) with MoKα radiation (λ = 0.71073 Å) and a Helios mirror optic by using the APEX III software package.[S6] The measurements were performed on single crystals coated with perfluorinated ether. The crystals were fixed on the top of a microsampler, transferred to the diffractometer and frozen under a stream of cold nitrogen. A matrix scan was used to determine the initial lattice parameters. Reflections were merged and corrected for Lorenz and polarization effects, scan speed, and background using SAINT.[S7] Absorption corrections, including odd and even ordered spherical harmonics were performed using SADABS.[S7] Space group assignments were based upon systematic absences, E statistics, and successful refinement of the structures. Structures were solved by direct methods with the aid of successive difference Fourier maps, and were refined against all data using the APEX III software in conjunction with SHELXL-2014[S8] and SHELXLE[S9]. H atoms bound to aluminium atoms were allowed to refine freely. Other H atoms were placed in calculated positions and refined using a riding model, with methylene and aromatic C–H distances of 0.99 and 0.95 Å, respectively, and $U_{iso}(H) = 1.2 \cdot U_{eq}(C)$. Full-matrix least-squares refinements were carried out by minimizing $\Delta w(F_o^2 - F_c^2)^2$ with SHELXL-97[S10] weighting scheme. Neutral atom scattering factors for all atoms and anomalous dispersion corrections for the non-hydrogen atoms were taken from International Tables for Crystallography.[S11] The image of the crystal structure was generated by Mercury.[S12] CCDC 1577580-1577584 contain the supplementary data for the structures. These data can be obtained free of charge from the Cambridge Crystallographic Data Centre.

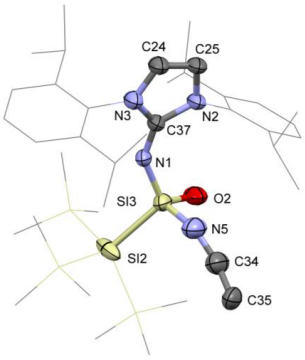

Figure S54: Molecular structure of silanone **2a** × **CD_3CN** in the solid state with ellipsoids set at the 50% probability level. For clarity, hydrogen atoms and co-crystallized solvent molecules are omitted and TMS as well as Dipp groups are simplified as wireframes. Selected bond lengths (Å) and angles (deg): Si3–O2 1.632(6), Si3–N5 1.749(7), Si3–N1 1.670(5), N1–C37 1.277(7), C37–N2 1.390(8), C37–N3 1.397(9), N1–Si3–Si2 114.1(4), C37–N1–Si3 142.1(9).

Table S1: Sample and crystal data for **2a** × **CD_3CN**.

Identification code	WenDa48	
Chemical formula	$C_{38}H_{66}N_4OSi_5$	
Formula weight	735.39	
Temperature	100(2) K	
Wavelength	0.71073 Å	
Crystal size	0.133 mm x 0.276 mm x 0.278 mm	
Crystal habit	clear colorless fragment	
Crystal system	monoclinic	
Space group	*P* 1 $2_1/n$ 1	
Unit cell dimensions	a = 10.3704(11) Å	α = 90°
	b = 33.835(3) Å	β = 97.371(3)°
	c = 12.9525(12) Å	γ = 90°
Volume	4507.2(8) Å^3	
Z	4	
Density (calculated)	1.084 g/cm^3	
Absorption coefficient	0.190 mm^{-1}	
F(000)	1600	

Table S2: Data collection and structure refinement for **2a** × **CD_3CN**.

Diffractometer	Bruker D8 Venture, CMOS detector (Bruker Photon-100)	
Radiation source	IMS microsource, Mo	
Theta range for data collection	2.32 to 25.03°	
Index ranges	-12<=h<=12, -40<=k<=40, -15<=l<=15	
Reflections collected	48889	
Independent reflections	7974 [R(int) = 0.0423]	
Coverage of independent reflections	99.9%	
Absorption correction	multi-scan	
Min. and max. transmission	0.6905 and 0.7453	
Refinement method	Full-matrix least-squares on F^2	
Refinement program	SHELXL-2014/7 (Sheldrick, 2014)	
Function minimized	$\Sigma\, w(F_o^2 - F_c^2)^2$	
Data / restraints / parameters	7974 / 682 / 902	
Goodness-of-fit on F^2	1.217	
Δ/σ_{max}	0.011	
Final R indices	5222 data; I>2σ(I)	R1 = 0.0941, wR2 = 0.2488
	all data	R1 = 0.1366, wR2 = 0.2777
Weighting scheme	$w=1/[\sigma^2(F_o^2)+(0.1137P)^2+6.2488P]$ where $P=(F_o^2+2F_c^2)/3$	
Largest diff. peak and hole	1.312 and -0.629 eÅ^{-3}	
R.M.S. deviation from mean	0.073 eÅ^{-3}	

Table S3: Sample and crystal data for **2b**.

Identification code	ReiDo8	
Chemical formula	$C_{30}H_{63}N_3OSi_3$	
Formula weight	646.10	
Temperature	100(2) K	
Wavelength	0.71073 Å	
Crystal size	0.138 mm x 0.144 mm x 0.517 mm	
Crystal habit	clear colorless fragment	
Crystal system	monoclinic	
Space group	$P\ 1\ 2_1/c\ 1$	
Unit cell dimensions	a = 13.987(10) Å	α = 90°
	b = 21.397(15) Å	β = 92.58(2)°
	c = 27.532(12) Å	γ = 90°
Volume	8231(10) Å^3	
Z	8	
Density (calculated)	1.043 g/cm^3	
Absorption coefficient	0.117 mm^{-1}	
F(000)	2832	

Table S4: Data collection and structure refinement for **2b**.

Diffractometer	Bruker D8 Venture, CMOS detector (Bruker Photon-100)	
Radiation source	TXS rotating anode, Mo	
Theta range for data collection	1.92 to 25.03°	
Index ranges	-16<=h<=16, -25<=k<=25, -32<=l<=32	
Reflections collected	193064	
Independent reflections	14326 [R(int) = 0.0786]	
Coverage of independent reflections	98.4%	
Absorption correction	multi-scan	
Min. and max. transmission	0.6460 and 0.7453	
Refinement method	Full-matrix least-squares on F^2	
Refinement program	SHELXL-2014/7 (Sheldrick, 2014)	
Function minimized	$\Sigma\ w(F_o^2 - F_c^2)^2$	
Data / restraints / parameters	14326 / 557 / 1300	
Goodness-of-fit on F^2	1.108	
Δ/σ_{max}	0.001	
Final R indices	11065 data; I>2σ(I)	R1 = 0.0788, wR2 = 0.1647
	all data	R1 = 0.1059, wR2 = 0.1786
Weighting scheme	$w=1/[\sigma^2(F_o^2)+(0.0344P)^2+20.6132P]$ where $P=(F_o^2+2F_c^2)/3$	
Largest diff. peak and hole	0.533 and -0.469 eÅ^{-3}	
R.M.S. deviation from mean	0.062 eÅ^{-3}	

Table S5: Sample and crystal data for **4a**.

Identification code	WenDa39	
Chemical formula	$C_{37}H_{67}N_3O_2Si_5$	
Formula weight	726.38	
Temperature	100(2) K	
Wavelength	0.71073 Å	
Crystal size	0.134 mm x 0.180 mm x 0.509 mm	
Crystal habit	clear colorless fragment	
Crystal system	monoclinic	
Space group	$P\ 1\ 2_1/n\ 1$	
Unit cell dimensions	a = 13.2302(14) Å	α = 90°
	b = 11.9923(13) Å	β = 96.613(3)°
	c = 28.620(3) Å	γ = 90°
Volume	4510.7(8) Å^3	
Z	4	
Density (calculated)	1.070 g/cm^3	
Absorption coefficient	0.190 mm^{-1}	
F(000)	1584	

Table S6: Data collection and structure refinement for **4a**.

Diffractometer	Bruker D8 Venture, CMOS detector (Bruker Photon-100)	
Radiation source	IMS microsource, Mo	
Theta range for data collection	2.22 to 25.03°	
Index ranges	-15<=h<=15, -11<=k<=11, -34<=l<=34	
Reflections collected	39229	
Independent reflections	7963 [R(int) = 0.0595]	
Coverage of independent reflections	99.9%	
Absorption correction	multi-scan	
Min. and max. transmission	0.5815 and 0.7453	
Refinement method	Full-matrix least-squares on F^2	
Refinement program	SHELXL-2014/7 (Sheldrick, 2014)	
Function minimized	$\Sigma\, w(F_o^2 - F_c^2)^2$	
Data / restraints / parameters	7963 / 0 / 446	
Goodness-of-fit on F^2	1.082	
Δ/σ_{max}	0.001	
Final R indices	5981 data; I>2σ(I)	R1 = 0.0563, wR2 = 0.1234
	all data	R1 = 0.0832, wR2 = 0.1342
Weighting scheme	$w=1/[\sigma^2(F_o^2)+(0.0351P)^2+9.0134P]$ where $P=(F_o^2+2F_c^2)/3$	
Largest diff. peak and hole	0.483 and -0.402 eÅ^{-3}	
R.M.S. deviation from mean	0.065 eÅ^{-3}	

Table S7: Sample and crystal data for **6**.

Identification code	WenDa40	
Chemical formula	$C_{43}H_{75}N_5OSi_5$	
Formula weight	818.53	
Temperature	100(2) K	
Wavelength	0.71073 Å	
Crystal size	0.133 mm x 0.148 mm x 0.167 mm	
Crystal habit	clear orange fragment	
Crystal system	triclinic	
Space group	*P* -1	
Unit cell dimensions	a = 12.4388(5) Å	α = 103.4770(10)°
	b = 20.3429(7) Å	β = 99.6220(10)°
	c = 20.7659(8) Å	γ = 94.4910(10)°
Volume	5000.2(3) $Å^3$	
Z	2	
Density (calculated)	1.087 g/cm^3	
Absorption coefficient	0.178 mm^{-1}	
F(000)	1784	

Table S8: Data collection and structure refinement for **6**.

Diffractometer	Bruker D8 Venture, CMOS detector (Bruker Photon-100)	
Radiation source	IMS microsource, Mo	
Theta range for data collection	1.39 to 25.03°	
Index ranges	-14<=h<=14, -24<=k<=24, -24<=l<=24	
Reflections collected	93632	
Independent reflections	17649 [R(int) = 0.0682]	
Coverage of independent reflections	99.9%	
Absorption correction	multi-scan	
Min. and max. transmission	0.7185 and 0.7453	
Refinement method	Full-matrix least-squares on F^2	
Refinement program	SHELXL-2014/7 (Sheldrick, 2014)	
Function minimized	$\Sigma\, w(F_o^2 - F_c^2)^2$	
Data / restraints / parameters	17649 / 84 / 1095	
Goodness-of-fit on F^2	1.025	
Δ/σ_{max}	0.001	
Final R indices	13203 data; I>2σ(I)	R1 = 0.0476, wR2 = 0.0957
	all data	R1 = 0.0748, wR2 = 0.1063
Weighting scheme	$w=1/[\sigma^2(F_o^2)+(0.0327P)^2+5.0730P]$ where $P=(F_o^2+2F_c^2)/3$	
Largest diff. peak and hole	0.469 and -0.419 $eÅ^{-3}$	
R.M.S. deviation from mean	0.051 $eÅ^{-3}$	

Table S9: Sample and crystal data for **7**.

Identification code	WenDa47	
Chemical formula	$C_{39}H_{63}N_3OSi_3$	
Formula weight	646.10	
Temperature	100(2) K	
Wavelength	0.71073 Å	
Crystal size	0.176 mm x 0.179 mm x 0.217 mm	
Crystal habit	clear colorless fragment	
Crystal system	monoclinic	
Space group	$P\ 1\ 2_1/c\ 1$	
Unit cell dimensions	a = 34.475(3) Å	α = 90°
	b = 10.6878(9) Å	β = 107.847(3)°
	c = 22.1910(19) Å	γ = 90°
Volume	7783.1(12) Å^3	
Z	4	
Density (calculated)	1.103 g/cm^3	
Absorption coefficient	0.123 mm^{-1}	
F(000)	2832	

Table S10: Data collection and structure refinement for **7**.

Diffractometer	Bruker D8 Venture, CMOS detector (Bruker Photon-100)	
Radiation source	IMS microsource, Mo	
Theta range for data collection	2.20 to 25.03°	
Index ranges	-41<=h<=41, -12<=k<=12, -26<=l<=26	
Reflections collected	152111	
Independent reflections	13754 [R(int) = 0.0652]	
Coverage of independent reflections	99.9%	
Absorption correction	multi-scan	
Min. and max. transmission	0.7188 and 0.7452	
Refinement method	Full-matrix least-squares on F^2	
Refinement program	SHELXL-2014/7 (Sheldrick, 2014)	
Function minimized	$\Sigma\ w(F_o^2 - F_c^2)^2$	
Data / restraints / parameters	13754 / 54 / 905	
Goodness-of-fit on F^2	1.081	
Δ/σ_{max}	0.001	
Final R indices	10907 data; I>2σ(I)	R1 = 0.0491, wR2 = 0.1006
	all data	R1 = 0.0704, wR2 = 0.1084
Weighting scheme	$w=1/[\sigma^2(F_o^2)+(0.0377P)^2+6.6255P]$ where $P=(F_o^2+2F_c^2)/3$	
Largest diff. peak and hole	0.378 and -0.326 eÅ^{-3}	
R.M.S. deviation from mean	0.049 eÅ^{-3}	

3. Computational Calculations

A) General

All calculations were performed at the B3LYP[S13-S15]/6-311+G(d) level of theory using Gaussian 09[S16]. The geometry of compounds **2b**, **6** and **7** were optimized starting from the solid state structures. The nature of stationary points found was assessed by frequency calculations, excluding **6**, where due to the size of the system, frequency calculations where only performed on the reduced system (Dipp groups replaced by 2,6-dimethyl-phenyl groups). Natural bond orbital (NBO)[S17] analyses were performed using the NBO 3.1 program implemented in Gaussian.

B) Theoretical Investigations

Influences on Si=O bonds and Related Structures

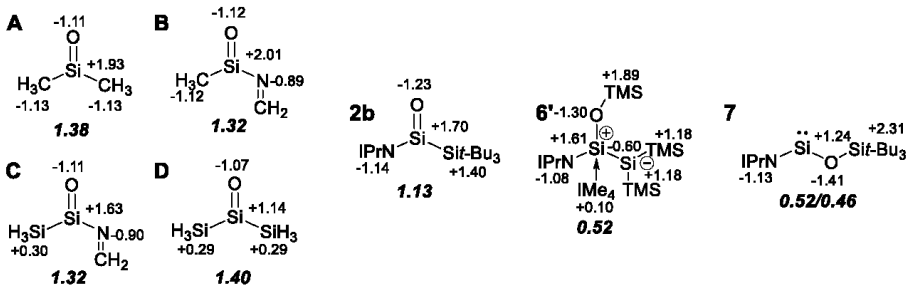

Figure S55: NPA charges and WBIs (bold & italic) of the corresponding Si-O bond of **2b**, **6**, **7** and comparable smaller silanones **A**-**D**.

By comparing smaller silanones **A**, **B**, **C** and **D**, the influence of silyl and imino groups on the Si=O moiety were investigated. As expected implementation of a π-donating imino function increases the polarization of the Si=O bond (see NPA charges O/Si of **A**: -1.11/+1.93 and **B**: -1.12/+2.01). However, addition of silyl moieties effectively reduces the positive charge at the silicon center (**B** (+2.01) and **C** (+1.63) or **A** (+1.93) and **D** (+1.14)). Most likely this is a result of inductive σ-donation of the silyl group to the electron deficient silicon center. Further, hyperconjugation of Si-C σ-orbitals with the π*-orbital of the Si=O moiety may also have a similar effect.

For compound **6** the obtained crystallographic and theoretical data point to resonance form **6'** with a zwitterionic Si1-Si2 bond (WBI 1.04) and a dative Si-NHC bond (WBI 0.60) as most fitting representation (Table S11). Still, we would like to note, that several more, but less likely, canonical forms (e.g. delocalization of the positive charge inside the NHI or NHC moiety) are generally imaginable.

Table S11: Selected WBI and NPA charges of **6**.

Bond	WBI	NPA charges
Si1Si2	1.04	1.61/-0.60
Si2Si3	0.99	-0.60/1.18
Si2Si4	0.98	-0.60/1.18
Si1O	0.52	1.61/-1.30
$Si1C^{IMe4}$	0.60	1.61/0.10
Si1N	0.73	1.61/-1.08
NC^{Imin}	1.60	-1.08/0.67

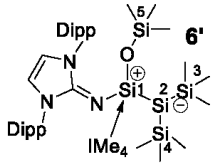

Calculated IR Stretching Frequencies of 2b, 6 and 7

Table S12: Experimental and calculated IR frequencies B3LYP/6-311+G(2d,2p)).

Compound	Mode	Exp. ν [cm^{-1}]	Calc. ν [cm^{-1}]
2b	stretch. Si=O	1144	1155
	stretch. C=N	1649	1647
6	asym. stretch. Si-O-Si	978	967
	stretch. C=N	1690	1751
7	asym. stretch. Si-O-Si	980	992
	stretch. C=N	1624	1684

asym. stretch.: asymmetric stretching

Calculated NMR Values

NMR chemical shifts were calculated at the SMD-B3LYP/6-311+G(2d,2p) level of theory based on the optimized geometries and referenced to tetramethylsilane. In the case of **5** and **6** the NMR shifts on this level where not satisfying (only the *Si*TMS_2 moiety showed a huge variance compared to experiment, indicating an incorrect representation of this moiety), inclusion of Grimme's dispersion[S18] improved the results in these cases, whereas only negligible effects occurred for **2b** and **7**.

Table S13: Experimental and calculated NMR chemical shifts(δ(TMS) = 0; SMD-B3LYP/6-311+G(2d,2p)).

Compound	Si	Exp. δ(^{29}Si) [ppm]	Calc. δ(^{29}Si) [ppm]	Δ [ppm]
2b	*central Si*	28.8	33.3[a]	-4.5
	Si-Bu_3	13.7	18.6[a]	-4.9
5	O*TMS*	4.3	2.0[b,c]	2.3
	Si*TMS*$_2$	-14.6	-19.8[b,c]	5.2
	Si*TMS*$_2$	-14.8	-20.1[b,c]	5.3
	*Si*OTMS	-35.7	-37.6[b,c]	1.9
	SiTMS_2	-39.8	-41.4[b,c]	1.6

6	O*TMS*	6.1	11.7 [a,c]	-5.6
	Si*TMS*$_2$	-7.1	-3.4 [a,c]	-3.7
	*Si*OTMS	-35.2	-32.8 [a,c]	-2.4
	*Si*TMS$_2$	-174.6	-170.5 [a,c]	-4.1
7	*central Si*	58.9	54.4 [a]	4.5
	Si-Bu$_3$	4.4	5.5 [a]	-1.1
INT	O*TMS*	4.3	17.1 [b,c]	-12.8
	Si*TMS*$_2$	-7.2	-3.0 [b,c]	-4.2
	*Si*OTMS	-8.0	59.5 [b,c]	-67.5
	*Si*TMS$_2$	-196.6	-198.2 [b,c]	1.6

[a] solvent benzene, [b] solvent tetrahydrofuran, [c] calculated including Grimme's dispersion[S18]

Calculated UV-VIS Values

Table S14: Excerpt of the TD-DFT calculation of **2b**.

Wavelength [nm]	MO contributions	f	Contributions
285.07	HOMO→LUMO	0.0019	92.97%
	HOMO→LUMO+4		3.83%
283.97	HOMO-1→LUMO+4	0.0035	6.10%
	HOMO→LUMO		5.23%
	HOMO→LUMO+1		30.30%
	HOMO→LUMO+4		53.32%
273.99	HOMO→LUMO+1	0.0046	45.36%
	HOMO→LUMO+2		7.75%
	HOMO→LUMO+3		17.04%
	HOMO→LUMO+4		25.10%
272.50	HOMO→LUMO+1	0.0030	21.56%
	HOMO→LUMO+2		45.32%
	HOMO→LUMO+3		28.56%
	HOMO→LUMO+4		3.05%
269.98	HOMO→LUMO+2	0.0004	44.09%
	HOMO→LUMO+3		52.74%
273.99	HOMO-1→LUMO+1	0.0046	15.04%
	HOMO-1→LUMO+4		70.11%
	HOMO→LUMO+4		10.86%

Table S15: Excerpt of the TD-DFT calculation of **7**

Wavelength [nm]	MO contributions	f	Contributions
340.57	HOMO→LUMO	0.0262	94.98%
	HOMO→LUMO+3		2.16%
335.05	HOMO→LUMO+1	0.0001	98.87%
320.66	HOMO→LUMO+2	0.0007	6.52%
	HOMO→LUMO+3		81.48%
	HOMO→LUMO+4		9.88%
319.73	HOMO→LUMO+2	0.0006	92.63%
	HOMO→LUMO+3		4.90%
318.47	HOMO→LUMO	0.0010	2.14%
	HOMO→LUMO+3		10.14%
	HOMO→LUMO+4		85.79%
291.46	HOMO→LUMO+5	0.0026	93.82%
	HOMO→LUMO+6		2.69%

Energy Difference between 2b and 7

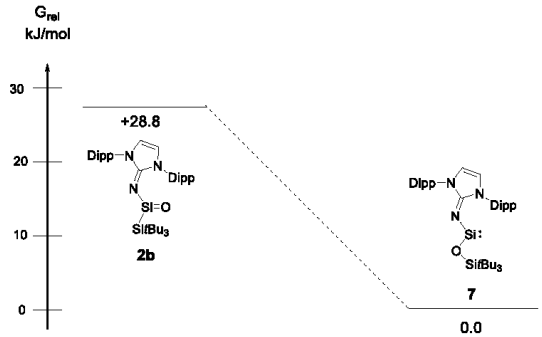

Figure S56: Energy difference between **2b** and **7**.

Orbitals of Calculated Species

Silanone 2b and Comparable Smaller Silanones

To illustrate the electronic influences of NHI and silyl ligands on the Si=O orbitals, the energy and shape of π and π* orbitals of silanone **2b** and analogue orbitals of smaller silanones **A**, **B**, **C** and **D** were compared. In general, both orbitals of **2b** look similar to structure **C**, but are significantly higher in energy than those of Me_2Si=O **A**. Furthermore, the π/π*-energy splitting is increased (ΔE in **2b** 7.37 eV vs. **A** 6.92 eV), illustrating its total stabilization, which can mainly be attributed to the NHI ligand by general decreasing the energy of the π-orbital and increasing the energy of the π*-orbital (see orbitals of **A** and **B**

for comparison) by mixing with the corresponding orbital of the imino group. By comparing the orbitals of structure **A** and **D** as well as **B** and **C**, it becomes evident that silyl groups not only decrease π/π*-orbitals in energy, but also lower the energy difference between these Si=O orbitals. On the first sight this observation may be considered as counteracting stabilization effect. However, we believe that hyperconjugation of the Si-C σ-orbitals of the silyl group with the π*-orbital of the Si=O moiety (see LUMO of **D**) is far more relevant to preserve the Si=O double bond nature and to effectively reduce the positive charge at the silicon center (already seen at the WBI and NPA charges of **A** and **D**).

Table S16: Representation of the most important orbitals of **2b**.

2b 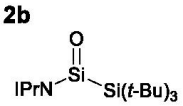	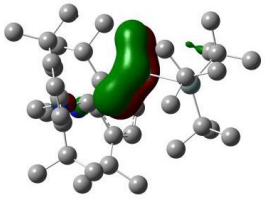 **π (Si=O)** **HOMO-10 (-7.78 eV)**	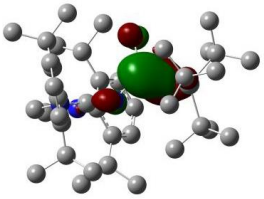 **π* (Si=O)** **LUMO+4 (-0.41 eV)**
	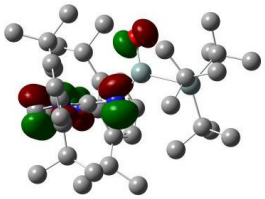 **HOMO (-5.82 eV)**	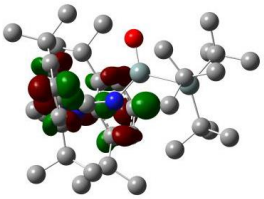 **LUMO (-0.73 eV)**

Table S17: Representation of π and π* orbitals of **A**, **B**, **C** and **D**.

A 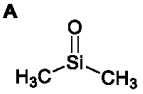	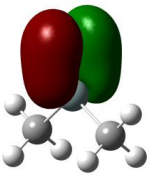	**π (Si=O)** **HOMO-1 (-8.18 eV)**	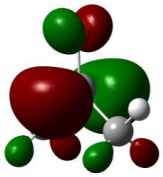	**π* (Si=O)** **LUMO (-1.26 eV)**
B 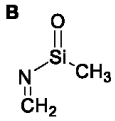	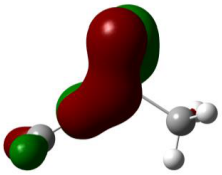	**π (Si=O)** **HOMO-2 (-8.44 eV)**	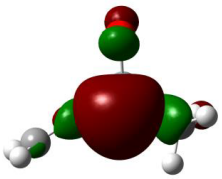	**π* (Si=O)** **LUMO+1 (-1.00 eV)**
C 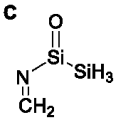	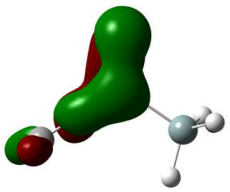	**π (Si=O)** **HOMO-2 (-8.61 eV)**	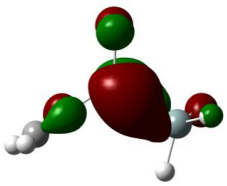	**π* (Si=O)** **LUMO+1 (-1.53 eV)**
D 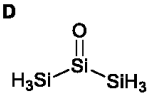	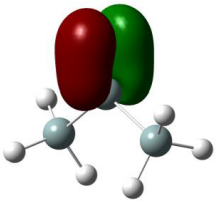	**π (Si=O)** **HOMO-1 (-8.65 eV)**	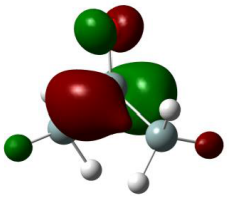	**π* (Si=O)** **LUMO (-2.76 eV)**

IMe$_4$ Zwitterionic Disilene 6

Table S18: Representation of the most important orbitals of **6**.

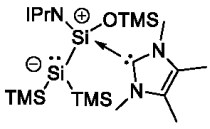

6'

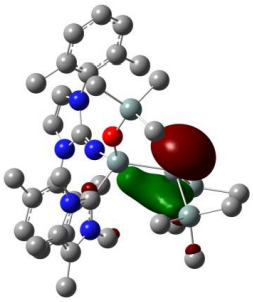

mainly lone pair of Si(2)

HOMO (-3.54 eV)

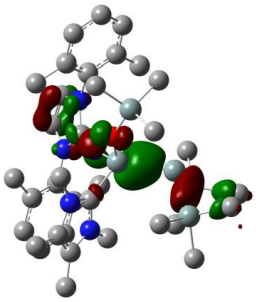

σ-bond (Si1Si2)

HOMO-3 (-6.11 eV)

***N,O*-Silylene 7**

The HOMO of *N,O*-silylene **7** exhibits mainly lone pair character (Si_n), the LUMO resembles the empty Si_{3p} orbital with a HOMO-LUMO gap of 4.33 eV. Both orbitals show only minor contributions from donating N or O atoms. For orbitals lower in energy some interactions of silicon with nitrogen, and even lower, minor interactions with oxygen can be found. HOMO-6 represents the lone pair on nitrogen atom N_n with obvious mixing with the empty Si_{3p} orbital, illustrating partial Si-N double bond character (similarly to HOMO-10 of silanone **2b**). For oxygen, the related lone pair orbital O_n (seen in HOMO-2, HOMO-15 and even HOMO-21) shows almost no extent towards the silicon center. Similar low-lying orbital interactions (Si-S) have been found for related dithiolato silylene by Power *et al.*.[S19]

Table S19: Representation of the most important orbitals of **7**.

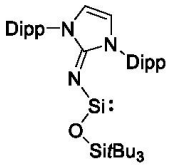

7

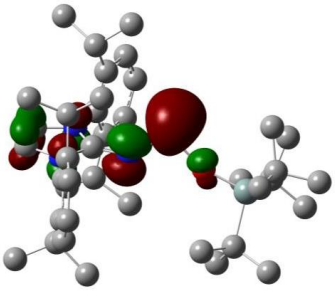

lone pair Si_n

HOMO (-5.04 eV)

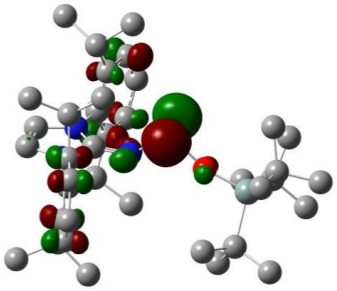

empty Si_{3p}

LUMO (-0.71 eV)

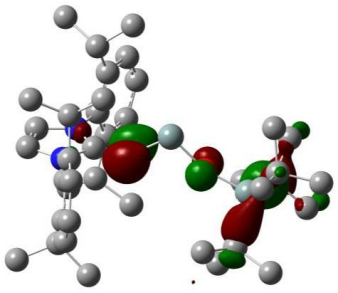

HOMO-2 (-6.56 eV)

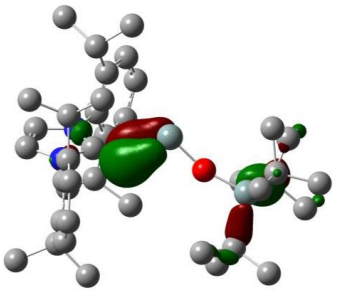

Mixing of N_n and Si_{3p} orbital

HOMO-6 (-6.96 eV)

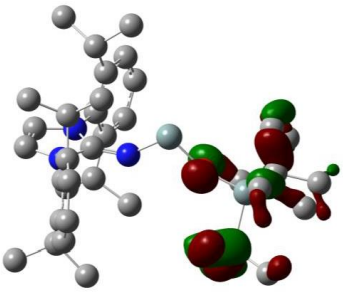

HOMO-15 (-8.82 eV)

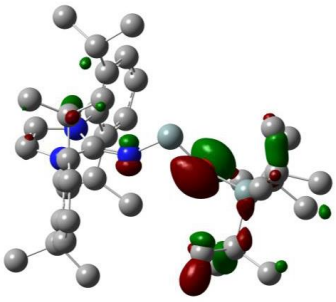

HOMO-21 (-9.09 eV)

S56

The explicit cartesian coordinates (S57-S64) of all calculated structures were removed due to space-saving issues, but the data is available free of charge at the ACS publications homepage.

4. References

(S1) Wendel, D.; Porzelt, A.; Herz, F. A. D.; Sarkar, D.; Jandl, C.; Inoue, S.; Rieger, B., *J. Am. Chem. Soc.* **2017**, *139*, 8134-8137.

(S2) Lui, M. W.; Merten, C.; Ferguson, M. J.; McDonald, R.; Xu, Y.; Rivard, E., *Inorg. Chem.* **2015**, *54*, 2040-2049.

(S3) Kuhn, N.; Kratz, T., *Synthesis* **1993**, *1993*, 561-562.

(S4) Wiberg, N.; Amelunxen, K.; Lerner, H. W.; Schuster, H.; Nöth, H.; Krossing, I.; Schmidt-Amelunxen, M.; Seifert, T., *J. Organomet. Chem.* **1997**, *542*, 1-18.

(S5) Ishida, S.; Abe, T.; Hirakawa, F.; Kosai, T.; Sato, K.; Kira, M.; Iwamoto, T., *Chem. Eur. J.* **2015**, *21*, 15100-15103.

(S6) *APEX suite of crystallographic software,* APEX 3 version 2015.5-2; Bruker AXS Inc.: Madison, Wisconsin, USA, **2015**.

(S7) *SAINT*, Version 7.56a and SADABS Version 2008/1; Bruker AXS Inc.: Madison, Wisconsin, USA, **2008**.

(S8) Sheldrick, G. M., *SHELXL-2014*, University of Göttingen, Göttingen, Germany, **2014**.

(S9) Huebschle, C. B.; Sheldrick, G. M.; Dittrich, B., *J. Appl. Cryst.* **2011**, 44, 1281.

(S10) Sheldrick, G. M., *SHELXL-97,* University of Göttingen, Göttingen, Germany, **1998**.

(S11) Wilson, A. J. C. *International Tables for Crystallography*, Vol. C, Tables 6.1.1.4 (pp. 500-502), 4.2.6.8 (pp. 219-222), and 4.2.4.2 (pp. 193-199); Kluwer Academic Publishers: Dordrecht, The Netherlands, **1992**.

(S12) Macrae, C. F., Bruno, I. J., Chisholm, J. A., Edgington, P. R., McCabe, P., Pidcock, E., Rodriguez-Monge, L., Taylor, R., van de Streek, J. & Wood, P. A., *J. Appl. Cryst.* **2008**, *41*, 466–470.

(S13) Becke, A. D., *J. Chem. Phys.* **1993**, *98*, 5648-5652.

(S14) Vosko, S. H.; Wilk, L., Nusair, M., *Can. J. Phys.* **1980**, *58*, 1200-1211.

(S15) Lee, C.; Yang, W.; Parr, R. G., *Phys. Rev. B* **1988**, *37*, 785-789.

(S16) Frisch, M. J.; Trucks, G. W.; Schlegel, H. B.; Scuseria, G. E.; Robb, M. A.; Cheeseman, J. R;.Scalmani, G.; Barone, V.; Petersson, G. A.; Nakatusji, H.; Li, X.; Caricato, M.; Marenich, A.; Bloino, J.; Janesko, B. G.; Gomperts, R.; Mennucci, B.; Hratchian, H. P.; Ortiz, J. V.; Izmaylov, A. F.; Sonnenberg, J. L.; Williams-Young, D.; Ding, F.; Lipparini, F.; Egidi, F.; Goings, J.; Peng, B.; Petrone, A.; Henderson, T.; Ranashinghe, D.; Zakrzewski, V. G.; Gao, J.; Rega, N.; Zheng, G.; Liang, W.; Hada, M.; Ehara, M.; Toyota, K.; Fukuda, R.; Hasekawa, J.; Ishida, M.; Nakajima, T.; Honda, Y; Kitao, O.; Nakao, H.; Vreven, T.; Throssell, K.; Montgomery, Jr., J. A.; Peralta, J. E.; Ogliaro, F.; Bearpark, M.; Heyd, J. J.; Brothers, E.; Kudin, K. N.; Staroverov, V. N.; Keith, T.; Kobayashi, R.; Normand, J.; Raghavachari, K; Rendell, A.; Burant, J. C.; Iyengar, S. S.; Tomasi, J.; Cossi, M.; Millam, J. M.; Klene, M.; Adamo, C.; Cammi, R.; Ochterski, J. W.; Martin, R. L.; Morokuma, K.; Farkas, O.; Forseman, J. B.; Fox, D.J., *Gaussian 09, Revision E.01,* Gaussian, Inc., Wallingford CT, **2016**.

(S17) Reed, A. E.; Curtiss, L. A.; Weinhold, F., *Chem. Rev.* **1988**, *88*, 899-926.

(S18) Grimme, S.; Antony, J.; Ehrlich, S.; Krieg, H., *J. Chem. Phys* **2010**, *132*, 154104-154119.

(S19) Rekken, B. D.; Brown, T. M.; Fettinger, J. C.; Tuononen, H. M.; Power, P. P., *J. Am. Chem. Soc.* **2012**, *134*, 6504-6507.

14.5 Supporting Information Chapter 10

Precise Ammonia Activation and Oxygenation by an Iminodisilene

Daniel Wendel,[a] Tibor Szilvási,[d] Daniel Henschel,[a] Philipp J. Altmann,[c] Christian Jandl,[c] Shigeyoshi Inoue*[b] and Bernhard Rieger*[a]

[a]WACKER-Chair of Macromolecular Chemistry, [b]WACKER-Institute of Silicon Chemistry, [c]Catalysis Research Center, Technische Universität München, Lichtenbergstraße 4, 85748 Garching bei München, Germany.

[d]Department of Chemical and Biological Engineering, University of Wisconsin Madison, 1415 Engineering Drive, Madison, Wisconsin 53706-1607, USA.

*s.inoue@tum.de; rieger@tum.de

Supporting Information

Total: S144 pages

1. Experimental Procedures

A) General Methods and Instrumentation

All manipulations were carried out under argon atmosphere using standard Schlenk or glovebox techniques. Glassware was heat-dried under vacuum prior to use. Unless otherwise stated, all chemicals were purchased from Sigma-Aldrich or ABCR and used as received. *n*-Hexane, THF and toluene were refluxed over sodium/benzophenone, distilled and deoxygenated prior to use. Deuterated benzene (C_6D_6) and THF-d_8 were obtained from Deutero Deutschland GmbH and were dried over 3 Å molecular sieves. All NMR samples were prepared under argon in J. Young PTFE tubes. Iminosilyldisilene **1** was synthesized according to a procedure described in literature.[S1] Carbon dioxide (5.0), nitrogen monoxide (5.0) and oxygen gas (5.0) were purchased from Westfalen AG and used as received. Ammonia (5.0) was first condensed into a cooling trap and dried over sodium before usage. NMR spectra were recorded on Bruker AV-500C and AV-500 spectrometers at ambient temperature (300 K), unless otherwise stated. ^{1}H, ^{13}C and ^{29}Si NMR spectroscopic chemical shifts δ are reported in ppm relative to tetramethylsilane. δ(^{1}H) and δ(^{13}C) were referenced internally to the relevant residual solvent resonances. δ(^{29}Si) was referenced to the signal of tetramethylsilane (TMS) (δ = 0 ppm) as external standard. Elemental analyses (EA) were conducted with a EURO EA (HEKA tech) instrument equipped with a CHNS combustion analyzer. Mass spectra (MS-CI) were recorded on a double focusing Finnigan MAT 90 mass spectrometer (isobutene, 150 eV). ATR-FTIR spectra were recorded on a Perkin Elmer FTIR spectrometer (diamond ATR, Spectrum Two; located inside an argon-filled glovebox) in a range of 400 – 4000 cm^{-1}.

B) Synthesis and Characterization of New Compounds

Synthesis of I*t*-BuN(SiTMS$_3$)NH$_2$Si-SiH(SiTMS$_3$)NI*t*-Bu (2a)

Ammonia gas was passed through a solution of disilene **1** (47.1 mg, 0.050 mmol) in *n*-hexane (10 mL) at –78 °C for approximately 5 min. The reaction temperature was constantly held at –78 °C for 16 h until the characteristic dark purple color vanished completely. Removal of all volatiles *in vacuo* gave a white crude product, which was re-dissolved in fresh *n*-hexane (3 × 5 mL). Concentration of this solution and cooling to –35 °C for several days yielded colorless crystals of 1,2-disilane **2a** (31.2 mg, 0.032 mmol, 64%) suitable for single crystal X-ray analysis.

To experimentally exclude a mechanism for the formation of **2a** that follows the dissociation of **1** into two silylene fragments, followed by instant activation of NH_3 by one silylene to form **2b**, and final insertion of the other silylene into the Si–H or Si–NH_2 bond of **2b**, we treated 2 eq. of isolated 1,1-monosilane **2b** in C_6D_6 with 1 eq. of disilene **1** at room temperature. Monitoring this reaction via ^{1}H NMR spectroscopy (Figure S5) did not show any conversion to 1,2-disilane **2a** even after one day at room temperature. Thus, in line with our theoretical calculations and the reported mechanism of H_2 activation[S1], we conclude that NH_3 directly adds to the Si=Si bond of **1**.

^{1}H NMR (500 MHz, C_6D_6, r.t.): δ = 6.37 (s, ^1J (Si-H) = 174 Hz, ^2J (SiSi-H) = 21.7 Hz, ^2J (TMS$_3$SiSi-H) = 13.8 Hz, 1H, Si*H*), 6.06 (d, ^3J = 3.3 Hz, 1H, C*H*-N), 5.96 (d, ^3J = 3.3 Hz, 1H, C*H*-N), 5.90 (d, ^3J = 3.3 Hz, 1H, C*H*-N), 5.88 (d, ^3J = 3.3 Hz, 1H, C*H*-N), 1.79 (bs, SiN*H*$_2$), 1.47 (s, 18H, CC*H*$_3$), 1.38 (s, 18H, CC*H*$_3$), 0.54 (s, 27H, Si*TMS*$_3$), 0.52 (s, 27H, Si*TMS*$_3$).

^{13}C NMR (126 MHz, C_6D_6, r.t.): δ = 140.6 (*C*=N), 138.6 (*C*=N), 108.4 (*C*H-N), 108.3 (*C*H-N), 108.1 (*C*H-N), 107.8 (*C*H-N), 56.2 (*C*CH$_3$), 55.8 (*C*CH$_3$), 55.0 (*C*CH$_3$), 54.9 (*C*CH$_3$), 31.8 (C*C*H$_3$), 31.6 (C*C*H$_3$), 30.4 (C*C*H$_3$), 29.6 (C*C*H$_3$), 5.3 (Si*TMS*$_3$), 4.8 (Si*TMS*$_3$).

^{29}Si NMR (99 MHz, C_6D_6, r.t.): δ = -9.5 (*TMS*$_3$), -9.7 (*TMS*$_3$), -48.6 (d, ^2J (SiSi-H) = 21.7 Hz, *Si*NH$_2$,), -62.4 (m, ^1J (Si-H) = 174 Hz, *Si*H), -123.5 (SiNH$_2$*Si*TMS$_3$) -128.9 (SiH*Si*TMS$_3$).

MS-CI (150 eV): m/z (%) = 955 [M]$^+$ (15), 485 [M-SiH(SiTMS$_3$)NI*t*-Bu]$^+$ (87), 470 [M-SiNH$_2$(SiTMS$_3$)NI*t*-Bu]$^+$ (29).

EA experimental (calculated): C 49.55 (50.02), H 10.21 (10.22), N 11.07 (9.94) %.

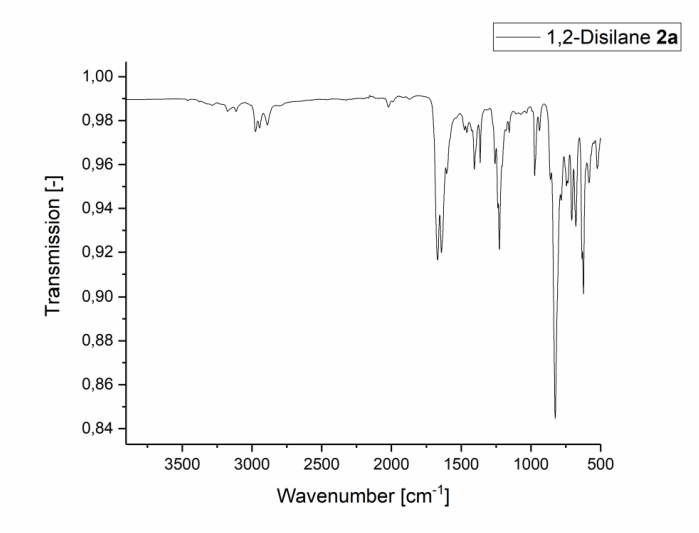

Figure S4: IR spectrum of 1,2-disilane **2a** (cm^{-1}): 3463 (w, $SiNH_2$), 3378 (w, $SiNH_2$), 2970 (w), 2902 (w), 2021 (w, Si-H), 1673 (m), 1633 (m), 1400 (w), 1223 (m), 970 (w), 813 (s), 705 (m), 674 (m), 629 (m).

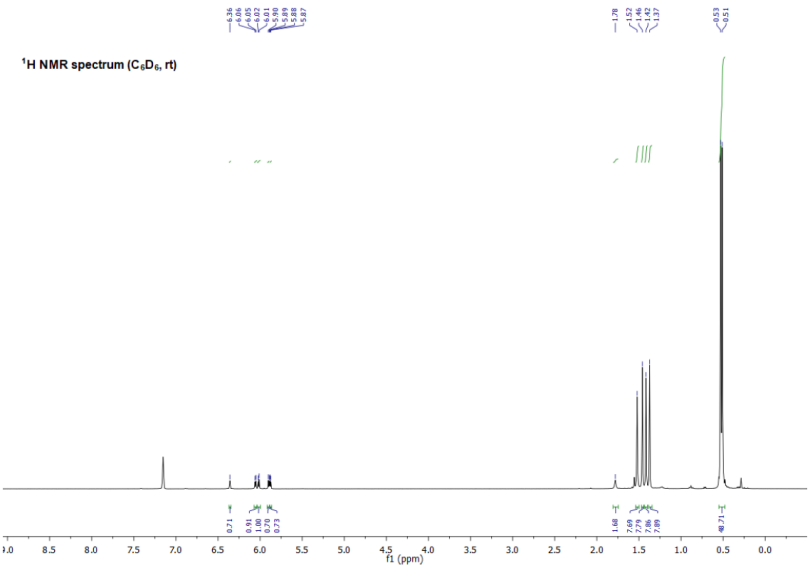

Figure S1: ^1H NMR spectrum of 1,2-disilane **2a** (C_6D_6, r.t.).

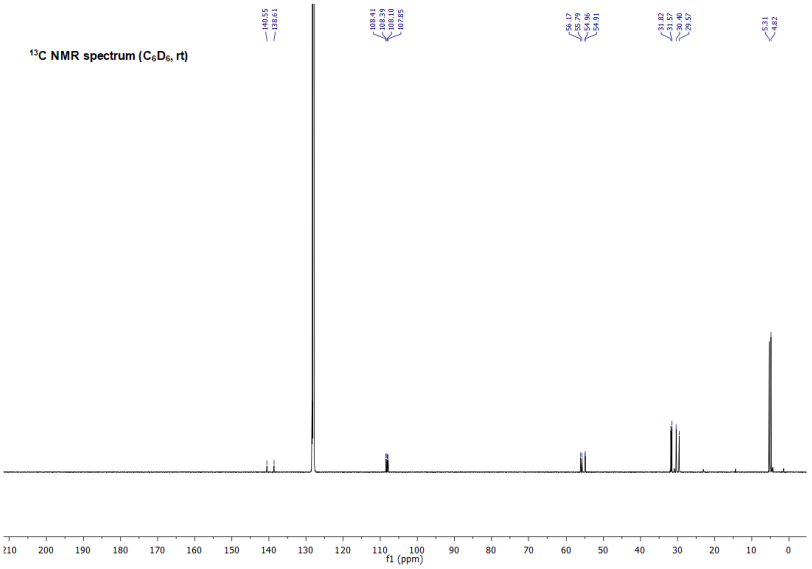

Figure S2: ^{13}C NMR spectrum of 1,2-disilane **2a** (C_6D_6, r.t.).

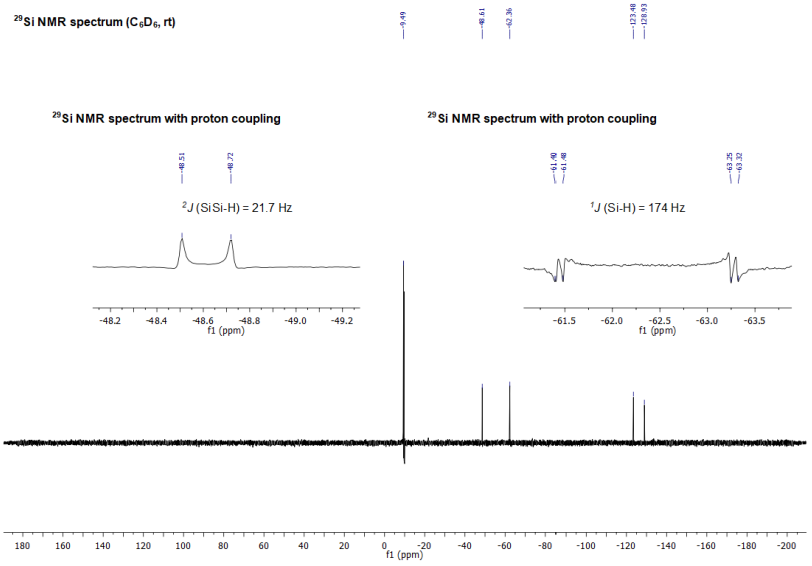

Figure S3: ^{29}Si NMR spectrum of 1,2-disilane **2a** (C_6D_6, r.t.).

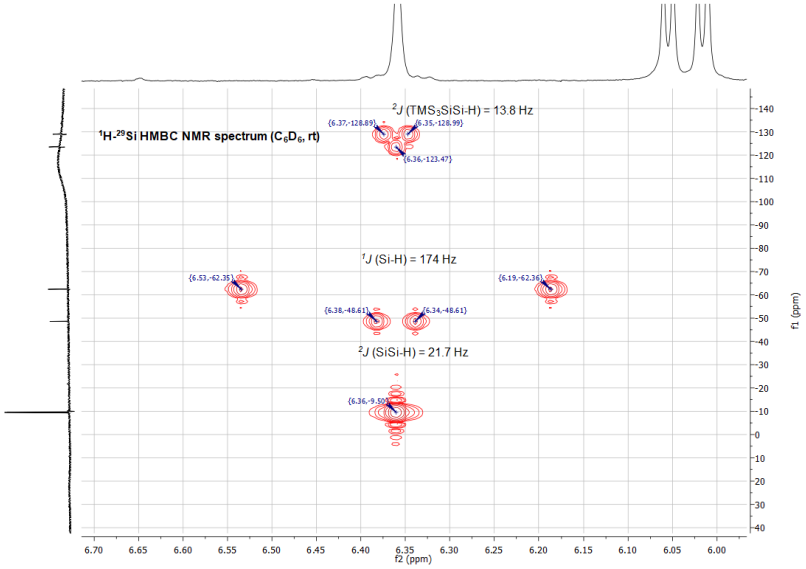

Figure S4:. ^{1}H-^{29}Si HMBC NMR spectrum of 1,2-disilane **2a** (C_6D_6, r.t.).

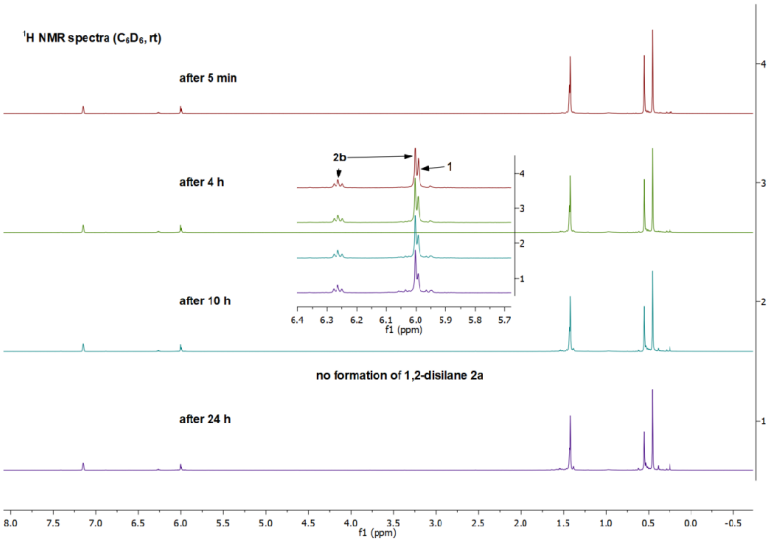

Figure S5: ^{1}H NMR spectra of NMR reaction of 1,1-monosilane **2b** (1 eq) and disilene **1** (2 eq) (C_6D_6, r.t.).

Synthesis of I*t*-BuN(SiTMS$_3$)SiHNH$_2$ (2b)

Ammonia gas was passed through a solution of disilene **1** (103 mg, 0.110 mmol) in *n*-hexane (10 mL) at –78 °C for approximately 5 min. The reaction solution was stirred further at -78 °C for 10 min, then it was allowed to warm to room temperature, whereupon the characteristic dark purple color vanished instantly. Removal of all volatiles *in vacuo* gave a white crude product, which was re-dissolved in fresh *n*-hexane (ca. 5 mL). Slow evaporation of the solvent led to colorless crystals of 1,1-monosilane **2b** (101 mg, 0.207 mmol, 94%) suitable for single crystal X-ray analysis.

^{1}H NMR (500 MHz, C_6D_6, r.t.): δ = 6.27 (t, ^1J (Si-H) = 202 Hz, ^3J (NH_2SiH) = 4.2 Hz, 1H, Si-*H*), 6.01 (s, 2H, C*H*-N), 1.42 (s, 18H, CC*H*$_3$), 0.98 (bs, 2H, SiN*H*$_2$), 0.46 (s, 27H, Si*TMS*$_3$).

^{13}C NMR (126 MHz, C_6D_6, r.t): δ = 140.0 (*C*=N), 107.5 (*C*H-N), 54.8 (*C*CH$_3$), 28.8 (C*C*H$_3$), 3.3 (Si*TMS*$_3$).

^{29}Si NMR (99 MHz, C_6D_6, r.t.): δ = -9.8 (*TMS*$_3$), -49.9 (d, ^1J (Si-H) = 202 Hz, H*Si*NH$_2$), -135.8 (*Si*TMS$_3$).

MS-CI (150 eV): m/z (%) = 486 $[M]^+$ (92).

EA experimental (calculated): C 48.70 (49.32), H 9.94 (10.35), N 11.07 (11.50) %.

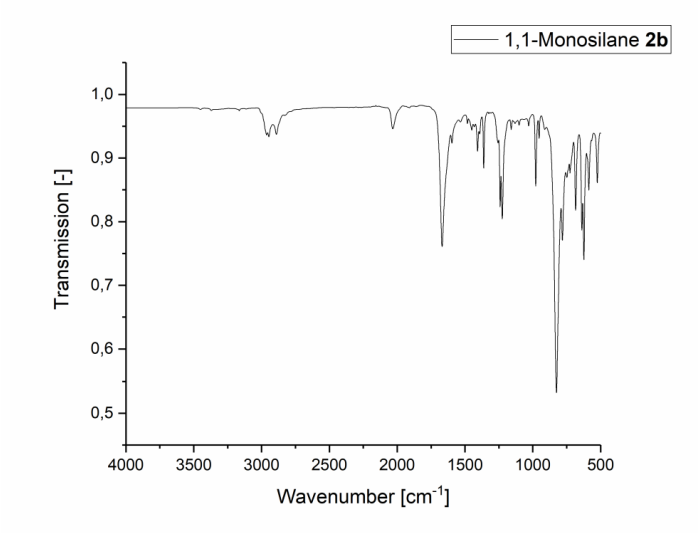

Figure S4: IR spectrum of 1,1-monosilane **2b** (cm^{-1}): 3441 (w, $SiNH_2$), 3370 (w, $SiNH_2$), 2952 (w), 2889 (w), 2030 (w, Si-H), 1662 (m), 1405 (w), 1358 (w), 1232 (m), 977 (w), 817 (s), 682 (m), 627 (m).

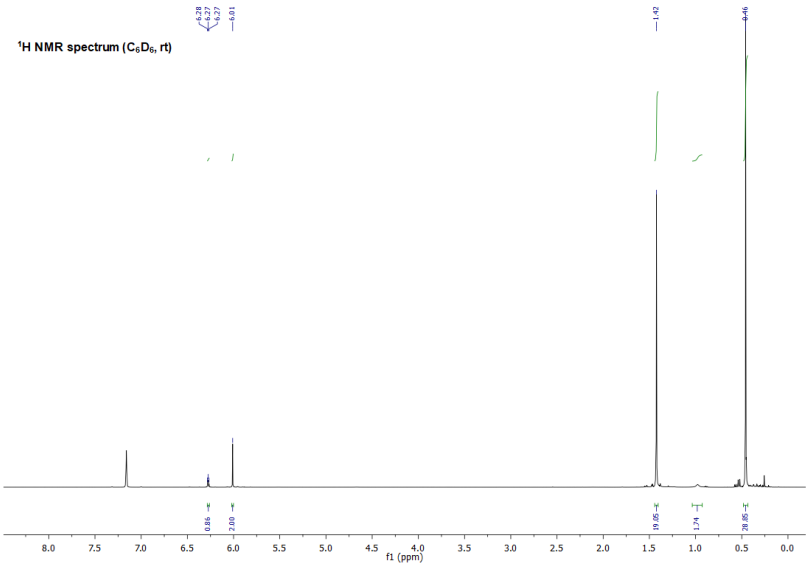

Figure S6: ^{1}H NMR spectrum of 1,1-monosilane **2b** (C_6D_6, r.t.).

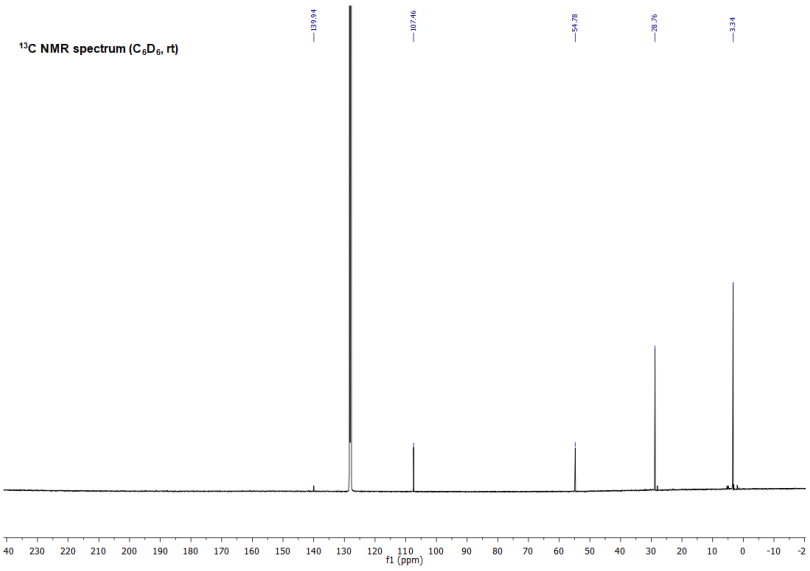

Figure S7: ^{13}C NMR spectrum of 1,1-monosilane **2b** (C_6D_6, r.t.).

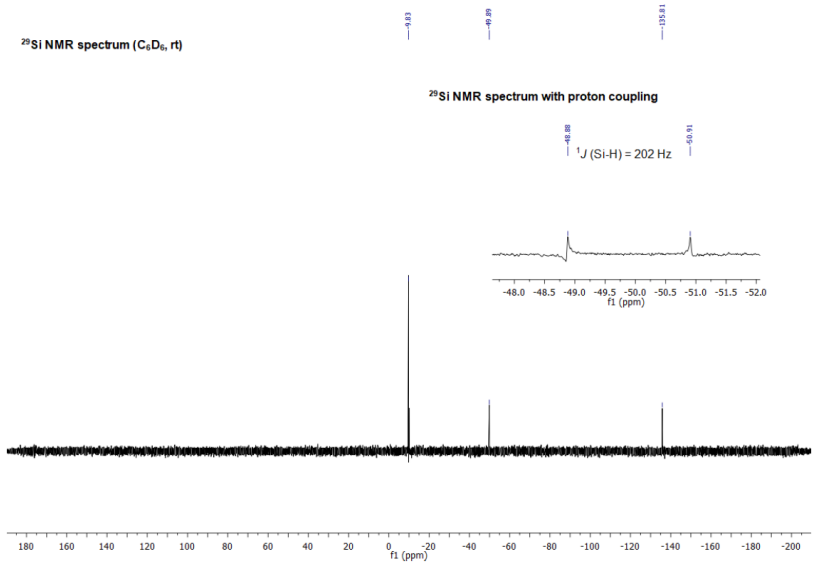

Figure S8: ^{29}Si NMR spectrum of 1,1-monosilane **2b** (C_6D_6, r.t.).

Synthesis of I*t*-BuN(SiTMS$_3$)Si(II)-B(C$_6$F$_5$)$_3$ (3)

B(C$_6$F$_5$)$_3$ (26.7 mg, 0.052 mmol, 2.00 eq) in *n*-hexane (2 mL) was added to a solution of disilene **1** (24.6 mg, 0.026 mmol, 1.00) in *n*-hexane (1 mL) at room temperature. The color rapidly changed to yellow with formation of a yellowish precipitate. To promote further precipitation, the flask was placed in a freezer at –35 °. Separation of the solvent and removal of all volatiles gave a yellowish powder of pure silylene-BCF adduct **3** (40.8 mg, 0.041 mmol, 79%). Re-dissolving the product in toluene (ca. 1 mL) and cooling to –35 °C for several days yielded yellow crystals of **3** suitable for single crystal X-ray analysis. Compound **3** is indefinitely stable as a solid and in C$_6$D$_6$ solution.

^{1}H NMR (500 MHz, C$_6$D$_6$, r.t.): δ = 5.81 (s, 2H, C*H*-N), 1.09 (s, 18H, CC*H*$_3$), 0.21 (s, 27H, Si*TMS*$_3$).

^{13}C NMR (126 MHz, C$_6$D$_6$, r.t): δ = 149.9 (*C*-F), 148.0 (*C*-F), 144.7 (*C*=N), 141.0 (*C*-F), 139.0 (*C*-F), 136.7 (*C*-F), 111.4 (*C*H-N), 58.3 (*C*CH$_3$), 29.4 (C*C*H$_3$), 3.4 (Si*TMS*$_3$).

^{29}Si NMR (99 MHz, C$_6$D$_6$, r.t.): δ = 161.9 (q, $^1J_{SiB}$ = 58.7 Hz, *central Si*), -7.7 (*TMS*$_3$), -113.4 (*Si*TMS$_3$).

^{11}B NMR (96 MHz, C$_6$D$_6$, r.t.): δ = -16.2.

^{19}F NMR (471 MHz, C$_6$D$_6$, r.t.): δ = -127.1, -158.2, -163.9.

MS-CI (150 eV): m/z (%) = 981 [M]$^+$ (4), 801 [M-NHC]$^+$ (11), 787 [M-NHI]$^+$ (8).

EA experimental (calculated): C 47.65 (46.48), H 4.94 (4.82), N 4.10 (4.28) %.

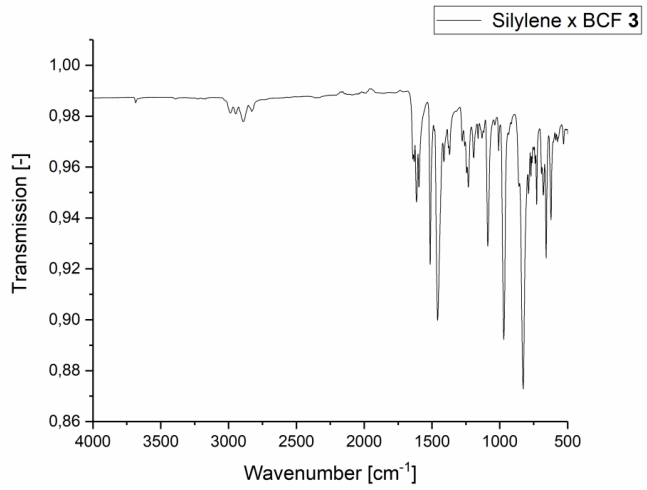

Figure S4: IR spectrum of silylene-BCF adduct **3** (cm^{-1}): 2947 (w), 2898 (w), 1617 (m), 1515 (m), 1443 (s), 1235 (w), 1083 (m), 968 (s), 829 (s), 659 (m), 618 (m).

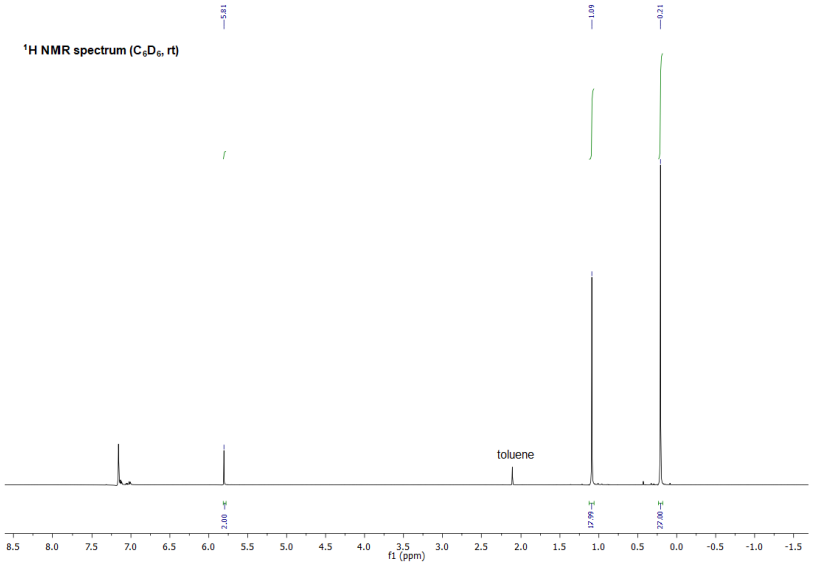

Figure S9:.^{1}H NMR spectrum of silylene-BCF adduct **3** (C_6D_6, r.t.).

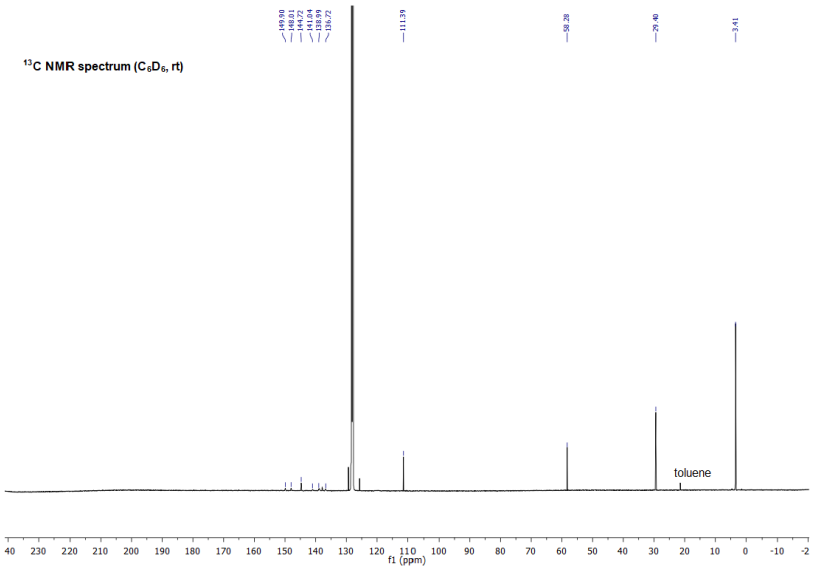

Figure S10: ^{13}C NMR spectrum of silylene-BCF adduct **3** (C_6D_6, r.t.).

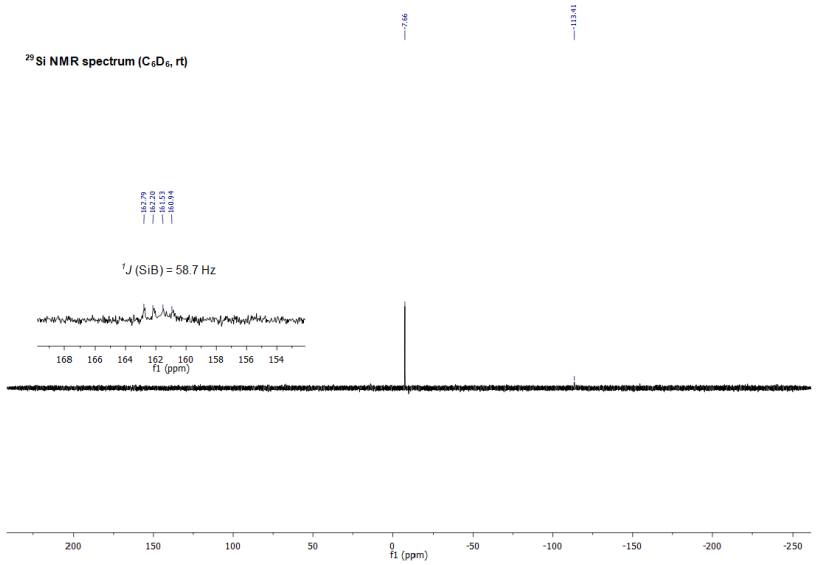

Figure S11: ^{29}Si NMR spectrum of silylene-BCF adduct **3** (C_6D_6, r.t.).

Synthesis of (*t*-BuN(SiTMS$_3$)Si)$_2$O (4-t)

A pressurizable Schlenk flask filled with disilene **1** (40.0 mg, 0.042 mmol) in toluene (2 mL) was exposed to N_2O gas (1 bar) at room temperature. The characteristic dark purple color vanished instantly, resulting in a clear yellow solution. The excess N_2O was removed and the solution was stirred for 4 h, whereupon a yellow crystalline solid formed. The reaction solution was put in a freezer at -35 °C, which increased the formation of yellow crystals of *trans*-disilaoxirane **4-t** (31.1 mg, 0.032 mmol, 76%) suitable for single crystal X-ray analysis.

To investigate the underlying mechanism of this reaction, the synthesis was repeated in a J. Young PTFE tube (C_6D_6) and monitored *via* ^{1}H and ^{29}Si NMR spectroscopy. As seen in the ^{1}H NMR spectra (Figure S15), exposure of disilene **1** to N_2O gas directly formed a symmetric intermediary product whose intensity decreased over time while simultaneously the signals of *trans*-disilaoxirane **4-t** increased. According to the ^{29}Si NMR spectrum (Figure S16) the shifts of this intermediary product are very close to those of the isolated *trans*-isomer, pointing to similar chemical constitution. We propose that this product is the *cis*-disilaoxirane **4-c**, which then fully isomerizes to the respective *trans*-isomer **4-t**. This assumption is in line with our calculated mechanism and the GIAO-DFT NMR data (see computational calculations). Furthermore, heating the solution of **4-t** in N_2O atmosphere to 50 °C for 16 h triggered the formation of two new products, a minor fraction of *cis*-dioxadisiletane **5-c** (identified by comparison of the NMR data with the selective O_2 reaction) and a major proportion of a compound with similar chemical shifts, that consistently is assumed to be the *trans*-isomer **5-t** (fitting computational NMR shifts).

Intermediary *cis*-isomer 4-c:

^{1}H NMR (500 MHz, C_6D_6, r.t.): δ = 5.97 (s, 4H, C*H*-N), 1.48 (s, 18H, CC*H*$_3$), 1.42 (s, 18H, CC*H*$_3$), 0.56 (s, 54H, Si*TMS*$_3$).

^{29}Si NMR (99 MHz, C_6D_6, r.t.): δ = -9.2 (*TMS*$_3$), -39.0 (*Si*O), -121.8 (*Si*TMS$_3$).

Isolated *trans*-isomer 4-t:

^{1}H NMR (500 MHz, C_6D_6, r.t.): δ = 6.03 (d, ^3J = 3.2 Hz, 2H, C*H*-N), 6.06 (d, ^3J = 3.2 Hz, 2H, C*H*-N), 1.59 (s, 18H, CC*H*$_3$), 1.55 (s, 18H, CC*H*$_3$), 0.51 (s, 54H, Si*TMS*$_3$).

^{1}H NMR (500 MHz, THF-d_8, r.t.): δ = 6.44 (d, ^3J = 3.2 Hz, 2H, C*H*-N), 6.43 (d, ^3J = 3.2 Hz, 2H, C*H*-N), 1.61 (s, 18H, CC*H*$_3$), 1.60 (s, 18H, CC*H*$_3$), 0.23 (s, 54H, Si*TMS*$_3$).

^{13}C NMR (126 MHz, C_6D_6, r.t.): δ = 140.7 (*C*=N), 108.7 (*C*H-N), 108.4 (*C*H-N), 56.1 (*C*CH$_3$), 55.6 (*C*CH$_3$), 31.0 (C*C*H$_3$), 30.9 (C*C*H$_3$), 4.6 (Si*TMS*$_3$).

^{13}C NMR (126 MHz, THF-d_8, r.t.): δ = 141.6 (*C*=N), 109.7 (*C*H-N), 109.5 (*C*H-N), 56.9 (*C*CH$_3$), 56.5 (*C*CH$_3$), 31.6 (C*C*H$_3$), 31.5 (C*C*H$_3$), 4.8 (Si*TMS*$_3$).

^{29}Si NMR (99 MHz, C_6D_6, r.t.): δ = -9.5 (*TMS*$_3$), -42.8 (*Si*O), -124.9 (*Si*TMS$_3$).

^{29}Si NMR (99 MHz, THF-d_8, r.t.): δ = -9.6 (*TMS*$_3$), -43.0 (*Si*O), -124.9 (*Si*TMS$_3$).

MS-CI (150 eV): m/z (%) = 485 [M-Si(SiTMS$_3$)NI*t*-Bu]$^+$ (17), 469 [M-OSi(SiTMS$_3$)NI*t*-Bu]$^+$ (21).

EA experimental (calculated): C 50.21 (50.25), H 9.78 (9.91), N 8.39 (8.79) %.

Second oxygenation with N_2O to *trans*-dioxadisiletane 5-t:

^{1}H NMR (500 MHz, C_6D_6, r.t.): δ = 6.02 (s, 4H, C*H*-N), 1.56 (s, 36H, CC*H*$_3$), 0.52 (s, 54H, Si*TMS*$_3$).

^{13}C NMR (126 MHz, C_6D_6, r.t.): δ = 139.4 (*C*=N), 108.6 (*C*H-N), 56.1 (*C*CH$_3$), 30.9 (C*C*H$_3$), 4.3 (Si*TMS*$_3$).

^{29}Si NMR (99 MHz, C_6D_6, r.t.): δ = -10.2 (*TMS*$_3$), -46.0 (*Si*O), -132.5 (*Si*TMS$_3$).

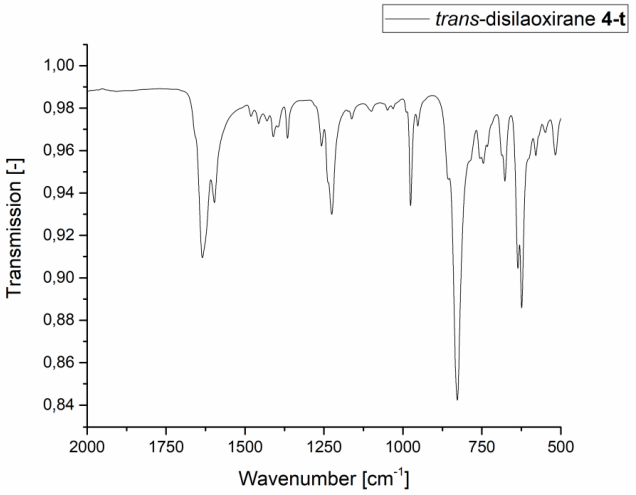

Figure S4: IR spectrum of *trans*-disilaoxirane **4-t** (cm^{-1}):1633 (m), 1595 (m), 1363 (w), 1228 (m), 976 (w), 825 (s), 629 (s).

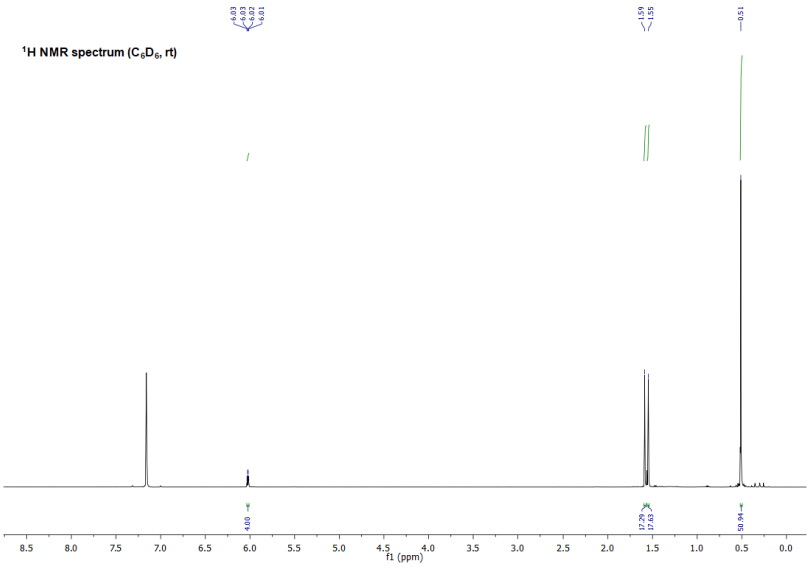

Figure S12: ^{1}H NMR spectrum of *trans*-disilaoxirane **4-t** (C_6D_6, r.t.).

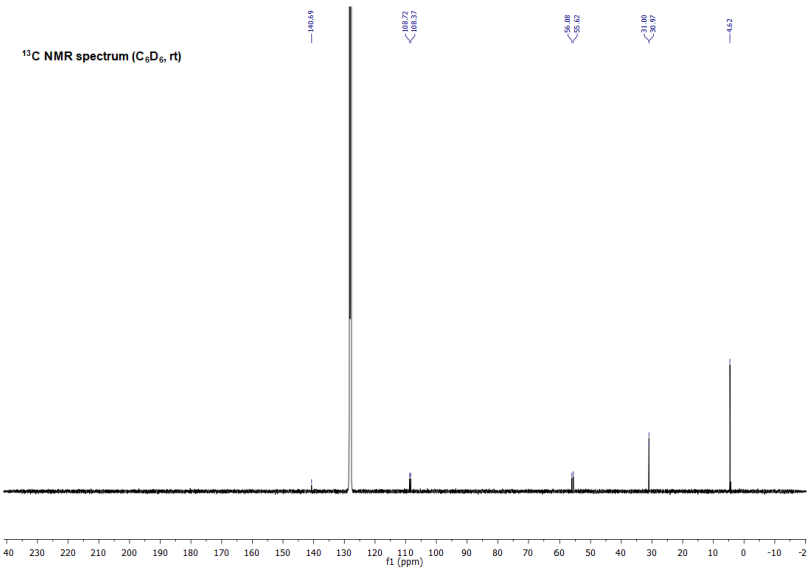

Figure S13: ^{13}C NMR spectrum of *trans*-disilaoxirane **4-t** (C_6D_6, r.t.).

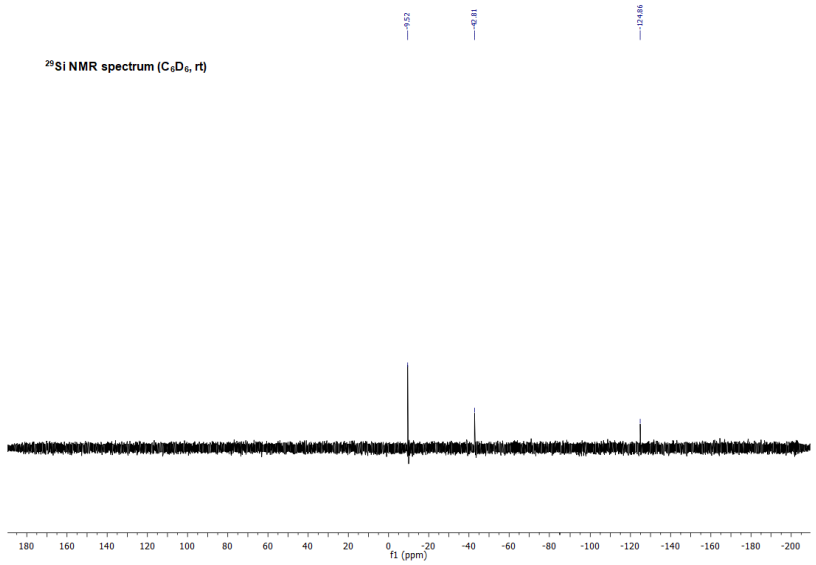

Figure S14: ^{29}Si NMR spectrum of *trans*-disilaoxirane **4-t** (C_6D_6, r.t.).

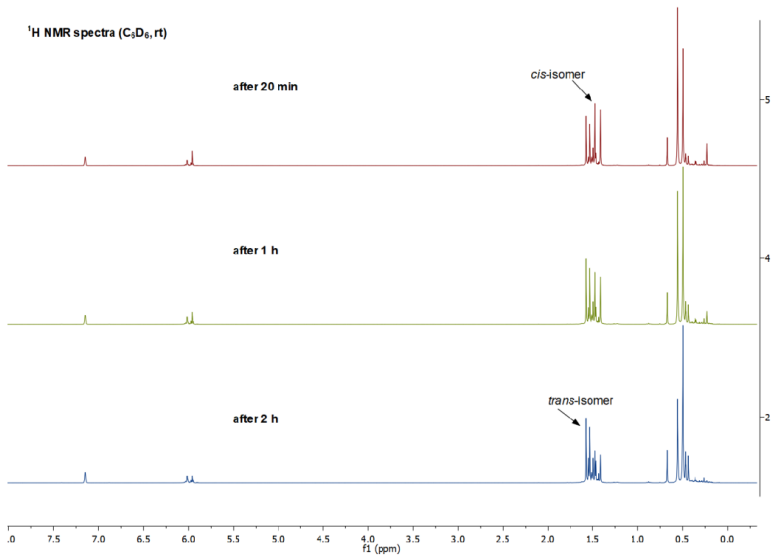

Figure S15: ^{1}H NMR spectra of the reaction of disilene **1** with N_2O after certain intervals (20 min, 1 h, 2 h) (C_6D_6, r.t.).

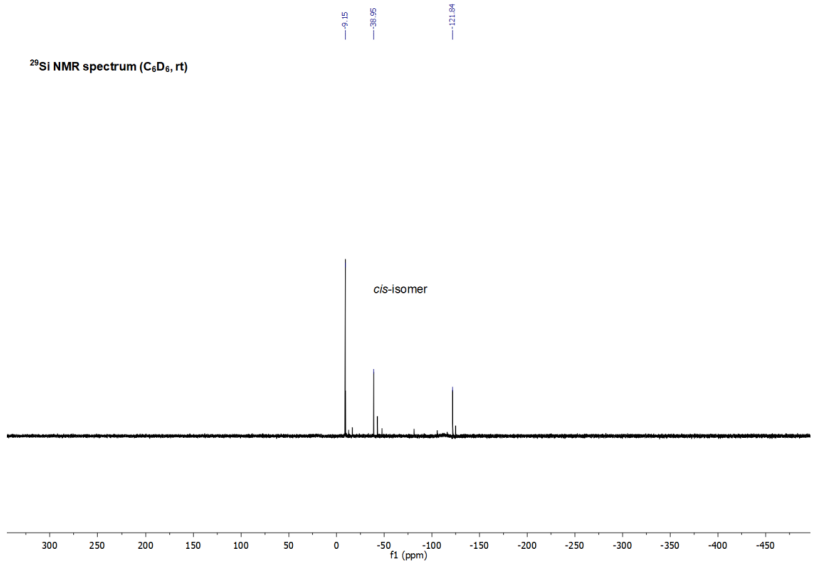

Figure S16: ^{29}Si NMR spectrum of intermediary *cis*-disilaoxirane **4-c** directly after addition of N_2O to **1** (C_6D_6, r.t.).

Synthesis of (*t*-BuN(SiTMS$_3$)SiO)$_2$ (5-c)

A pressurizable Schlenk flask filled with disilene **1** (39.9 mg, 0.042 mmol) in *n*-hexane (3 mL) was exposed to O_2 gas (1 bar) at -78 °C. The characteristic dark purple color vanished instantly, resulting in a cloudy colorless solution, which was stirred further for 10 min. Removal of all volatiles *in vacuo* gave a white crude product, which was re-dissolved in a mixture of toluene/*n*-hexane (1 mL respectively). Cooling to –35 °C for several days yielded colorless crystals of *cis*-dioxadisiletane **5-c** (33.4 mg, 0.034 mmol, 80%) suitable for single crystal X-ray analysis.

A spectroscopic investigation of the underlying mechanism similar to compound **4-t** was not feasible, since the oxygenation reaction with O_2 proceeded within seconds even at -78 °C.

Isolated *cis*-isomer 5-c:

^{1}H NMR (500 MHz, C_6D_6, r.t.): δ = 5.96 (s, 4H, C*H*-N), 1.47 (s, 36H, CC*H*$_3$), 0.56 (s, 54H, Si*TMS*$_3$).

^{13}C NMR (126 MHz, C_6D_6, r.t.): δ = 138.8 (*C*=N), 107.9 (*C*H-N), 55.7 (*C*CH$_3$), 30.3 (C*C*H$_3$), 5.0 (Si*TMS*$_3$).

^{29}Si NMR (99 MHz, C_6D_6, r.t.): δ = -9.8 (*TMS*$_3$), -44.0 (*Si*O), -129.8 (*Si*TMS$_3$).

EA experimental (calculated): C 49.42 (49.30), H 9.75 (9.79), N 8.65 (8.61) %.

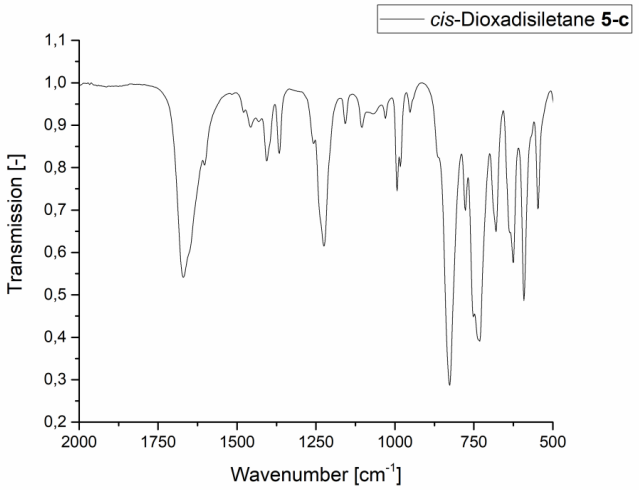

Figure S4: IR spectrum of *cis*-dioxadisiletane **5-c** (cm^{-1}):1670 (s), 1402 (w), 1365 (w), 1228 (m), 993 (w), 825 (s), 737 (s), 684 (m), 637 (m), 584 (m).

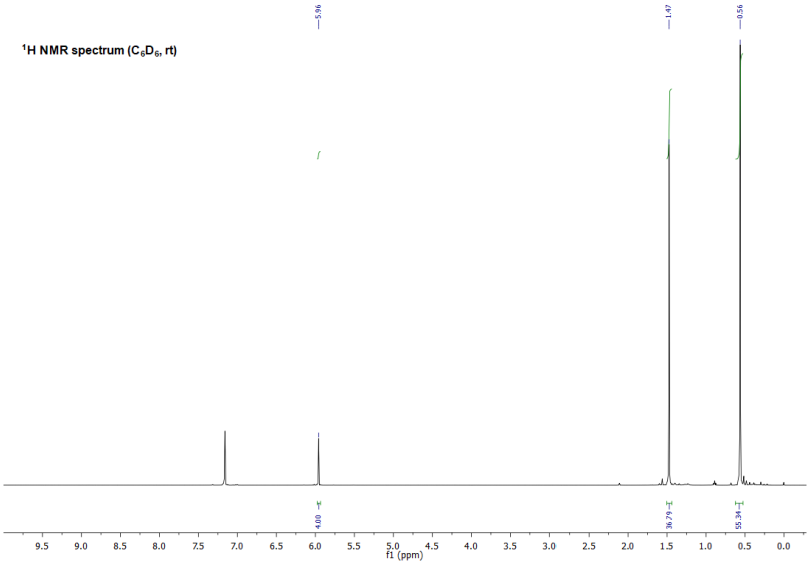

Figure S17: ^{1}H NMR spectrum of *cis*-dioxadisiletane **5-c** (C_6D_6, r.t.).

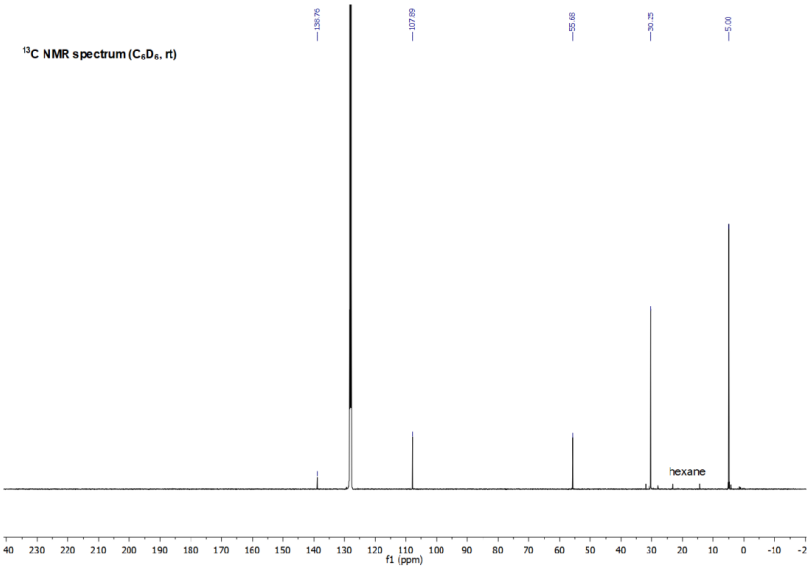

Figure S18: ^{13}C NMR spectrum of *cis*-dioxadisiletane **5-c** (C_6D_6, r.t.).

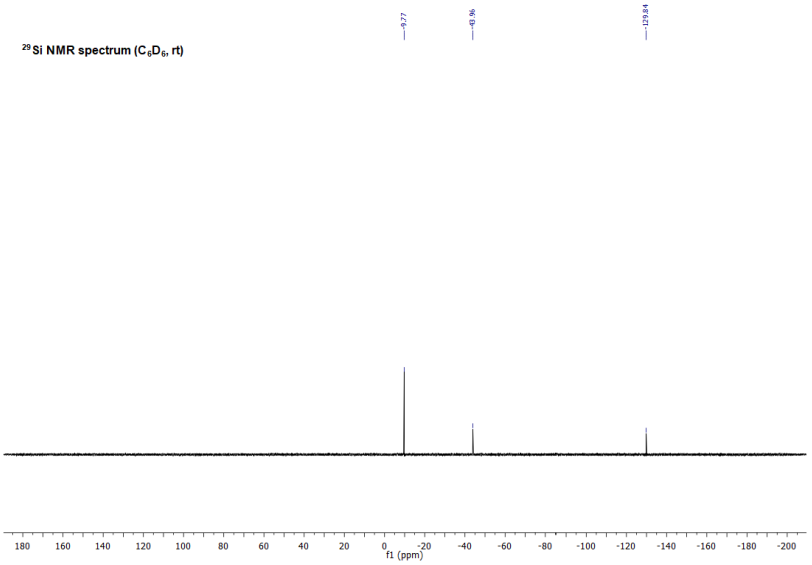

Figure S19: ^{29}Si NMR spectrum of *cis*-dioxadisiletane **5-c** (C_6D_6, r.t.).

Synthesis of (I*t*-BuN(SiTMS$_3$)Si)$_2$O(CO$_2$) (6-t)

A J. Young PTFE tube filled with *trans*-disilaoxirane **4-t** (421 mg, 0.44 mmol) in C_6D_6 (0.5 mL) (moderate solubility, yellow suspension) was exposed to CO_2 gas (1 bar) at room temperature. The characteristic yellow color of the solution slowly faded while the reaction progress was monitored *via* ^{1}H NMR spectroscopy (1 day at r.t). To overcome the low solubility of **4-t** in C_6D_6 and simultaneously increase the rate of this reaction, the solution was heated to 50 °C. Full conversion to silacycle **6-t** was detected after 4 h (note: no CO formation in ^{13}C NMR spectrum). Removal of all volatiles *in vacuo* gave a white crude product, which was re-dissolved in a mixture of toluene/*n*-hexane (1 mL respectively). Cooling to –35 °C for several days yielded colorless crystals of silacycle **6-t** (279 mg, 0.28 mmol, 63%) suitable for single crystal X-ray analysis. Repetition of this reaction in the more polar solvent THF-d_8 as well led to compound **6-t**, but was accompanied with a loss of selectivity. Compound **6-t** is permanently stable as a solid and in solution (C_6D_6). In line with our calculations, no elimination of CO to form the *trans*-isomer of disilaoxirane **4** was detected even after heating a solution of **6-t** at 90 °C for 16 h.

^{1}H NMR (500 MHz, C_6D_6, r.t.): δ = 6.08 (d, ^3J = 3.2 Hz, 1H, C*H*-N), 6.05 (d, ^3J = 3.2 Hz, 1H, C*H*-N), 5.97 (dd, ^3J = 3.2 Hz, 2H, C*H*-N), 1.57 (s, 9H, CCH_3), 1.56 (s, 9H, CCH_3), 1.53 (s, 9H, CCH_3), 1.48 (s, 9H, CCH_3), 0.47 (s, 27H, Si*TMS*$_3$), 0.46 (s, 27H, Si*TMS*$_3$).

^{13}C NMR (126 MHz, C_6D_6, r.t.): δ = 186.8 (O*C*O), 140.5 (*C*=N), 139.3 (*C*=N), 109.0 (*C*H-N), 108.8 (*C*H-N), 108.1 (*C*H-N), 107.9 (*C*H-N), 56.2 (*C*CH$_3$), 56.1 (*C*CH$_3$), 56.0 (*C*CH$_3$), 31.4 (C*C*H$_3$), 31.1 (C*C*H$_3$), 30.1 (C*C*H$_3$), 29.9 (C*C*H$_3$), 4.2 (Si*TMS*$_3$), 4.1 (Si*TMS*$_3$).

^{29}Si NMR (99 MHz, C_6D_6, r.t.): δ = -9.7 (*TMS*$_3$), -9.9 (*TMS*$_3$), -54.4 (*Si*O$_2$), -63.2 (*Si*(O)C), -132.2 (*Si*TMS$_3$), -132.8 (*Si*TMS$_3$).

EA experimental (calculated): C 49.55 (49.24), H 9.62 (9.47), N 8.28 (8.40) %.

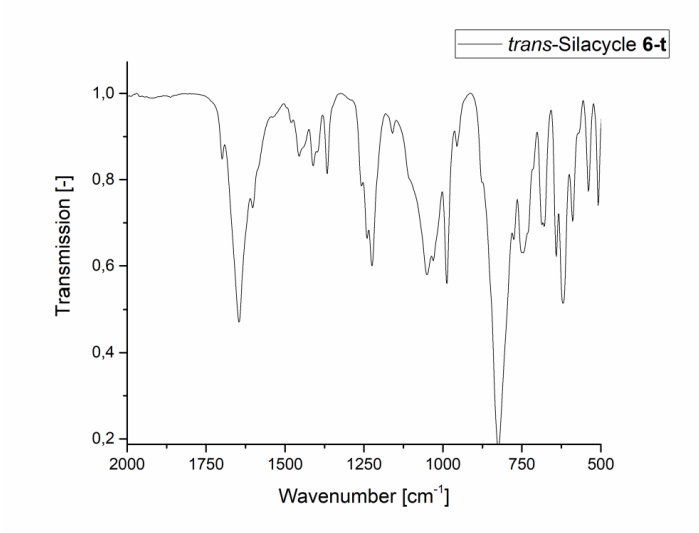

Figure S4: IR spectrum of *trans*-silacycle **6-t** (cm^{-1}):1644 (s), 1408 (w), 1366 (w), 1232 (m), 1054 (m), 979 (m), 813 (s), 745 (s), 680 (m), 616 (m).

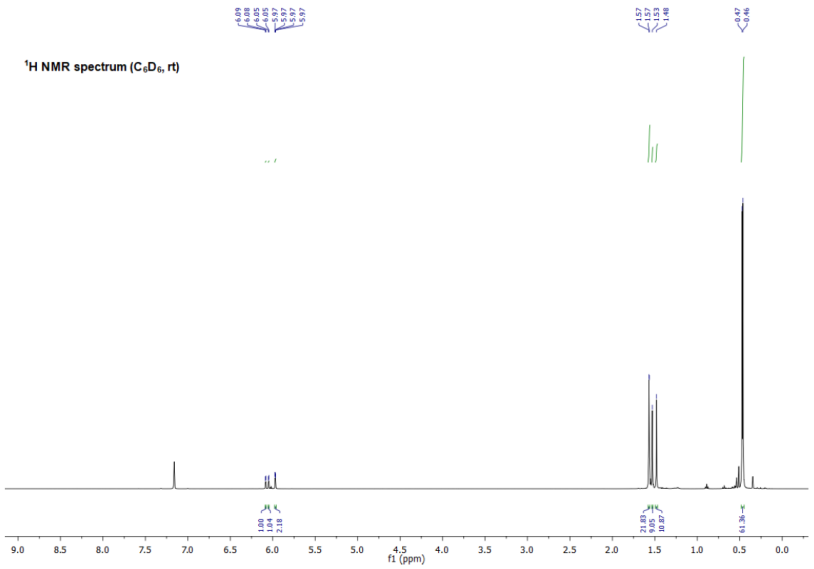

Figure S20: ^{1}H NMR spectrum of silacycle **6-t** (C_6D_6, r.t.).

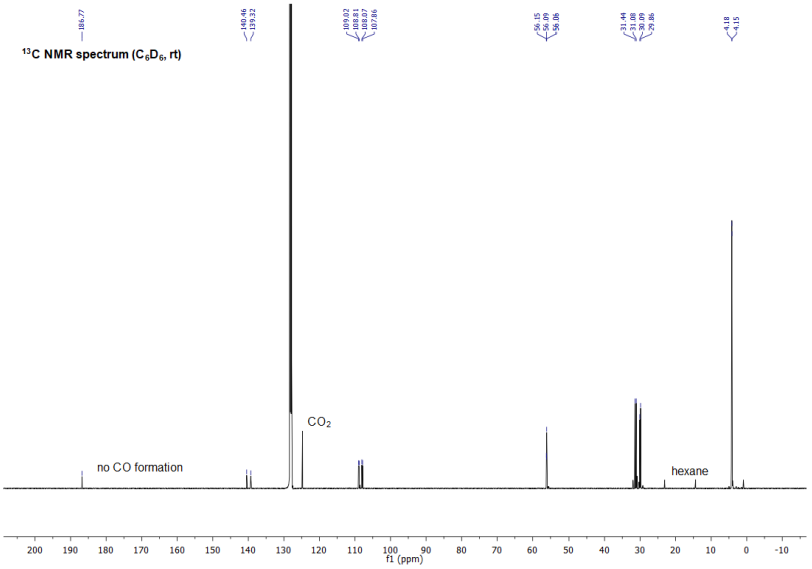

Figure S21: ^{13}C NMR spectrum of silacycle **6-t** (C_6D_6, r.t.).

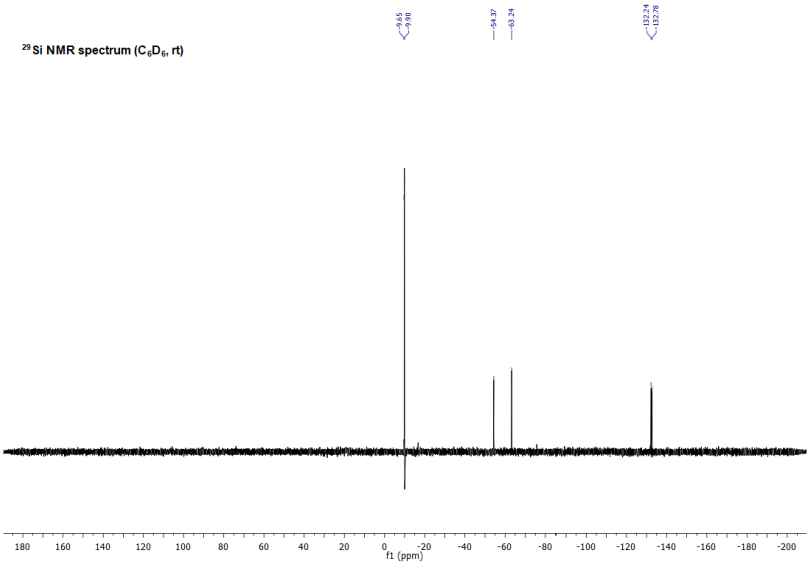

Figure S22: ^{29}Si NMR spectrum of silacycle **6-t** (C_6D_6, r.t.).

NMR experiments of disilene 1 directly with CO_2:

A J. Young PTFE tube filled with disilene **1** (14.2 mg, 0.015 mmol) in 0.5 mL C_6D_6 was exposed to CO_2 gas (1 bar) at room temperature. The characteristic dark purple color vanished instantly, resulting in a clear yellow solution. Since several products are formed in this reaction, their structures were only determined by monitoring their reaction progress *via* ^{1}H NMR spectroscopy and comparison of the NMR data with the isolated and fully characterized equivalents. The instant formation of intermediary *cis*-disilaoxirane **4-c** was detected, which in analogy to the reaction with N_2O constantly isomerizes to *trans*-isomer **4-t** (Figure S23). In line with our proposed mechanism, the formation of **4-c** was accompanied with the release of carbon monoxide (^{13}C 184.5 ppm)[S2], which as well was found in the reaction mixture (Figure S24). Interestingly, already in the first ^{1}H spectra of this experiment (Figure S23) the presence of *cis*-dioxadisiletane **5-c** was detectable, whose formation necessarily involves the elimination of two equivalents of carbon monoxide. As the observation of **5-c** occurred already in the early stages of the reaction and its concentration did not increase over time, a potential formation *via* the high-energy consuming CO release of precursors **6-c** or **6-t** (28.2 kcal/mol) can likely be excluded. We rather attribute the formation of **5-c** to the partly splitting of the Si=Si bond by the harsh oxygenation agent CO_2, similarly to the mechanism of the formation of 1,1-monosilane **2b** in the NH_3 activation. Besides, in accordance with the independently conducted CO_2 reaction of **4-t**, longer reaction times (^{29}Si NMR checked after approx. 2 days, Figure S25) revealed increasing amounts of *trans*-silacycle **6-t** due to the slow addition of CO_2 to **4-t** at room temperature. Consistently, also low intensity signals assignable to the *cis*-isomer **6-c** were identified, which was formed logically from intermediary **4-c**. This assumption was verified by a second NMR experiment, in which first disilene **1** was pressurized with N_2O (1 bar) to give a mixture of **4-c** and **4-t**. Subsequently, the excess N_2O is removed and replaced with CO_2 gas (1 bar). As seen in the ^{13}C and ^{29}Si NMR spectra of this reaction (Figure S26 and Figure S27) both five-membered silacycles **6-c** and **6-t** were formed. For this second separate experiment again no CO formation was detected, in accordance with a non-reductive addition of CO_2 to **4**.

NMR data for **6-c**:

^{1}H NMR: strong overlap with major product **6-t**: no reliable assignment possible.

^{13}C NMR (126 MHz, C_6D_6, r.t.): δ = 186.3 (O*C*O), 140.8 (*C*=N), 138.8 (*C*=N), 108.7 (*C*H-N), 108.6 (*C*H-N), 107.7 (*C*H-N), 107.6 (*C*H-N), 55.8 (*C*CH$_3$), 55.7 (*C*CH$_3$), 55.6 (*C*CH$_3$), 30.9 (C*C*H$_3$), 30.7 (C*C*H$_3$), 29.8 (C*C*H$_3$), 29.4 (C*C*H$_3$), 4.9 (Si*TMS*$_3$), 4.5 (Si*TMS*$_3$).

^{29}Si NMR (99 MHz, C_6D_6, r.t.): δ = -10.0 (*TMS*$_3$), -10.2 (*TMS*$_3$), -53.5 (*Si*O$_2$), -62.1 (*Si*(O)C), -130.3 (*Si*TMS$_3$), -131.7 (*Si*TMS$_3$).

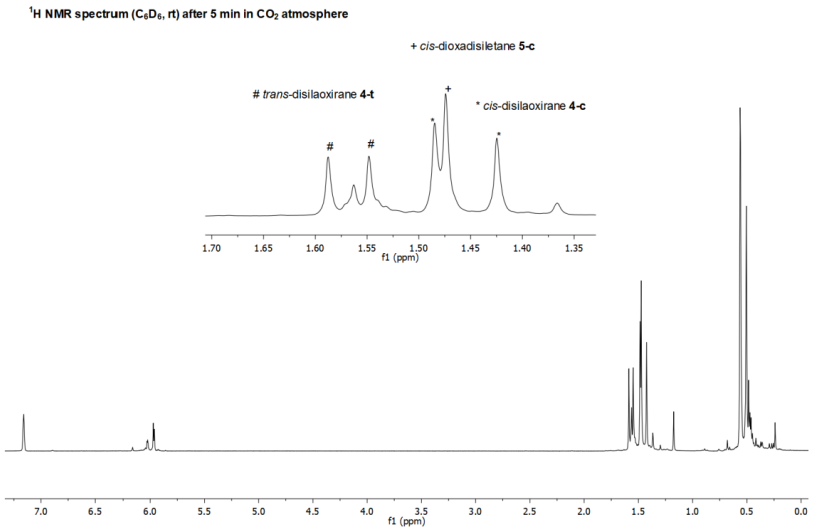

Figure S23: ^{1}H NMR spectrum of reaction of disilene **1** with CO_2 after 5 min at room temperature (C_6D_6, r.t.).

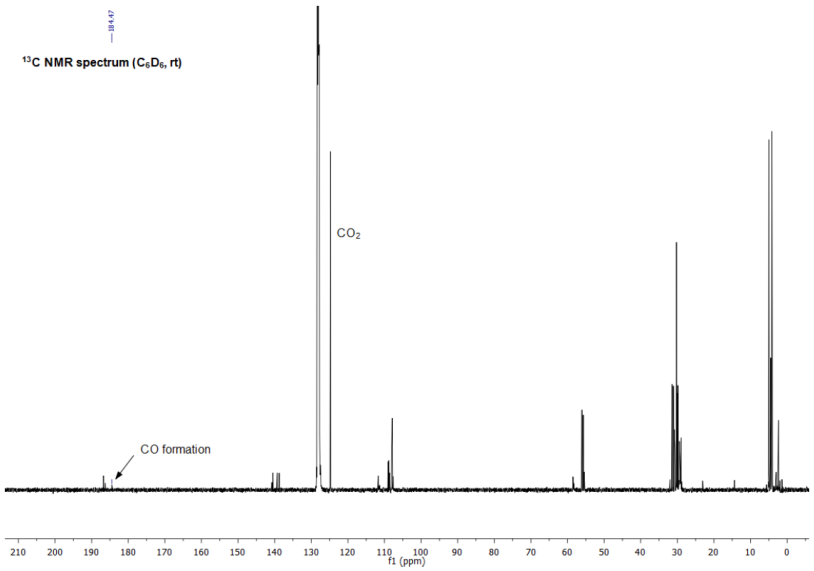

Figure S24: ^{13}C NMR spectrum of reaction of disilene **1** with CO_2 after approx. 2 days at room temperature (C_6D_6, r.t.).

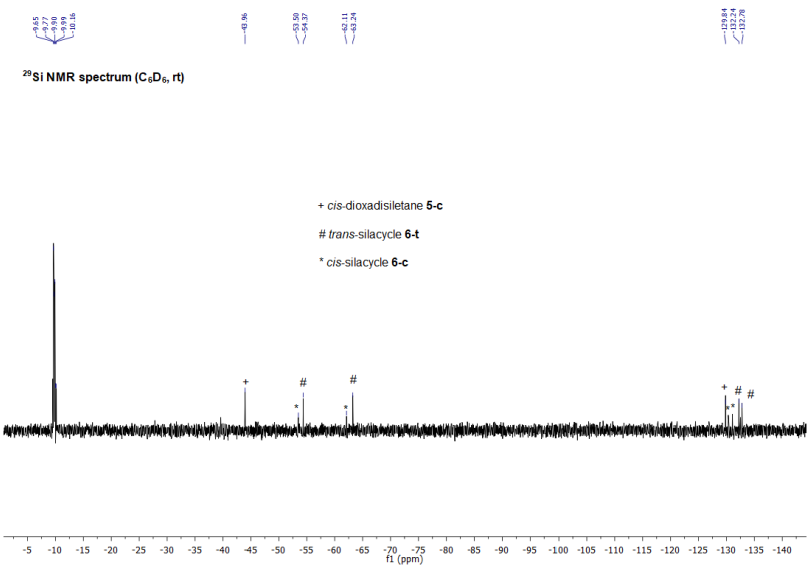

Figure S25: ^{29}Si NMR spectrum of reaction of disilene **1** with CO_2 after approx. 2 days at room temperature (C_6D_6, r.t.).

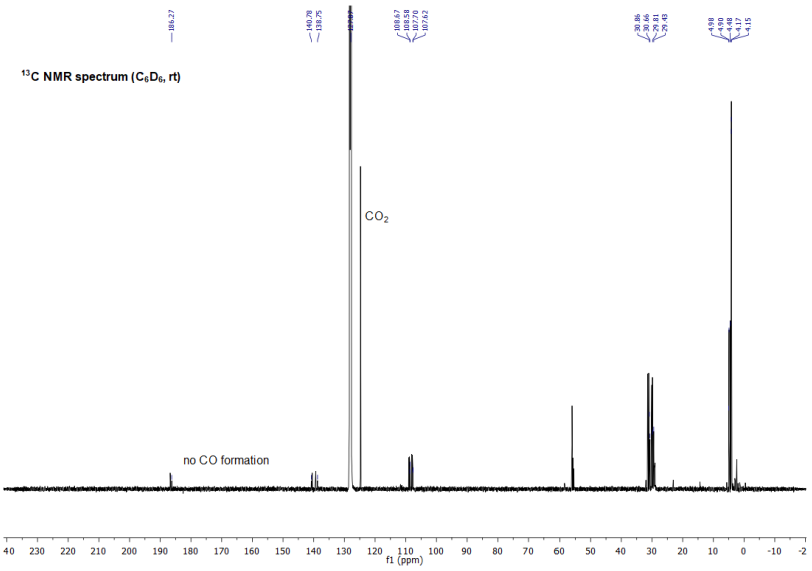

Figure S26:^{13}C NMR spectrum of reaction of disilene **1** with N_2O directly followed by CO_2 after approx. 1 day (C_6D_6, r.t.).

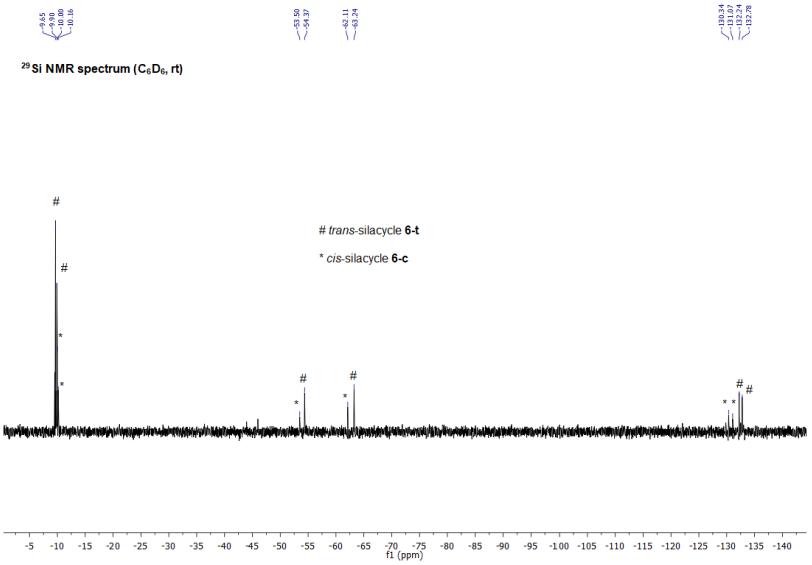

Figure S27: ^{29}Si NMR spectrum of reaction of disilene **1** with N_2O directly followed by CO_2 after approx. 1 day (C_6D_6, r.t.).

2. X-ray Crystallographic Data

General:

Data were collected on a single crystal X-ray diffractometer equipped with a CCD detector (APEX II, κ-CCD), a fine-focus sealed tube and a Triumph monochromator using the APEX II software package (**2b**, **3**, **4-t**) or with a CMOS detector (APEX III, κ-CMOS), an IMS microsource (**2a**) or a TXS rotating anode (**5-c**, **6-t**) and a Helios optic using the APEX III software package.[S3-4] All measurements were performed using MoK_α radiation (λ = 0.71073 Å). The crystals were fixed on the top of a Kapton micro sampler with perfluorinated ether, transferred to the diffractometer and frozen under a stream of cold nitrogen. A matrix scan was used to determine the initial lattice parameters. Reflections were corrected for Lorentz and polarization effects, scan speed, and background using SAINT.[S5] Absorption corrections, including odd and even ordered spherical harmonics were performed using SADABS.[S5] Space group assignments were based upon systematic absences, *E* statistics, and successful refinement of the structures. Structures were solved using SHELXT with the aid of successive difference Fourier maps, and were refined against all data using SHELXL-2014 in conjunction with SHELXLE.[S6-8] Hydrogen atoms were calculated in ideal positions as follows: methyl hydrogen atoms were refined as part of rigid rotating groups, with a C–H distance of 0.98 Å and $U_{iso}(H) = 1.5 \cdot U_{eq}(C)$. Methylene, aromatic and other H atoms were placed in calculated positions and refined using a riding model with C–H distances of 0.99 Å, 0.95 Å and 1.00 Å, respectively, and $U_{iso}(H) = 1.2U_{eq}(C)$. N–H distances and Si–H distances were set to 0.91 Å and 1.44 Å, respectively and additional constraints on angles were used to idealize typical environments for amino-groups and tetrahedrally coordinated Si at the reaction centers of ammonia activation. Non-hydrogen atoms were refined with anisotropic displacement parameters. Full-matrix least-squares refinements were carried out by minimizing $\Sigma w(F_o^2-F_c^2)^2$ with the SHELXL weighting scheme.[S7] Neutral atom scattering factors for all atoms and anomalous dispersion corrections for the non-hydrogen atoms were taken from *International Tables for Crystallography*.[S9] A split layer refinement was used for disordered groups and SIMU, DELU and SAME restraints were employed to stabilize the refinement of the layers. In the case of **2a** and **2b**, the NH_2-group and the hydrogen atom originating from NH_3 were found to be disordered and additional SADI and EADP restraints were employed. For **2b**, a free refinement of the occupancies showed an overstoichiometric ratio of NH_2-groups, which is probably due to an intermolecular H/NH_2-exchange during crystallization leading to the formation some amount of 1,1-diaminosilane. For **6-t**, the central Si(O)(OCO)Si unit showed a high degree of disorder, thus a considerable amount of constraints were necessary to carve out the structural motif. **3** contains one

disordered toluene molecule and **4-t** contains one disordered benzene molecule which both were treated as a diffuse contribution to the overall scattering without specific atom positions using the PLATON/SQUEEZE procedure.[S10] Images were created with Mercury.[S11]

Compound **2a** (CCDC XYZ)

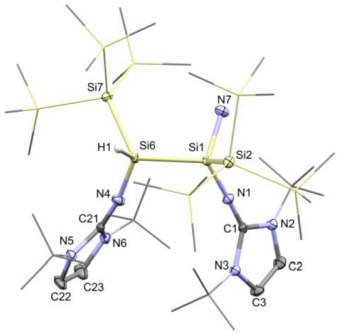

Figure S28. Molecular structure of compound **2a**.

Table S1. Crystallographic data for compound **2a**.

Diffractometer operator C. Jandl
scanspeed 5 s per frame
dx 50 mm
1809 frames measured in 5 data sets
phi-scans with delta_phi = 0.5
omega-scans with delta_omega = 0.5
shutterless mode

Crystal data

$C_{40}H_{97}N_7Si_{10}$

M_r = 956.84	D_x = 1.078 Mg m^{-3}
Monoclinic, $P2_1/c$	Melting point: ? K
Hall symbol: -P 2ybc	Mo $K\alpha$ radiation, λ = 0.71073 Å
a = 19.7763 (11) Å	Cell parameters from 9274 reflections
b = 14.2972 (9) Å	θ = 2.4–26.4°
c = 22.3661 (14) Å	μ = 0.26 mm^{-1}
β = 111.182 (2)°	T = 100 K
V = 5896.7 (6) Å^3	Fragment, colourless
Z = 4	0.56 × 0.47 × 0.38 mm
F(000) = 2103	

Data collection

Bruker Photon CMOS diffractometer	11615 independent reflections
Radiation source: IMS microsource	10166 reflections with $I > 2\sigma(I)$
Helios optic monochromator	R_{int} = 0.042
Detector resolution: 16 pixels mm^{-1}	θ_{max} = 26.0°, θ_{min} = 2.2°
phi– and ω–rotation scans	h = –24 22
Absorption correction: multi-scan *SADABS* 2014/5	k = –17 17
T_{min} = 0.705, T_{max} = 0.745	l = –27 27
117894 measured reflections	

Refinement

Refinement on F^2	Secondary atom site location: difference Fourier map
Least-squares matrix: full	Hydrogen site location: mixed
$R[F^2 > 2\sigma(F^2)]$ = 0.037	H atoms treated by a mixture of independent and constrained refinement
$wR(F^2)$ = 0.087	$W = 1/[\Sigma^2(FO^2) + (0.0315P)^2 + 6.1294P]$ WHERE $P = (FO^2 + 2FC^2)/3$
S = 1.04	$(\Delta/\sigma)_{max}$ = 0.001
11615 reflections	$\Delta\rho_{max}$ = 0.67 e Å^{-3}
560 parameters	$\Delta\rho_{min}$ = –0.65 e Å^{-3}
14 restraints	Extinction correction: none
0 constraints on non-H atoms	Extinction coefficient: -
Primary atom site location: intrinsic phasing	

Compound **2b** (CCDC XYZ)

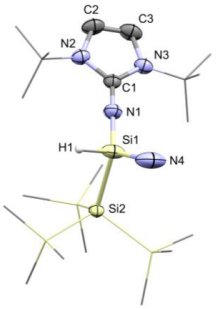

Figure S29. Molecular structure of compound **2b**.

Table S2. Crystallographic data for compound **2b**.

Diffractometer operator C. Jandl
scanspeed 10 s per frame
dx 40 mm
3279 frames measured in 7 data sets
phi-scans with delta_phi = 0.5
omega-scans with delta_omega = 0.5

Crystal data

$C_{20}H_{50.25}N_{4.25}Si_5$

M_r = 490.78	D_x = 1.058 Mg m^{-3}
Monoclinic, $P2_1/c$	Melting point: ? K
Hall symbol: -P 2ybc	Mo $K\alpha$ radiation, λ = 0.71073 Å
a = 9.636 (3) Å	Cell parameters from 9670 reflections
b = 19.228 (6) Å	θ = 2.4–25.2°
c = 16.630 (5) Å	μ = 0.25 mm^{-1}
β = 90.278 (17)°	T = 100 K
V = 3081.2 (16) Å^3	Fragment, colourless
Z = 4	0.41 × 0.24 × 0.21 mm
F(000) = 1080	

Data collection

Apex II CCD diffractometer	6067 independent reflections

Radiation source: fine-focus sealed tube	4521 reflections with $I > 2\sigma(I)$
Triumph monochromator	R_{int} = 0.064
Detector resolution: 16 pixels mm^{-1}	θ_{max} = 26.0°, θ_{min} = 1.6°
phi– and ω–rotation scans	h = –11 11
Absorption correction: multi-scan *SADABS* 2016/2	k = –23 23
T_{min} = 0.693, T_{max} = 0.745	l = –20 20
79359 measured reflections	

Refinement

Refinement on F^2	Secondary atom site location: difference Fourier map
Least-squares matrix: full	Hydrogen site location: mixed
$R[F^2 > 2\sigma(F^2)]$ = 0.041	H atoms treated by a mixture of independent and constrained refinement
$wR(F^2)$ = 0.109	$W = 1/[\Sigma^2(FO^2) + (0.0526P)^2 + 0.9484P]$ WHERE $P = (FO^2 + 2FC^2)/3$
S = 1.03	$(\Delta/\sigma)_{max} < 0.001$
6067 reflections	$\Delta\rho_{max}$ = 0.33 e Å^{-3}
426 parameters	$\Delta\rho_{min}$ = –0.21 e Å^{-3}
329 restraints	Extinction correction: none
0 constraints on non-H atoms	Extinction coefficient: -
Primary atom site location: intrinsic phasing	

Compound **3** (CCDC XYZ)

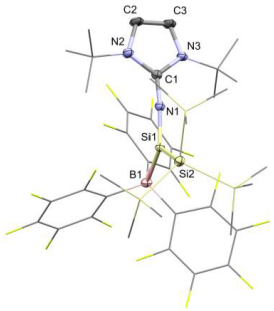

Figure S30. Molecular structure of compound **3**.

Table S3.Crystallographic data for compound **3**.

Diffractometer operator P. Altmann
scanspeed 3 s per frame
dx 44 mm
2690 frames measured in 7 data sets
phi-scans with delta_phi = 0.5
omega-scans with delta_omega = 0.5

Crystal data

$C_{38}H_{47}BF_{15}N_3Si_5 \cdot C_7H_8$	$F(000)$ = 1112
M_r = 1074.18	
Triclinic, $P\bar{1}$	D_x = 1.303 Mg m^{-3}
Hall symbol: -P 1	Melting point: ? K
a = 11.5650 (13) Å	Mo $K\alpha$ radiation, λ = 0.71073 Å
b = 12.5830 (15) Å	Cell parameters from 9847 reflections
c = 21.645 (3) Å	θ = 2.2–25.7°
α = 95.265 (5)°	μ = 0.22 mm^{-1}
β = 100.829 (5)°	T = 100 K
γ = 115.527 (5)°	Fragment, yellow
V = 2738.2 (6) Å^3	0.37 × 0.29 × 0.17 mm
Z = 2	

Data collection

Apex II CCD diffractometer	9653 independent reflections

Radiation source: fine-focus sealed tube	8128 reflections with i > 2σ(i)
Triumph monochromator	R_{int} = 0.034
Detector resolution: 16 pixels mm^{-1}	θ_{max} = 25.0°, θ_{min} = 2.0°
phi– and ω–rotation scans	h = –13 13
Absorption correction: multi-scan *SADABS* 2016/2	k = –14 14
T_{min} = 0.687, T_{max} = 0.745	l = –25 25
51416 measured reflections	

Refinement

Refinement on F^2	Secondary atom site location: difference Fourier map
Least-squares matrix: full	Hydrogen site location: inferred from neighbouring sites
$R[F^2 > 2\sigma(F^2)]$ = 0.033	H-atom parameters constrained
$wR(F^2)$ = 0.086	W = 1/[$\Sigma^2(FO^2) + (0.0395P)^2 + 1.4469P$] WHERE $P = (FO^2 + 2FC^2)/3$
S = 1.02	$(\Delta/\sigma)_{max}$ = 0.001
9653 reflections	$\Delta\rho_{max}$ = 0.34 e Å^{-3}
638 parameters	$\Delta\rho_{min}$ = –0.28 e Å^{-3}
0 restraints	Extinction correction: none
0 constraints on non-H atoms	Extinction coefficient: -
Primary atom site location: intrinsic phasing	

Compound **4-t** (CCDC XYZ)

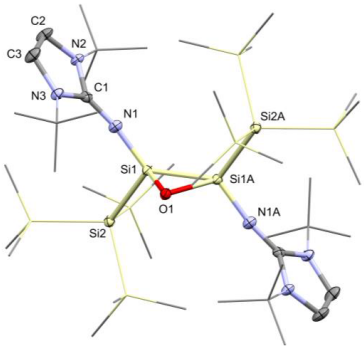

Figure S31. Molecular structure of compound **4-t**.

Table S4. Crystallographic data for compound **4-t**.

Diffractometer operator Philipp J. Altmann
scanspeed 5 s per frame
dx 35 mm
2617 frames measured in 9 data sets
phi-scans with delta_phi = 0.5
omega-scans with delta_omega = 0.5

Crystal data

$C_{40}H_{94}N_6OSi_{10}$	$F(000)$ = 524
M_r = 956.11	
Triclinic, *P*	D_x = 1.018 Mg m^{-3}
Hall symbol: -P 1	Melting point: ? K
a = 10.1005 (15) Å	Mo $K\alpha$ radiation, λ = 0.71073 Å
b = 12.3755 (16) Å	Cell parameters from 8406 reflections
c = 13.755 (2) Å	θ = 2.3–25.5°
α = 75.131 (6)°	μ = 0.24 mm^{-1}
β = 73.172 (6)°	T = 100 K
γ = 75.088 (6)°	Fragment, clear pale orange
V = 1559.2 (4) Å^3	0.24 × 0.14 × 0.11 mm
Z = 1	

Data collection

Apex II CCD diffractometer	5495 independent reflections
Radiation source: fine-focus sealed tube	4423 reflections with $I > 2\sigma(I)$
Triumph monochromator	R_{int} = 0.056
Detector resolution: 16 pixels mm^{-1}	θ_{max} = 25.0°, θ_{min} = 2.1°
phi– and ω–rotation scans	h = −12 12
Absorption correction: multi-scan *SADABS* 2014/5	k = −14 14
T_{min} = 0.709, T_{max} = 0.745	l = −16 16
45737 measured reflections	

Refinement

Refinement on F^2	Secondary atom site location: difference Fourier map
Least-squares matrix: full	Hydrogen site location: inferred from neighbouring sites
$R[F^2 > 2\sigma(F^2)]$ = 0.033	H-atom parameters constrained
$wR(F^2)$ = 0.074	$W = 1/[\Sigma^2(FO^2) + (0.0302P)^2 + 0.6826P]$ WHERE $P = (FO^2 + 2FC^2)/3$
S = 1.03	$(\Delta/\sigma)_{max} \leq 0.001$
5495 reflections	$\Delta\rho_{max}$ = 0.29 e Å^{-3}
277 parameters	$\Delta\rho_{min}$ = −0.19 e Å^{-3}
0 restraints	Extinction correction: none
0 constraints on non-H atoms	Extinction coefficient: -
Primary atom site location: intrinsic phasing	

Compound **5-c** (CCDC XYZ)

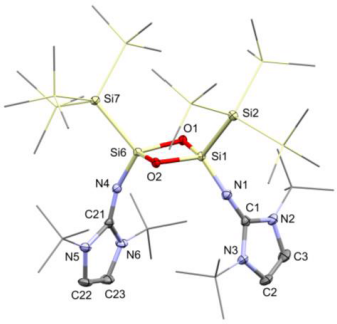

Figure S32. Molecular structure of compound **5-c**.

Table S5.Crystallographic data for compound **5-c**.

Diffractometer operator Philipp J. Altmann
scanspeed 10 s per frame
dx 50 mm
2140 frames measured in 7 data sets
phi-scans with delta_phi = 0.5
omega-scans with delta_omega = 0.5
shutterless mode

Crystal data

$C_{40}H_{94}N_6O_2Si_{10}$	$F(000)$ = 2128
M_r = 972.11	
Triclinic, *P*	D_x = 1.100 Mg m^{-3}
Hall symbol: -P 1	Melting point: ? K
a = 13.1009 (12) Å	Mo *K*α radiation, λ = 0.71073 Å
b = 19.8564 (18) Å	Cell parameters from 9174 reflections
c = 24.454 (2) Å	θ = 2.4–25.7°
α = 72.371 (3)°	μ = 0.26 mm^{-1}
β = 89.894 (3)°	T = 100 K
γ = 76.245 (3)°	Fragment, clear colourless
V = 5871.8 (9) Å^3	0.15 × 0.07 × 0.06 mm
Z = 4	

Data collection

Bruker Photon CMOS diffractometer	20741 independent reflections
Radiation source: TXS rotating anode	15834 reflections with $I > 2\sigma(I)$
Helios optic monochromator	R_{int} = 0.072
Detector resolution: 16 pixels mm^{-1}	θ_{max} = 25.0°, θ_{min} = 2.3°
phi– and ω–rotation scans	h = −15 15
Absorption correction: multi-scan *SADABS* 2014/5	k = −23 23
T_{min} = 0.725, T_{max} = 0.745	l = −29 29
160309 measured reflections	

Refinement

Refinement on F^2	Secondary atom site location: difference Fourier map
Least-squares matrix: full	Hydrogen site location: inferred from neighbouring sites
$R[F^2 > 2\sigma(F^2)]$ = 0.038	H-atom parameters constrained
$wR(F^2)$ = 0.081	W = 1/[$\Sigma^2(FO^2)$ + (0.0292P)^2 + 4.3779P] WHERE P = (FO^2 + 2FC^2)/3
S = 1.01	$(\Delta/\sigma)_{max}$ = 0.001
20741 reflections	$\Delta\rho_{max}$ = 0.38 e Å^{-3}
1105 parameters	$\Delta\rho_{min}$ = −0.29 e Å^{-3}
0 restraints	Extinction correction: none
0 constraints on non-H atoms	Extinction coefficient: -
Primary atom site location: intrinsic phasing	

Compound **6-t** (CCDC XYZ)

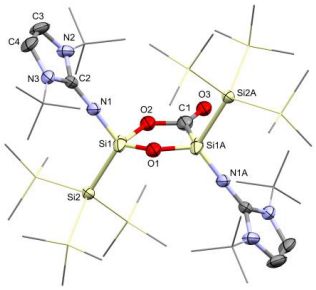

Figure S33. Molecular structure of compound **6-t**.

Table S6. Crystallographic data for compound **6-t**.

Diffractometer operator Philipp J. Altmann
scanspeed 10 s per frame
dx 34 mm
995 frames measured in 7 data sets
phi-scans with delta_phi = 0.5
omega-scans with delta_omega = 0.5
shutterless mode

Crystal data

$C_{41}H_{94}N_6O_{2.75}Si_{10}$

M_r = 996.19	D_x = 1.133 Mg m^{-3}
Monoclinic, $P2_1/n$	Melting point: ? K
Hall symbol: -P 2yn	Mo $K\alpha$ radiation, λ = 0.71073 Å
a = 13.4486 (6) Å	Cell parameters from 9994 reflections
b = 14.1316 (7) Å	θ = 2.2–25.6°
c = 15.7287 (8) Å	μ = 0.26 mm^{-1}
β = 102.323 (2)°	T = 115 K
V = 2920.4 (2) Å^3	Block, clear colourless
Z = 2	0.18 × 0.10 × 0.08 mm
F(000) = 1088	

Data collection

Bruker Photon CMOS diffractometer	5341 independent reflections
Radiation source: TXS rotating anode	4653 reflections with $I > 2\sigma(I)$
Helios optic monochromator	R_{int} = 0.048
Detector resolution: 16 pixels mm^{-1}	θ_{max} = 25.4°, θ_{min} = 2.3°
phi– and ω–rotation scans	h = −16 16
Absorption correction: multi-scan *SADABS* 2014/5	k = −17 17
T_{min} = 0.699, T_{max} = 0.745	l = −18 18
41739 measured reflections	

Refinement

Refinement on F^2	Secondary atom site location: difference Fourier map
Least-squares matrix: full	Hydrogen site location: inferred from neighbouring sites
$R[F^2 > 2\sigma(F^2)]$ = 0.084	H-atom parameters constrained
$wR(F^2)$ = 0.173	$W = 1/[\Sigma^2(FO^2) + (0.0068P)^2 + 12.9514P]$ WHERE $P = (FO^2 + 2FC^2)/3$
S = 1.17	$(\Delta/\sigma)_{max} \leq 0.001$
5341 reflections	$\Delta\rho_{max}$ = 0.91 e Å^{-3}
326 parameters	$\Delta\rho_{min}$ = −0.75 e Å^{-3}
96 restraints	Extinction correction: none
0 constraints on non-H atoms	Extinction coefficient: -
Primary atom site location: intrinsic phasing	

3. Computational Calculations

General:

All geometry optimizations were carried out at B3LYP-D3(BJ)/def2-SVP level of theory[S12-15]. Harmonic frequency calculations were used to verify the stable minimum energy structures. Further theoretical analyses (Natural Population Analysis, Wiberg Bond Index, and IR) were conducted at the same level of theory which had been proved to be satisfactory to describe the electronic structure disilene compounds.[S12] NMR shifts were calculated using a special basis set for Si (IGLO-III) instead of def2-SVP, which was developed for NMR shift calculations,[S16,S17] together with B3LYP functional using the previously optimized geometries. All calculations were executed using Gaussian 09[S18].

Theoretical Investigations:

Analysis of the HOMOs in the transition states of the H_2 and NH_3 activation (Figure S34 and Figure S35) shows the interaction of the σ*-orbital of the H–H and N–H bonds with the HOMO of **1** leading to the cleavage of both bonds and the formation of Si–H bonds, respectively. In the LUMOs of the transition states, the presence of the LUMO of **1** is very distinct in both cases. The σ-orbital of the H_2 molecule is also evident in the LUMO of the H_2 activation but the σ-orbital of the N–H bond is less clear. We think that this is because before the transition state the lone pair of the NH_3 interacts with the LUMO of **1** facilitating the reaction between NH_3 and **1**. Therefore, both orbitals (σ-orbital of the N–H bond and the lone pair of NH_3) participates in the overall reaction. The presence of the lone pair on the NH_3 can be one important feature why the calculated transition state energy is significantly lower in case of NH_3 than that of H_2. Figure S36 shows the alternative reaction pathway of NH_3 and **1**. The HOMO depicts the lone pairs of the silylene moieties (also resembling the HOMO of **1**) while the LUMO shows the vacant p-orbital of the leaving silylene and the σ*-orbital of the forming Si–N bond.

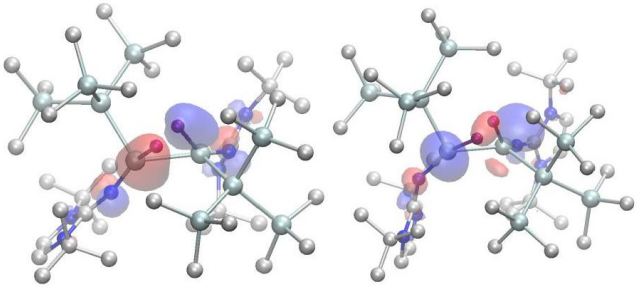

Figure S34: HOMO (left, -4.34 eV) and LUMO (right, -0.53 eV) of *anti*-addition transition state of compound **1** and H_2. Hydrogens except for the reacting H_2 molecule are omitted for clarity.

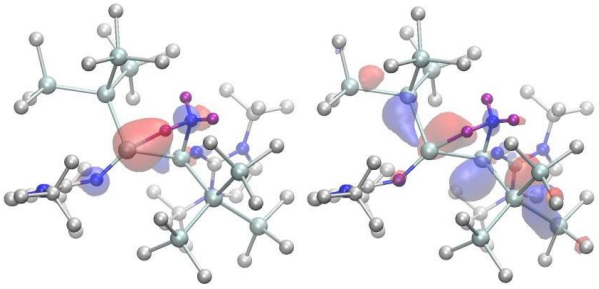

Figure S35: HOMO (left, -3.78 eV) and LUMO (right, -0.10 eV) of *anti*-addition transition state of compound **1** and NH_3 (TS1). Hydrogens except for the reacting NH_3 molecule are omitted for clarity.

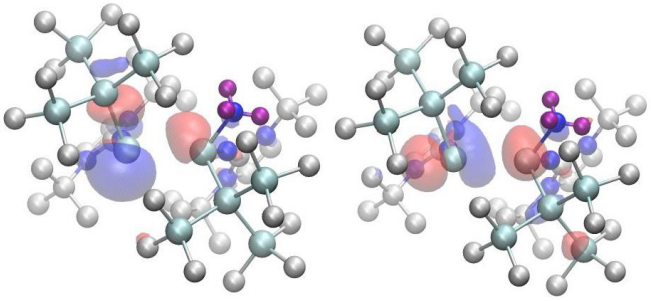

Figure S36: HOMO (left, -3.46 eV) and LUMO (right, -0.31 eV) of transition state of compound **1** and NH_3 (TS2). Hydrogens except for the reacting NH_3 molecule are omitted for clarity.

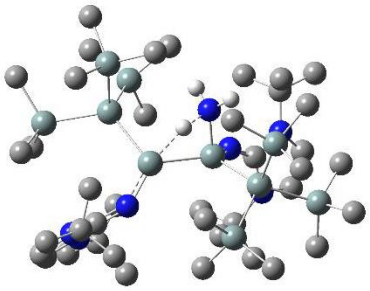

Figure S37: *Anti*-addition transition state (TS1) of compound **1** and NH_3. Hydrogens except for the reacting NH_3 molecule are omitted for clarity. White, blue, tan, and gray colors refer to H, N, Si, and C atoms, respectively.

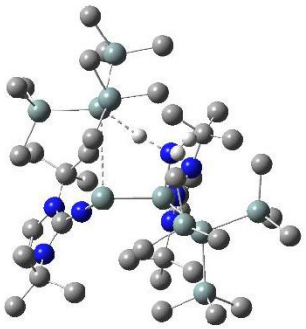

Figure S38: Alternative transition state (TS1') of compound **1** and NH_3. Hydrogens except for the reacting NH_3 molecule are omitted for clarity. White, blue, tan, and gray colors refer to H, N, Si, and C atoms, respectively.

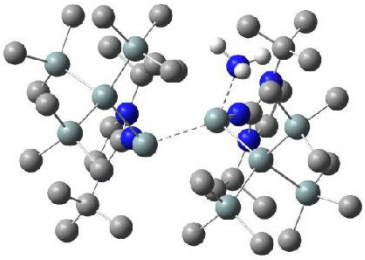

Figure S39: Transition state (TS2) of compound **1** and NH_3. Hydrogens except the reacting NH_3 molecule are omitted for clarity. White, blue, tan, and gray colors refer to H, N, Si, and C atoms, respectively.

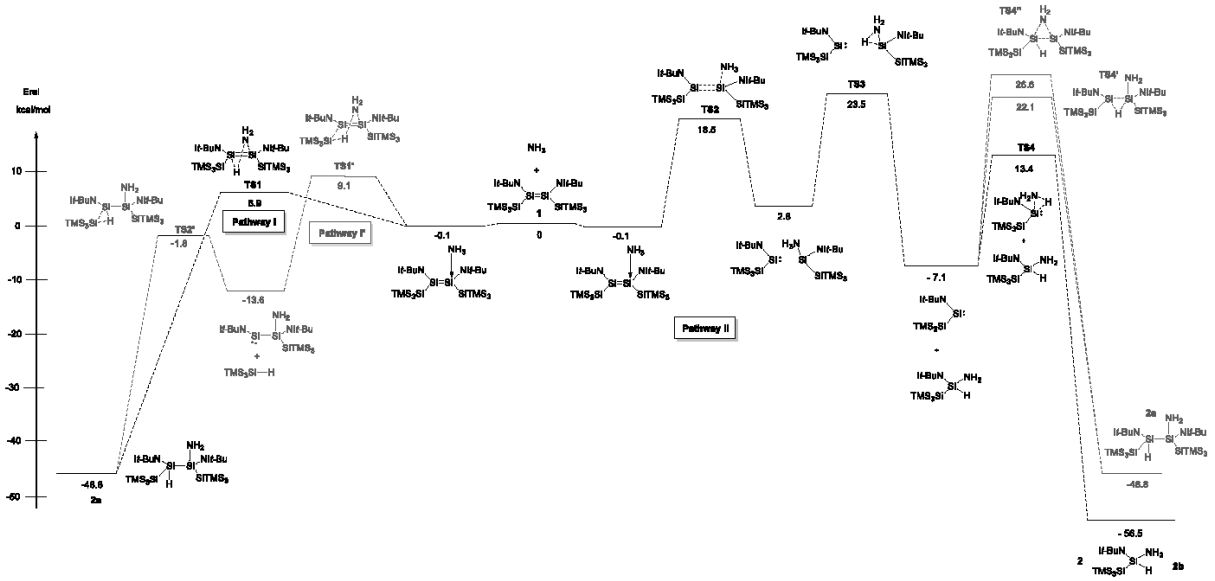

Scheme 1: Energy profile of the NH_3 activation by imino(silyl)disilene **1** to give 1,2-disilane **2a** and 1,1-monosilane **2b**, respectively.

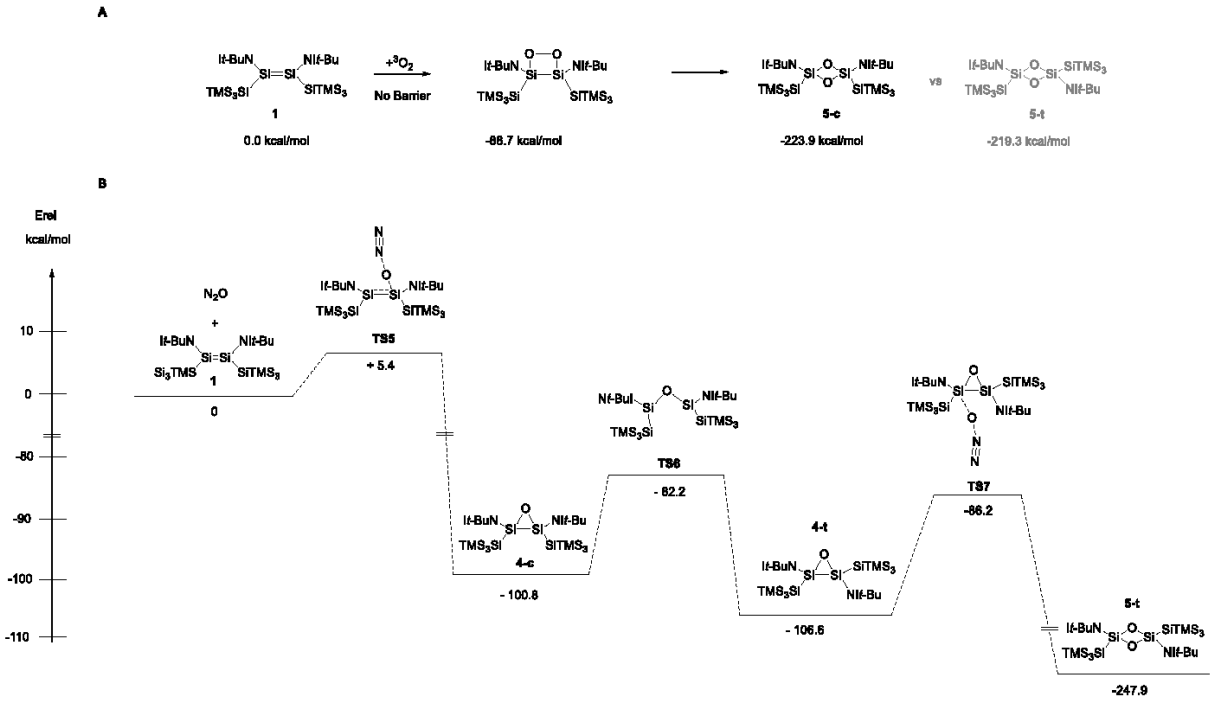

Scheme 2: A) Energetics of the oxygenation of imino(silyl)disilene **1** with $^3O_2$ to afford *cis*-dioxadisiletane **5-c** and energetic comparison to less stable *trans*-isomer **5-t** B) Energy profile of the reaction of **1** with N_2O to disilaoxiranes **4-c** and **4-t** including the second N_2O attack to give **5-t**.

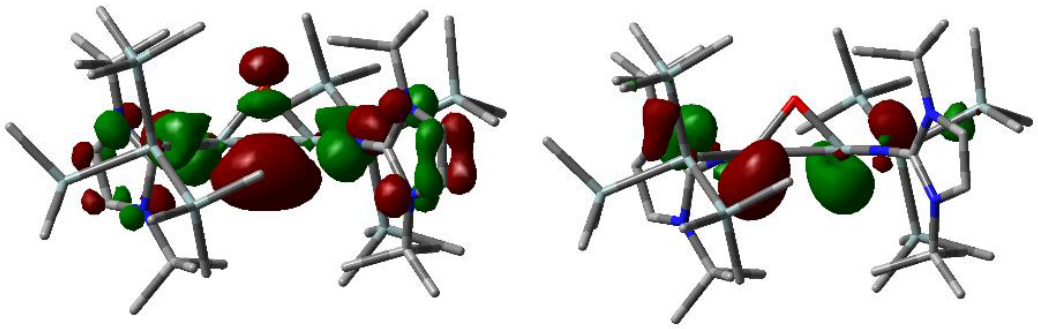

Figure S40: HOMO (-4.28 eV) and LUMO (-0.39 eV) of *trans*-disilaoxirane **4-t**.

The interaction of N_2O and CO_2 with the depicted orbitals in Figure S39 can explain their relative difference in reactivity. In case of N_2O, the interaction with the LUMO of **4-t** is the main factor, however the LUMO lies high in energy (-0.39 eV) and is sterically protected by the hypersilyl and IPrN groups. Note that the presence of an oxygen atom in **4-t** forced all the bulky groups to the other side of the molecule causing significantly larger steric hindrance compared to **1**. In case of the electrophilic carbonyl center of CO_2, the interaction with the HOMO of **4-t** is the dominating factor, which is still available in terms of energy and spatially as well. Therefore, reaction of **4-t** with CO_2 is predicted to be faster than that of N_2O (see also energy barrier $\Delta E^{\ddagger}$ (CO_2) = 11.9 kcal/mol vs. $\Delta E^{\ddagger}$ (N_2O) = 20.4 kcal/mol).

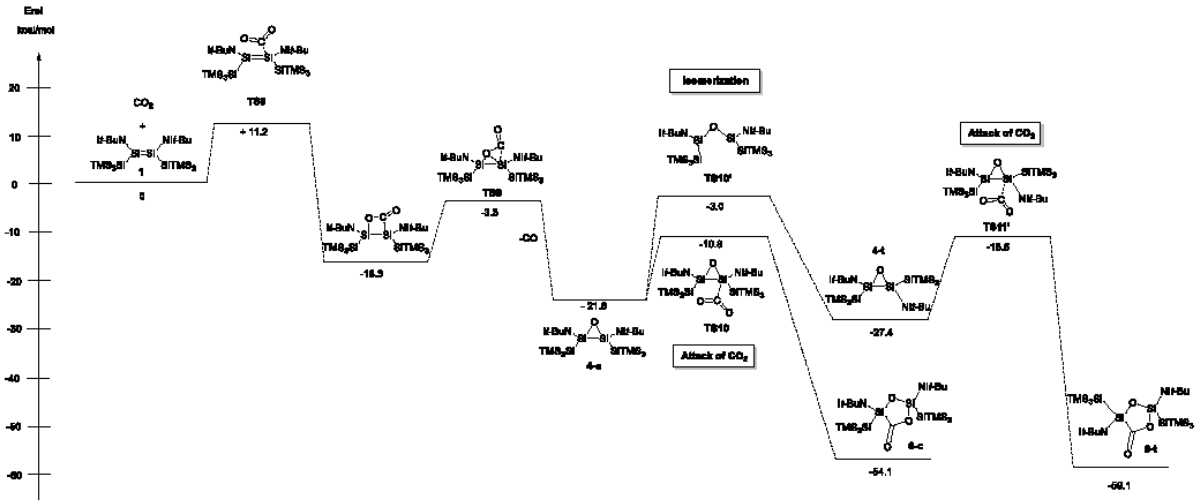

Scheme 3: Energy profile of the reaction of CO_2 and imino(silyl)disilene **1** to disilaoxiranes **4-c** and **4-t** and the following pathways to the five-membered silacycles **6-c** and **6-t**.

Electronic description of compound 6-t

Table S7: Selected WBI and NPA charges of **6-t**.

Bond	WBI	NPA charges
$Si_{1A}O_1$	0.55	+1.60/-1.23
Si_1O_1	0.58	+1.91/-1.23
$Si_{1A}C_1$	0.73	+1.60/+0.45
Si_1O_2	0.48	+1.91/-0.88
C_1O_2	1.02	+0.45/-0.88
C_1O_3	1.73	+0.45/-0.62
$Si_{1A}N_{1A}$	0.78	+1.60/-1.15
$N_{1A}C_{2A}$	1.47	-1.15/+0.71
Si_1N_1	0.78	+1.91/-1.17
N_1C_2	1.46	-1.17/+0.71

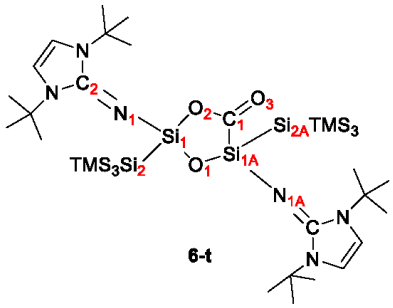

6-t

Calculated IR Stretching Frequencies of 4-t, 5-c and 6-t

Table S8: Experimental and calculated IR frequencies.

Compound	Mode	Exp. ν [cm^{-1}]	Calc. ν [cm^{-1}]
2a	Si–H	2021	2067
	$SiNH_2$	3463, 3378	3517, 3425
2b	Si–H	2030	2059
	$SiNH_2$	3441, 3370	3497, 3404
4-t	Si–O–Si	825	808
	N=C	1633	1753, 1784
5-c	Si–O–Si	825	826, 834
	N=C	1670	1749, 1777
6-t	Si–O–Si	813	840
	C–O	1054	1091
	C=O/N=C	1644	1717, 1690, 1688

Calculated NMR Values

Table S9: Experimental and calculated NMR chemical shifts ($\delta(SiMe_4) = 0$).

Compound	Si	Exp. $\delta(^{29}Si)$ [ppm]	Calc. $\delta(^{29}Si)$ [ppm]	Δ [ppm]
4-c	*TMS*$_3$	-9.2	-7.1	2.1
	*Si*O	-39.0	-41.0	2.0
	*Si*TMS$_3$	-121.8	-119.5	2.3
4-t	*TMS*$_3$	-9.5	-7.1	2.4
	*Si*O	-42.8	-45.6	2.8
	*Si*TMS$_3$	-124.9	-119.5	5.4
5-c	*TMS*$_3$	-9.8	-8.5	1.3
	*Si*O	-44.0	-41.1	2.9
	*Si*TMS$_3$	-129.8	-126.8	3.0
5-t	*TMS*$_3$	-10.2	-8.0	2.2
	*Si*O	-46.0	-45.3	0.7
	*Si*TMS$_3$	-132.5	-131.1	1.4
6-c	*TMS*$_3$	-10.0	-6.7	3.3
	TMS$_3$	-10.2	-6.7	3.5
	*Si*O$_2$	-53.5	-47.3	6.2
	Si(O)C	-62.1	-65.6	3.5
	*Si*TMS$_3$	-130.3	-126.6	3.7
	*Si*TMS$_3$	-131.7	-126.8	4.1
6-t	*TMS*$_3$	-9.7	-7.9	1.8
	TMS$_3$	-9.9	-7.9	2.0
	*Si*O$_2$	-54.4	-53.2	1.2
	Si(O)C	-63.2	-62.7	0.5
	*Si*TMS$_3$	-132.2	-130.8	1.4
	*Si*TMS$_3$	-132.8	-132.1	0.7

The explicit cartesian coordinates (S49-S143) of all calculated structures were removed due to space-saving issues, but the data can be provided anytime.

4. References

(S1) Wendel, D.; Szilvási, T.; Jandl, C.; Inoue, S.; Rieger, B., *J. Am. Chem. Soc.* **2017**, *139*, 9156-9159.

(S2) A separate measurement of pure CO in C_6D_6 gave a shift at 184.5 ppm in the ^{13}C NMR spectrum.

(S3) *APEX suite of crystallographic software*, APEX 2 Version 2014-9.0; Bruker AXS Inc.: Madison, Wisconsin, USA, **2014**.

(S4) *APEX suite of crystallographic software*, APEX 3 Version 2015-5.2; Bruker AXS Inc.: Madison, Wisconsin, USA, **2015**.

(S5) *SAINT*, Version 8.34A and 8.37A and *SADABS*, Version 2014/5 and 2016/2; Bruker AXS Inc.: Madison, Wisconsin, USA, **2014**.

(S6) Sheldrick, G. M., *Acta Crystallogr., Sect. A* **2015**, *71*, 3–8.

(S7) Sheldrick G. M., *Acta Crystallogr., Sect. C* **2015**, *71*, 3–8.

(S8) Huebschle, C. B.; Sheldrick, G. M.; Dittrich, B., *J. Appl. Cryst.* **2011**, *44*, 1281–1284.

(S9) Wilson, A. J. C. (Ed.) *International Tables for Crystallography, Vol. C*, Tables 6.1.1.4 (pp. 500-502), 4.2.6.8 (pp. 219-222), and 4.2.4.2 (pp. 193-199); Kluwer Academic Publishers: Dordrecht, The Netherlands, **1992**.

(S10) Spek, A. L., *Acta Crystallogr., Sect. C* **2015**, *71*, 9–18.

(S11) Macrae, C. F.; Edgington, P. R.; McCabe, P., Pidcock E.; Shields, G. P.; Taylor, R.; Towler, M.; van de Streek, J., *J. Appl. Cryst.* **2006**, *39*, 453–457.

(S12) A. D. Becke, *J. Chem. Phys.*, **1993**, *98*, 5648-5652.

(S13) Vosko, S. H.; Wilk, L.; Nusair, M. *Can. J. Phys.*, **1980**, *58*, 1200-1211.

(S14) Lee, C.; Yang, W.; R. G. Parr, *Phys. Rev. B*, **1988**, *37*, 785-789.

(S15) F. Weigend, R. Ahlrichs, *Phys. Chem. Chem. Phys.*, **2005**, *7*, 3297-3305.

(S16) K. L. Schuchardt, B. T. Didier, T. Elsethagen, L. Sun, V. Gurumoorthi, J. Chase, J. Li, T. L. Windus, *J. Chem. Inf. Model.*, **2007**, *47*, 1045-1052.

(S17) W. Kutzelnigg, U. Fleischer, M. Schindler, Springer-Verlag, Heidelberg, 1990, vol. 23.

(S18) Gaussian 09, Revision D.01, M. J. Frisch, G. W. Trucks, H. B. Schlegel, G. E. Scuseria, M. A. Robb, J. R. Cheeseman, G. Scalmani, V. Barone, B. Mennucci, G. A. Petersson, H. Nakatsuji, M. Caricato, X. Li, H. P. Hratchian, A. F. Izmaylov, J. Bloino, G. Zheng, J. L. Sonnenberg, M. Hada, M. Ehara, K. Toyota, R. Fukuda, J. Hasegawa, M. Ishida, T. Nakajima, Y. Honda, O. Kitao, H. Nakai, T. Vreven, J. A. Montgomery, Jr., J. E. Peralta, F. Ogliaro, M. Bearpark, J. J. Heyd, E. Brothers, K. N. Kudin, V. N. Staroverov, R. Kobayashi, J. Normand, K. Raghavachari, A. Rendell, J. C. Burant, S. S. Iyengar, J. Tomasi, M. Cossi, N. Rega, J. M. Millam, M. Klene, J. E. Knox, J. B. Cross, V. Bakken, C. Adamo, J. Jaramillo, R. Gomperts, R. E. Stratmann, O. Yazyev, A. J. Austin, R. Cammi, C. Pomelli, J. W. Ochterski, R. L. Martin, K. Morokuma, V. G. Zakrzewski, G. A. Voth, P. Salvador, J. J. Dannenberg, S. Dapprich, A. D. Daniels, Ö. Farkas, J. B. Foresman, J. V. Ortiz, J. Cioslowski, and D. J. Fox, Gaussian, Inc., Wallingford CT, 2009.

14.6 Licenses for Copyrighted Content

“Reactivity of an Acyclic Silylsilylene toward Ethylene: Migratory Insertion into the Si–Si Bond”

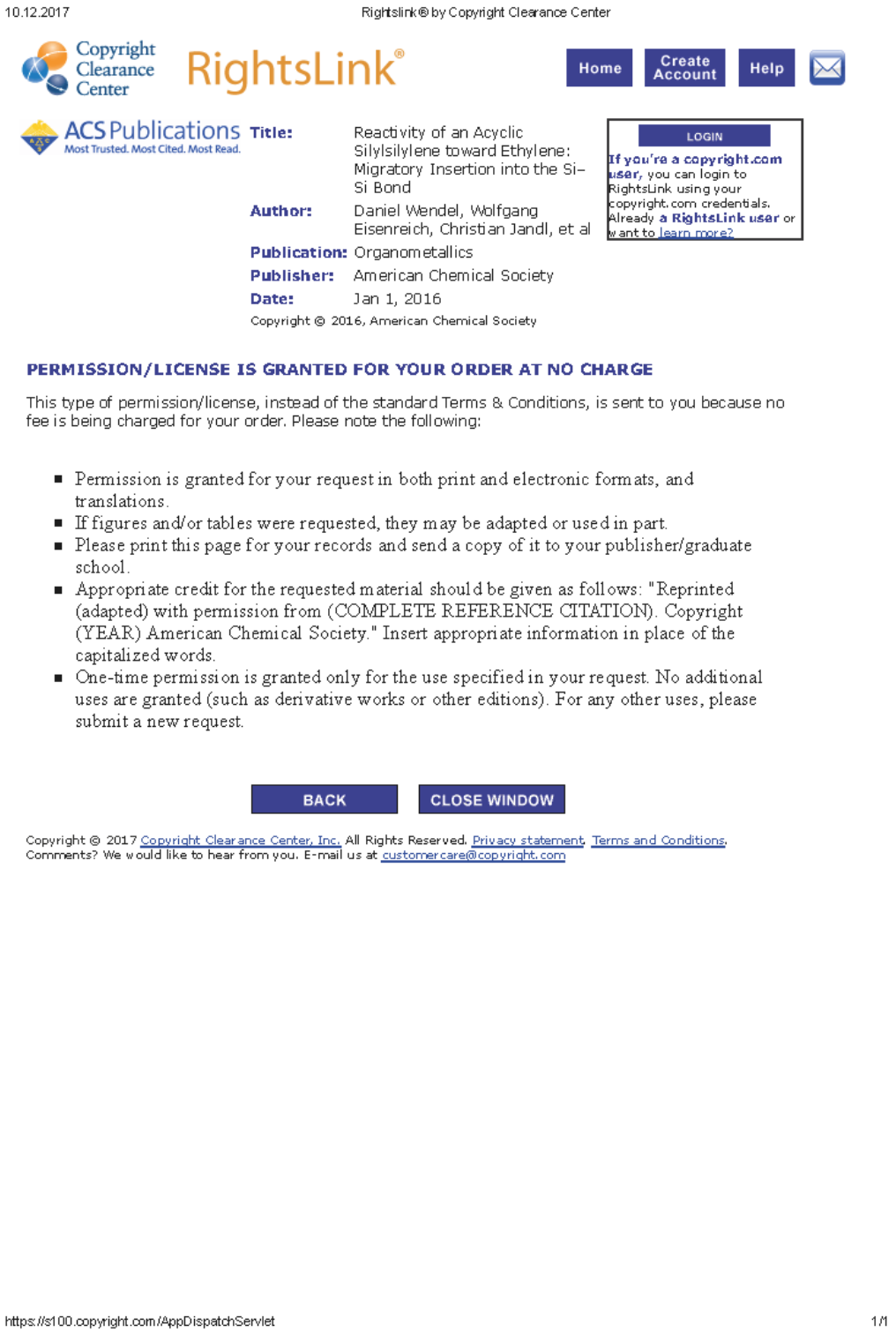

10.12.2017 Rightslink® by Copyright Clearance Center

Copyright Clearance Center RightsLink® Home Create Account Help

ACS Publications Most Trusted. Most Cited. Most Read.

Title: Reactivity of an Acyclic Silylsilylene toward Ethylene: Migratory Insertion into the Si–Si Bond

Author: Daniel Wendel, Wolfgang Eisenreich, Christian Jandl, et al

Publication: Organometallics

Publisher: American Chemical Society

Date: Jan 1, 2016

Copyright © 2016, American Chemical Society

LOGIN

If you're a copyright.com user, you can login to RightsLink using your copyright.com credentials. Already a RightsLink user or want to learn more?

PERMISSION/LICENSE IS GRANTED FOR YOUR ORDER AT NO CHARGE

This type of permission/license, instead of the standard Terms & Conditions, is sent to you because no fee is being charged for your order. Please note the following:

- Permission is granted for your request in both print and electronic formats, and translations.
- If figures and/or tables were requested, they may be adapted or used in part.
- Please print this page for your records and send a copy of it to your publisher/graduate school.
- Appropriate credit for the requested material should be given as follows: "Reprinted (adapted) with permission from (COMPLETE REFERENCE CITATION). Copyright (YEAR) American Chemical Society." Insert appropriate information in place of the capitalized words.
- One-time permission is granted only for the use specified in your request. No additional uses are granted (such as derivative works or other editions). For any other uses, please submit a new request.

BACK CLOSE WINDOW

Copyright © 2017 Copyright Clearance Center, Inc. All Rights Reserved. Privacy statement. Terms and Conditions. Comments? We would like to hear from you. E-mail us at customercare@copyright.com

https://s100.copyright.com/AppDispatchServlet 1/1

“Twist of a Silicon–Silicon Double Bond: Selective *Anti*-Addition of Hydrogen to an Iminodisilene”

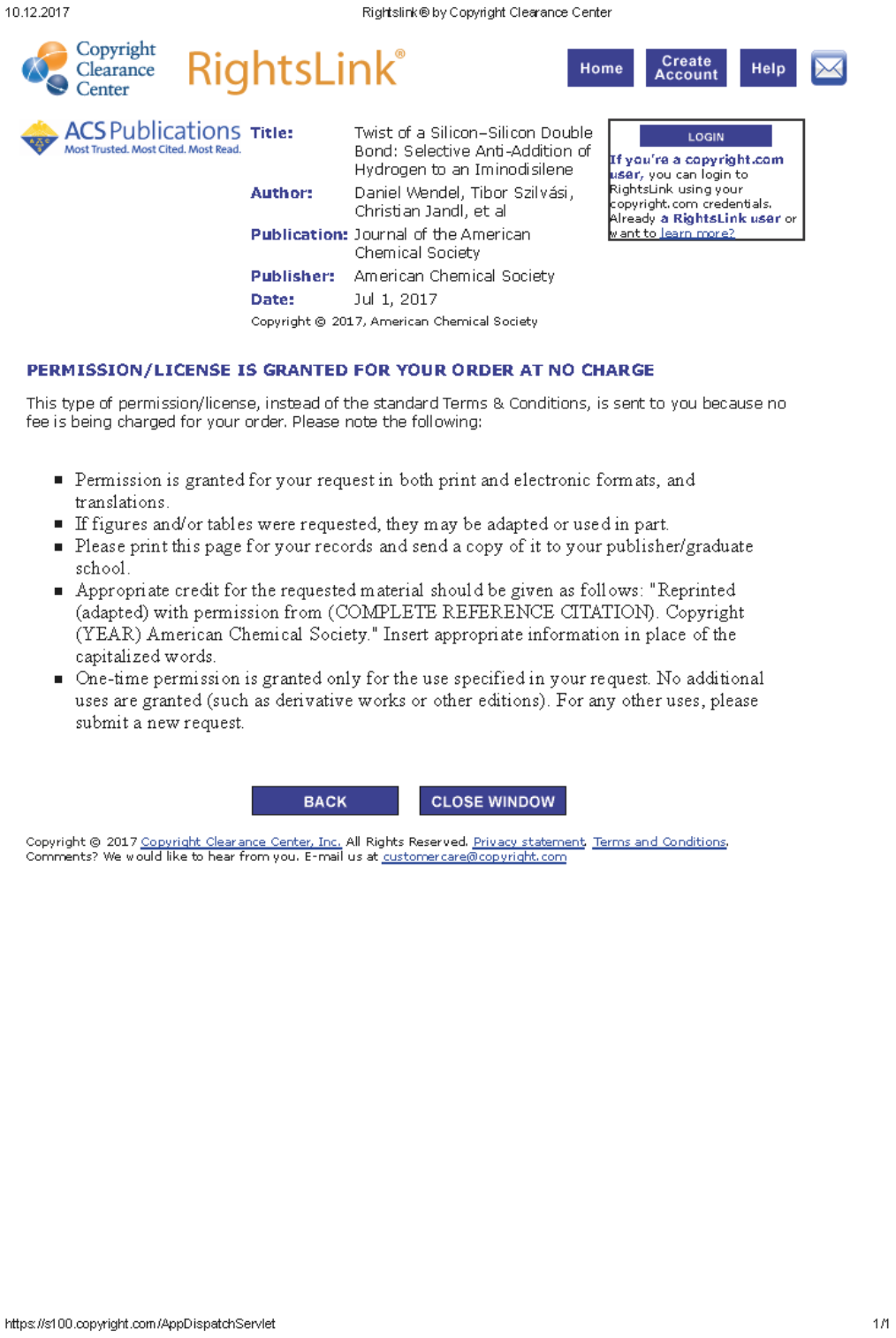

10.12.2017 Rightslink® by Copyright Clearance Center

Copyright Clearance Center RightsLink® Home Create Account Help

ACS Publications Most Trusted. Most Cited. Most Read.

Title: Twist of a Silicon–Silicon Double Bond: Selective Anti-Addition of Hydrogen to an Iminodisilene

Author: Daniel Wendel, Tibor Szilvási, Christian Jandl, et al

Publication: Journal of the American Chemical Society

Publisher: American Chemical Society

Date: Jul 1, 2017

Copyright © 2017, American Chemical Society

LOGIN

If you're a copyright.com user, you can login to RightsLink using your copyright.com credentials. Already a RightsLink user or want to learn more?

PERMISSION/LICENSE IS GRANTED FOR YOUR ORDER AT NO CHARGE

This type of permission/license, instead of the standard Terms & Conditions, is sent to you because no fee is being charged for your order. Please note the following:

- Permission is granted for your request in both print and electronic formats, and translations.
- If figures and/or tables were requested, they may be adapted or used in part.
- Please print this page for your records and send a copy of it to your publisher/graduate school.
- Appropriate credit for the requested material should be given as follows: "Reprinted (adapted) with permission from (COMPLETE REFERENCE CITATION). Copyright (YEAR) American Chemical Society." Insert appropriate information in place of the capitalized words.
- One-time permission is granted only for the use specified in your request. No additional uses are granted (such as derivative works or other editions). For any other uses, please submit a new request.

BACK CLOSE WINDOW

Copyright © 2017 Copyright Clearance Center, Inc. All Rights Reserved. Privacy statement. Terms and Conditions. Comments? We would like to hear from you. E-mail us at customercare@copyright.com

https://s100.copyright.com/AppDispatchServlet 1/1

“From Si(II) to Si(IV) and Back: Reversible Intramolecular Carbon–Carbon Bond Activation by an Acyclic Iminosilylene”

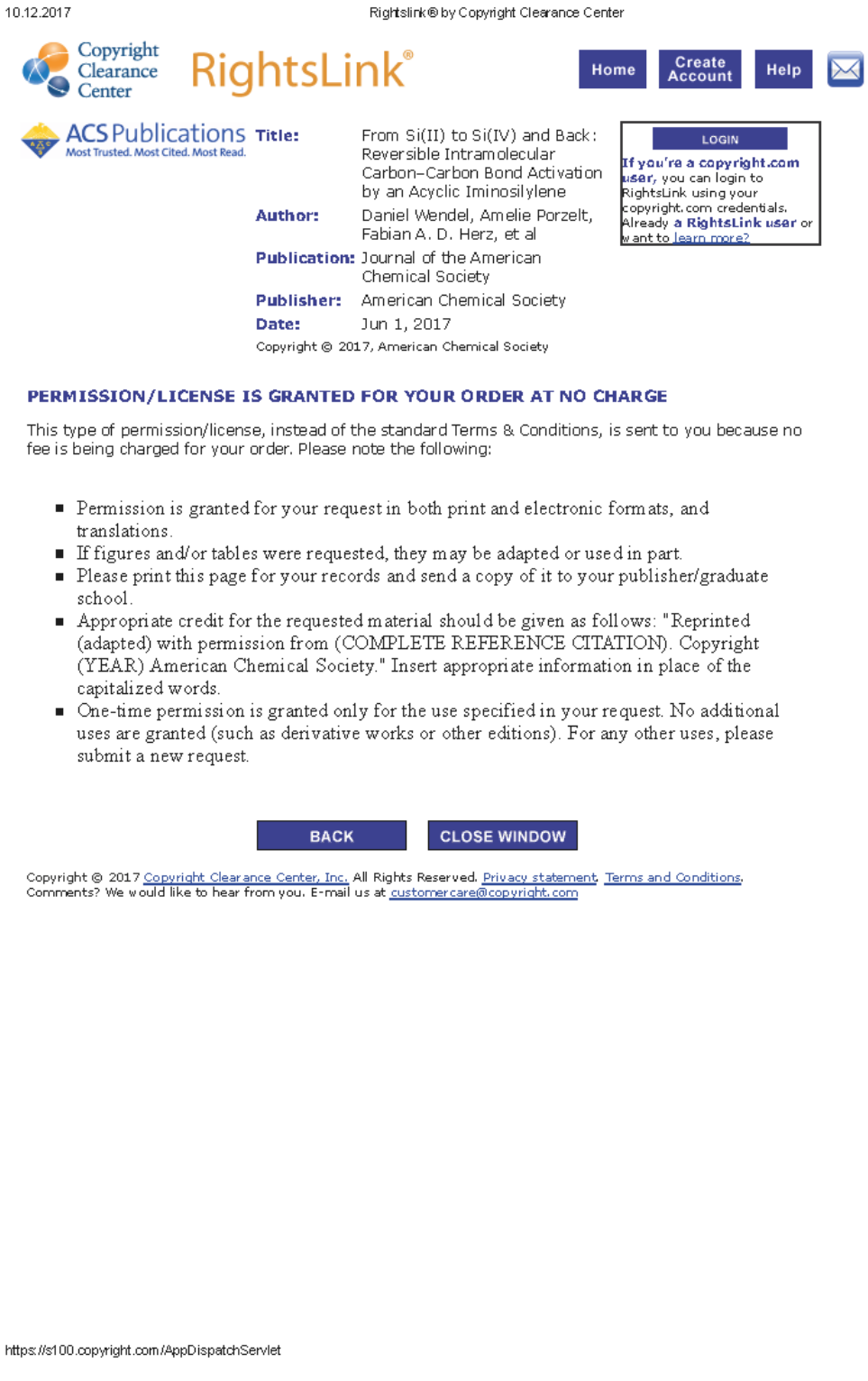

10.12.2017 Rightslink® by Copyright Clearance Center

Copyright Clearance Center RightsLink® Home Create Account Help

ACS Publications Most Trusted. Most Cited. Most Read.

Title: From Si(II) to Si(IV) and Back: Reversible Intramolecular Carbon–Carbon Bond Activation by an Acyclic Iminosilylene

Author: Daniel Wendel, Amelie Porzelt, Fabian A. D. Herz, et al

Publication: Journal of the American Chemical Society

Publisher: American Chemical Society

Date: Jun 1, 2017

Copyright © 2017, American Chemical Society

LOGIN

If you're a copyright.com user, you can login to RightsLink using your copyright.com credentials. Already a RightsLink user or want to learn more?

PERMISSION/LICENSE IS GRANTED FOR YOUR ORDER AT NO CHARGE

This type of permission/license, instead of the standard Terms & Conditions, is sent to you because no fee is being charged for your order. Please note the following:

- Permission is granted for your request in both print and electronic formats, and translations.
- If figures and/or tables were requested, they may be adapted or used in part.
- Please print this page for your records and send a copy of it to your publisher/graduate school.
- Appropriate credit for the requested material should be given as follows: "Reprinted (adapted) with permission from (COMPLETE REFERENCE CITATION). Copyright (YEAR) American Chemical Society." Insert appropriate information in place of the capitalized words.
- One-time permission is granted only for the use specified in your request. No additional uses are granted (such as derivative works or other editions). For any other uses, please submit a new request.

BACK CLOSE WINDOW

Copyright © 2017 Copyright Clearance Center, Inc. All Rights Reserved. Privacy statement. Terms and Conditions. Comments? We would like to hear from you. E-mail us at customercare@copyright.com

https://s100.copyright.com/AppDispatchServlet 1/1

“Silicon and Oxygen’s Bond of Affection: An Acyclic Three-Coordinate Silanone and Its Transformation to an Iminosiloxysilylene”

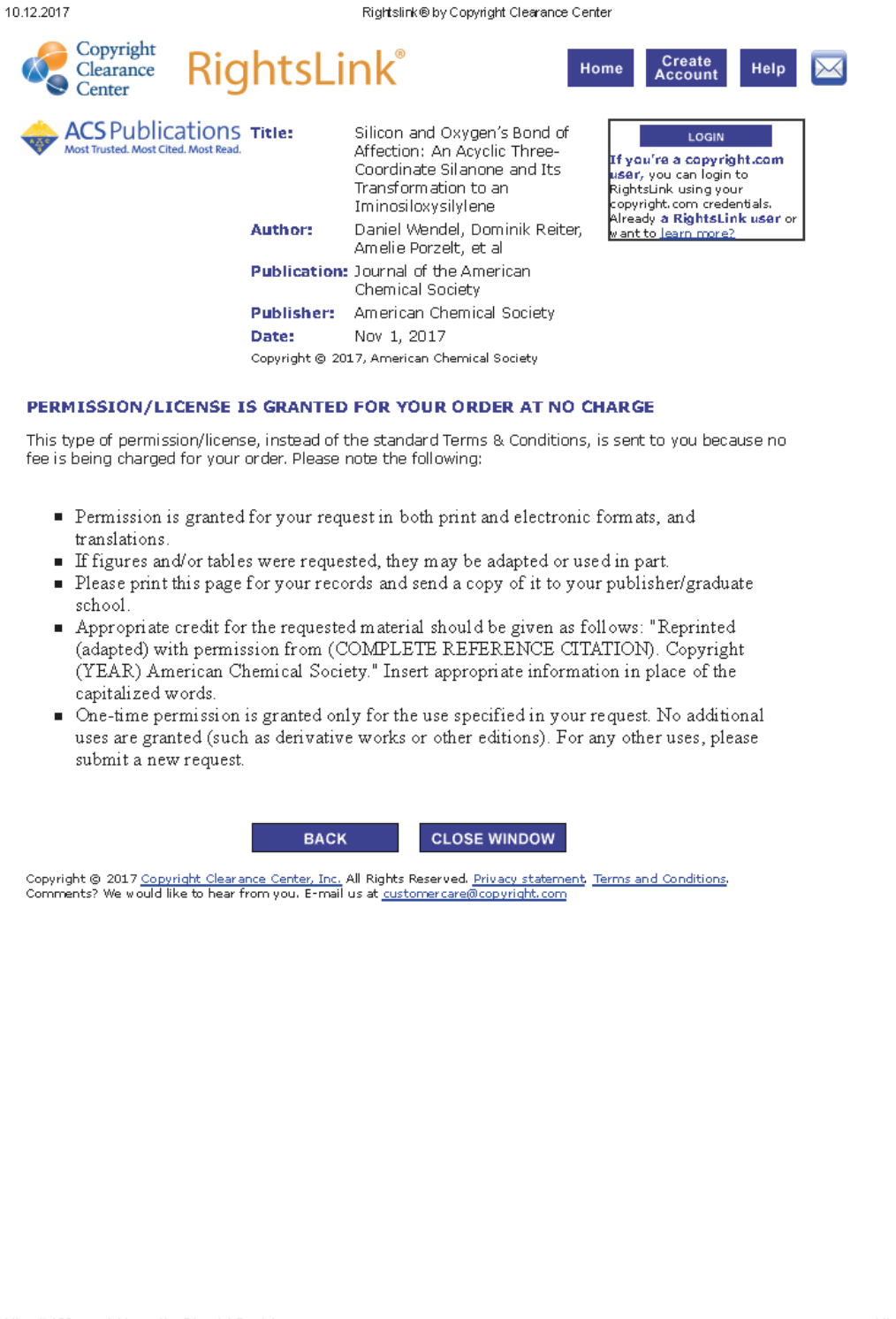

10.12.2017 Rightslink® by Copyright Clearance Center

Copyright Clearance Center RightsLink® Home Create Account Help

ACS Publications Most Trusted. Most Cited. Most Read.

Title: Silicon and Oxygen’s Bond of Affection: An Acyclic Three-Coordinate Silanone and Its Transformation to an Iminosiloxysilylene

Author: Daniel Wendel, Dominik Reiter, Amelie Porzelt, et al

Publication: Journal of the American Chemical Society

Publisher: American Chemical Society

Date: Nov 1, 2017

Copyright © 2017, American Chemical Society

LOGIN

If you’re a copyright.com user, you can login to RightsLink using your copyright.com credentials. Already a RightsLink user or want to learn more?

PERMISSION/LICENSE IS GRANTED FOR YOUR ORDER AT NO CHARGE

This type of permission/license, instead of the standard Terms & Conditions, is sent to you because no fee is being charged for your order. Please note the following:

- Permission is granted for your request in both print and electronic formats, and translations.
- If figures and/or tables were requested, they may be adapted or used in part.
- Please print this page for your records and send a copy of it to your publisher/graduate school.
- Appropriate credit for the requested material should be given as follows: "Reprinted (adapted) with permission from (COMPLETE REFERENCE CITATION). Copyright (YEAR) American Chemical Society." Insert appropriate information in place of the capitalized words.
- One-time permission is granted only for the use specified in your request. No additional uses are granted (such as derivative works or other editions). For any other uses, please submit a new request.

BACK CLOSE WINDOW

Copyright © 2017 Copyright Clearance Center, Inc. All Rights Reserved. Privacy statement. Terms and Conditions.
Comments? We would like to hear from you. E-mail us at customercare@copyright.com

https://s100.copyright.com/AppDispatchServlet 1/1